NASA CONTRACTOR REPORT

NASA CR-134762

NASA CR-134762

INVESTIGATION OF SCRUBBING AND IMPINGEMENT NOISE

by Martin R. Fink

Prepared by
UNITED AIRCRAFT RESEARCH LABORATORIES
East Hartford, Conn. 06108
for Lewis Research Center

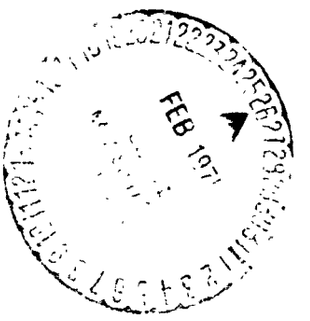

NATIONAL AERONAUTICS AND SPACE ADMINISTRATION. WASHINGTON, D.C. · FEBRUARY 1975

1. Report No.	2. Government Accession No.	3. Recipient's Catalog No.
NASA CR-134762		

4. Title and Subtitle	5. Report Date
INVESTIGATION OF SCRUBBING AND IMPINGEMENT NOISE	February 1975
	6. Performing Organization Code

7. Author(s)	8. Performing Organization Report No.
M. R. Fink	
	10. Work Unit No.

9. Performing Organization Name and Address	11. Contract or Grant No.
United Aircraft Research Laboratories East Hartford, Connecticut 06108	NAS3-17863
	13. Type of Report and Period Covered
12 Sponsoring Agency Name and Address	Contractor Report
National Aeronautics and Space Administration Washington, D.C. 20546	14. Sponsoring Agency Code

15. Supplementary Notes

Project Manager, William A. Olsen, V/STOL and Noise Division, NASA Lewis Research Center, Cleveland, Ohio

16. Abstract

Tests were conducted in an acoustic wind tunnel to determine surface pressure spectra and far-field noise caused by turbulence impinging on an airfoil and turbulence convected past a sharp trailing edge. Measured effects of flow velocity and turbulence intensity were compared with predictions from several theories. Also, tests were conducted in an anechoic chamber to determine surface pressure spectra and far-field noise caused by a deflected airfoil scrubbed by a subsonic jet. This installation simulated both an under-the-wing and an upper-surface-blowing externally blown flap, depending on the deflection angle. Surface and far-field spectra, and cross-correlation coherence and delay time, were utilized to infer the major noise-producing mechanisms.

17. Key Words (Suggested by Author(s))	18 Distribution Statement
Acoustics; Aerodynamic noise; Aircraft noise; Incidence fluctuation noise; Installation noise; Scrubbing noise; Trailing edge noise.	Unclassified-Unlimited

19. Security Classif. (of this report)	20 Security Classif. (of this page)	21 No. of Pages	22 Price*
Unclassified	Unclassified	149	$3.00

* For sale by the National Technical Information Service, Springfield, Virginia 22151

NASA CR-134762

INVESTIGATION OF SCRUBBING AND IMPINGEMENT NOISE

By Martin R. Fink

UNITED AIRCRAFT CORPORATION RESEARCH LABORATORIES

prepared for

NATIONAL AERONAUTICS AND SPACE ADMINISTRATION

NASA Lewis Research Center
Contract NAS3-17863

CONTENTS

INVESTIGATION OF SCRUBBING AND IMPINGEMENT NOISE

By Martin R. Fink

United Aircraft Corporation Research Laboratories

SUMMARY

Tests were conducted in an acoustic wind tunnel to determine surface pressure spectra and far-field noise caused by turbulence impinging on an airfoil and turbulence convected past a sharp trailing edge. Measured effects of flow velocity and turbulence intensity were compared with predictions from several theories. Cross-correlations were utilized to assure that measurements were dominated by the aeroacoustic mechanism of interest. Also, tests were conducted in an anechoic chamber to determine surface pressure spectra and far-field noise caused by a deflected airfoil scrubbed by a subsonic jet. This installation simulated both an under-the-wing and an upper-surface-blowing externally blown flap, depending on the deflection angle. Surface and far-field spectra, and cross-correlation coherence and delay time, were utilized to infer the major noise-producing mechanisms.

Surface pressure spectra for the airfoil with incident turbulence were best predicted by the theory of Filotas. This theory uses separate asymptotic solutions for large and for small Strouhal numbers. Far-field acoustic spectra were well predicted by use of that theory for lift force spectra, combined with Hayden's modification for sound radiation from acoustically noncompact sources.

Trailing edge noise was found to vary with velocity to the fifth power and turbulence intensity squared as predicted by the theories of Ffowcs Williams and Hall and of Chase. Amplitude is predicted by the theory of Ffowcs Williams and Hall if turbulent eddy spacing is taken as four times the turbulence transverse integral scale length.

Noise from an airfoil scrubbed by a jet was found to arise from three mechanisms. Trailing edge noise, caused when turbulent eddies in the jet were convected past the airfoil trailing edge, had large contributions to low-frequency noise and overall sound pressure level. Scrubbing noise, the dipole noise that is strongest normal to the deflected chord of an under-the-wing (UTW) blown flap, was found to be caused by lift force fluctuations induced by large-scale vortex instabilities of the jet as they are convected along the chord. The resulting noise is like that from discrete spanwise vortices moving past an airfoil. Thus, scrubbing noise is increased when the vortices

are brought close to the airfoil as by deflecting an UTW externally blown flap. It is decreased when the flap chord is made so large that the vortices are dissipated by viscosity along the chord. Jet mixing noise, increased in amplitude by jet deflection and reflected toward the ground by UTW installations but shielded by upper-surface-blowing (USB) installations, affects spectra at high frequencies. Thus, major differences between the two types of externally blown flaps are that (1) UTW scrubbing noise is large and oriented normal to the deflected flap segments while USB scrubbing noise is smaller and oriented normal to the undeflected wing, and (2) UTW jet quadrupole noise below the flaps is increased by reflection while USB jet quadrupole noise below the flaps is reduced by shielding.

This report describes work conducted during the first year of this contract. Validated noise prediction methods for different aeroacoustic mechanisms will be combined and applied to practical airframe installation noise problems in subsequent years.

SYMBOLS

Values of dimensional quantities are given in both SI and U.S. Customary Units.

a	speed of sound, m/sec (ft/sec)
b	airfoil span, m (ft)
c	airfoil chord, m (ft)
$\bar{c}$	effective radius of acoustic source, taken as c/2
C_{p_α}	derivative of airfoil pressure coefficient with respect to angle of incidence
D	nozzle diameter, m (ft)
E	spectral density of turbulence intensity, m^2/sec (ft^2/sec)
f	frequency, Hz
I	acoustic intensity, w/m^2 (lb/ft sec)
k	reduced frequency, $\omega c/U$
L	ratio of integral scale length to half-chord, $2\Lambda/c$
$\overline{p^2}$	mean square acoustic pressure, n^2/m^4 (lb^2/ft^4)
p_{ref}	acoustic reference pressure, 2×10^{-5} n/m^2
R	far field radius, m (ft)
S	Sears function (ratio of unsteady to quasi-steady response)
St	Strouhal number, fc/U or $f\delta/U$
$\overline{u^2}$	mean square streamwise velocity fluctuation, m^2/sec^2 (ft^2/sec^2)
U	streamwise mean velocity, m/sec (ft/sec)
$\overline{v^2}$	mean square transverse velocity fluctuation, m^2/sec^2 (ft^2/sec^2)
V	volume of turbulent eddy, m^3 (ft^3)

SYMBOLS (Concluded)

W	width of trailing edge, m (ft)
x	streamwise distance from midchord, m (ft)
α	normalized turbulence intensity, $\overline{v^2}/U^2$
δ	transverse correlation radius of turbulence, m (ft)
θ	angle from upstream direction, deg
Λ	streamwise integral scale length, m (ft)
ρ	density, kg/m^3 ($lb\ sec^2/ft^4$)
ϕ	normalized spectral density, Hz^{-1}, also sideline angle, deg
ω	angular frequency, $2\pi f$, rad/sec

Subscripts

F	lift force
o	original solution by Sears
P	acoustic pressure
S	surface pressure
T	turbulence

INTRODUCTION

Noise generated by solid bodies in the presence of engine airflow determines the inherent minimum noise of installed aircraft engines. For example, acoustically treated splitters within the engine inlet and exhaust ducts can attenuate turbomachinery noise but produce noise at their outer edges. Internal struts, necessary for structural support of the engine and splitters, are likely to be immersed in high-velocity turbulent engine airflows. Externally blown flaps utilize engine exit airflow to generate wing supercirculation lift force at low flight speeds while impinging the high turbulence levels of a jet mixing region onto the wing surface. In all these cases, a solid surface of finite extent is scrubbed by airflow containing velocity and pressure fluctuations generated upstream, within the boundary layer, and within the near wake. The same relatively small number of basic aeroacoustic mechanisms should be present for all of these examples; the magnitude of noise generated by each mechanism should be predictable if the airstream mean velocity, rms turbulence intensity, integral scale lengths, and turbulence spectrum shape are known.

Numerous analyses with varying degrees of complexity are available for calculating noise caused by different mechanisms. A few of these analyses are aerodynamically and aeroacoustically rigorous. Their applicability is limited only by one's ability to predict required properties of the aerodynamically imposed turbulence. Others are little better than dimensional analysis with a proportionality constant chosen to match selected data. Such methods are likely to give poor agreement with data for other tests having different turbulence intensities, different ratios of turbulence length scale to model dimension, and on occasion different Reynolds number. In some cases, different aeroacoustic analyses which yield different predicted trends have been developed for the same basic process. Generally, each analysis contains some fundamental assumptions connecting the aerodynamic flow to the amplitude, correlation area, spectrum shape, and phase relationship of surface pressure fluctuations and connecting these to the far-field acoustic amplitude, directivity shape, and spectrum shape. If all these quantities were measured, it would be possible to (1) accept some analyses as providing good agreement with data for conditions and directions at which the assumed aeroacoustic mechanism should dominate, (2) reject some analyses as clearly contradicted by data, and (3) improve some analyses by revising key assumptions to provide agreement with data. The combination of analyses which survives this examination could then have its total prediction compared with available far-field data for practical engine installations in which several noise mechanisms exist.

ANALYTICAL METHODS

Incidence Fluctuation Noise

A procedure for calculating dipole noise caused by incident turbulence was developed by Sharland (ref. 1), who expressed overall acoustic pressure in terms of a fluctuating lift force. This was written as a product of dynamic pressure, mean square turbulence in the upwash direction, and an effective lift coefficient slope. In order to match his data, this lift slope was taken as approximately half its steady-state value. It is now known that for calculation of overall sound pressure level, the effective lift coefficient slope is a function of the ratio of turbulence integral scale length to airfoil chord.

Noise caused by incident turbulence thus is viewed as caused by lift force fluctuations generated by fluctuations of angle of attack associated with upwash turbulence. Noise from turbulent fluctuations of streamwise velocity was examined analytically by Clark (ref. 2), who showed that it was small relative to that from incidence fluctuation. Other details associated with a dipole noise process have been verified experimentally for airfoils with incidence turbulence. Measured directional patterns reported in references 1 and 3 varied approximately with cosine squared of the angle from normal to the flow direction. Acoustic signals measured at equal distances above and below an airfoil were reported in references 4 and 5 to be of equal magnitude and opposite phase.

As improved theories were developed by Filotas (refs. 6 and 7) and Mugridge (ref. 8) for predicting lift fluctuations in unsteady flow, attempts were made (refs. 2 and 5) to evaluate the use of such theories for predicting noise spectra from airfoils in a measured spectrum of turbulence. The tests reported by Dean (ref. 5) included surface loading data from pressure transducers at an airfoil quarter-chord. Assuming that all pressure fluctuations at a given point on the airfoil are caused by fluctuating incidence, the spectral density ϕ_S of static pressure fluctuation can be related to the spectral density ϕ_T of normalized upwash turbulence $\overline{v^2}/U^2$ by

$$\phi_s = \left(\frac{1}{2}\rho U^2\right)^2 C_{p_\alpha}{}^2 \phi_T \tag{1}$$

where C_{p_α}, the rate of change of pressure coefficient with angle of attack, generally is a function of chordwise position, reduced frequency, turbulence scale length, and Mach number. For incompressible flow and two-dimensional turbulence, the chordwise distribution of C_{p_α} was shown by Sears (ref. 9) to have the same shape as that for a two-dimensional flat plate in steady flow. Then $C_{p_\alpha}{}^2$ can be written as

$$C_{p_a}^2 = \frac{1-2x/c}{1+2x/c}\,\frac{4}{\pi^2}\left(2\pi S_s\right)^2 = 16\,\frac{1-2x/c}{1+2x/c}\,S_s^2 \tag{2}$$

where chordwise distance x is positive downstream of mid-chord and S_s is defined herein as an effective Sears function for surface pressure fluctuation. Then

$$S_s^2 = \frac{1+2x/c}{1-2x/c}\left(2\rho U^2\right)^{-2}\phi_s/\phi_T \tag{3}$$

can be determined experimentally for different chordwise positions. If the turbulence could be represented by a series of two-dimensional gusts having their axis parallel to the leading edge, S_s would be predicted (ref. 6) to be independent of chordwise position and equal to the Sears function. The magnitude of the Sears function can be approximated (ref. 10, p. 411) by

$$\left|S_0\right|^2 = (a+k)\left[a + (\pi a+1)\,k + 2\pi k^2\right]^{-1},\quad a = 0.1811 \tag{4}$$

or, at high frequencies

$$\left|S_0\right|^2 = \left(1+2\pi k\right)^{-1} \tag{5}$$

where k is the unsteady-aerodynamics reduced frequency

$$k = \omega c/(2U) = \pi fc/U = \pi St \tag{6}$$

and St is the Strouhal number or acoustic reduced frequency.

Three-dimensional turbulence is represented by a summation of gusts that are skewed relative to the leading edge. As shown analytically by Filotas in reference 6, skewed gusts cause the chordwise distribution of pressure response to differ from the flat-plate distribution. Pressure fluctuations become relatively larger near the leading edge but the overall amplitude is

decreased. The equations for local pressure spectrum have not been evaluated for incident turbulence. It is clear that for positions at and downstream of mid-chord, the effective Sears function for pressure response should be less than the two-dimensional Sears function.

In the absence of analytical solutions, the simplest approximation would be to neglect distortion in shape of the chordwise loading distribution. The effective Sears function for pressure, at low reduced frequencies, would then be approximately equal to the effective Sears function for lift force response on a chordwise segment having negligible spanwise extent. This quantity was evaluated numerically by Filotas for isotropic turbulence and is shown in figure 4 of reference 7. It decreases with decreasing ratio L of turbulence integral scale length to airfoil half-chord and is approximately independent of reduced frequency at low reduced frequencies. This low-frequency effective Sears function was approximated by equation (35) of reference 7

$$\left|S_F\right|^2 = \frac{\ell n\,(1.2+\pi^2/L^2)}{\ell n\ 1.2+3\pi^2/L^2} \quad ,k < 1/L \tag{7}$$

This constant low value is caused by the spanwise variation of upwash. As reduced frequency k is increased above 1/L, phase cancellation is predicted along the chord. The resulting effective Sears function for lift force on a narrow strip is approximated by equation (7) above with 1/L replaced by k. At large reduced frequencies the resulting function decays as k^{-2} which is more rapid than k^{-1} behavior of the two-dimensional Sears function, equation (5). Static pressure fluctuation should not be affected by phase variation along the chord and should have the smaller high-frequency decay rate of the two-dimensional Sears function. As a crude approximation, the effective Sears function for pressure fluctuation at high frequencies would then be

$$S_s^2 = \frac{\ell n\,(1.2+\pi^2/L^2)}{\ell n\ 1.2+3\pi^2/L^2}\ \frac{1+2\pi/L}{1+2\pi k} \quad ,k > 1/L \tag{8}$$

This would be rewritten as

$$10\log_{10} S_s^2\,(k) = 10\log_{10}\left|S_F(1/L)\right|^2 - 10\log_{10}\left|S_0(1/L)\right|^2 + 10\log_{10}\left|S_0(k)\right|^2 \tag{9}$$

for comparison with values determined from turbulence and surface pressure spectra by use of equation (3).

The above expressions were derived in analyses that neglected the effects of compressibility. Such analyses are not valid when the acoustic wavelength is not large relative to the chord, or equivalently when the time required for an acoustic signal to travel upstream from the trailing edge to the leading edge is a significant fraction of the period. The criterion for which the analyses should be affected by compressibility is

$$k M (1-M)^{-1} > 1 \tag{10}$$

Expressions for local loading distribution in two-dimensional, slightly compressible flow ($kM<1$) have been derived by Osborne (ref. 11). Mean square loading is proportional to the Sears function evaluated at a larger reduced frequency (and thus decreased in amplitude), divided by the Prandtl-Glauert compressibility factor $1-M^2$. For acoustics calculations, the predicted compressible flow loading can be adequately approximated by the incompressible-flow Sears function evaluated at the actual reduced frequency and without the Prandtl-Glauert correction.

Solutions have been developed by Adamczyk (refs. 12 and 13) for two-dimensional and three-dimensional subsonic compressible flow at large reduced frequencies. In this case, both the turbulence scale length and the acoustic wavelength are small relative to the chord. Thus the predicted loading distribution tends to resemble that for a semi-infinite flat plate. The local loading response is predicted to vary inversely with reduced frequency like the corresponding expression obtained from the incompressible-flow Sears function. In contrast, compressibility causes a variation in phase such that the integral of loading along the chord, for large kM, is predicted to vary inversely with reduced frequency squared for two-dimensional unswept gusts.

As with incompressible flow, three-dimensional turbulence or gusts in subsonic compressible flow can be represented by a summation of gusts skewed at different angles relative to the leading edge. The point at which a two-dimensional skewed gust intersects the leading edge can have either subsonic or supersonic velocity, depending on the Mach number and skew angle. If this velocity is subsonic, the resulting equation was shown in reference 12 to resemble that for three-dimensional gusts and incompressible flow. If this velocity is supersonic, the equation resembles that for two-dimensional gusts and compressible flow. For both of these solutions, the effective Sears function for static pressure fluctuation varies inversely with reduced frequency squared. These tails were examined in order to assure that the

effect on lift per unit span caused by changing from two-dimensional to three-dimensional incompressible gusts, and the effect caused by changing from incompressible to subsonic compressible two-dimensional gusts, should not be directly multiplied.

The spectrum of mean square lift force generated by an airfoil in incident turbulence can be written in terms of the turbulence spectrum and an effective Sears function for lift force

$$\phi_F = \left(\frac{1}{2}\rho U^2\right)^2 (cb)^2 \left(2\pi S_F\right)^2 \phi_T \tag{11}$$

following the approach of reference 5. If this force distribution is acoustically compact, it will generate dipole acoustic radiation in the far field whose spectrum will have the amplitude

$$\phi_p = \left(\frac{f\cos\theta}{2ra}\right)^2 \phi_F \tag{12}$$

Combining equations (11) and (12), the effective Sears function for lift force is

$$S_F^2 = \left(\frac{2}{\pi\rho U^2}\ \frac{a}{fb}\ \frac{r}{c\cos\theta}\right)^2 \phi_p/\phi_T \tag{13}$$

This quantity could be determined experimentally from measurements of far-field acoustic spectrum and incident turbulence spectrum. At large reduced frequencies it should be smaller than the effective Sears function derived by Filotas (ref. 7) for lift force on a narrow strip because spanwise variations of phase were omitted in that analysis. An approximate analytic solution for S_F^2 was obtained by Mugridge as equation (3) of reference 8. However, in the limit of large reduced frequency that solution reduces to a product of the Sears function and a function of the ratio of turbulence integral scale length to model span. Thus its frequency decay rate would be that predicted for two-dimensional turbulence rather than the larger rate predicted by Filotas (ref. 7) for three-dimensional turbulence.

If the model dimensions are not small relative to the acoustic wavelength, regions which are nearly in phase with respect to their contributions to aerodynamic lift may have acoustic contributions that differ significantly in phase. That is, the compact source assumption may not be valid. Mugridge (ref. 14) has estimated that high-frequency rapid decay of the sound spectrum from a compact acoustic source should occur for reduced frequencies $\pi fc/U$ greater than 3, and that noncompact-source phase cancenllation effects occur for $\pi fc/a$ greater than unity. Thus, high-frequency acoustic effects are inherently combined with acoustic noncompactness if the Mach number is greater than 1/3. An approximate prediction of whole-body dipole source noise for compact and noncompact sources was developed by Hayden (ref. 15). The acoustic transfer function $(\omega/a)^2$ for compact sources was replaced by the quantity $(\omega/a)^2[1 + (\omega\bar{c}/a)^2]^{-1}$ where $\bar{c}$ is an otherwise undefined effective radius of the acoustic source. Once the ratio of this dimension to a geometric dimension such as chord or the square root of planform area is known, the far-field sound spectrum of a noncompact lift force fluctuation can be calculated. At large reduced frequencies referenced to both the flow speed and speed of sound, power spectral density of far-field sound caused by three-dimensional turbulence should decay at least as rapidly as inversely with the fourth power of frequency. However, the actual calculation process recommended by Hayden in reference 15 used the lift response equations of reference 8 and yields a power spectral density that decays inversely with frequency cubed.

In all of these methods, overall sound pressure level must be calculated by computing the sound pressure spectrum and integrating over frequency. Values of frequency-averaged rms lift coefficient are given in figure 5 of reference 7 as a function of the ratio of turbulence scale length to chord. If these are inserted within Sharland's equation (8) of reference 1 for overall acoustic power, that quantity will be overestimated as compared with the integral of calculated power spectral density.

Trailing-Edge Noise

The earliest analytic solution for edge noise was that of Powell (ref. 16), who used dimensional analysis to develop approximate predictions for several noise mechanisms associated with a flat-plate turbulent boundary layer. These were described as surface noise associated with turbulence far from an edge, edge noise from streamwise and trailing edges, and boundary layer noise and wake noise from quadrupoles in the turbulent boundary layer and wake. Surface noise was claimed to vanish, using an approach similar to that by which Sharland (ref. 1) later found it to be two orders of magnitude smaller than most other types of noise for an isolated airfoil. Edge noise, caused by turbulent eddies very near a sharp edge, was shown to be proportional to the product of turbulence intensity squared and velocity to the

fifth power. For this case of boundary layer turbulence, it was given by equation (12a) of reference 16 as proportional to velocity raised to the 4.6 power. Power spectral density was found to vary inversely with frequency cubed at high frequencies. Directivity was stated to be biased in the upstream direction but was not determined explicitly.

More recently, Ffowcs Williams and Hall (ref. 17) obtained solutions for noise caused by quadrupoles in a turbulent stream near a sharp leading or trailing edge of a long plate relative to the acoustic wavelength. Intensity was found to vary with velocity to the fifth power, as would have been obtained in equation (12a) of reference 16 if the dependence of turbulent velocity fluctuation on Reynolds number had been omitted from equation (2) therein. Intensity was shown to be maximum in the direction within the plane surface (downstream for a sharp leading edge and upstream for a sharp trailing edge) and to vary with $\cos^2(\theta/2)$ where θ is the angle from the plane. This directivity agrees with the qualitative result of reference 16. Edge noise would therefore be expected to vary with velocity to the fifth power and to have a distinctive single-lobed directivity pattern. For edges with large half-angles, the velocity exponent was shown in reference 18 to be equal to $4 + 2/n$ for an exterior wedge angle $n\pi$. Thus the exponent should increase from 5 for a cusp to 5 1/3 for an included right angle and 6 for a surface perpendicular to the flow.

Using a slight modification of the notation of reference 17, rms intensity of edge noise caused by one eddy is given by equation (15) of reference 17 as

$$I_{edge} = \frac{\rho k U^4 V^2 \alpha^2}{\pi^3 a R^2 \delta^3} \cos^2(\theta/2) \tag{14}$$

where k is the wave number, V is the volume of the turbulent eddy, α is the normalized turbulence velocity intensity, and δ is the correlation radius. The quantities ρ, U, a, and R are the density, velocity, and speed of sound of the uniform flow in which the edge is immersed, and distance from the edge to a field point. From the paragraph following equation (15) of reference 17,

$$k = \pi U/a\,\delta \tag{15}$$

and the volume of each turbulent eddy probably can be approximated by that of a sphere with radius δ

$$V = (4/3)\pi\delta^3 \tag{16}$$

Mean square acoustic pressure is given by

$$\overline{p^2} = \rho a I \tag{17}$$

so the mean square acoustic pressure for edge noise caused by one eddy would be given by the following equation:

$$\overline{p^2}_{edge} = (16/9)\left(\rho^2/a\right) U^5 a^2 (\delta/R)^2 \cos^2(\theta/2) \tag{18}$$

A trailing edge normal to the flow and having spanwise extent L would be expected to have roughly L/ (2δ) eddies near it. Thus the mean square acoustic pressure for edge noise radiated by the entire edge would be

$$\overline{p^2}_{edge} = (8/9)\left(\rho^2/a\right) U^5 a^2 \left(\delta L/R^2\right) \cos^2(\theta/2) \tag{19}$$

This quantity is proportional to velocity to the fifth power, turbulence intensity squared, and the product of correlation radius and spanwise dimension.

Solutions for acoustic pressure spectra of edge noise caused by boundary layer turbulence and by isotropic turbulence had been developed by Chase (ref. 19). As noted therein, integration of these spectra to obtain mean square acoustic pressure gives the same functional dependence as that of reference 17. Because turbulence properties are described differently in the two analyses, absolute levels cannot be compared directly. The autospectrum of point pressure in isotropic turbulence, as given by equation (36) of reference 16, has a frequency dependence given by

$$\omega^{-7/3}\left[1 + K(\omega\delta/U)^2\right]^{-7/6}$$

which is independent of frequency at low reduced frequencies and varies inversely with frequency to the 7/3 power at high reduced frequencies. Here the constant K is a function of the distribution of energy within different eddy sizes and of the eddy convection velocity. The corresponding power spectral density of acoustic pressure can be obtained from equation (41) of reference 19 as proportional to

$$\omega^{-10/3}\left[1 + K\,(\omega\delta/U)^2\right]^{-5/3}$$

At high reduced frequencies this factor varies inversely with frequency to the -10/3 power, in good agreement with Powell's early estimate (ref. 16) of an inverse frequency cubed dependence. The frequency factor approaches a constant as reduced frequency approaches zero, but as noted in reference 19 the analysis is not valid near that limit. Measured edge noise spectra were shown in figure 4 of reference 19 to be correlated when plotted as $\omega\pi/U^5$ against a scaled frequency ω/U and to decay approximately inversely with scaled frequency to the -10/3 power at large values of scaled frequency. Rather than being constant at small values of scaled frequency, they increased strongly with frequency (roughly, with frequency to the fifth power). A more recent solution by Chase (ref. 20) used a revised expression for turbulence and got a frequency exponent of -8/3.

Hayden (refs. 15 and 21) has used a dimensional analysis similar to that of Powell (ref. 16) in which acoustic intensity of trailing edge noise was assumed proportional to the product of frequency squared, mean square pressure fluctuation, spanwise correlation length, and edge length. Spanwise correlation length was assumed by Hayden in references 15 and 21 to vary inversely with jet velocity while in reference 16 the relevant velocity was assumed by Powell to be the speed of sound. Thus, Hayden predicted that trailing-edge noise should vary with the sixth rather than the fifth power of velocity. Normalized one-third-octave spectra and overall levels are given in figure 6 of reference 15 as proportional to

$$U^6\left(\delta L/R^2\right)\cos^2(\theta/2)$$

From equation (5) of reference 15, overall sound pressure level can be calculated from

$$OASPL = 10\log_{10}\left(\delta_H L U^6\right) - 20\log_{10} R + 10\log\left[\sin^2\phi\cos^2(\theta/2)\right] + \text{constant} \qquad (20)$$

where U is the maximum jet velocity at the edge (fps), δ_H is the distance from the surface to the maximum-velocity position, and L is the spanwise width between positions at which the local maximum of jet velocity is half of the largest maximum. The distance R from the center of the trailing edge to the far field has the same length dimension units as the jet thickness and width, and ϕ is the sideline angle (zero or π in the sideline direction, $\pi/2$ in a direction normal to the plane surface). The constant is equal to -18.5 if the jet has a potential core extending to the trailing edge, -13.5 if it has considerable viscous decay in all directions (radial decay region), and -16.5 for an intermediate type of flow. In the context of other analyses, these represent a change in the ratio of rms velocity fluctuation to local mean velocity by a factor of about 1.8.

Normalized one-third-octave spectra were given by Hayden in figure 6 of reference 15. In the radial decay region they correspond to a PSD that varies inversely with frequency cubed at high frequencies and directly with frequency to the first power at low frequencies. The curve for the potential core regime would have a SPL that decays inversely with frequency to the fourth power at high frequencies and increases at about the same exponent at low frequencies. Thus one empirical curve has a high-frequency decay rate close to that predicted by others but has a relatively small increase at low frequencies. Another has a more rapid decay at high frequencies than was predicted in reference 16 and 19 but has a very steep increase at low frequencies as was shown in a data correlation within reference 19.

APPARATUS AND PROCEDURE

Acoustic Research Tunnel

The UARL acoustic wind tunnel permits the concurrent measurement of both near- and far-field aerodynamic noise and the unsteady static pressures on surfaces of airfoil models. A detailed description of this tunnel was given in reference 22. The acoustic research tunnel, shown in figure 1, is of the open-circuit open-test-section type. Use of an open circuit and a muffling section with two right-angle bends and parallel baffles downstream of the diffuser greatly reduces the contribution of the tunnel fan to the test section ambient noise level. The free-jet test section has a two-stage nozzle that provides nominal maximum velocities of 80 m/sec (270 fps) and 205 m/sec (670 fps) at flow cross section areas of 0.93 and 0.42 sq m (10 and 4.5 sq ft), respectively. For these tests the smaller cross section area, 0.79 m (31 in.) high and 0.53 m (21 in.) wide, was used with a 1.24 m (49 in.) open jet length. By locating the free jet within a 5.5 m (18 ft) long, 4.9 m (16 ft) high, and 6.7 m (22 ft) wide anechoic chamber, reflection-free conditions are obtained above the 270 Hz free-field cutoff frequency (99% absorption at normal incidence) determined by the acoustic wedge dimensions. The chamber has been found to be anechoic within a 200 Hz to 20,000 Hz range of calibration frequencies for broadband noise. Measurements can be taken in the acoustic far field within the chamber but outside the high-velocity airstream.

The inlet section has a contraction ratio of 16.5 for the smaller test section area. It is equipped with five removable screens and a high length-to-diameter honeycomb section. These provide controlled turbulence levels with a minimum value less than 0.2% in the test section. Grids can be inserted at the junction of the two nozzle contractions to provide a range of turbulence levels. The test section airflow is brought into the diffuser by a collector that has anechoic treatment on its flow-impingement lip. The test section collector and three-stage diffuser have been designed to avoid local flow separation. The 1500 hp electric induction motor and the acoustically lined muffling sections on both sides of the centrifugal fan were selected to reduce noise radiated from the tunnel drive system.

Jet Exhaust Equipment

Clean dry air for jet exhaust tests is obtained from a large air storage system at 2.7×10^3 kN/m^2 (400 lb/in.^{2}) nominal supply pressure. As sketched in figure 2, this air passes through a flow control valve, flow straighteners, a flowmeter, another flow control valve, three 0.915 m (3 ft) noise mufflers in series, and a straight pipe. Each of the three tubular mufflers has a dynamic insertion loss greater than 35 dB in the 850 and 1700 Hz mid-frequency

octave bands for noise propagating in the flow direction at flow rates of these tests. The straight pipe was approximately 2.9 m (9.5 ft) long and had an 0.15 m (6 in.) inside diameter. It ended at a fitting that provided smooth transition to an 0.049 m (1.925 in.) exit diameter axisymmetric nozzle contoured to give uniform exit flow. The pipe passed into the anechoic chamber which contains the test section of the acoustic research tunnel and was aimed at a large door in this chamber. This door was opened to allow undisturbed exit of the jet. The nozzle centerline was 1.07 m (42 in.) above the tips of the floor anechoic wedges.

Exhaust velocity was defined as that for isentropic expansion from the stagnation pressure and temperature measured near the start of the straight pipe to a static pressure equal to ambient pressure in the chamber. Stagnation temperatures for these tests generally ranged from about 4 C to 10 C (40 F to 50 F) as did the static temperature within the anechoic chamber. Velocity was set by maintaining the difference between stagnation pressure and atmospheric static pressure at predetermined values within about 2.5 mm (0.1 in.) of water at pressure differences less than about 16 kN/m^2 (70 in. of water) and about 2.5 mm (0.1 in.) of mercury at larger pressure differences.

Airfoil Models

Two airfoil models were used in this investigation. One model was an instrumented flat plate which represents a hard-wall splitter plate, engine duct strut, or wing with retracted flaps. This model, shown in figures 3 and 4, had 46 cm (18 in.) chord and 53 cm (21 in.) span. It had constant 2.54 cm (1.0 in.) thickness except for the cylindrical leading edge and the aft 6.35 cm (2.5 in.) which had circular arc upper and lower surfaces and a nominally sharp trailing edge. This model thickness was chosen to allow easy installation of conventional 0.635 cm (1/4 in.) condenser microphones mounted on right-angle adaptors and preamplifiers. Microphones were flush mounted without protective grids on both the upper and lower surfaces at positions offset $\pm$0.5 cm (0.2 in.) from mid-span at three chordwise locations: 5 cm (2 in.), 23 cm (9 in.), and 41 cm (16 in.) downstream of the leading edge. These positions were chosen because, for the chordwise loading distribution predicted for two-dimensional turbulence at low frequencies and incompressible flow, surface pressure fluctuation levels at the forward and aft positions would be 9 dB larger and smaller, respectively, than at mid-chord. Also, if the forward and mid-chord microphones were in the two-dimensional far field of noise originating at the trailing edge, signals from these two positions would be predicted to differ by 5 dB.

This flat plate model could be mounted in the wind tunnel test section between sidewalls at zero incidence and each of two positions sketched in figure 5. Noise caused by incident turbulence was examined with the airfoil in the tunnel center plane and its leading edge 27 cm (10.5 in.) downstream of the nozzle exit. Sidewalls were used because noise from portions of an end-plated model that are within the thin low-turbulence sidewall boundary layers is much smaller than noise from portions of an airfoil that extend through thick high-turbulence shear layers. Trailing edge noise caused by turbulence convected past a sharp trailing edge was examined with this airfoil raised and moved forward to the nozzle exit. The airfoil's rounded leading edge was faired into the test section nozzle and the flat lower surface became an extension of the nozzle (fig. 5). In both positions the model was attached to the sidewalls.

The other airfoil model had 23 cm (9 in.) chord, 53 cm (21 in.) span, and an NACA 0018 airfoil section. As shown in figure 6, it contained sliders at 30% and 70% chord that could be moved manually within keyhole-shaped slots that extend to the airfoil surface. A 0.635 cm (1/4 in.) flush-mounted microphone with its right-angle adaptor and preamplifier was contained within each slider and could be traversed along the airfoil span. Four fixed flush-mounted microphones were installed in a chordwise row at one-third span and 20, 30, 62, and 80% chord. (The number of active microphones was limited by space available for cables and preamplifiers.) The airfoil was mounted between circular end-plates and could be rotated about 30% chord within a support stand. For tests representing an under-the-wing externally blown flap, the leading edge at zero deflection was 2.5 cm (1.0 in.) beneath and 2.5 cm (1.0 in.) downstream of the lip of a 4.9 cm (1.925 in.) diameter convergent nozzle. Airfoil position relative to the nozzle, and relative to lines of constant mean square pressure fluctuation of an undistorted jet as determined from reference 23, is sketched in figure 7 for -10, 0, 9, 18, and 30° deflection. At zero deflection (fig. 7b) the scrubbed surface was approximately along a line on which the pressure fluctuation was 80% of maximum, and at 9° the scrubbed surface was in line with the nozzle lip where pressure fluctuations would be largest. The two larger angles placed the airfoil trailing edge either on the extended nozzle centerline or in line with the nozzle opposite lip. For tests that represented an over-the-wing (upper surface blowing) externally blown flap, the leading edge at zero deflection was 2.5 cm (1.0 in.) above and 2.5 cm (1.0 in.) downstream of the nozzle lip. Airfoil position relative to the nozzle and relative to lines of constant mean square pressure fluctuation of an undistorted jet for this installation are sketched in figure 7a for -10° deflection angle. Because the airfoil leading edge moved into the jet as negative angle was increased, the jet became split between the airfoil surfaces and did not detach from the airfoil scrubbed surface with increasing deflection angle.

Acoustic Instrumentation

Far-field noise spectra and surface pressure spectra were measured with commercially available 0.635 cm (1/4 in.) condenser microphones. Frequency response of these microphones to pressure fluctuations is flat from 6 Hz to 20,000 Hz. Free-field directivity corrections at grazing (90°) incidence are less than 0.2 dB at frequencies to 16,000 Hz and about 0.5 dB at 20,000 Hz without the protecting grid. Far-field microphones were oriented at grazing incidence and used without the protecting grid. To permit flush mounting the microphones in the airfoil models as sketched in figure 6, right-angle adaptors were used. Each microphone and adaptor was clamped in a bracket that was attached to the airfoil by set screws. These set screws were adjusted to optically aline the microphone diaphragm with the airfoil surface.

Atmospheric attenuation of the far-field acoustic data was calculated as about 0.1 dB at 10 kHz and 0.4 dB at 20 kHz. Because this correction is approximately equal and opposite to that for free-field directivity of the microphones, no corrections were applied to the measured spectra.

Far-field sound pressure levels and surface pressure fluctuation levels, cited herein as SPL and surface SPL, respectively, were measured in decibels referenced to 2×10^{-5} newtons per square meter (2×10^{-4} microbar). All microphones were calibrated daily with a 250 Hz pistonphone.

For all tests, far-field microphones were located at three positions on an arc of 2.14 m (7 ft) radius in a vertical plane through the wind tunnel or jet nozzle centerline. The microphones were at 60°, 90°, and 120° angular position relative to the undeflected flow velocity. The microphone arc was centered at the flat plate trailing edge for the plate upper position, mid-chord for the flat plate lower position, and the center of the axisymmetric nozzle for the jet scrubbing noise tests.

Test Conditions and Procedures

Background noise measurements were obtained at the far field measurement locations of the acoustic wind tunnel without an upstream grid and with each of two turbulence grids at five test velocities. Hot wire measurements of transverse and axial velocity fluctuation spectra produced in the test section by these grids had been conducted at other airspeeds within another test program. Wind tunnel velocities for the tests described herein were 31.5, 50, 80, 125, and 177 m/sec (103, 164, 262, 410, and 580 ft/sec). The lower velocities divide the nominal operating range of this test section in approximately equal logarithmic increments that differ by multiples of $2^{2/3}$.

Comparison of one-third-octave spectra measured at different velocities is facilitated by use of this spacing. The highest velocity was the maximum test section velocity that could be obtained with the turbulence grids.

Because wind tunnel turbulence grids could be changed easily without disturbing the model and far-field instrumentation, tests were conducted through the range of turbulence levels at constant flat plate model positions. Surface and far-field one-third-octave spectra were automatically plotted on-line. These data were monitored during each run for qualitative comparison with expected trends. Additional one-third-octave or constant-bandwidth spectra in other ranges of frequency were obtained if unusual effects were noted. Combinations of microphones that would be expected to have strong signal coherence were then chosen for cross correlation. Autocorrelations and cross correlations could be displayed on an oscilloscope to assure that signal delay times were consistent with the assumed noise origins and propagation path lengths. After satisfactory results were obtained, the correlation functions were automatically plotted on-line.

This procedure was followed at each of the three turbulence levels with the flat plate airfoil in its upper position. The airfoil was then lowered to mid-height of the test section and moved aft, the far-field microphones were lowered to their new positions, and the above process was repeated at each turbulence level.

Jet scrubbing noise tests were conducted at 125, 160, 200, 250 and 295 m/sec (410, 525, 656, 820, and 967 ft/sec) jet velocities. These velocities differ by multiples of $2^{1/3}$ except for the highest velocity, which was somewhat smaller to avoid supersonic jet velocities and shock wave noise. The lowest and three highest of these velocities correspond to the nominal nozzle pressure ratios of 1.1, 1.25, 1.4, and 1.7 that have been used in NASA model tests of EBF noise (e.g., ref. 24). Surface and far field one-third-octave spectra were obtained on-line for all jet velocities at each deflection angle that corresponded to an under-the-wing EBF installation. At several velocities, the sliders were moved spanwise and spectra were monitored on an oscilloscope to determine the lateral extent of significant surface pressure fluctuations. Spectra and filtered surface-to-surface cross correlations were obtained at selected spanwise locations. Surface to far-field cross correlations also were obtained for use in relating local surface pressure fluctuation to local acoustic source strength. The airfoil model was then moved to its over-the-wing EBF position and the above process repeated. Shear layer refraction effects on far-field noise measurements were calculated for lift dipole directivity as expected for noise caused by incident turbulence. As can be inferred from the calculated distortions of directivity shown in figure 8 of reference 22, these effects were less than 1 dB for the velocities and microphone positions of this test program. Corrections for these effects were not applied.

Grid-Produced Turbulence

Turbulence was generated in the test section of the acoustic research tunnel by use of grids in the contraction nozzle (fig. 5). The flow cross-section area at the nozzle exit was 45% of that for the grid location. Grids used in these tests are denoted as the large and medium grid; a small grid did not raise the tunnel turbulence level enough so that clearly measurable noise would be expected. Turbulence streamwise integral scale lengths were determined from autocorrelation of the hot wire measurement of axial velocity fluctuation at four velocities from 26 to 67 m/sec. These measurements were conducted at mid-span, mid-height, and approximately the axial position that would be occupied by the flat plate airfoil's leading edge in tests of noise caused by incident turbulence. This streamwise integral scale length was found to be approximately 3.2 cm (1.27 in.) for both grids and the test range of velocity. Transverse integral scale length was determined from cross correlation of hot wire measurements from two probes, one at the centerline and the other moved spanwise, to be approximately 1.9 cm (0.75 in.). This distance was about 60% of the streamwise integral scale length and exceeds the 50% ratio expected for isotropic turbulence. Precisely isotropic behavior had not been expected because of the nozzle contraction downstream of the grids. Measured normalized spectral distributions of streamwise turbulence for both grids are compared in figure 8 with the analytic expression

$$\frac{UE_1}{U_1^2 \Lambda} = 4\left[1+(2\pi f \Lambda / U^2\right]^{-1} \qquad (21)$$

given by equation (1-95) of reference 25 for isotropic behavior. This equation, which includes streamwise velocity, power spectral density, mean square velocity fluctuation, mean velocity, turbulence integral scale length, and frequency gives a reasonable prediction of these spectra. However, the measured high-frequency decay rate was smaller than inversely with Strouhal number squared as is given by the equation. The data are more closely approximated by a decay inversely with Strouhal number to the 5/3 power, shown as a dashed line.

Streamwise and transverse rms turbulence intensities were found to be approximately equal within about 5% and to vary within about 15% over a transverse distance of about 21.6 cm (8.5 in.) from the centerline (within about 5 cm (2 in.) from one sidewall). Measured streamwise rms turbulence intensities are plotted in figure 9 for both grids, a range of free-stream velocities, and axial positions corresponding roughly to the flat plate airfoil's leading edge, mid-chord, and trailing edge in tests with incident

turbulence. Turbulence intensity decreased with increasing velocity and increasing streamwise distance, and was about 2/3 as large for the medium grid as for the large grid. Intensity varied approximately with velocity to the -0.2 power and decayed at midchord to about 86% of its value at the leading edge but had little change from there to the trailing edge. Empirical curves (straight lines on a logarithmic plot) were fit to these data to allow prediction of turbulence at higher velocities. These curves and their equation are also given in figure 9.

Background Noise

Measured background noise spectra of the acoustic research tunnel without a turbulence grid are given in figure 10 for microphone direction angles 60°, 90°, and 120° from the downstream direction. The microphones were on a vertical arc of 2.13 cm (7 ft) radius centered at a point 46 cm (18 in.) downstream of the nozzle upper exit lip and in the lateral plane of symmetry. This center point was the flat plate airfoil's trailing edge location when the airfoil was in its upper position for tests of trailing edge noise. One-third-octave spectra are shown for center frequencies from 200 to 20,000 Hz; the chamber is not anechoic to broadband noise below 200 Hz center frequency (ref. 22). In these tests, tabs with triangular aft portions (fig. 4 of ref. 22) protruded into the upper and lower shear layers to prevent edge tones caused by feedback between the collector and nozzle. These tabs generated the relatively flat high-frequency portions of the spectra which were spaced at increments of about 12 dB at successive lower velocities and 9 dB between the two highest velocities. These increments correspond to a sixth-power dipole velocity dependence but the amplitudes had little variation with direction angle. The low-frequency part of the spectra had a rapid decay with increasing frequency and maximum amplitude in the direction perpendicular to the flow.

Measured background noise spectra in these three directions and with each of two turbulence grids are given in figure 11. Nozzle tabs were installed for these runs. Background noise was increased markedly by the presence of upstream turbulence. This noise generally was strongest in the downstream direction and is attributed to impingement of the turbulent shear layer onto the collector. Increasing the grid size from medium to large, which increased the turbulence level, raised the noise level at low frequencies. Unexpectedly, background noise at high frequencies was larger for the medium than for the large grid.

Background noise also was measured with the microphones moved downward 39 cm (15.5 in.) and downstream 4 cm (1.5 in.). In this position they defined an arc centered at mid-chord of the flat plate airfoil in its center position for measurement of incident turbulence noise. One-third-octave sound pressure levels were within one dB of those shown in figure 11 and are not given herein.

Jet mixing noise spectra of the exhaust nozzle used for scrubbing noise tests are compared in figures 12(a)-(c) with those calculated by the semi-empirical method of reference 26. That method is based primarily on jet noise measurements obtained at NASA Lewis Research Center. Data of these tests for directions 90° and 120° from downstream agreed with the calculated spectra within ±2 dB, the typical scatter cited in reference 26, except for the lower frequencies and lower velocities. At jet velocities less than 125 m/sec (410 ft/sec), measured one-third-octave spectra did not decay with decreasing frequency at Strouhal numbers less than about 0.2. This excess low-frequency noise caused measured overall sound pressure levels to vary less rapidly with decreasing jet velocity. Excess noise is a familiar property of jet noise measurements at low exhaust velocities. The data given in references 24 and 26 do not extend below 130 and 123 m/sec (426 and 409 ft/sec), respectively, and do not appear to contain excess noise, in agreement with results of these tests. The spectra measured in these tests at a direction angle 60° from downstream (fig. 12c) have up to 3 dB scatter about the predicted curves. The spectrum shown for 200 m/sec (565 ft/sec) jet velocity is about 4 dB above what would be expected by interpolation of spectra for adjacent velocities and may have been affected by an incorrectly recorded amplifier setting.

RESULTS AND DISCUSSION

Trailing Edge Noise

Presentation of Data. - Typical measured one-third-octave spectra on the airfoil surface and in the far field are shown in figure 13 for the large grid. Trailing edge tabs were not used with the airfoil when used as a nozzle extension; the shortened streamwise extent of open shear layer apparently prevented edge tones at frequencies of interest. Refraction of sound by the shear layer was neglected because the trailing edge was not below the shear layer. The upper spectrum is that measured at the aft microphone 5 cm (2 in.) ahead of the trailing edge on the lower surface scrubbed by turbulent flow generated by the large grid. Approximately the same spectra were measured by all of the microphones on this scrubbed surface. This spectrum shape would be expected to be a composite of grid-generated turbulence at low frequencies, convected at the flow speed and impressed across the boundary layer, and the nozzle wall turbulent boundary layer at high frequencies. Static pressure fluctuations produced by turbulence within the free stream would be expected to have a power spectral density (PSD) that decayed inversely with frequency to the 7/3 power at high frequencies. The corresponding one-third-octave slope of -4 dB per octave is shown to match a portion of these spectra At higher frequencies the spectra tend to level off and then decrease steeply. Here the spectra were dominated by fluctuations of the wall boundary layer. An underestimate of this boundary layer spectrum is provided by the spectra measured at this microphone for the low free-stream turbulence achieved without an upstream grid, also shown in the figures. Such spectra would have slowly increasing PSD at low frequencies (one-third-octave slope somewhat larger than 3 dB per octave) and an apparent rapid decay at high frequencies caused by averaging of pressures over the relatively large sensing area of the transducer. Increased free-stream turbulence would raise the turbulence level within the boundary layer. Thus the actual contribution of the wall boundary layer to pressure fluctuations measured at the surface when an upstream grid was installed was larger than that shown for runs without the grid. The no-grid spectrum thus cannot merely be subtracted from the aft scrubbed surface spectrum to yield the portion of the aft scrubbed spectrum caused by free-stream turbulence.

The next largest spectra shown on these curves are those measured on the aft unscrubbed surface for runs with the large grid. Unlike the spectra measured on the scrubbed surface, these decay at the relatively large rate (PSD varying approximately inversely with frequency cubed, one-third-octave spectra decay 6 dB per octave) expected for trailing edge noise. These measurement positions on scrubbed and unscrubbed surfaces were less than two streamwise integral scale lengths ahead of the trailing edges, but sound pressure levels were 10 to 20 dB apart [illegible] and 20 to 30 dB

apart at high frequencies. Static pressure fluctuations caused by convected turbulence on the scrubbed surface, varying with velocity to the fourth power, always were much larger than the near-field acoustic pressures which varied approximately with velocity to the fifth power. Because of these lower amplitudes and rapid decay with increasing frequency, pressure spectra on the unscrubbed surface decayed into the background noise at high frequencies.

The spectrum measured at the middle microphone on the unscrubbed surface also is shown. This position was 4.5 times further from the trailing edge than was the aft microphone. Spectra for these two positions were similar in shape. Because these microphones were relatively near the trailing edge, one might expect the variation of acoustic intensity with distance to be that for a line source (inverse with radius) rather than that for a point source (inverse with radius squared). Thus a 6.5 dB difference between amplitudes measured at these positions had been expected. The measured difference was about this large at the lowest velocity of 31.5 m/sec (103 ft/sec) but was smaller (about 3 dB) at large velocities.

The lowest spectrum shown is that measured in the far field at a direction 120° from downstream. Far-field data for trailing edge noise were not corrected for background noise because the presence of the plate and absence of nozzle tabs would have altered the background noise. Spectra measured at 90° from downstream, not shown, were about 2 dB smaller at low frequencies. This difference is consistent with the 1.75 dB decrease expected for the angular directivity of trailing edge noise. Values measured at 60° from downstream were about as large as or larger than those 120°, contrary to the expected directivity. These higher levels of uncorrected spectra are believed to arise from collector noise, as was established from cross correlations to be discussed below. The measured far-field spectra generally decreased rapidly with increasing frequency at low frequencies and decreased moderately at middle frequencies. Levels measured at middle and high frequencies with the airfoil and without tabs were about as large as background levels measured without the airfoil but with nozzle tabs.

Spectra measured for the same microphone positions and test velocities but with the medium grid are presented in figure 14. The trends are the same as those discussed for tests with the large grid, but amplitudes at low frequencies are smaller and the spectra are dominated by grid turbulence and trailing-edge noise for a smaller range of frequency.

Cross correlations of measured spectra were utilized to validate the assumed trailing edge noise process. Amplified signals were sent through adjustable matched filters prior to correlation. A high-pass filter was needed to remove a tone at the tunnel fan shaft rotation frequency near 30 Hz; this tone is known to propagate up the diffuser and, of course, produces a well-correlated signal at microphones on the model and in the anechoic chamber.

Filtered cross correlations were obtained for spectra measured at the middle and aft positions on the scrubbed surface at several velocities. At each velocity, measured coherence (cross correlation, normalized by the square root of the product of autocorrelations evaluated at zero time delay) was maximum at a time roughly given by the ratio of separation distance to free-stream velocity. Coherence at fixed axial spacing varied approximately directly with velocity. Also, cross-correlation of microphones on the unscrubbed side gave peaks at delay times corresponding to upstream propagation at the velocity of sound as would be expected for noise from the trailing edge, tunnel collector, or tunnel drive system.

Cross-correlations between the aft scrubbed microphone and the far-field microphone 120° from downstream are shown in figure 15a for 31.5 and 50 m/sec (103 and 164 ft/sec) velocities. Because sound pressure is proportional to the first derivative of surface pressure, the delay time of interest is that for which the coherence is zero and has maximum negative slope between positive and negative peaks (see ref. 27). The zero crossings between maximum-amplitude peaks occurred at roughly the sum of fluid convection time to the trailing edge and acoustic propagation time to the far field, as expected for noise originating near the trailing edge. When this aft scrubbed microphone was cross-correlated with the other far field microphones (not shown), this region of largest positive and negative coherence decreased in amplitude but remained constant in time delay as expected. However, the small region of positive coherence shown in figure 15a for delays of 4 to 5 milliseconds increased in amplitude and shifted to smaller delay times with increasing downstream position and constant radial distance from the trailing edge. These delay times at local maximum coherence correspond approximately to the difference between times required for an acoustic wave to travel from the wind tunnel downstream collector lip to the far field positions and to the surface microphone. That is, both the far field microphones and the airfoil aft scrubbed microphone were detecting drag dipole noise caused by the shear layer striking the collector lip. Delay times for these secondary peaks were approximately unaffected by test section velocity as would be expected for sound waves traveling outside the tunnel airflow until they neared the airfoil trailing edge.

To establish that the pressure fluctuations measured on the unscrubbed side were sound waves generated at the trailing edge by turbulence convected along the scrubbed surface, the aft scrubbed microphone was cross-correlated with the middle unscrubbed microphone. This cross-correlation is shown in figure 15b for 31.5 and 50 m/sec (103 and 164 ft/sec) velocities. At both velocities, the delay time at zero coherence was the sum of the time expected for turbulence to be convected from the aft microphone to the trailing edge at the free-stream velocity and the time expected for a sound wave to travel upstream adjacent to the unscrubbed surface. This result

confirms that the acoustic signal was generated by turbulence convected past the trailing edge. Cross-correlations between other pairs of microphones on the scrubbed and unscrubbed surfaces validated this conclusion.

Autocorrelations (not shown) were smooth damped oscillatory functions that were approximately symmetrical about zero time delay. The autocorrelations of scrubbed-surface microphones had no local irregularity at delay times corresponding to the sum of fluid convection time to the trailing edge and acoustic wave propagation time upstream to the microphone. This absence of a secondary peak would be expected from the measured spectra on scrubbed and unscrubbed surfaces; the acoustic pressure fluctuations were much weaker than the pressure fluctuations of turbulent flow.

Comparison With Theories. - According to the analyses of Ffowcs Williams and Hall (ref. 17) and of Chase (ref. 19), one-third-octave spectra of trailing edge noise should agree when intensity is normalized with respect to velocity to the fifth power and mean square turbulence amplitude. Frequencies should be normalized with respect to transverse turbulence integral scale length and flow velocity. Far-field spectra at the microphone 120° from downstream were normalized in this manner and the resulting adjusted spectra are shown separately in figure 16 for the large and the medium grid. The resulting normalized spectra are coalesced over the test range of a factor of 5.6 in velocity ratio (a factor of 7.5 dB) by use of this fifth-power velocity law. The high-frequency portion of the spectrum at the highest test velocity was in worst agreement with this adjustment. For the medium grid, this portion of the data followed a sixth-power velocity law and had a smaller frequency decay as with wind tunnel background noise.

According to Hayden's analysis (ref. 15), one-third-octave spectra of trailing edge noise should agree when intensity is normalized with respect to velocity to the sixth power. Turbulence level does not enter directly into the prediction method, but its effect is implied by the need to choose one of three flow regions for which empirical curves are given. The tests described herein had a uniform potential core along the model span and for considerable distance normal to the surface so they should correspond to Hayden's potential core regime. Other flows, denoted the characteristic decay and radial decay regions, had relatively thicker mixing regions and presumably larger turbulence levels. The adjustment parameter of reference 15 for standard atmospheric density and speed of sound was modified to apply for velocities measured in m/sec rather than ft/sec, and the resulting prediction curves for the extreme cases of the potential core region and radial decay regions are shown in figure 17. Also shown in this figure are the spectra previously used in figure 16 but plotted according to this other adjustment parameter. The spectra measured for different velocities are spread out between the two prediction curves and also fall below the lower curve. Clearly, this parameter does not coalesce the data of this investigation.

The data bands for the two sets of data in figure 16 are overlaid in figure 18 to form a final comparison of adjusted measured trailing edge noise spectra for uniform velocity and turbulence. The results agree well for low reduced frequency where the data were dominated by trailing edge noise. They differ for the two different grids at Strouhal numbers above 0.2 (not shown) where the spectra were dominated by background noise. Thus the parameters derived by Ffowcs Williams and Hall in reference 17 are validated by these data.

While trying to compare the empirical prediction curve from figure 6 of reference 15 for the potential core regime with these data, it was noted in figure IV.15(a) of reference 21 that five of the seven spectra used in that comparison were obtained at velocities between approximately 61 and 64 m/sec (200 and 209 ft/sec). The empirical curve of reference 15 was then assumed to be valid for the 63.4 m/sec (208 ft/sec) velocity of two reference 21 test spectra and was scaled using the scaling laws of reference 17. The turbulence scale length was arbitrarily taken equal to the wall-jet boundary layer thickness. As shown in figure 18, the resulting average far field spectrum from the data of reference 21 would agree with these data if a 2% turbulence level is assumed for those tests.

In principle, it should be possible to compute this normalized spectrum from the analysis within Section VI of reference 19. The wavevector representation of the inertial subrange of homogeneous turbulence requires so many details about the turbulence structure that even the data comparisons given therein examined only the trends at large and small reduced frequencies. Power spectral density (PSD) is predicted from equation (41) of reference 19 to decay inversely with frequency to the 10/3 power at large frequencies. One-third-octave spectra would then be expected to decay 7 dB per octave, which is significantly larger than the 3 to 4 dB per octave decay rates associated with jet mixing noise. The data of figure 16 had this higher decay rate at Strouhal numbers up to 0.016 where the scatter was fairly small. At large Strouhal numbers the spectrum decay rate decreased to about 4 dB per octave and the high-velocity spectra systematically shifted above those measured at the lower velocities. These same trends are apparent in other correlated spectra plotted in figure 4 of reference 19. Somewhat smaller decay rates are given by the revised analysis in reference 20. The curve obtained from the data of reference 21 for 63 m/sec (208 ft/sec) velocity approximately follows the predicted steep decay. In the limit of low frequency, the spectrum calculated from reference 19 had a steep increase with increasing velocity (PSD roughly proportional to frequency to the fifth power) as with the data comparison in figure 4 of reference 19. The spectra from the tests described herein are approximately flat near the low-frequency limit of the chamber. From equations (36) and (42b) of reference 19, PSD of both the turbulence spectrum and the radiated sound should be independent of frequency in the limit of very small reduced frequencies. The trend of a

steep increase with increasing frequency, however, seems established by the majority of data. Additional discussion of low-frequency predicted and measured behavior is given in reference 20.

These adjusted spectra can be integrated over all Strouhal numbers to obtain a predicted overall sound pressure level. This quantity can be compared with that calculated from equation (15) of reference 17 for a turbulent eddy at a sharp trailing edge. If that equation is correct, the difference between the two quantities would be a measure of the number of eddies along the trailing edge at one time. The integrated OASPL corresponds to an adjustment parameter of about 63.5. That quantity would be given by roughly seven eddies, while twenty-eight would be expected if turbulent eddies were regarded as hard ellipsoids with a semi-minor axis equal to the transverse integral scale length. Thus the number of noise-producing eddies is one-fourth the maximum that could be stacked side-by-side in the simplified viewpoint of turbulent eddies as rigid objects.

Because these data clearly agreed with a fifth power velocity law and disagreed with a sixth power law, the tests on which the sixth power law was based were examined. The dimensional analysis in which trailing-edge noise was claimed to vary with velocity to the sixth power, and presentation of data to justify the analysis, was first given by Hayden in reference 21. The data were obtained with a slot nozzle that was tangent to a flat plate of adjustable length. Data were presented for three different regimes of wall-jet flow. In the core region, the plate length was sufficiently short so that a potential-flow core existed within the jet at the trailing edge. Adjusted acoustic spectra for this regime were given in figure IV.15(a) of reference 21 for four ratios of plate length to nozzle height at approximately constant velocity and three velocities at constant plate length. The spectra for different velocities, normalized in a manner based on assumed sixth-power velocity dependence, are reproduced in the upper part of figure 19 herein. If a fifth power velocity law were correct, the adjusted sound pressure levels should be increased by 10 $\log_{10} U/a_o$ at constant Strouhal number. Spectra modified in this manner are shown in the lower part of the figure. The low-frequency portion of these spectra (Strouhal numbers less than 0.1) is better fitted by a sixth-power velocity law, and about 4 dB spread of the data is obtained for both adjustments in the high-frequency portion.

In the characteristic decay region, there was no potential core in which the mean velocity was independent of distance normal to the plate but there was a central spanwise region in which the mean velocity profile was independent of lateral position. Adjusted spectra were given in figure IV.15(b) of reference 21 for eleven combinations of velocity and plate length. The approximately 6 dB spread of these measured spectra would not be significantly changed if a fifth-power rather than a sixth-power velocity law was assumed. At still larger plate lengths, the radial region is reached in which

mean flow properties vary laterally within the jet. Adjusted spectra for five velocities at one plate length and two velocities at another length were given in figure IV.15(c) of reference 21 for this regime. The data for five velocities at constant plate length are reproduced in the upper part of figure 20 herein. These spectra, modified for a fifth-power rather than a sixth-power velocity law, are plotted in the lower part of the figure. It can be seen that adjusting these spectra by a fifth-power velocity law approximately halves the 6 dB scatter. Thus, if attention is concentrated on large Strouhal numbers which have strong effects on perceived noise level, Hayden's data are in better agreement with a fifth-power velocity law in one flow regime and agree equally well with either a fifth or sixth power in the other two regimes.

Incidence Fluctuation Noise

Presentation of Data. - Typical far-field one-third-octave spectra radiated by the flat plate airfoil with incident turbulence generated by the large grid are plotted in figure 21 for 50 and 125 m/sec (164 and 410 ft/sec) velocities. Also shown are spectra for several conditions that represent possible reference background noise levels. All these spectra were measured at 90° from the free-stream direction. Sound pressure levels measured with the airfoil and grid were largest at a relatively low frequency, decreased rapidly with increasing frequency, and decreased less rapidly with further increase of frequency. Sound pressure levels measured with the grid but without the airfoil decreased rapidly and then became approximately constant with increasing frequency. It is apparent that the presence of the airfoil did not significantly change the high-frequency part of the spectrum, and at high velocities the low-frequency spectrum, from that measured with the grid alone. Other spectra shown are those for the airfoil without an upstream turbulence grid and therefore in a flow with less than 0.2% turbulence level and those for the empty tunnel with neither an airfoil nor a turbulence grid. These spectra were below those measured for the tunnel plus grid. Without a grid, the presence of the airfoil caused little or no increase of far-field noise.

Spectra measured with the airfoil and large grid, and a microphone direction 60° from upstream, generally were one to two dB lower than those at 90°. This small difference would be expected for noise having lift dipole directivity, for which a 1.25 dB decrease is predicted. Those measured at a microphone direction 120° from upstream tended to be about as large as at 90°, possibly because of the larger background noise in this direction and the expected refraction effect of the wind tunnel shear layer on measured directivity. Refraction of sound by the wind tunnel shear layer was calculated for the measurement directions, test Mach numbers, and lift dipole directivity to be less than 1 dB. Calculated refraction effects for a lift dipole are shown in figure 8 of reference 22.

Before the measured far-field spectra could be used for evaluation of different theories, it was necessary to subtract the background noise of the tunnel with grid. Only those portions of the measured spectra which exceeded background by at least 3 dB were used. The background noise was subtracted logarithmically to obtain corrected spectra for the airfoil with incidence fluctuation but without the low-frequency or high-frequency noise of the wind tunnel with the turbulence grid. These spectra for 90° direction are presented in figures 22 and 23 for the medium and large grid, respectively.

Uncorrected overall sound pressure levels for 90° direction angle and the frequency range from 200 Hz to 20 kHz are plotted against velocity in figure 24. Data are presented for the large grid, medium grid, and no turbulence grid, with and without the airfoil. Airfoil OASPL was increased about 3 dB by changing from the medium to the large grid at constant velocity, in good agreement with the 3.5 dB increase expected if acoustic intensity is proportional to turbulence level squared. They increased with velocity to the 5.6 power, in agreement with the expected variation with free-stream velocity to the sixth power and turbulence level squared (turbulence level varied with velocity to the -0.2 power for these upstream grids). In contrast, background noise measured with the grids and without the airfoil was found to vary approximately with velocity to the sixth power. Background noise of the tunnel without an upstream grid was increased about one dB by the presence of the airfoil. This relatively large (about 1/4 sq m) airfoil apparently generated little or no noise by itself. Its lowest test Reynolds number of about one million was greater than that for which the boundary layer would be expected to stay laminar to the trailing edge, so airfoil discrete tone vortex noise (ref. 28) was not expected. Airfoil OASPL calculated for different noise mechanisms listed in reference 1 are also shown in figure 24. Sound radiation from an airfoil surface boundary layer that is turbulent from the leading edge was calculated from equation (11) of reference 1 to be about 15 dB below background. Sound radiation caused by 0.2% incident turbulence level was calculated from equation (8) of reference 1 to be about 10 dB below background. Vortex shedding noise as defined in reference 1 and calculated from equation (9) therein was unexpectedly in good agreement with OASPL measured for the airfoil without an upstream grid. However, the sum of this calculated noise and the tunnel-empty background noise would overestimate levels measured for this airfoil. The far field spectra did not peak at a Strouhal number of 2 referenced to airfoil chord as assumed in reference 1. Measured spectra for the tunnel plus airfoil, and background noise for the tunnel without airfoil, were not given in reference 1. It is possible that the equation given in reference 1 for vortex noise of an airfoil was actually fitted to background noise of the open-jet wind tunnel. This good agreement between calculated OASPL for the airfoil alone and measured OASPL for the airfoil plus background noise would then result from use of comparable ratios of model size to tunnel size.

Surface pressure spectra measured by the three upper-surface and three lower-surface microphones at the five test velocities are given in figure 25 for incident turbulence produced by the medium grid. Surface pressure spectra for the same positions and velocities but for the large grid are given in figure 26. Because upper-surface and lower-surface microphones were located at slightly different spanwise locations, it would not have been proper to subtract the microphone output signals to obtain spectra of local loading. The surface pressure spectra contain a sum of pressure fluctuations caused by incidence fluctuation and, at high frequencies, the static pressure spectrum of the airfoil turbulent boundary layer.

Cross-correlations between upper surface microphones and the far-field microphone directly above the airfoil model are shown in figure 27 for 31.5 and 80 m/sec (103 and 262 ft/sec) velocities. These signals were filtered to cut off signals at frequencies lower than 100 and greater than 20,000 Hz. All of these traces passed through zero amplitude with maximum negative slope at approximately identical delay times. This delay time was equal to the expected time required for a sound wave to travel from the model to the far field. These data thus confirm the expectation (ref. 27) that noise caused by incident turbulence is radiated from all positions along the airfoil chord. Coherence between the surface and far field microphones was relatively large at the airfoil forward position and decreased with increasing distance from the leading edge. This would be expected because local loading due to incidence fluctuation would decrease with increasing chordwise distance while static pressure fluctuations within the airfoil boundary layer would increase or remain constant.

Cross-correlations between microphones at the same position on upper and lower surfaces were symmetrical about zero delay time and had a large negative peak at zero time. The negative peak denotes signals that are antisymmetric on the upper and lower surface as is expected for loading fluctuations. Coherence of these signals decreased with increasing distance from the leading edge. It was decreased somewhat by changing from the large to the medium grid and was approximately independent of airspeed. Cross-correlations between microphones at different chordwise positions on the same surface generally had three positive peaks. One was at a very small delay time that corresponded to downstream propagation of an acoustic wave and represented adjustment of surface loading to the incident convected turbulence. Another had a delay time equal to the ratio of streamwise separation to free-stream velocity and represented convection of free-stream turbulence. The third had a delay time somewhat less than twice that for the second peak and probably represented convection of turbulence within the airfoil boundary layer.

Comparisons With Theories. - Variations of measured surface pressure spectra with velocity, turbulence level, and chordwise position were correlated by a procedure chosen for ease in preparing summary plots. Power

spectral density of surface pressure fluctuations can be written as the product of dynamic pressure squared, the square of the derivative of pressure coefficient with respect to incidence, and the power spectral density of incident turbulence. Expressing the surface pressure spectra in terms of the one-third-octave surface pressure level (SPL_S),

$$SPL_S - 10\log_{10}(0.232\,f) = 20\log_{10}(1/2\,\rho U^2/P_{ref}) + 20\log_{10} C_{p_\alpha} + 10\log_{10}(E/U^2) \qquad (22)$$

which can be rearranged as

$$SPL_S - 20\log_{10}\left(1/2\,\rho U^2/P_{ref}\right) - 10\log_{10}\left(\overline{v^2}/U^2\right) - 10\log_{10}(0.232\,\Lambda/c)$$
$$= 10\log_{10}\overline{C_{p_\alpha}^2} + 10\log_{10}(fc/U) + 10\log_{10}\left(UE/\overline{v^2}\,\Lambda\right) \qquad (23)$$

The left-hand side of equation (23) is a sum of a measured function of frequency and a function of velocity and grid size. The normalized turbulence spectrum on the right-hand side of the equation is a measured quantity that had been found to be well approximated by equation (21), an analytic function of reduced frequency based on turbulence integral scale length. Thus the right-hand side is the sum of functions of Strouhal number plus a loading coefficient that is expected to depend on chordwise position, Strouhal number, and Mach number. The left-hand side of the equation was determined from measured one-third-octave spectra by shifting the amplitudes by a function of velocity and grid size but not of frequency, and renumbering the frequency axis as a one-third-octave scale of Strouhal number. Spectra measured at successive velocities could then be overlaid by shifting the frequencies by two (or, for the highest velocity, $1\frac{1}{2}$) one-third-octave bands. The purpose of this procedure was to allow spectra measured at the same chordwise position but different turbulence levels to be overlaid and traced without further manipulation.

This measured comparison can then be compared with curves of the right-hand side of equation (23) as calculated using different theories for the derivative of pressure coefficient with respect to loading. Results are given in figure 28 for the upper- and lower-surface microphones at forward and mid-chord positions and incident turbulence produced by the medium and large grids. Surface pressure spectra were measured with the large grid and the three lower velocities (figs. 28(c) and (d)) at frequencies down to 10 Hz for comparison with theories over a larger range of Strouhal number. Spectra measured at corresponding positions on the upper and lower surface of this

symmetrical model often differed by several dB for unknown reasons. At constant microphone position and turbulence grid, spectra measured at velocities from 31.5 to 125 m/sec (103 to 410 ft/sec) coalesced within better than 3 dB over most of the range of Strouhal number. However, data for the highest and lowest of these velocities generally defined the upper and lower edge, respectively, of this band. Data for the highest test velocity of 177 m/sec (580 ft/sec, Mach number of 0.535) were significantly larger in amplitude and, for the forward microphone, different in shape. The cylinder-slab leading edge shape probably generated too strong an adverse pressure gradient downstream of the discontinuity of curvature, locally separating the boundary layer. The spectra are typified by an increase of about 3 dB per octave at low Strouhal numbers, a decrease of less than 6 dB per octave at moderate Strouhal numbers, and a second peak followed by rapid decay at high Strouhal numbers. This high-frequency part of the spectra is attributed to the airfoil surface turbulent boundary layer. From the right-hand side of equation (23) and the known shape of the incident turbulence spectrum, the derivative of unsteady pressure coefficient with respect to angle of incidence can be inferred. It must have been approximately constant for Strouhal numbers up to unity and decayed at the slope predicted for the Sears function at Strouhal numbers above four.

The curves shown were calculated from Sears theory (eq. (4) herein) and by arbitrary application of analytical results presented by Filotas (eqs. (7) and (9) herein) and Mugridge (eq. (17) of ref. 8). Filotas' equation for lift response at high frequencies was adjusted as described in the section, "ANALYTICAL METHODS". All of these calculated results have the same asymptotic slopes in the limits of very small or very large Strouhal numbers. The low-frequency approximation of Filotas yields a derivative of unsteady pressure coefficient with respect to incidence that is independent of Strouhal number for Strouhal numbers less than π^{-1} times the ratio of half-chord to turbulence streamwise integral scale length. The resulting calculated loading is in better agreement with the data than is the Mugridge solution at low Strouhal numbers. Those two solutions differ by little more than 2 dB at large Strouhal numbers and generally agree with the data at those conditions. Agreement between predictions and data is best at mid-chord, where distortion in shape of the chordwise loading is predicted in reference 7 to be least. Measured loading at the forward microphone position was overestimated by the procedure used herein that neglected this distortion.

Far field acoustic pressures caused by incidence fluctuation were expressed in equation (13) in terms of turbulence PSD and the effective Sears function for lift response of an acoustic compact source. If acoustic pressures are expressed as one-third-octave SPL, that equation can be rewritten as

$$SPL_{1/3} - 10 \log_{10}\left(\overline{v^2}/U^2\right) - 10 \log_{10}(0.232\,\Lambda/c) - 20 \log_{10}\left(\frac{\pi}{2}\,\frac{\rho U^3}{aP_{ref}}\,\frac{b\cos\theta}{r}\right)$$

$$= 10 \log_{10}\,\overline{S_F^2} + 10 \log_{10}\left(UE/\overline{v^2}\,\Lambda\right) + 30 \log_{10}(fc/U) \qquad (24)$$

Here the left-hand side consists of the measured spectrum and terms that are functions of free-stream velocity, turbulence mean properties, model geometry, and microphone location. The right-hand side is a sum of terms that are functions of Strouhal number. Thus the left-hand side was determined by over-laying measured one-third-octave spectra with approximately shifted amplitude and frequency axis. The right-hand side was calculated using different analytical solutions for effective Sears function in three-dimensional turbulence. Analytical methods used were conventional Sears theory for two-dimensional turbulence, the solution of Mugridge (eq. (3) of ref. 8), and the solution by Filotas (ref. 7). Lift response in turbulence had been calculated by Filotas only for a narrow strip at constant spanwise position. However, the calculated decay rate is steeper than that given by Mugridge (ref. 8) for either a two-dimensional airfoil or a three-dimensional rectangular wing in three-dimensional turbulence.

Predicted far-field one-third-octave spectra calculated from the right-hand side of equation (24) are given in figure 29. Spectra calculated by the theories of Sears and Mugridge increase to a constant asymptote with increasing Strouhal number. The method of Filotas for a narrow two-dimensional strip gives a high-frequency decay inverse with frequency. Measured spectra are shown for the far-field microphone directly above the airfoil, medium turbulence grid, and 31.5, 80, and 177 m/sec (103, 262, and 580 ft/sec) velocities. The measured spectra for different velocities clearly were not coalesced by this set of parameters. Low-frequency data approximately agreed with spectra calculated by the theories of Mugridge and Filotas. As velocity was increased, the Strouhal number above which the predictions and data disagree was decreased. Spectra measured at large Strouhal numbers decreased roughly inversely with frequency cubed. This behavior is typical of that for a noncompact acoustic source.

Exact solutions for the change in far-field acoustic radiation as the acoustic source changes from compact to noncompact are not available. A qualitative solution proposed by Hayden (ref. 15) utilized a reduced frequency based on the speed of sound and an undefined effective radius of the source. Assuming that the source radius is proportional to airfoil chord, the appropriate frequency parameter for a noncompact source should then be the

product of Strouhal number and Mach number. However, because the onset of chordwise phase cancellation depends on Strouhal number alone, spectra measured at different velocities cannot be directly compared.

Measured and calculated far-field one-third-octave spectra are compared in figure 30 for each of the five test velocities. The envelope of measured spectra is shown for microphone positions 60 and 90° from upstream and both turbulence levels. The top of this envelope at low frequencies always was set by the 90° microphone at the highest turbulence level; scatter between the other three combinations of microphone position and turbulence level at low frequencies was about equal to that shown for all four at high frequencies. The curves shown for the combined predictions of Filotas and Hayden were calculated by arbitrarily taking the source radius as one-half the chord. At the lower velocities, rapid decay due to acoustic noncompactness was predicted by Hayden's equation to start at about the same frequency as rapid decay due to spanwise phase cancellation. Measured spectra decayed roughly at about 9 dB per octave as predicted for the combination of effects. As velocity was increased, decay of the measured spectra due to noncompactness continued to occur at products of Strouhal number and Mach number larger than about 0.5. However, the calculated incompressible-flow lift force response was still increasing with increasing value of this product. Thus the calculated and measured spectra became less sharply peaked as velocity was increased.

It should be noted that because the lift force spectrum was not measured, the acoustic noncompactness correction is not clearly identified. An alternate explanation might apply the same correction factor to calculation of lift force. This additional phase cancellation of surface pressure spectra would reduce the lift force spectrum at products of Mach number and Strouhal number greater than about 0.8. Such behavior was qualitatively predicted by Adamczyk (ref. 12) for gust response in subsonic compressible flow; the analysis had not been extended to incident turbulence. The resulting compressible-flow lift force response spectrum, regarded as producing an acoustically compact dipole, would yield the far-field spectrum attributed here to an incompressible-flow lift spectrum and noncompact source. This alternate viewpoint avoids the problem of explaining why acoustic noncompactness should occur for an overhead far-field point, and why it was the same for directions 60° and 90° from upstream.

If the solution of Mugridge had been modified in the same manner as that of Filotas to include a crude approximation for spanwise phase cancellation plus Hayden's factor for a noncompact source, it would have given equally good agreement with the measured spectra. Spectra calculated by the methods of Filotas and Mugridge would differ significantly only for low Strouhal numbers, at which the theory of Mugridge would predict stronger noise. Far-field data were not obtained at those conditions because the anechoic chamber is not

anechoic at low frequencies. Howeve., surface pressure spectra measured at those low frequencies were better predicted by the theory of Filotas. That theory plus Hayden's modification therefore give best agreement with both surface and far-field pressure spectra.

Subsonic Mach number effects can be found in other measurements of noise from airfoils in turbulent flow. Tests reported by Dean (ref. 5) had included measurements of upstream turbulence spectra, loading spectra at the airfoil quarter-chord, and far-field acoustic pressure spectra. The ratio L of turbulence integral scale length to airfoil half-chord was about 0.8 in those tests. That is, the turbulence scale was about three times larger relative to chord than for the tests reported herein. As with these tests, the local loading spectrum was adequately predicted by the theories of Mugridge and Filotas. Fluctuating lift force was assumed given by the product of local loading and a correlation area. The far-field spectra and compact-source acoustic dipole equation were then utilized to calculate the ratio of correlation area to planform area. The variation of this quantity with Strouhal number, taken from figure 14 of reference 5, is shown in figure 31 for the four test velocities from 55 to 175 m/sec (180 to 575 ft/sec). From the analysis developed herein, this effective correlation area is really a combination of chordwise phase cancellation and Hayden's compressibility effect. Curves calculated for these two processes, again using a correlation radius of half the chord, are also shown in figure 31. Data for the lowest velocity were bracketed by the calculated curves for spanwise phase cancellation with and without the noncompact source effect. The decay of effective Strouhal number was somewhat overestimated, but within about 4 dB this otherwise unexplained correction factor between data and dipole noise theory is predicted by the recommended calculation method.

Scrubbing Noise

General Comparison of Far Field Acoustic Data. - The dominant type of noise radiated beneath under-the-wing (UTW) externally blown flaps has often been called scrubbing noise. For highly deflected flaps, its directivity resembles that of a lift dipole oriented perpendicular to the deflected flap panels. Intensity of scrubbing noise varies approximately with local jet velocity to the sixth power. Its power spectral density decays almost inversely with frequency squared at large Strouhal numbers. This noise process as considered herein does not include quadrupole noise from deflected distorted portions of the exhaust jet, sometimes called impingement or impact noise. In contrast to scrubbing noise, this noise is strongest at moderate angles (less thn 40°) from the deflected exhaust and has an intensity that varies with exhaust velocity to the eighth or larger power.

The airfoil model used in the present study differed from conventional externally blown flaps because it was a single deflected airfoil rather than a multiple slotted flap having separately deflected flap panels. Therefore, far field acoustic spectra were compared with NASA data of reference 24 for a double slotted UTW blown flap model to assure that results were representative of UTW noise. The two models had about the same nozzle diameter but the single airfoil had about 71% as large a chord. Because the NASA tests used a 3.28 m (10 ft) microphone distance and these tests used a 2.3 m (7 ft) distance, tabulated NASA data were increased 3 dB for this comparison.

One-third-octave spectra measured at 90° to the nozzle centerline, in the direction beneath a UTW model, are shown in figure 32 for zero airfoil deflection at 200 and 250 m/sec (656 and 820 ft/sec) exhaust velocities. The circle symbols are the average of NASA data shown in reference 24 for 80° and 100° from the nozzle centerline, flaps retracted, and the closest velocities to these conditions (Runs 94 and 93). Those data, taken at 190 and 231 m/sec (623 and 758 ft/sec), were increased 1.3 and 2.1 dB, respectively, to compensate for the differences in exhaust velocity assuming a sixth-power velocity scaling law as reported in reference 24. Except for the region of low frequencies in which the data of reference 24 were affected by ground reflections, the two sets of data are in good agreement.

One-third-octave spectra for the UTW configuration at 30° airfoil deflection, 200 m/sec exhaust velocity, and directions perpendicular to the deflected chord (60° from upstream) and perpendicular to the nozzle centerline are shown in figure 33. These are compared with data for Runs 56 and 100 of reference 24 for those directions and 190 and 194 m/sec (623 and 636 ft/sec) velocities, at 10° - 20° deflection of the double slotted flaps. Because these deflections were taken relative to a chord line with 5° incidence from the nozzle, the aft flap segment was deflected 25° relative to the nozzle centerline. The spectra for the single airfoil are in general agreement with the two sets of NASA data. Externally blown flap noise measured with the deflected single airfoil therefore is in both qualitative and quantitative agreement with data for an airfoil having double slotted flaps. Thus the noise mechanisms which occur for the deflected single airfoil should be the same as those for more complicated, less easily instrumented airfoils having deflected flaps.

An indication of one noise mechanism that causes a difference between far-field spectra of UTW and upper surface blowing (USB) installations can be obtained by comparing spectra measured in the scrubbed and unscrubbed directions at zero airfoil deflection. These spectra and those for the nozzle alone are presented in figure 34 for 160 and 250 m/sec (525 and 820 ft/sec) velocity at direction angles 60, 90, and 120° from upstream. Spectra measured in the far field on the scrubbed side of the airfoil decayed less

rapidly with increasing frequency than did spectra measured on the unscrubbed side. It seemed likely that this difference of decay rates could be explained by the presence of direct and reflected jet noise on one side of the airfoil and shielding of that noise from the other side. To test this assumption, one-third-octave levels were calculated as the sum of measured sound from the unscrubbed side, measured directly radiated sound from the nozzle alone, and reflection of nozzle sound by the airfoil. Reflection was arbitrarily assumed to double the acoustic intensity at 60° and 90° but to have no effect at 120° direction. The resulting spectra, shown as circle symbols in figure 34, are in close agreement with those measured in the direction of the scrubbed side. In these directions, one-third-octave spectra for the airfoil had a relatively sharp peak at Strouhal numbers of 0.20 to 0.25 while nozzle jet noise spectra had a more gradual maximum which peaked at Strouhal numbers closer to 1.0. As discussed later, reflection effects apparently were absent at the direction 120° from upstream because the spectrum on the unscrubbed side already contained some jet noise. The two exhaust velocities for which this comparison is shown correspond to Mach numbers near 0.5 and 0.8. These bracket the value of 0.608 at which a significant change has been predicted to occur (ref. 29) in the instability modes of an isolated cold axisymmetric jet. Apparently, any change of airfoil noise caused by changes in jet instability structure did not alter the radiated directivity pattern. Adding the direct and reflected jet noise to far-field noise measured in the unscrubbed direction yielded a close prediction of measured spectrum in the scrubbed direction. This result would not be valid for large deflection angles where quadrupole noise generated in the shear layer downstream of the airfoil trailing edge may be significant relative to quadrupole noise of the isolated jet.

A previous analysis (ref. 30) had assumed that scrubbing noise was produced by locally correlated turbulent regions on each scrubbed surface. Pressure fluctuations generated in the jet mixing region and imposed on the surface were assumed to produce dipole noise as in Sharland's (ref. 1) analysis of turbulent boundary layer dipole noise. Because pressure fluctuations in a jet mixing region are an order of magnitude larger than those in a turbulent boundary layer, calculated OASPL was about 20 dB larger than that calculated from reference 1 for boundary layer noise. If that description of the scrubbing noise mechanism was correct, scrubbing noise would be radiated only from the scrubbed side of an airfoil. In contrast, if scrubbing noise is associated with a fluctuation of local loading, its directivity would be the same on both the scrubbed and unscrubbed sides. The data of figure 34 clearly demonstrate that scrubbing noise is symmetrical about the airfoil chord. They disprove a fundamental assumption of the scrubbing noise analysis given in reference 30.

If changes of jet instability mode cause changes in EBF noise mechanisms, then suitability normalized spectra obtained at different Mach numbers should not coalesce. One-third-octave frequencies can be readily normalized as Strouhal numbers. However, if several noise mechanisms each have different velocity dependence, then no one correction to one-third-octave SPL should be valid for all Strouhal numbers. A sixth-power velocity dependence was arbitrarily assumed because OASPL of externally blown flaps is empirically found (e.g., ref. 24) to vary approximately in this manner. Thus any portion of the spectrum dominated by trailing edge noise, which should vary with velocity to the fifth power, would be overcorrected. A normalized spectrum for the highest velocity would be smallest, and that for the lowest velocity would be highest, by a predictable increment. Similarly, portions of the spectrum dominated by quadrupole noise should vary with velocity to the eighth power and would be undercorrected.

Amplitudes were normalized by subtracting $60 \log_{10} U$, where U is the jet exhaust velocity (m/sec), from spectra measured at 100, 160, and 250 m/sec (328, 525, and 820 ft/sec) velocity. Thus, successive one-third-octave spectra were decreased 12 dB in amplitude and two one-third-octave bands. The resulting velocity-adjusted far field spectra at directions 60, 90, and 120° from upstream are presented in figure 35 for six combinations of deflection angle and measurement direction. Straight lines showing 10 dB per octave increase of amplitude at low Strouhal numbers, 7 dB per octave decrease at moderate Strouhal numbers, and 4 dB per octave decrease at high Strouhal numbers are included as guides to observed trends. The larger decrease is typical of trailing edge noise; the smaller decrease is typical of jet exhaust noise and of UTW EBF spectra denoted as scrubbing noise.

Far field spectra in the scrubbed direction at zero deflection are shown in figure 35(a). The 10 dB per octave increase, which corresponds to a pressure-squared spectral density proportional to frequency to the 7/3 power, gives a good approximation to the slope for Strouhal numbers less than 0.16. At Strouhal numbers less than about one, the data decrease at about 7 dB per octave and, at constant Strouhal number, decrease with increasing velocity. The approximate 4 dB spread between spectra for the largest and smallest velocities corresponds to a fifth power velocity dependence. Thus the velocity dependence, spectrum slope, and directivity (least intensity in the most downstream direction) are consistent with trailing edge noise at Strouhal numbers up to about one. At larger Strouhal numbers, and at Strouhal numbers down to about 0.4 for the higher velocities, the spectra decayed at about 4 dB per octave as would be expected for both scrubbing noise and jet mixing noise. Because the spectra are coalesced by this sixth power velocity adjustment at forward angles but are spread apart at the aft direction angle, the high-frequency portion is dominated by scrubbing noise in forward directions and jet mixing noise in aft directions.

Velocity-adjusted far field spectra in the unscrubbed direction at zero deflection are shown in figure 35(b). As with the comparison in the scrubbed direction, spectrum slopes and variations of amplitude with velocity are consistent with dominant trailing edge noise for Strouhal numbers less than unity and forward direction angles. Spectra for larger Strouhal numbers and the aft direction decreased at about 4 dB per octave at levels roughly 4 dB larger at 250 m/sec (820 ft/sec) than at 160 m/sec (525 ft/sec) velocity. Those parts of the spectra therefore were dominated by jet mixing noise. The apparent discrepancy between calculation of high-frequency noise on the scrubbed side by use of jet noise with reflection for other directions but without reflection for this direction is then resolved. Noise on the unscrubbed side, in aft directions, already includes a quadrupole jet contribution at large Strouhal numbers.

Spectra taken in the unscrubbed direction correspond to data beneath an USB installation. Velocity-adjusted data for the unscrubbed direction and 10° deflection are shown in figure 35(c). A tone was present in spectra for this airfoil and nozzle at the higher test velocities and greater than about 3° deflection. The region of Strouhal numbers that could be characterized by 7 dB per octave decay was smaller for this deflection than for zero deflection. There was little effect of USB deflection on the portions of these spectra having Strouhal numbers less than about 0.2, but increased deflection increased the amplitudes at larger Strouhal numbers.

Velocity-adjusted spectra beneath the scrubbed side for 9, 18, and 30° UTW deflections are shown in figures 35(d), (e), and (f). Increasing deflection caused a gradual increase of velocity-adjusted sound pressure level at constant Strouhal number and a decrease in the importance of trailing edge noise relative to scrubbing noise. For 30° deflection (fig. 35(f)), spectra for the direction 60° from upstream (normal to the airfoil chord) and Strouhal numbers greater than 0.8 were coalesced by subtracting sixty times the logarithm of exhaust velocity. This portion of the data therefore varied with exhaust velocity to the sixth power as expected for scrubbing noise from a surface which does not extend beyond the jet potential core. For the same direction but smaller Strouhal numbers, each increase of velocity by a factor of $2^{2/3}$ caused about a 2 dB decrease in amplitude. This systematic effect of velocity corresponds to a fifth power velocity dependence as expected for trailing edge noise. At a measurement direction 120° from upstream and large Strouhal numbers, each increase of velocity caused roughly a 4 dB increase of amplitude as for eighth power jet mixing noise. Both scrubbing noise and trailing edge noise seem to have the same 10 dB per octave frequency dependence at low Strouhal numbers, and both scrubbing noise and jet mixing noise seem to have the same -4 dB per octave frequency dependence at high Strouhal numbers.

Surface Pressure Spectra. - Surface pressure spectra on the scrubbed airfoil surface are of interest for possible improved understanding of the noise radiation mechanisms and as direct input for estimating sonic fatigue of wing panels. Spectra measured at different chordwise positions along the flow plane of symmetry are examined first, followed by examination of the effects of spanwise distance.

Velocity-adjusted spectra measured at 15% and 30% chord on the plane of symmetry, for 125 and 250 m/sec (410 and 820 ft/sec) exhaust velocity, are shown in figure 36(a) for zero airfoil deflection. Amplitudes of these one-third-octave spectra were normalized by assuming a dependence on exhaust velocity to the fourth power, and frequencies were normalized as Strouhal numbers. Surface spectra for these velocities differing by a factor of 2 were in good agreement when compared in this manner. Amplitudes of adjusted overall surface pressure level also are shown. The largest rms pressure fluctuation within the mixing region of an isolated jet (ref. 23) is about 0.065 times the jet dynamic pressure. This maximum fluctuation for a jet without an airfoil corresponds to an adjusted overall level of about 66 dB. Thus the measured adjusted overall level of about 54 dB at 15% chord is an rms pressure fluctuation of one-fourth the maximum expected for an isolated jet. As shown in figure 7(b), this level would be a reasonable estimate of the pressure fluctuation at this measurement position within an isolated jet. The level of just less than 60 dB at 30% chord would be about half the jet maximum rms fluctuation, while a somewhat larger fluctuation is expected for this location in an undistorted isolated jet. Adjusted spectra for these two velocities and zero deflection are shown in figure 36(b) for 38, 62, 70, and 80% chord. Adjustment for the effect of exhaust velocity remains good, and adjusted overall levels were between one-fourth and one-half the maximum pressure fluctuation expected for an isolated jet. Overall level therefore seemed to be generated by the jet process and impressed upon the airfoil surface, rather than being generated by aeroacoustic interaction of the exhaust jet with the airfoil.

A distinctive feature of these spectra was the decrease of peak Strouhal number with increasing rearward distance. Maximum amplitude occurred at a Strouhal number of 1.6 at the forward positions, near 0.4 at positions near mid-chord, and near 0.2 at the aft positions. This behavior also occurs for pressure fluctuation spectra measured in the mixing region of an isolated jet, as shown in figures 14 through 17 of reference 31. An attempt to predict scrubbing noise by assuming that it was generated by coherent regions of jet mixing region turbulence (ref. 30) had assumed that surface pressure spectrum shape was independent of chordwise position. These surface data, in addition to the far-field acoustic data, prove that the explanation of scrubbing noise given in reference 30 is wrong.

Velocity-adjusted surface pressure spectra for 9° deflection are given in figures 36(c) and (d). At this deflection, much of the airfoil aft surface in the plane of symmetry was at a distance of about one radius from the extended nozzle centerline (fig. 7(c)). This region of an undistorted jet mixing region would have the largest intensity of static pressure fluctuations (refs. 23 and 31). Spectra for the two exhaust velocities were not as well coalesced for the forward locations (fig. 36(c)) as further aft. Overall levels remained at intensities that would be reasonable within an undistorted jet mixing region. Spectra measured at the forward chordwise stations were sharply peaked, increasing and then decreasing rapidly as Strouhal number was increased. These same trends occurred for 18° (figs. 36(e) and (f)) and 30° (figs. 36(g) and (h)) deflection. Spectra measured at chordwise positions where the high-shear part of the mixing region impinged against the airfoil surface were sharply peaked while those measured further aft had more gradual growth and decay. For large deflections the peak Strouhal number at aft locations was of order unity rather than the smaller levels typical of those locations at small deflection and of far-field acoustic spectra.

Velocity-adjusted surface spectra for the scrubbed surface at -9° deflection, representing an USB installation, are shown in figures 36(i) and (j). Overall levels were relatively low at forward positions and increased to near the maximum for an isolated jet mixing region with increasing downstream distance. Surface spectra for the higher velocity contained no indication of the tone observed (fig. 35(c)) in far-field acoustic spectra.

Spanwise measurements of one-third-octave spectra were taken at 9° and 30° deflection, 30% and 70% chord, and 125 and 250 m/sec (410 and 820 ft/sec) velocity. Overall levels were found to be symmetrical about the jet plane of symmetry; only data for measurement directions toward the furthest end of the airfoil from that plane are presented. Spectra for the smaller deflection and forward microphone are given in figures 37(a) and (b) for the two velocities. Surface pressures were approximately the same at the centerline and 0.25 diameters to the side. They decayed rapidly beyond 0.5 diameter, the width of the undistorted jet. At a spanwise distance of one diameter the overall levels were about 20 dB below the centerline and the peak frequencies decreased by a factor of about 4. (The constant levels of spectra for high frequencies and low amplitudes are noise floors of the amplifiers.) These peak frequencies agree with those of far-field noise at these test conditions. It is likely that the surface pressure spectra measured at distances of 1.0 to 1.5 diameters at the forward position and small deflections are near-field noise spectra rather than pressure fluctuations of the jet mixing region.

Spectra for the smaller deflection and aft traversed microphone are given in figures 37(c) and (d) for the two velocities. At this location, maximum surface pressure fluctuations occurred at half a diameter to each side of the exhaust centerline. This result is consistent with the viewpoint that

turbulence is generated in the jet mixing region, impressed upon the airfoil surface, and damped by prolonged exposure to the boundary constraint of a rigid surface. As at the forward position, the spectrum shape shifted to lower peak frequencies with increasing spanwise distance. Except for the portions of these spectra at low frequencies and large spanwise spacing, these spectra for velocities differing by a factor of two have similar shape. They would be in good agreement if compared at constant Strouhal number and adjusted 12 dB in amplitude as for a fourth power velocity dependence.

Spectra for the larger deflection are given in figures 37(e) through (h). The decrease of amplitude with increasing spanwise distance was less rapid at this larger deflection, as would be expected with the jet spread over a larger part of the span. For the aft microphone and spanwise positions near the centerline, high-frequency parts of the spectra were approximately equal in magnitude at constant velocity but different deflection. Sonic fatigue of airframe structure caused by high-frequency surface pressure fluctuations then would not be significantly eased by reducing the flap deflection. It is not obvious whether surface pressure spectra in the regions of largest intensity are related to acoustic radiation from those surfaces or merely are imposed by the turbulent jet mixing region.

Cross-Correlation of Scrubbing Noise.

Types of Data Interpretation. - At least three methods are commonly used for interpretation of cross-correlation measurements. Because different types of information can be learned from each method, these analysis methods should be discussed before presenting the results obtained. The simplest use of cross-correlations is the determination of coherence. Coherence of two quantities is defined as the ratio of maximum amplitude of cross-correlation to the square root of the product of maximum autocorrelations; its magnitude varies from zero to one. If coherence between two measured signals has non-negligible magnitude relative to one, then some physical process must exist that relates the two signals. Coherence thus is useful in assuring that a relationship exists but is of little help in understanding the relationship.

This difficulty is avoided if delay time is examined. For two microphones measuring free-field sound waves, the delay time at maximum coherence is the time difference between arrival of a sound wave at each of the two microphone positions. If the ratio of delay time to speed of sound is equal to the microphone separation distance, the sound wave traveled past one microphone on its way to the other. If the measured delay time is less than the acoustic travel time between the two microphones, the locus of all source points which would produce that difference of delay times can be determined. Cross-correlation of several free-field microphones would then yield enough

information to locate the sound source as in sonar triangulation. An important variation of this method occurs when a far-field microphone is cross-correlated with a surface pressure transducer on a surface believed to be radiating sound. The acoustic signal would be proportional to the negative of the first derivative of surface pressure, and this derivative should be maximum at zero signal amplitude. Thus the appropriate delay time is that for a zero crossing with negative slope, located between positive and negative peaks of coherence. If this delay time is equal to the acoustic propagation time, acoustic radiation from the surface location has a significant contribution to far-field sound. More important, differences between delay time and acoustic propagation time represent differences between the time when turbulent eddies generate noise and the time they are convected past the surface transducer. One could locate the origin of sound radiation by use of delay time if the convection speed were known. By cross-correlating a streamwise row of surface microphones with one far-field microphone, and comparing delay times with propagation time, a discrete noise source along the surface can be located. This location can be identified even though physical constraints may prevent placement of a transducer near the region of large local source strength.

In contrast to the use of delay times to infer source locations at positions other than the surface measurement point, causality analysis (e.g., ref. 27) yields the surface dipole source strength at the measurement point. Absolute values of cross-correlation slope at the acoustic delay time and of autocorrelations evaluated at zero delay time, along with speed of sound and field-point distance and direction, are utilized to calculate local source strength. Distribution of source strength along the surface must be obtained from a large number of surface-to-far-field cross-correlations. This measured distribution can be checked for self-consistency by integrating over the surface, calculating far-field sound, and comparing with far-field data. Of the three methods, the causality analysis is the most rigorous but it requires the largest number of surface pressure transducers and the largest amount of data processing per measurement. The approach used herein has been directed primarily toward use of coherence and delay time for identifying locations of sound-radiating mechanisms. When those methods show that two different mechanisms each have significant contributions, causality analysis is used only to examine the effect of some variable on source strengths at locations that are important for each mechanism. Thus the emphasis was directed toward understanding the aeroacoustic mechanisms rather than determining the surface distributions of combined source strength.

Cross-Correlation Data. - Signals from the far-field microphone at 90° direction to the exhaust nozzle were cross-correlated with those from surface microphones along the airfoil in the jet exhaust plane of symmetry. Some results for 9° deflection angle and two different velocities are given in figure 38. As sketched in figure 38(a), cross-correlation signals for such data were relatively simple in appearance with a large positive peak followed by an approximately equal large negative peak. The two measured quantities were coherence (maximum cross-correlation normalized with respect to rms level of the two autocorrelations at zero delay time) and the delay time at which cross-correlation passed through zero amplitude between the two peaks. Delay times for the two jet velocities of 125 and 250 m/sec (410 and 820 ft/sec) are shown in figure 38(b) for overall spectra filtered to exclude frequencies below 200 Hz. These times exceeded the 6.4×10^{-3} sec required for a sound wave to travel from the airfoil to the far-field microphone. The amount by which this delay time exceeded the acoustic travel time increased approximately linearly with distance from the trailing edge and was halved when jet velocity was doubled. Time required for a fluid disturbance to be convected from a surface microphone to the airfoil trailing edge at 0.8 times the jet velocity, added to the acoustic travel time, is shown as solid straight lines for the two jet velocities. Overall noise at this deflection angle was apparently dominated by a process in which fluid disturbances were convected along the surface at about 80% of jet exhaust velocity and produced noise as they moved past the trailing edge. That is, measured overall signals were dominated by trailing edge noise.

Measured levels of coherence for overall signals at the two velocities are shown in figure 38(c). They decreased with increasing distance from the trailing edge and with increasing velocity. If it is assumed that coherence between surface pressure fluctuations and far-field acoustic pressures would be unity for surface measurements at the trailing edge, then the data can be seen to be approximated by an exponential decay. The argument of the exponential is proportional to the product of velocity and upstream distance. Such behavior has been predicted (ref. 20) for trailing edge noise.

Cross-correlations were obtained at the lower velocity for spectra filtered in octave bandwidths with center frequencies of 500, 1000, 2000, and 4000 Hz. Delay times for these filtered signals were approximately equal to those for overall spectra and are not shown. Coherence measured in these four octave bands and with the overall signal are shown in figure 38(d). Overall coherence approximately matched that which was measured at 1000 Hz. At higher frequencies, coherence decreased as center frequency was increased. The argument of the exponential decay was approximately directly proportional to frequency at the higher frequencies.

When airfoil deflection was increased to 18° and 30°, cross-correlation curves became more complicated in appearance. Cross-correlations measured at upstream locations along the airfoil had two pairs of prominent signals. Delay times for the two zero crossings at 30° deflection and 125 m/sec velocity, for signals filtered to exclude frequencies below 200 Hz, are shown in figure 39(a). One set of zero crossings occurred at about the acoustic travel time. This corresponded to sound radiated from a surface as the fluid disturbance was convected along the surface. The other set occurred at somewhat larger than the sum of fluid convection time and acoustic travel time and corresponded to trailing edge noise. Values of coherence for these two peaks are shown in figure 39(b) for the overall signals and for octave bands centered at 1000 and 2000 Hz. Coherence of the peak occurring at the acoustic travel time decreased with increasing distance from the leading edge and either was independent of frequency or increased as center frequency was increased. In contrast, coherence of the peak associated with trailing edge noise decreased with increasing distance from the trailing edge and decreased as center frequency was increased.

Coherence of this trailing edge peak was smaller than that for trailing edge noise at the same velocity but smaller deflection angle (fig. 38(d)). This does not mean that trailing edge noise was weaker at the larger angle. The actual levels of trailing edge noise could be calculated by a causality analysis (ref. 32) of properly obtained autocorrelations and cross-correlations. As a rapid approximation to a causality analysis, it can be noted from figures 36(d) and (h) that overall surface pressure levels at 80% chord were about 3 dB larger for the larger deflection but, from figures 35(d) and (f), peak one-third-octave sound pressure levels were essentially unchanged. The smaller coherence at larger deflection angle represents approximately the same local acoustic source strength in both cases, but the ratio of source strength to surface pressure fluctuation was smaller at the larger deflection angle.

With all surface microphones located along the jet plane of symmetry, streamwise cross-correlations were obtained between the 30% chord position and 38, 62, 70, and 80% chord. In addition, cross-correlations were obtained between the three most rearward chord positions. These results can be used for determining whether coherence of surface pressure fluctuations is strongly dependent on streamwise position (30 or 70% chord) or whether it depends primarily on distance between the two correlated microphones. For these surface-to-surface comparisons, delay times were measured to maximum coherence. Delay times and coherence are given in figure 40 for 125 m/sec (410 ft/sec) velocity and 9° and 30° deflection. Signals were filtered for various octave bandwidths. Measured delay times at both deflection angles were consistent with disturbances being convected along the chord at about 80% of the jet exhaust velocity. This ratio of convection to velocity to jet velocity is

larger than the values near 60% usually assumed in jet noise theories for convection velocity of small eddies in undistorted jets. Approximately the same convection velocity ratio of 60% is also found for predicted convection of large-scale vortex instabilities (ref. 29). However, convection velocities determined from cross-correlation of surface pressure spectra on a simulated under-the-wing externally blown flap were described (ref. 32, p. 227) as nearly the same as the local maximum mean speed. This maximum mean speed of the jet attached to a simulated 45° deflected flap was given in figure 8(b) of reference 32 as about 90% of jet exhaust velocity. The convection velocity ratio of 80% determined from both surface-to-surface and surface-to-far-field cross-correlations then is reasonable for an attached wall jet. The flow disturbances convected along the surface were described in reference 32 as large-scale vortex structures that were relatively coherent in the spanwise direction. Formation of these ring vortices in the free shear layer of an undistorted exhaust jet was described in reference 29. Distortion of ring vortices by an externally blown flap was described in reference 33, but convection velocities for the distorted vortices were not given in that study.

Cross-correlations were obtained at 125 m/sec (410 ft/sec) velocity and 9° deflection with the surface pressure microphones at 30 and 70% chord traversed spanwise. Each traversed microphone was cross-correlated with the nearest chordwise position on the exhaust centerline and with the 90° far field microphone. Delay times for maximum coherence between the centerline and traversed surface microphones were approximately independent of spanwise position. That is, the convected pressure disturbances had relatively large spanwise extent rather than being small relative to jet diameter. These delay times were roughly equal to the flow convection time. Maximum coherence of these measurements is plotted in figure 41(a) for the overall signal and the 1000 Hz octave band at both chordwise positions. The highly correlated region was somewhat wider at the downstream position. Generally similar results had been presented in reference 32 for 45° flap deflection. Coherence along a spanwise line at zero time delay was shown in figure 12(a) of reference 32 to decay to zero in about half a diameter near the impingement region but, in figure 12(b) to be about 0.4 at spanwise distances of half to one diameter at a further downstream position.

Cross-correlations of the far-field microphone with the spanwise traversed microphone had zero crossings at the sum of flow convection time and acoustic travel time. At the larger spanwise positions, cross-correlations with the 30% chord microphone had a second peak that was maximum at a time roughly 0.4 milliseconds less than the acoustic travel time. This signal corresponds to a sound wave radiated from the trailing edge and detected by both the surface microphone and far-field microphone. Coherence of the other peak is plotted in figure 41(b). These values were approximately independent of spanwise position and were larger at the aft position. Probably they show

that the pressure pattern associated with large-scale structure of the exhaust jet was felt outside of the exhaust jet and was associated with noise production.

Interpretation of Scrubbing Noise Mechanism. - When this investigation was begun, it had been tentatively assumed that scrubbing noise was produced by locally correlated turbulent eddies in the exhaust jet adjacent to the airfoil surface. This process was assumed identical to that described in references 1 and 34 for turbulent boundary layer dipole noise. Because jet mixing regions have turbulence intensities an order of magnitude larger than those of turbulent boundary layers, calculated sound intensities would be of the order of 20 dB larger than given by equation (11) of reference 1. Several results of this investigation which disprove this assumed process for scrubbing noise are (1) large variations in coherence between surface pressures and far-field acoustic pressures in regions having roughly equal amplitudes of surface pressure fluctuation, so that local source strength is clearly not proportional to local surface pressure fluctuation, (2) symmetry of scrubbing noise directivity measured in the scrubbed and unscrubbed directions, and (3) surface pressure spectrum shapes that differ from that which would yield observed far-field scrubbing noise spectra as predicted by the analysis of reference 30. Other experimental results that disprove this assumed mechanism were given in reference 32. Increasing the length of an under-the-wing externally blown flap from 3.75 to 12.75 diameters was found to reduce the acoustic power, change the directivity pattern from one that was dominated by a lift dipole to one that was typical of jet mixing noise, and change the velocity dependence from fifth or sixth power to eighth power. Local mean velocity profiles, and presumably the local surface pressure fluctuations in the impingement and flow attachment region, were not changed by the increased flap length. Attributes associated with scrubbing noise were therefore eliminated relative to jet mixing noise by increasing the extent of surface that was scrubbed. The most easily measured surface pressure fluctuations apparently are not directly part of the acoustic radiation process.

An alternate qualitative mechanism for scrubbing noise was cited in reference 33 as stretching and distortion of large-scale vortex structure in the impingement region. Changes in area of a vortex ring at constant circulation were shown analytically in reference 35 to produce a dipole sound field. However, increasing the flap length as described in reference 32 should not have altered the changes in jet exhaust large-scale vortex structure near the impingement region. It is also difficult to understand why noise produced by vortex motion beneath an unslotted flap of moderate length would not be shielded by the flap rather than (ref. 32, fig. 5(b)) symmetrical above and below such a flap at low exhaust velocities. The Concluding Remarks of reference 32 attributed scrubbing noise to the motion of large-scale exhaust jet turbulence past the trailing edge. Reduced noise intensity at large flap

lengths was then attributed to the reduced flow velocity at that location. However, trailing edge noise differs in directivity shape, spectrum shape, and velocity exponent from what is characterized experimentally as scrubbing noise.

The investigation reported herein showed that coherence of scrubbing noise from a 30° deflected airfoil was large near the impingement region and decayed with increasing downstream distance. The measured large coherence near the trailing edge may have been produced by a second maximum of scrubbing noise in addition to trailing edge noise. It is possible that convection and distortion of the exhaust jet's large-scale ring vortices, as described in reference 33, generates airfoil lift force fluctuations similar to those for isolated vortexes convected past an airfoil. The local loading induced by each vortex would be concentrated along the chord near the vortex. It would be acoustically compact and in phase along the scrubbed span. Thus the power spectrum of lift force response should be independent of frequency at low frequencies and vary inversely with frequency squared at high frequencies as for a swept or unswept gust in subsonic compressible flow (ref. 12). Far-field sound from this compact source should vary as the product of frequency squared, lift response spectrum, and turbulence spectrum of the large-scale vortex structure. This vortex spectrum is likely (ref. 36) to have the same general behavior as small-scale jet turbulence, being essentially constant at low frequencies and decaying roughly inversely with frequency squared at high frequencies. The resulting acoustic spectrum would increase approximately with frequency squared at low frequencies and decay inversely with frequency squared at high frequencies. This is the spectrum shape observed (ref. 30) for scrubbing noise. The fluctuation of lift coefficient for an unswept single vortex convected past an airfoil was shown in figure 5 of reference 13 to be essentially independent of subsonic Mach number. Thus the far-field sound strength would vary approximately with some appropriate local velocity to the sixth power as is observed.

Lift force fluctuation due to a vortex encounter at constant velocity was shown in figure 9 of reference 13 to vary approximately inversely with vortex trajectory distance from the airfoil, divided by chord. If this force fluctuation mechanism is the cause of scrubbing noise, the major difference between effects of flap deflection on sound directivity of under-the-wing and upper-surface-blowing externally blown flaps (ref. 37) would be explained. For an under-the-wing configuration, increased flap deflection would decrease the distance from the flap surface to the outer edge of the deflected jet. Noise caused by large-scale vortex structures convected past the flaps would then be much larger than that for the undeflected, physically larger main part of the wing. Directivity would then be typified by a lift dipole that rotates and strengthens with increasing flap deflection. In contrast, deflecting the flaps of an upper-surface-blowing configuration would tend to increase the distance between the flap surface and the vortexes. Scrubbing

noise for such installations would be expected to be a lift dipole normal to the undeflected wing, with a strength that decreases slightly as deflection is increased. Noise beneath such configurations would be a sum of trailing edge noise that rotates with flap deflection and scrubbing noise that is essentially unaffected by flap deflection. Overall sound pressure levels measured below an upper-surface-blowing configuration thus are not significantly changed by flap deflection and are about 10 dB below those for a comparable under-the-wing model (fig. 14 of ref. 37). This increment corresponds (fig. 7 of ref. 24) to the difference between scrubbing noise measured for an under-the-wing model with maximum and zero flap deflections.

If vortex strength, position, and velocity could be known from studies of the jet impingement region such as were reported in reference 33, the calculation method of reference 13 might be used for predicting scrubbing noise. In the absence of such knowledge, an empirical approximation to vortex trajectory can be obtained from the description in Appendix A of reference 33. The initial distortion of an exhaust jet by an aerodynamically efficient slotted flap should be that for a shallow-angle oblique jet. The outer portion of the jet retains its undeflected shape and the primary distortion of velocity profile occurs near the airfoil. The jet is gradually rotated until it becomes a spreading wall jet attached to the airfoil. In contrast, large-angle oblique jet impingement may represent the effect of the aft flap panel. A complex recirculation region may be formed in the impingement region, and the jet is rapidly turned to the flap direction. Jet width is substantially increased and thickness is reduced to less than one-fourth the initial jet diameter.

CONCLUSIONS

1. Trailing edge noise has an intensity that varies with velocity to the fifth power, turbulence intensity squared, and cosine squared of half the direction angle measured from the upstream direction. This behavior is predicted by the analyses of Ffowcs Williams and Hall and of Chase. Overall magnitude is predicted by the analysis of Ffowcs Williams and Hall if the turbulence eddy spacing along the trailing edge is four times the spanwise integral scale length.

2. Incidence fluctuation noise has a spectrum shape that varies with subsonic Mach number at moderate and large Strouhal numbers. Magnitude and spectrum shape of far-field spectra are predicted by the theory of Filotas as modified by a Mach number dependence obtained by Hayden. Airfoil surface pressure spectra are not strongly affected by subsonic Mach number and are predicted by the theory of Filotas.

3. Scrubbing noise of externally blown flaps apparently is caused by fluctuations of airfoil loading, coherent along the scrubbed span, induced by large-scale vortex structure of the exhaust jet that is convected past the wing and flap surface. The resulting surface pressure fluctuations are small relative to those generating in the exhaust jet mixing region and impressed onto the scrubbed surface. A rigorous theory for predicting scrubbing noise is not presently available.

REFERENCES

1. Sharland, I. J.: Source of Noise in Axial Flow Fans. J. of Sound and Vib., Vol. 1, No. 3, July 1964, pp. 302-322.

2. Clark, L. T.: Results of an Experimental Investigation Relating to Sound Generation by a Single Airfoil in a Turbulent Flow. The Boeing Co., Commercial Division, Rep. No. D6-23274, April 1969.

3. Hersh, A. S. and Meecham, W. C.: Sound Directivity Pattern Radiated from Small Airfoils. J. Acoust. Soc. Am., Vol. 53, No. 2, Feb. 1973, pp. 602-606.

4. Clark, P. J. F. and Ribner, H. S.: Direct Correlation of Fluctuating Lift with Radiated Sound for an Airfoil in Turbulent Flow. J. Acoust. Soc. Am., Vol. 46, No. 3, Part 2, Sept. 1969, pp. 802-805.

5. Dean, L. W.: Broadband Noise Generated by Airfoils in Turbulent Flow. Paper 71-587, AIAA, June 1971. Also, Fan-Compressor Noise: Prediction, Research and Reduction Studies. Fed. Avia. Admin. FAA-RD-71-73, Feb. 1971, pp. 183-211.

6. Filotas, L. T.: Theory of Airfoil Response in a Gusty Atmosphere, Part I - Aerodynamic Transfer Function. Univ. of Toronto, Instit. for Aerospace Studies, UTIAS Rep. No. 139, AFOSR 69-2150TR, Oct. 1969.

7. Filotas, L. T.: Theory of Airfoil Response in a Gusty Atmosphere, Part II - Response to Discrete Gusts or Continuous Turbulence. Univ. of Toronto, Instit. for Aerospace Studies, UTIAS Rep. 141, AFOSR 69-3089TR, Nov. 1969.

8. Mugridge, B. D.: Sound Radiation from Aerofoils in Turbulent Flow. J. Sound Vib., Vol. 13, No. 3, Nov. 1970, pp. 362-363.

9. Sears, W. R.: Some Aspects of Non-Stationary Airfoil Theory and Its Practical Applications. J. Aero. Sci., Vol. 8, No. 3, Jan. 1941, pp. 104-108.

10. Fung, Y. C.: An Introduction to the Theory of Aeroelasticity. John Wiley & Sons, Inc., New York, 1955.

11. Osborne, C.: Unsteady Thin-Airfoil Theory for Subsonic Flow. AIAA J., Vol. 11, No. 2, Feb. 1973, pp. 205-209.

12. Adamczyk, J. J.: Passage of an Isolated Airfoil Through a Three-Dimensional Disturbance. PhD Thesis, Univ. of Conn., May 1971.

13. Adamczyk, J. J.: Passage of a Swept Airfoil Through an Oblique Gust. J. Aircraft., Vol. 11, No. 5, May 1974, pp. 281-287.

14. Mugridge, B. D.: Broadband Noise Generation by Aerofoils and Axial Flow Fans. Paper 73-1018, AIAA, Oct. 1973.

15. Hayden, R. E.: Noise from Interaction of Flow with Rigid Surfaces: A Review of Current Status of Prediction Techniques. NASA CR 2126, Oct. 1972.

16. Powell, A.: On the Aerodynamic Noise of a Rigid Flat Plate Moving at Zero Incidence. J. Acoust. Soc. Am., Vol. 31, No. 12, Dec. 1959, pp. 1649-1653.

17. Ffowcs Williams, J. and Hall, L. H.: Aerodynamic Sound Generation by Turbulent Flow in the Vicinity of a Scattering Half Plane. J. Fluid Mech., Vol. 40, Part 4, Mar. 1970, pp. 657-670.

18. Crighton, D. G. and Leppington, F. G.: On the Scattering of Aerodynamic Noise. J. Fluid Mech., Vol. 46, Part 3, April 1971, pp. 557-597.

19. Chase, D. M.: Sound Radiated by Turbulent Flow Off a Rigid Half Plane as Obtained From a Wavevector Spectrum of Hydrodynamic Pressure. J. Acoust. Soc. Am., Vol. 52, No. 3, Part 2, Sept. 1972, pp. 1011-1023.

20. Chase, D. M.: Noise Radiated from an Edge in Turbulent Flow According to a Model of Hydrodynamic Pressure; Comparison with a Jet Flow Experiment. Paper 74-570, AIAA, June 1974.

21. Hayden, R. E.: Sound Generation by Turbulent Wall Jet Flow Over a Trailing Edge. MS Thesis, Purdue Univ., 1969.

22. Paterson, R. W., Vogt, P. G., and Foley, W. M.: Design and Development of the United Aircraft Research Laboratories Acoustic Research Tunnel. J. Aircraft, Vol. 10, No. 7, July 1973, pp. 427-433.

23. Arndt, R. E. A., Tran, N., and Barefoot, G.: Turbulence and Acoustic Characteristics of Screen Perturbed Jets. Paper 72-644, AIAA, June 1972.

24. Olsen, W. A., Dorsch, R. G., and Miles, J. H.: Noise Produced by a Small-Scale, Externally Blown Flap. NASA TN D-6636, March 1972.

25. Hinze, J. O.: Turbulence. McGraw-Hill Book Co., New York, 1959.

26. Olsen, W. A., Gutierrez, O., and Dorsch, R. G.: The Effect of Nozzle Inlet Shape, Lip Thickness, and Exit Shape and Size on Subsonic Jet Noise. Paper 73-187, AIAA, Jan. 1973.

27. Siddon, T. E.: Surface Dipole Strength by Cross-Correlation Method. J. Acoust. Soc. Am., Vol. 53, No. 2, Feb. 1973, pp. 619-633.

28. Paterson, R. W., Vogt, P. G., Fink, M. R., and Munch, C. L.: Vortex Noise of Isolated Airfoils. J. Aircraft, Vol. 10, No. 5, May 1973, pp. 296-302.

29. Michalke, A.: Instabilitat eines Kompressiblen Runden Freistrahls unter Berucksichtigung des Einflusses der Strahlgrenzschichtdicke. ZFW, Vol. 19, No. 8/9, 1971, pp. 319-328.

30. Fink, M. R.: Mechanisms of Externally Blown Flap Noise. Paper 73-1029, AIAA, Oct. 1973.

31. Barefoot, G.: Fluctuating Pressure Characteristics in the Mixing Region of a Screen Perturbed Jet. Penn. State Univ., Ordnance Res. Lab. TM-72-165, Aug. 1972.

32. Yu, J. C., Reddy, N. N., and Whitesides, J. L., Jr.: Noise and Flow Characteristics of an Externally Blown Flap. Proceedings of the Second Interagency Symposium on Univ. Res. in Transp. Noise, June 1974, Vol. I, pp. 219-237.

33. Foss, J. F.: Research on Free and Impinging Jets for the Development of STOL Aircraft. NASA CR-138031, Jan. 1974.

34. Vecchio, E. A. and Wiley, C. A.: Noise Radiated from a Turbulent Boundary Layer. J. Acoust. Soc. Am., Vol. 52, No. 2, Feb. 1973, pp. 596-601.

35. Powell, A.: Theory of Vortex Sound. J. Acoust. Soc. Am., Vol. 36, No. 1, Jan. 1964, pp. 177-195.

36. Arndt, R. E. A. and George, W. K.: Investigation of the Large-Scale Coherent Structure in a Jet and Its Relevance to Jet Noise. Proceedings of the Second Interagency Symposium on Univ. Res. in Transp. Noise. June 1974, Vol. I, pp. 142-161.

37. Reshotko, M., Goodykoontz, J. H., and Dorsch, R. G.: Engine-Over-the-Wing Noise Research. Paper 73-631, AIAA, July 1973.

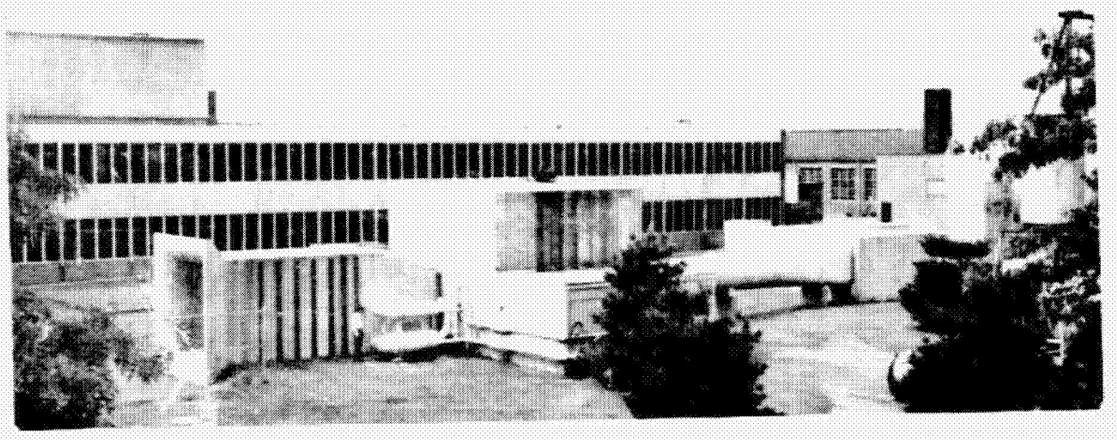

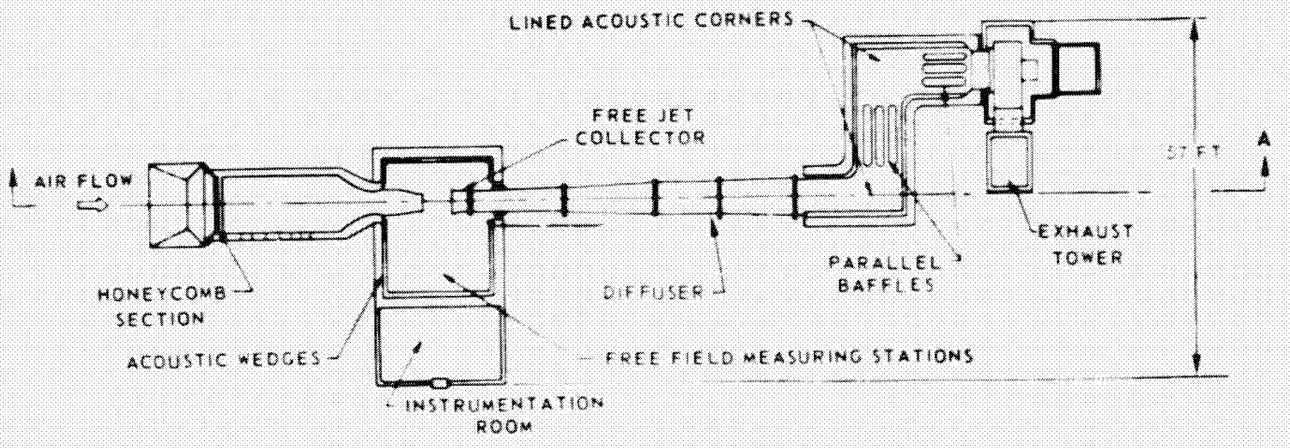

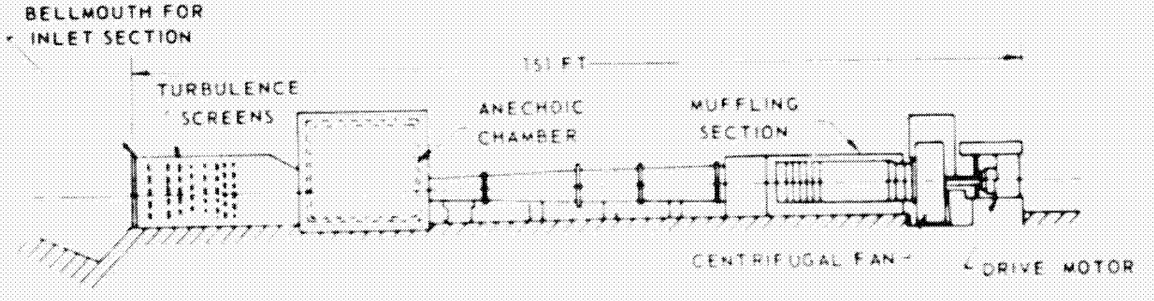

PARTIAL SECTION A–A

FIGURE 1. – UARL ACOUSTIC RESEARCH TUNNEL

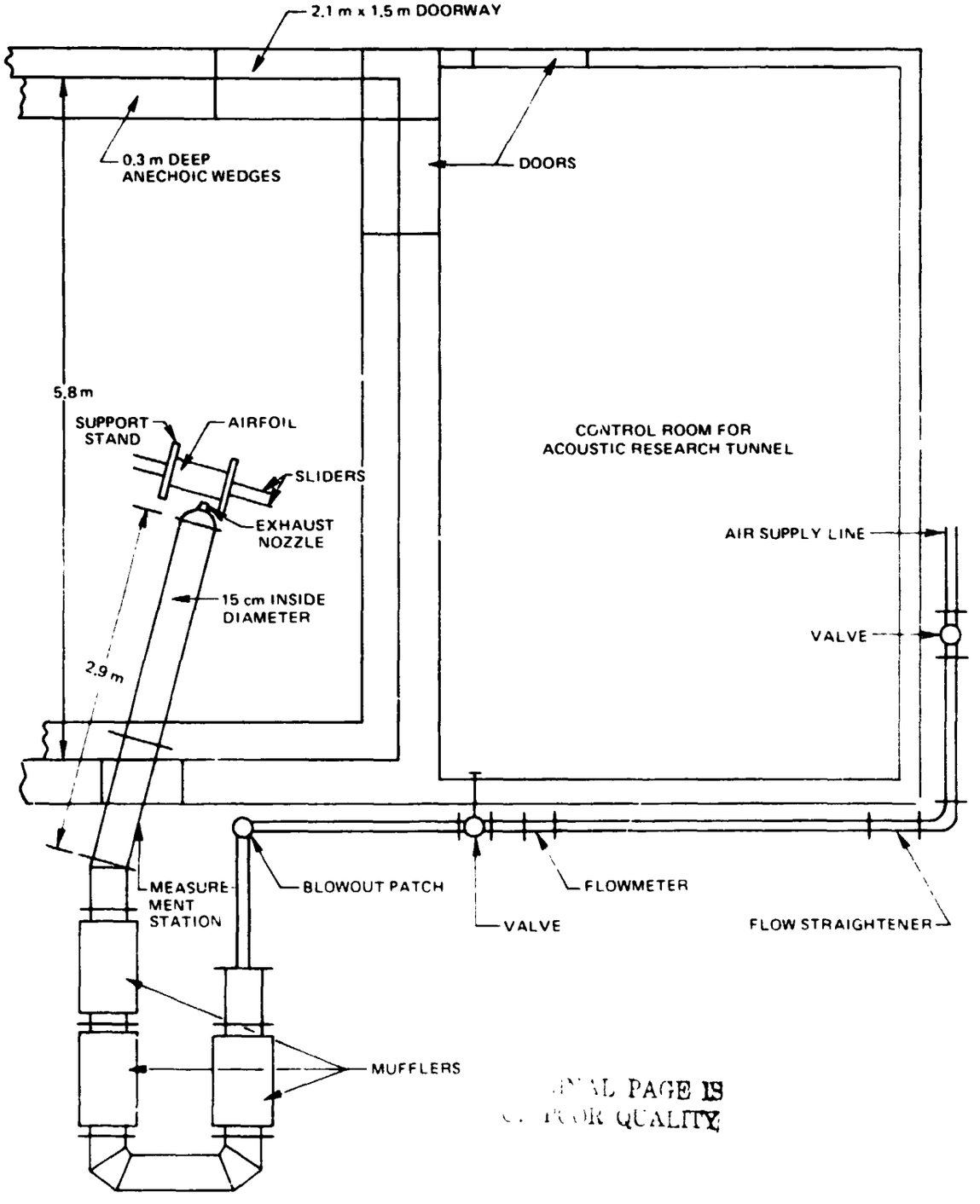

FIGURE 2. – SKETCH OF JET EXHAUST NOISE EQUIPMENT

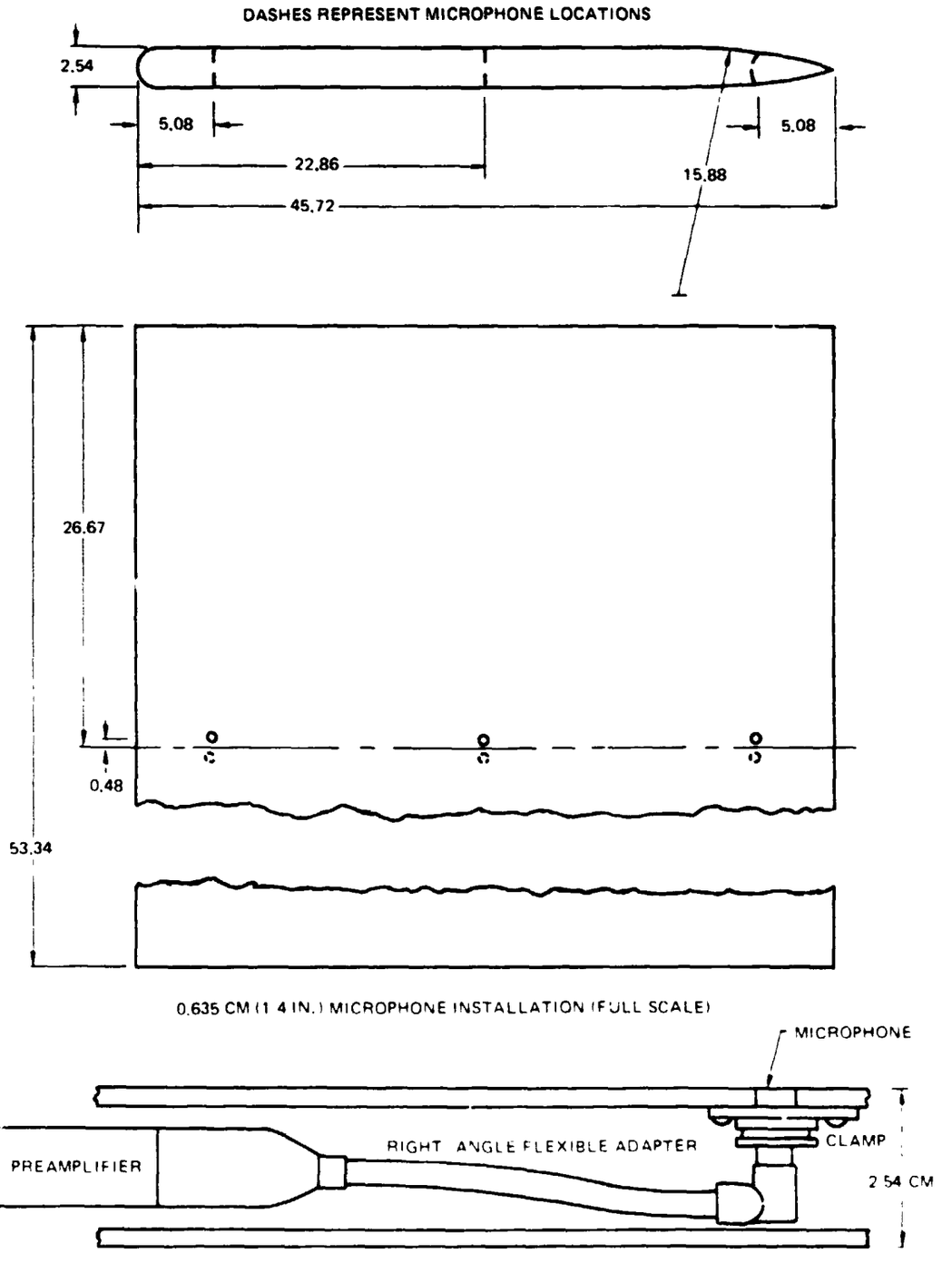

FIGURE 3. – FLAT PLATE AIRFOIL. ONE–QUARTER SCALE EXCEPT WHERE NOTED. ALL DIMENSIONS IN CENTIMETERS

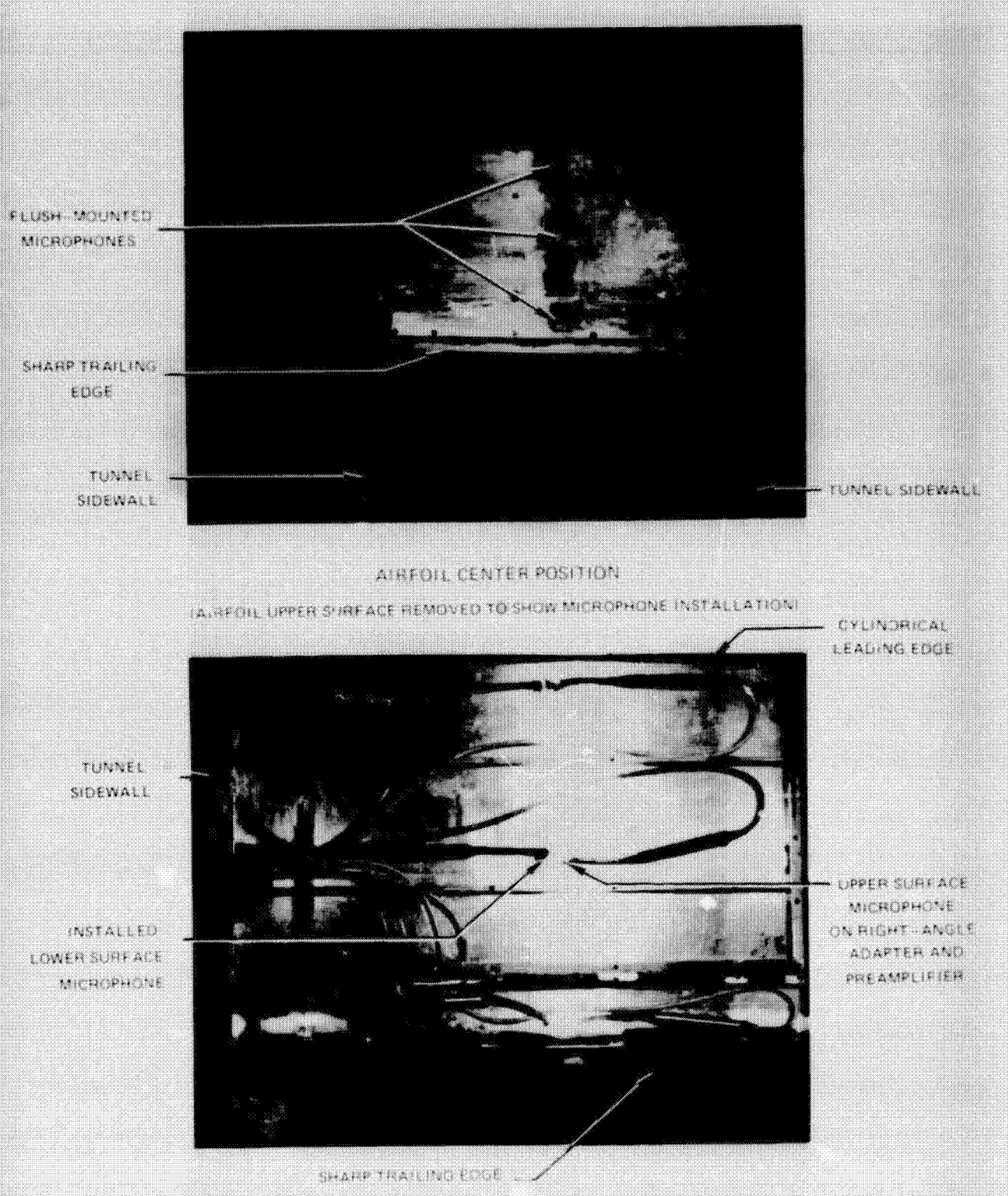

FIGURE 4. – FLAT PLATE AIRFOIL INSTALLATIONS

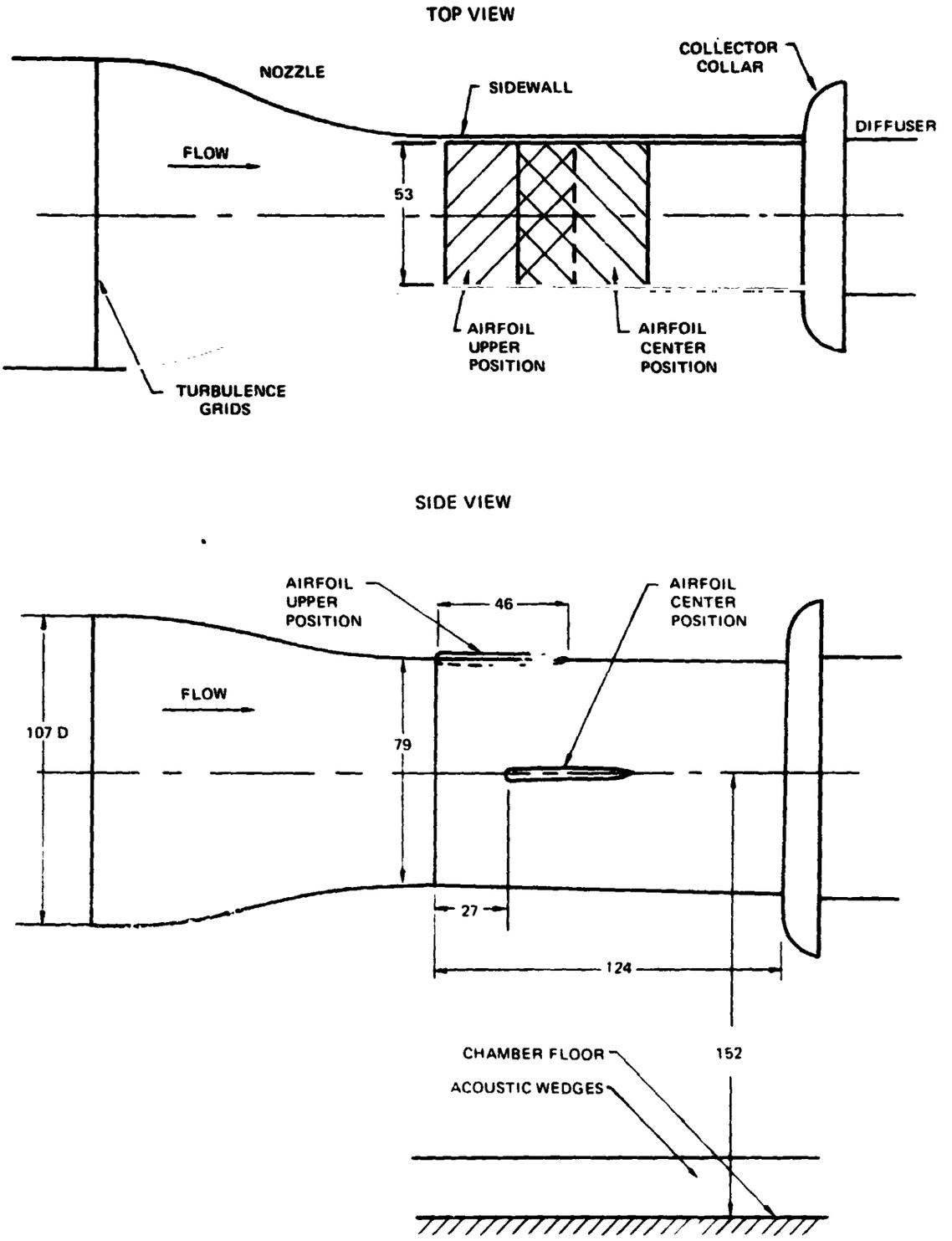

FIGURE 5. – ACOUSTIC TUNNEL TEST SECTION. ALL DIMENSIONS IN CENTIMETERS

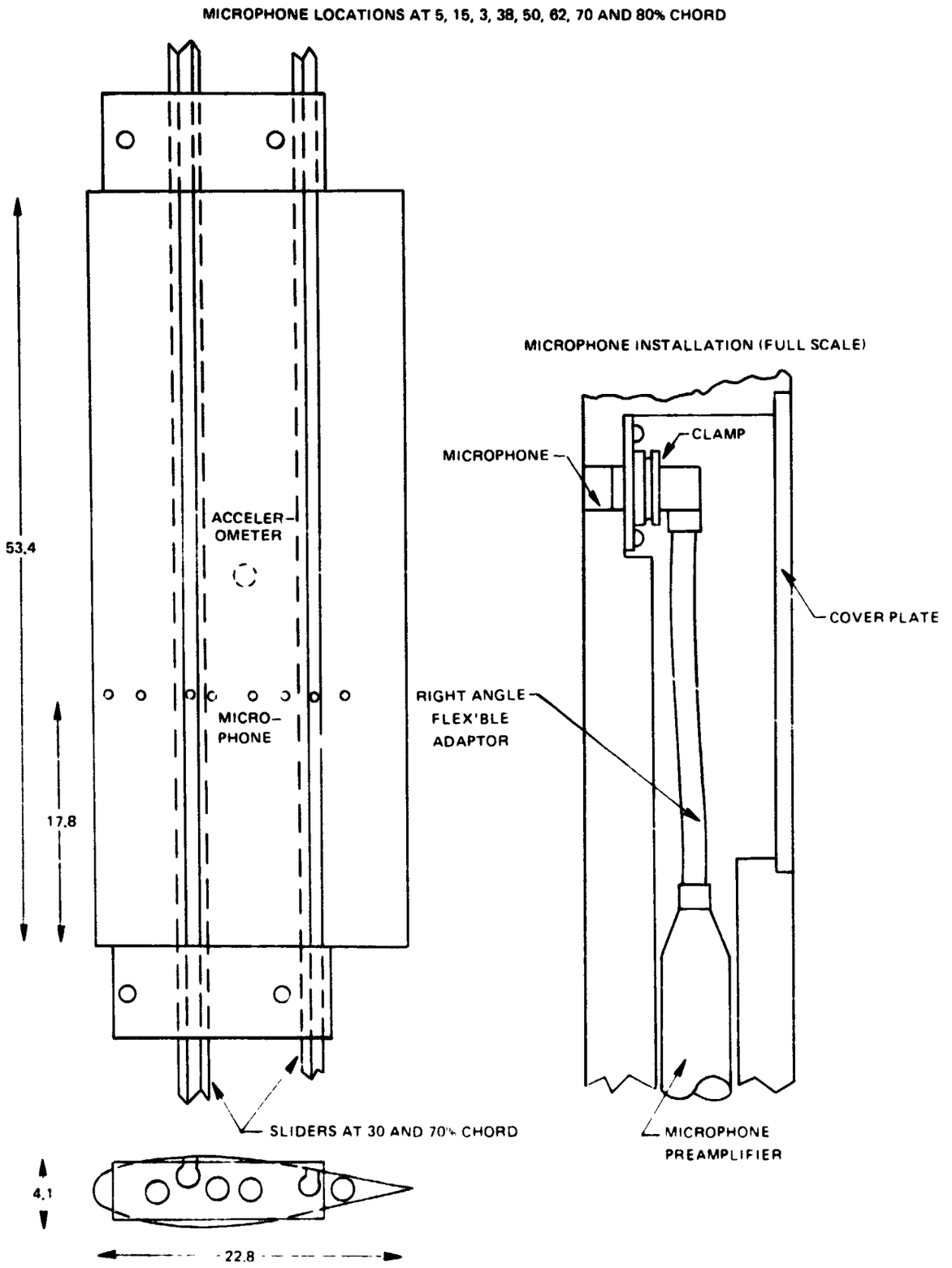

FIGURE 6. – NACA 0018 FULL–SPAN AIRFOIL. ONE–QUARTER SCALE, ALL DIMENSIONS IN CENTIMETERS.

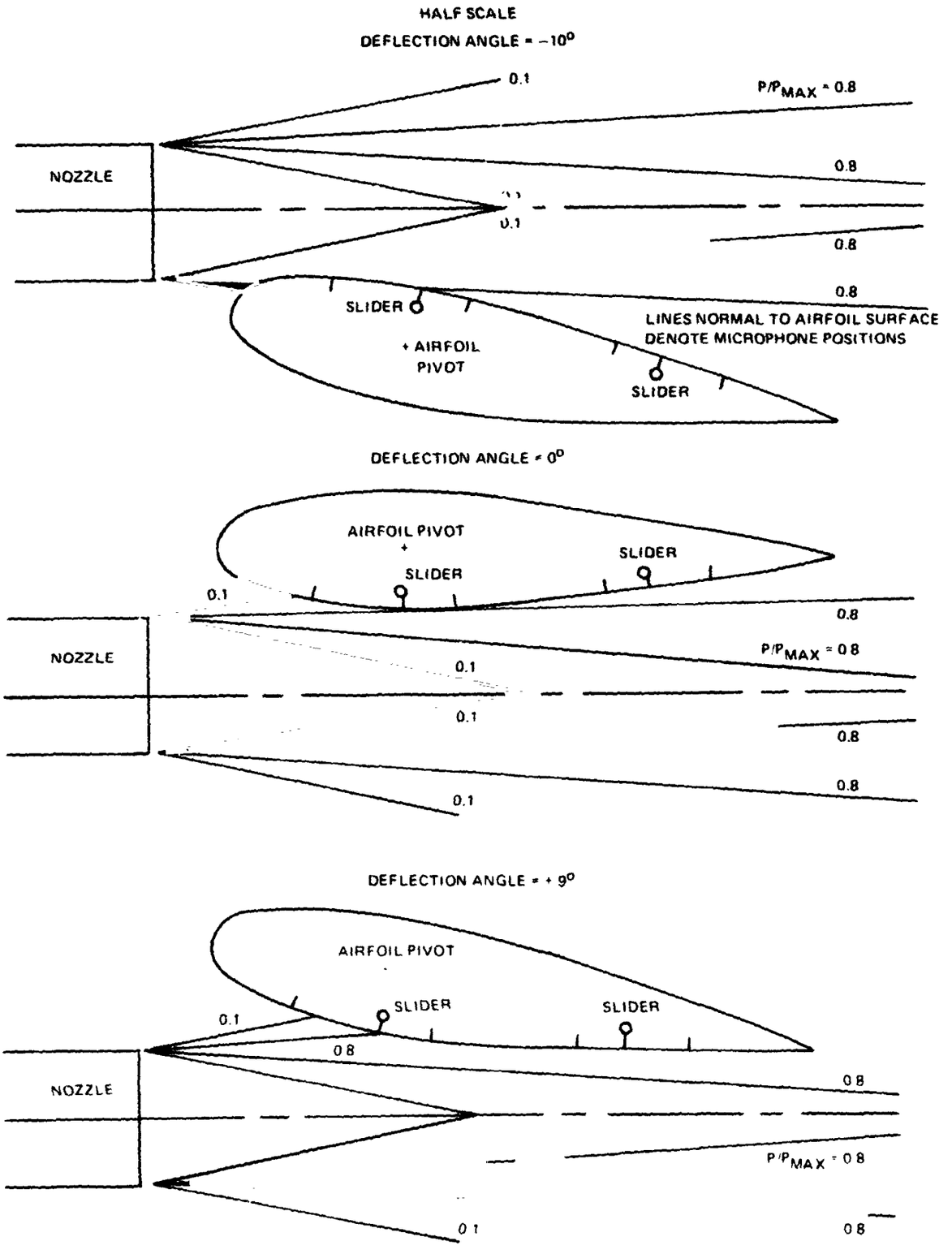

FIGURE 7. – SKETCH OF SELECTED AIRFOIL POSITIONS RELATIVE TO STATIC DISTRIBUTION OF PRESSURE FLUCTUATIONS IN JET

HALF SCALE

DEFLECTION ANGLE = + 18°

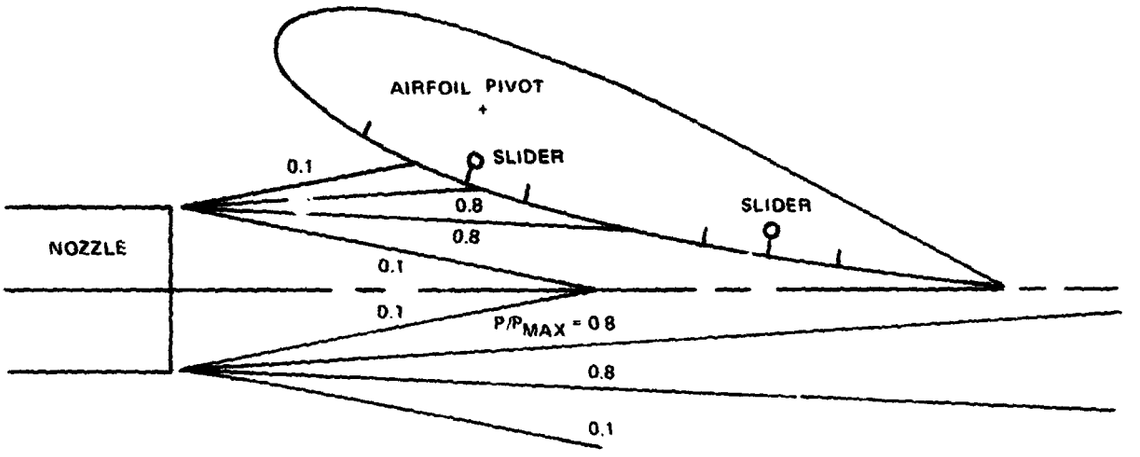

DEFLECTION ANGLE = + 30°

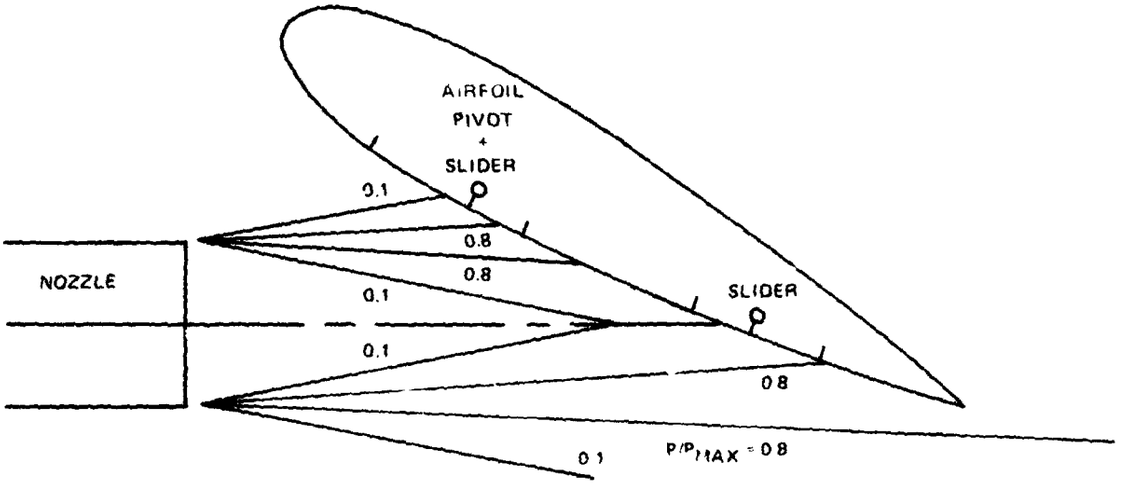

FIGURE 7. – CONCLUDED

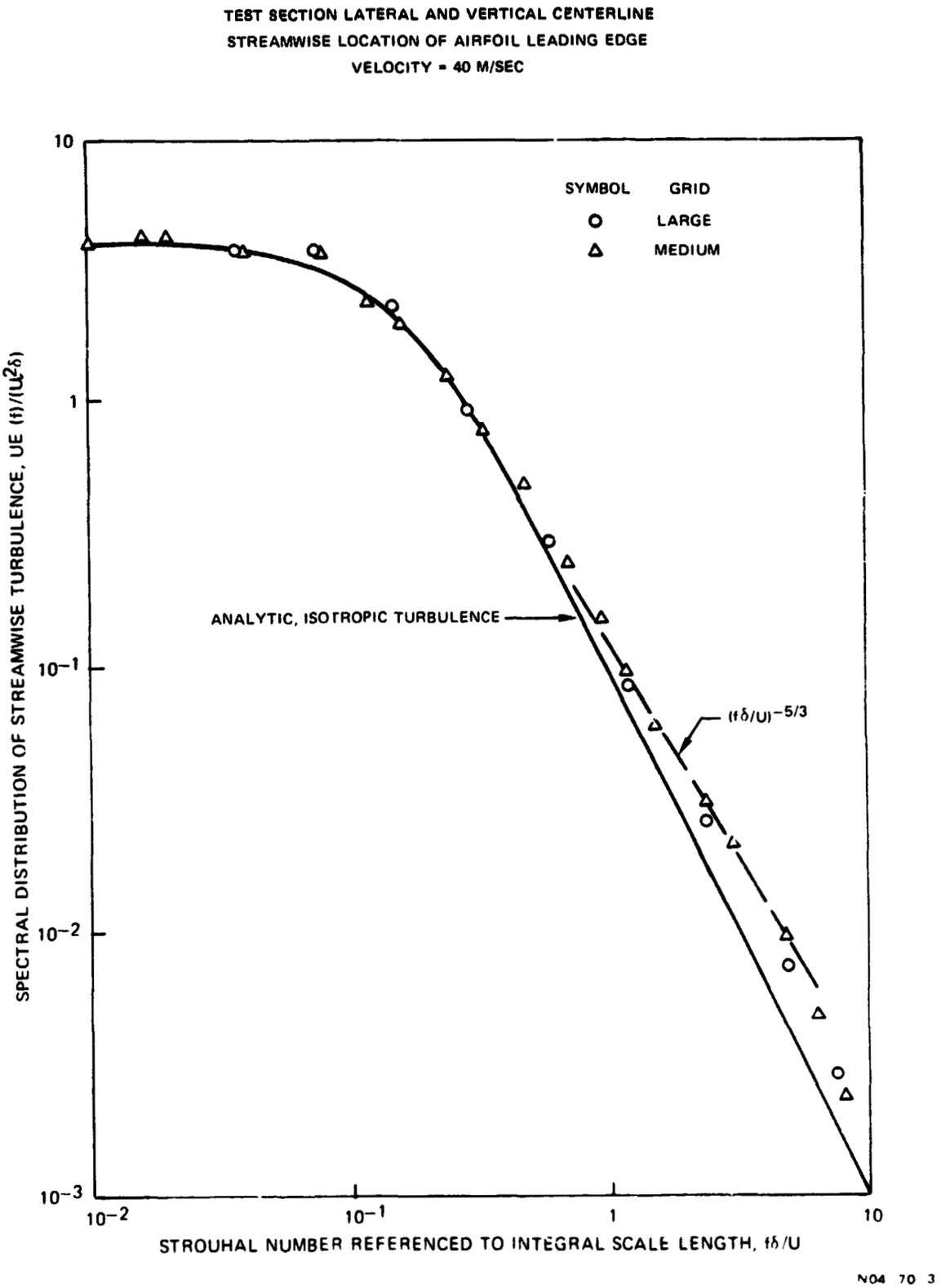

FIGURE 8. – COMPARISON OF MEASURED AND ANALYTIC NORMALIZED SPECTRAL DISTRIBUTION OF STREAMWISE TURBULENCE

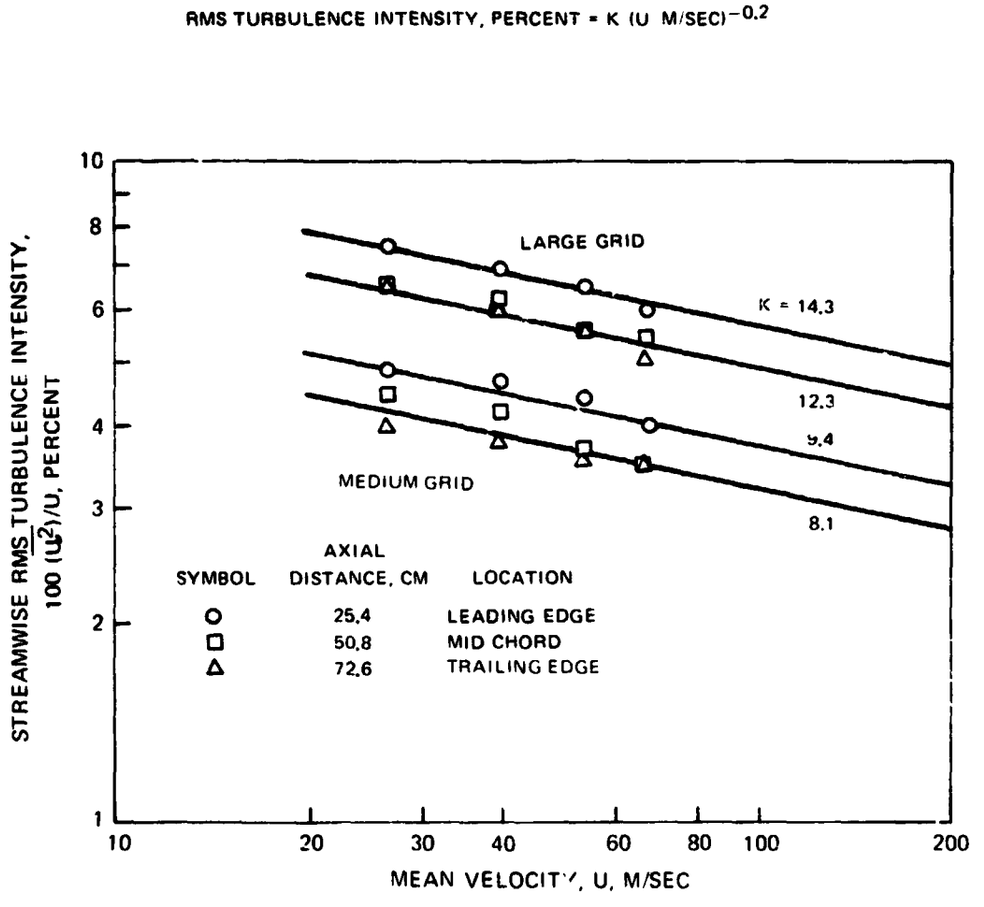

FIGURE 9 – VARIATION OF STREAMWISE RMS TURBULENCE WITH VELOCITY AND STREAMWISE DISTANCE

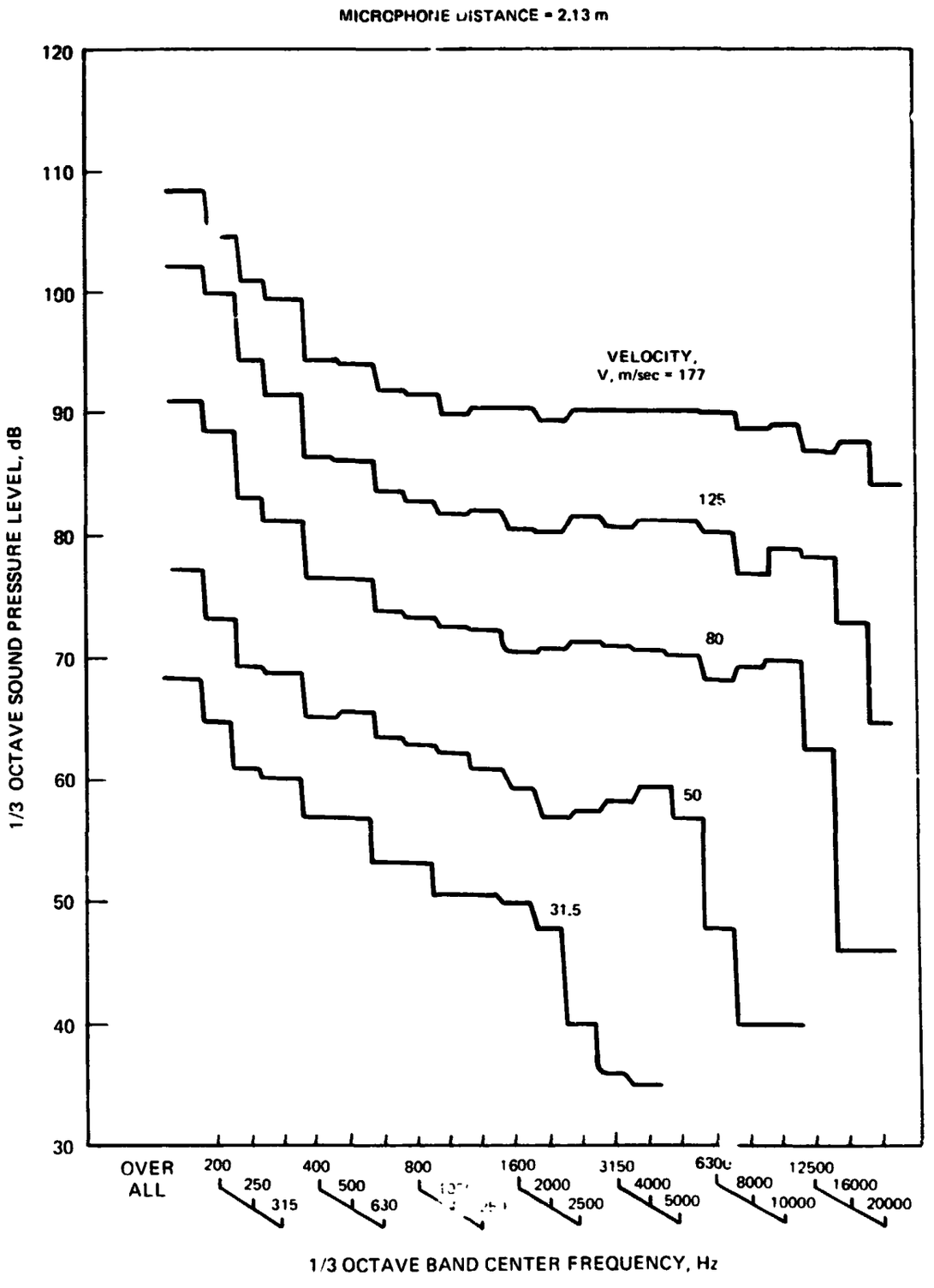

FIGURE 10. – BACKGROUND NOISE OF ACOUSTIC RESEARCH TUNNEL WITHOUT TURBULENCE GRID.
(a) 60° FROM DOWNSTREAM

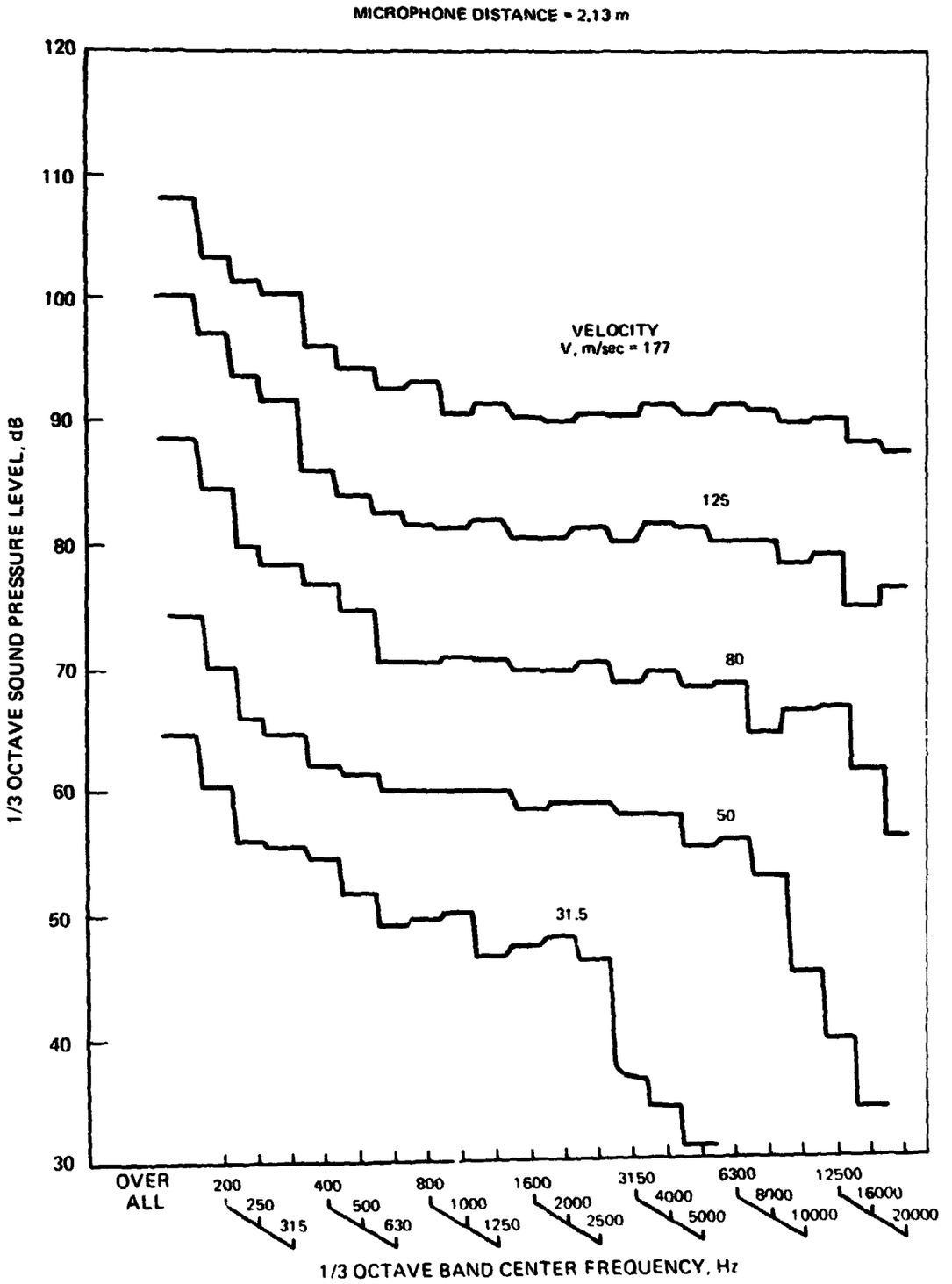

FIGURE 10. – CONTINUED (b) 90° FROM DOWNSTREAM

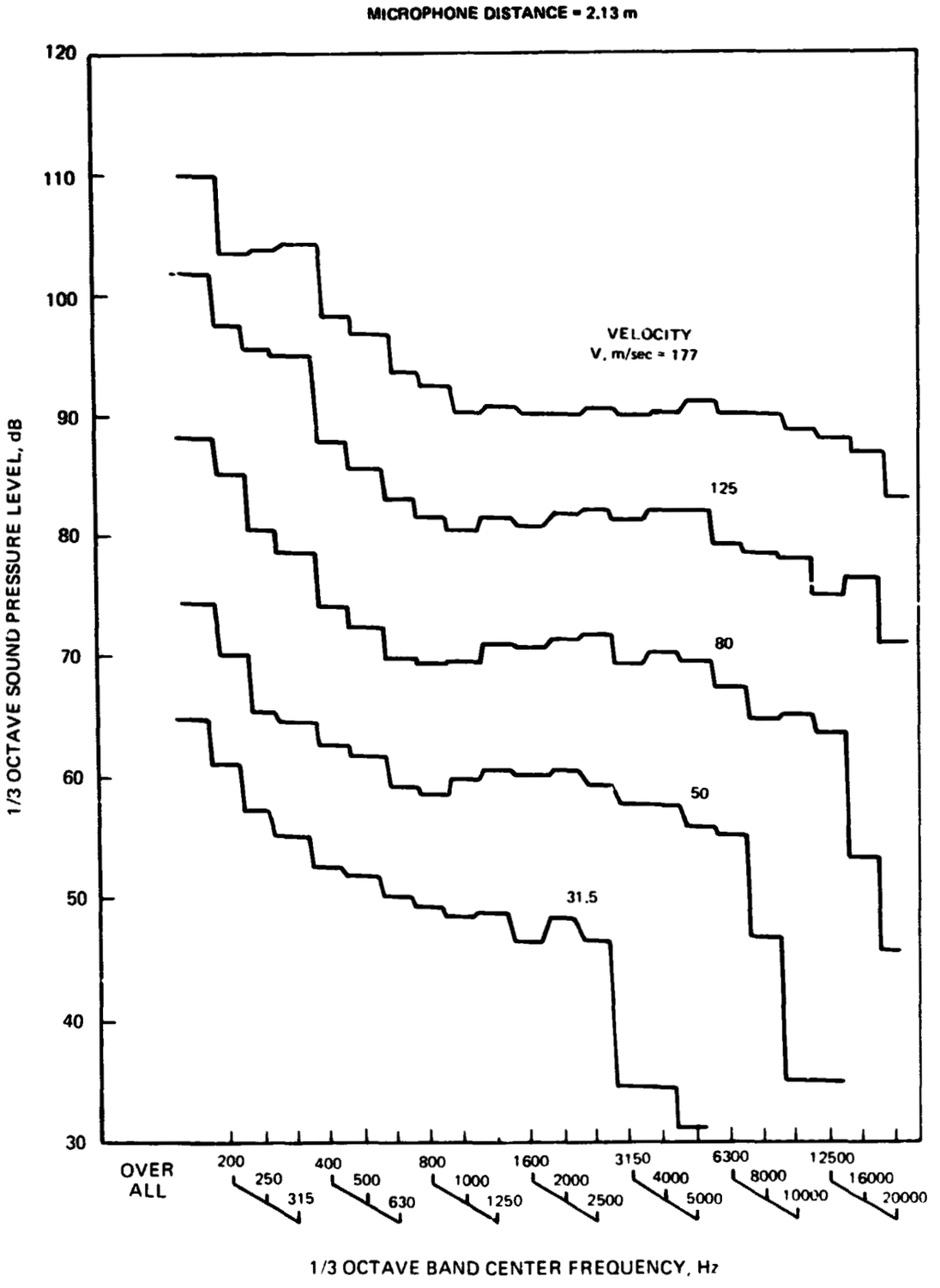

FIGURE 10. – CONCLUDED. (c) 120° FROM DOWNSTREAM

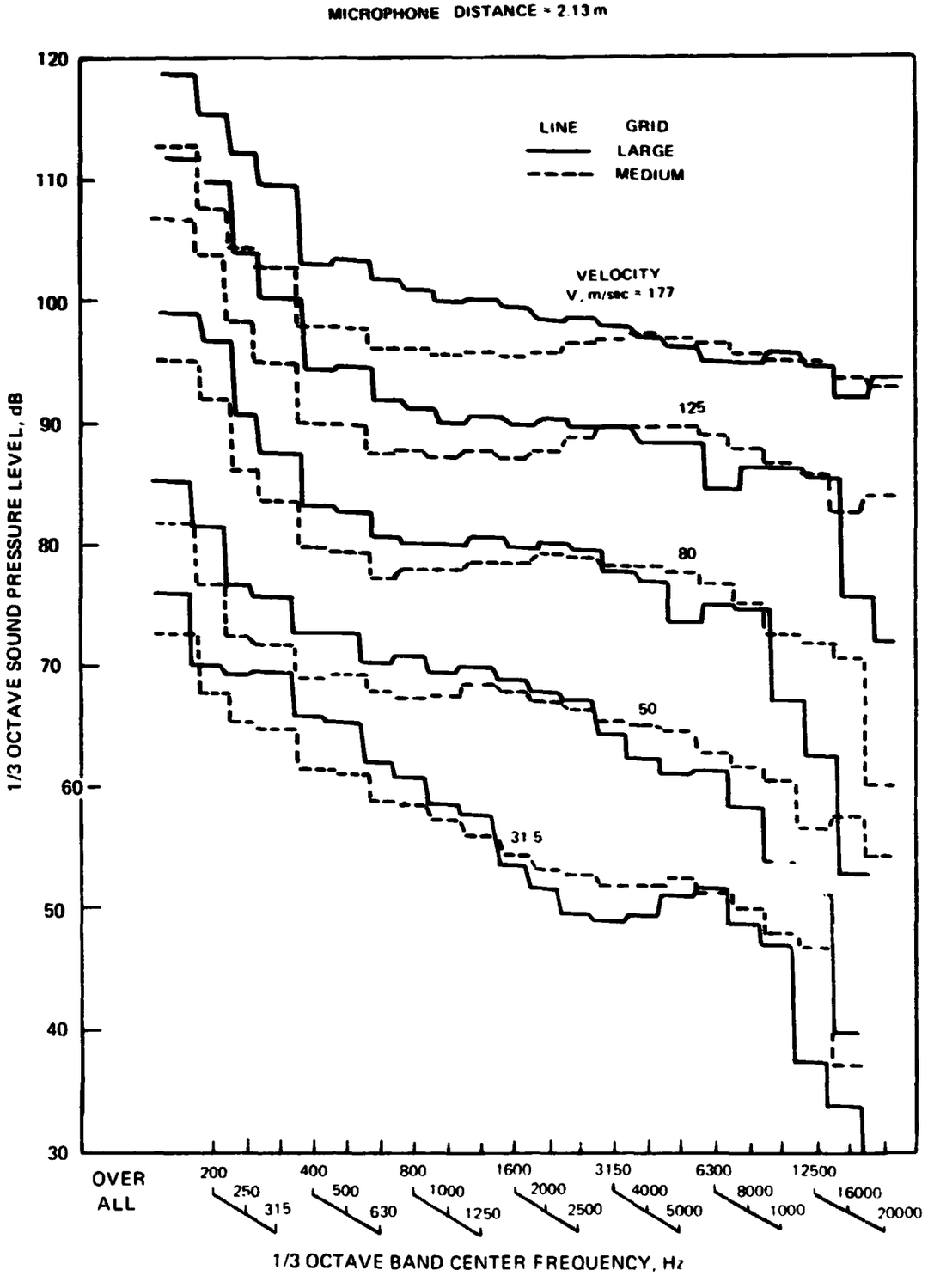

FIGURE 11. – BACKGROUND NOISE OF ACOUSTIC RESEARCH TUNNEL WITH TURBULENCE GRIDS. (a) 60° FROM DOWNSTREAM

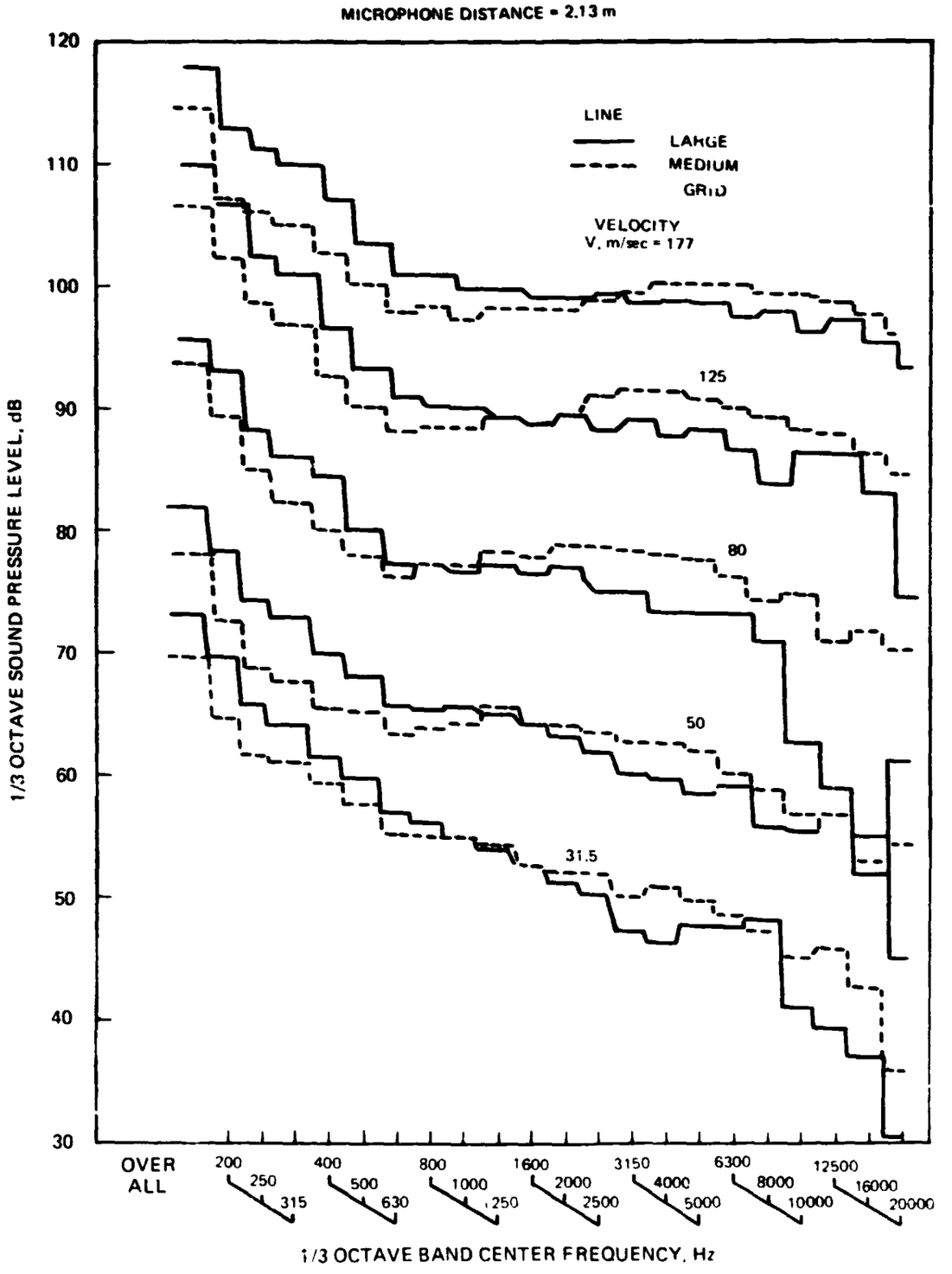

N05-136-11

FIGURE 11. – CONTINUED (b) 90° FROM DOWNSTREAM

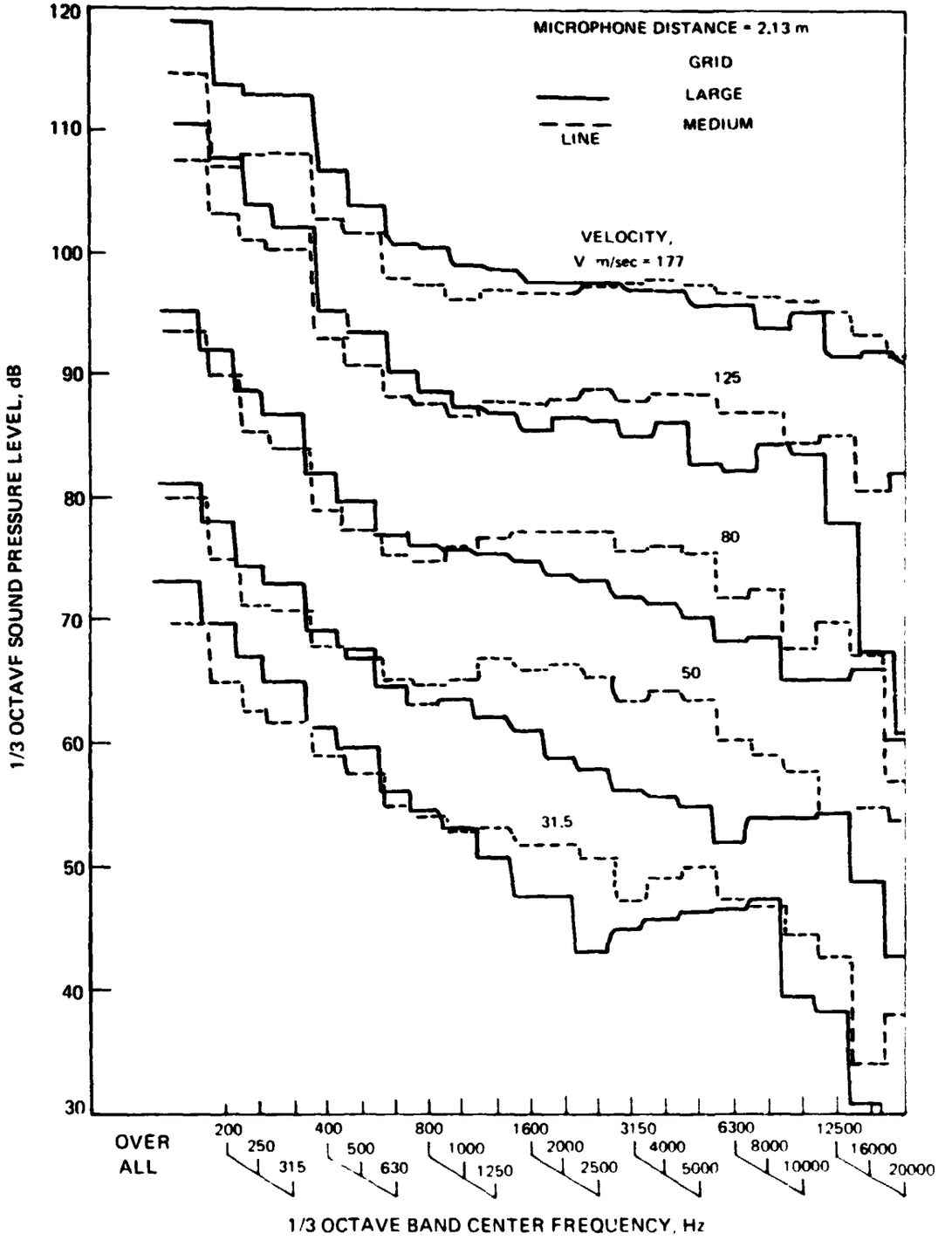

FIGURE 11. – CONCLUDED. (c) 120° FROM DOWNSTREAM

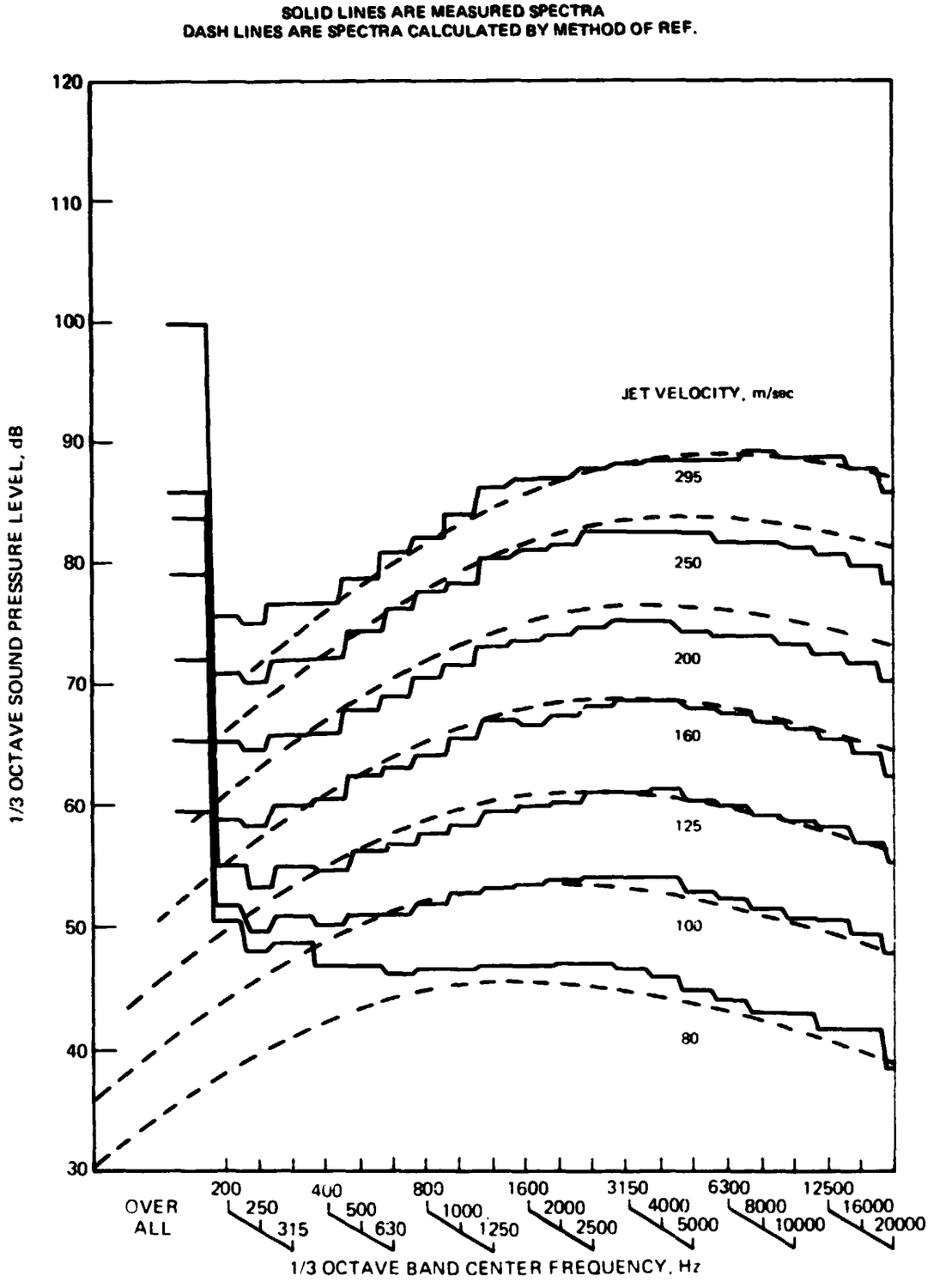

FIGURE 12. – MEASURED AND PREDICTED FAR FIELD SPECTRA FOR A 4.9 cm (1.9 IN.) UNHEATED SUBSONIC JET. (a) 120° FROM DOWNSTREAM

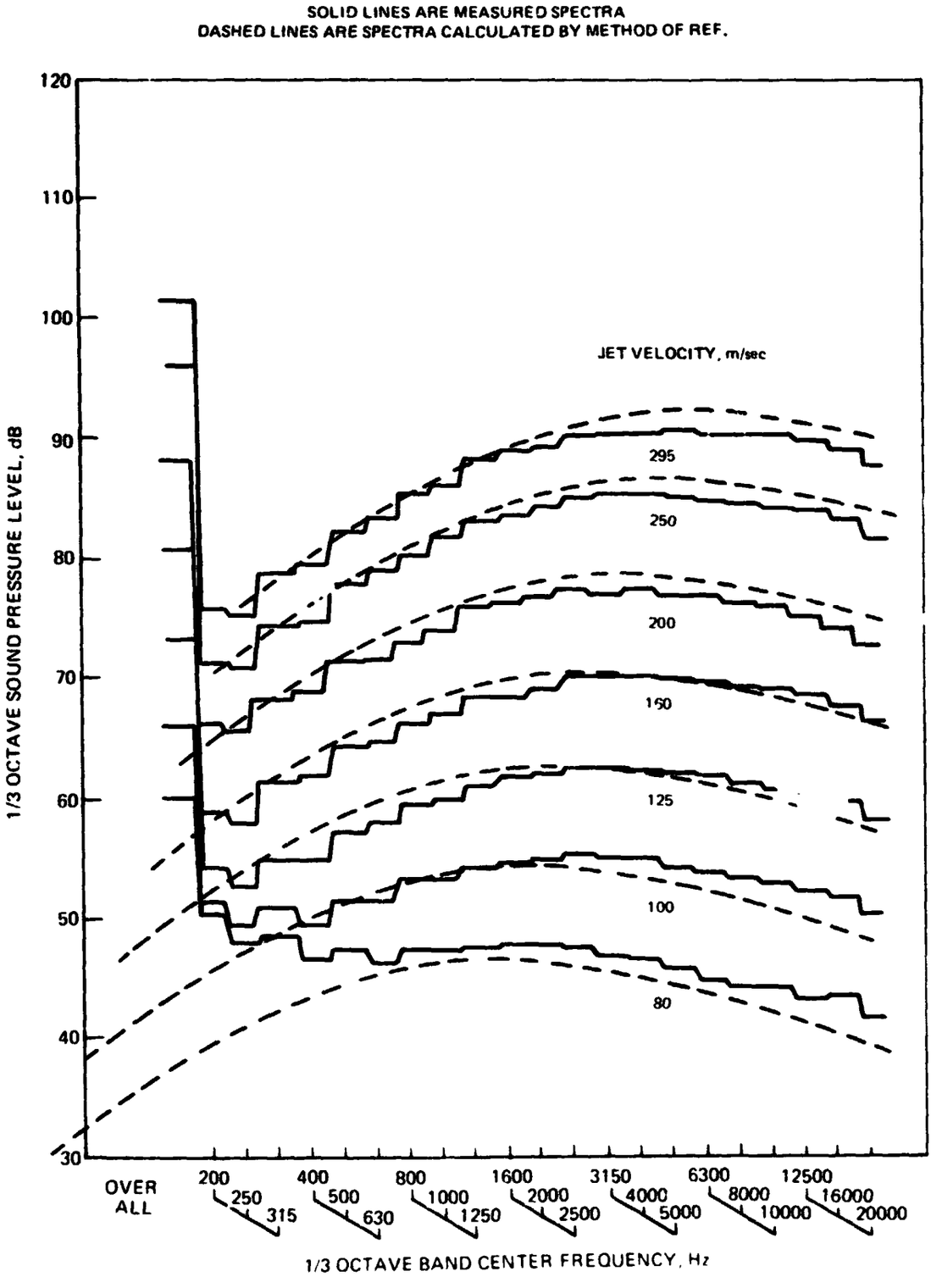

FIGURE 12. – CONTINUED. (b) 90° FROM DOWNSTREAM.

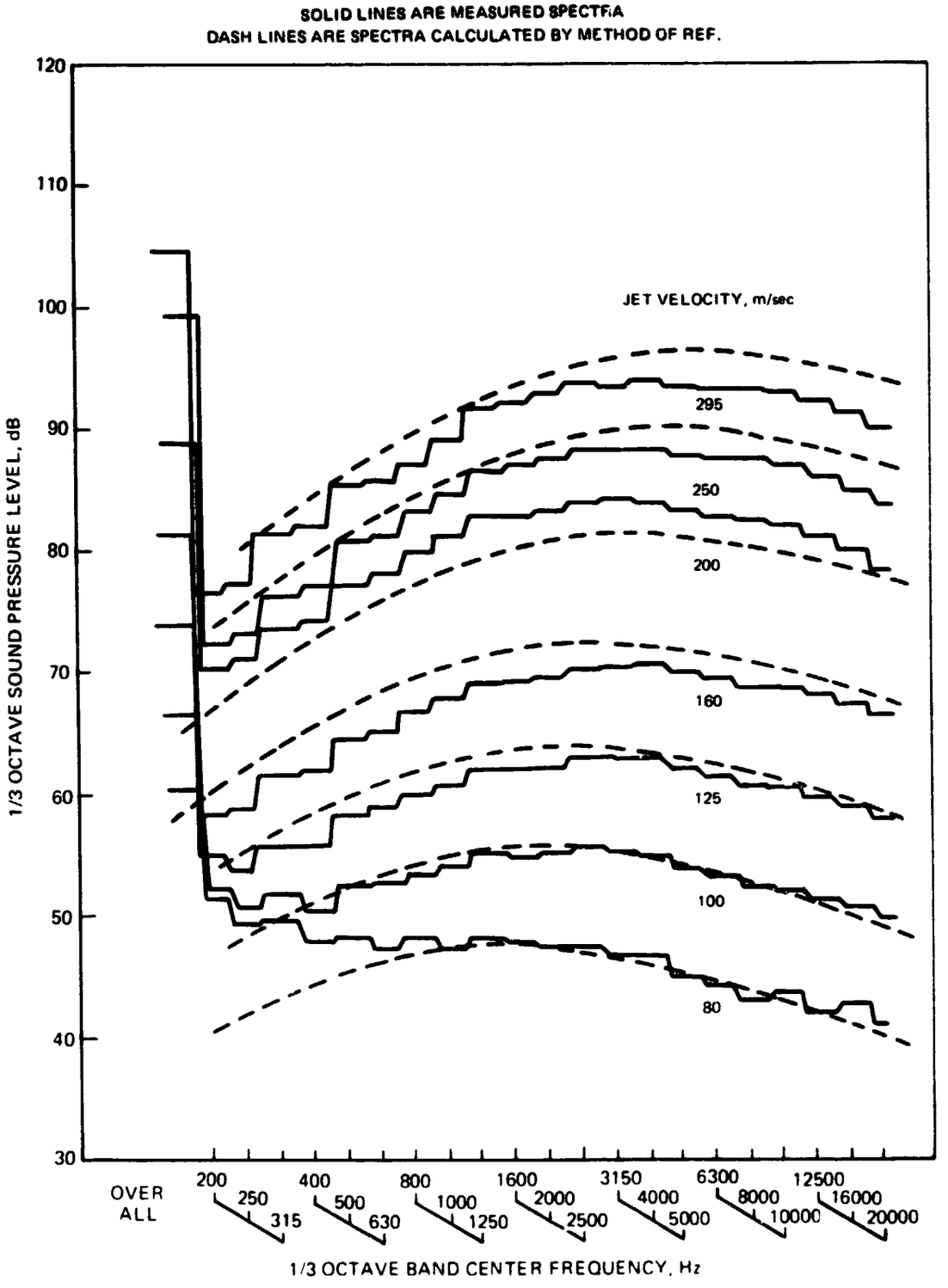

FIGURE 12. – CONCLUDED (c) 60° FROM DOWNSTREAM

LARGE GRID

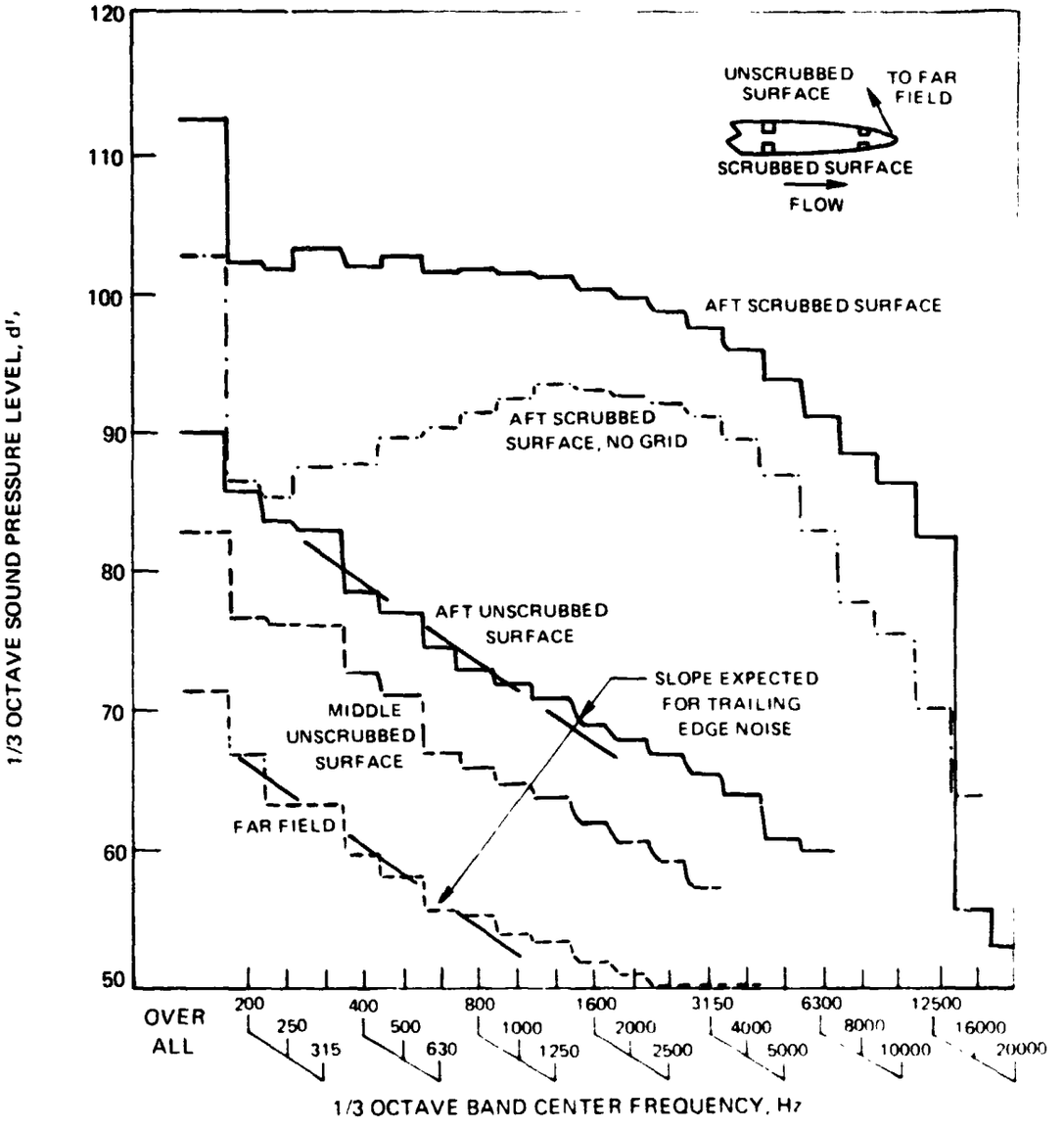

FIGURE 13. TYPICAL SPECTRA FOR TRAILING EDGE NOISE, LARGE GRID.

(a) 31.5 m/sec VELOCITY

LARGE GRID

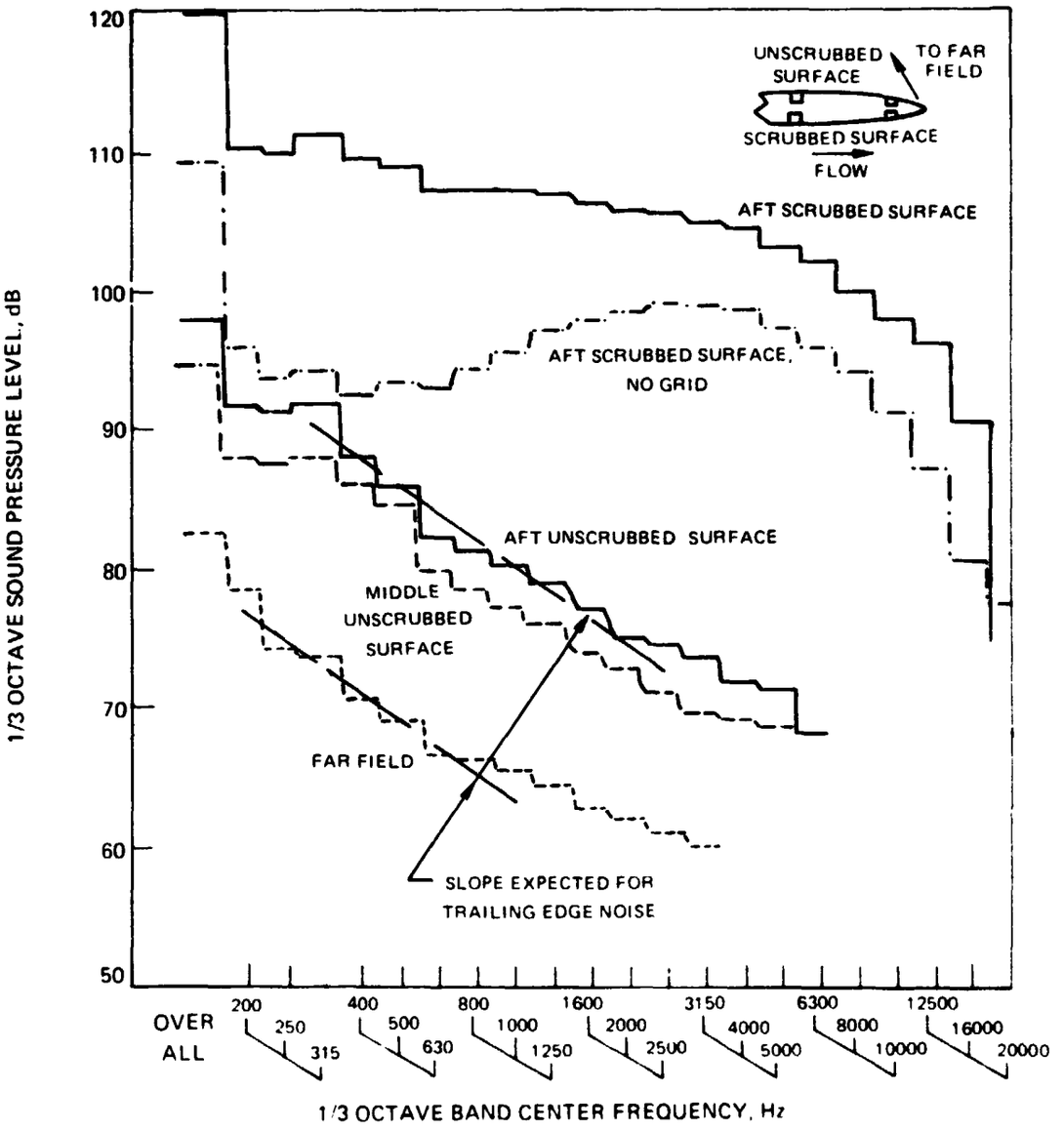

FIGURE 13. -- CONTINUED. (b) 50 M/SEC VELOCITY

LARGE GRID

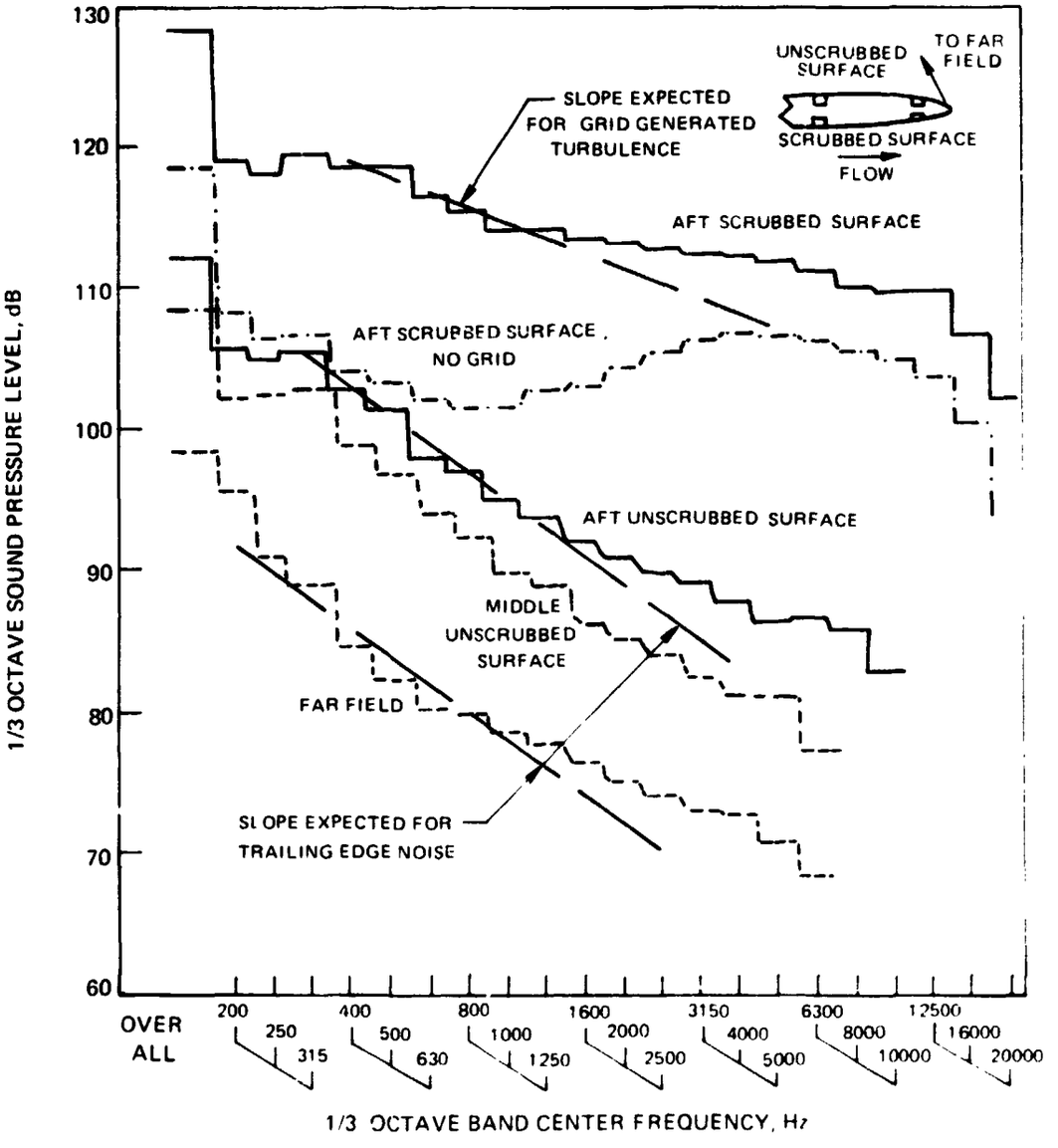

FIGURE 13. – CONTINUED. (c) M/SEC VELOCITY

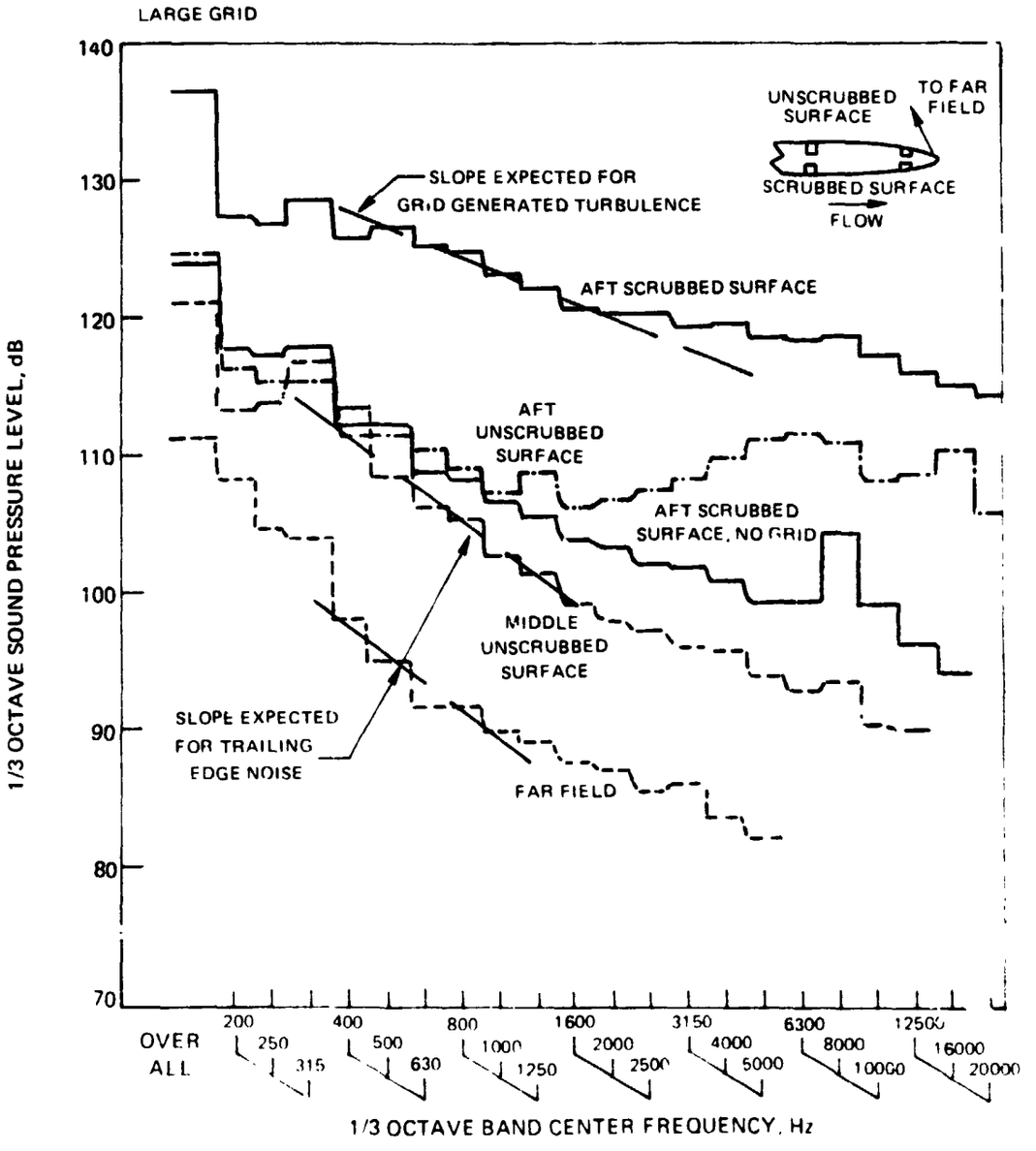

FIGURE 13. – CONTINUED. (d) 125 M/SEC VELOCITY

LARGE GRID

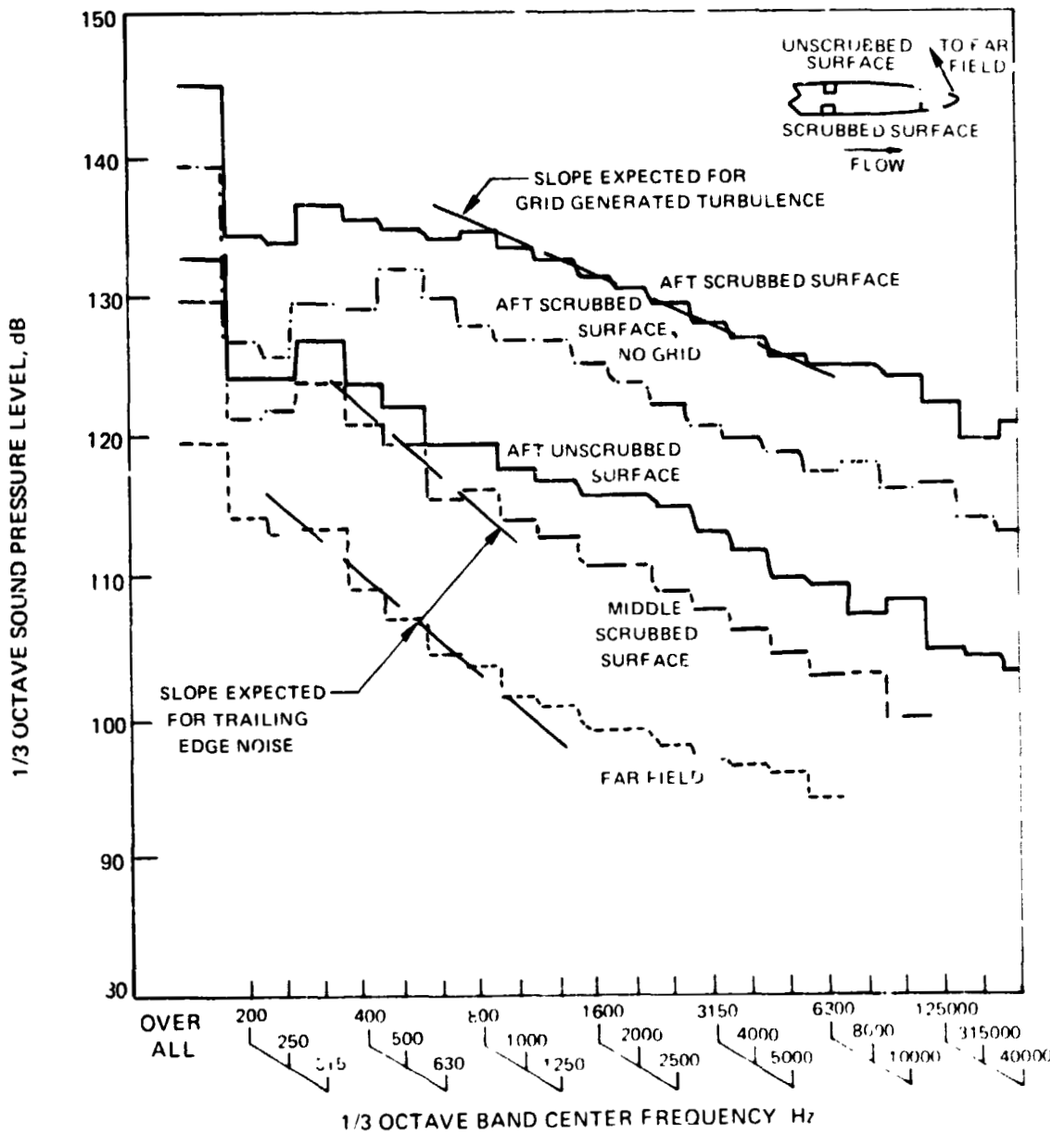

FIGURE 13. – CONCLUDED. (e) 177 M/SEC VELOCITY

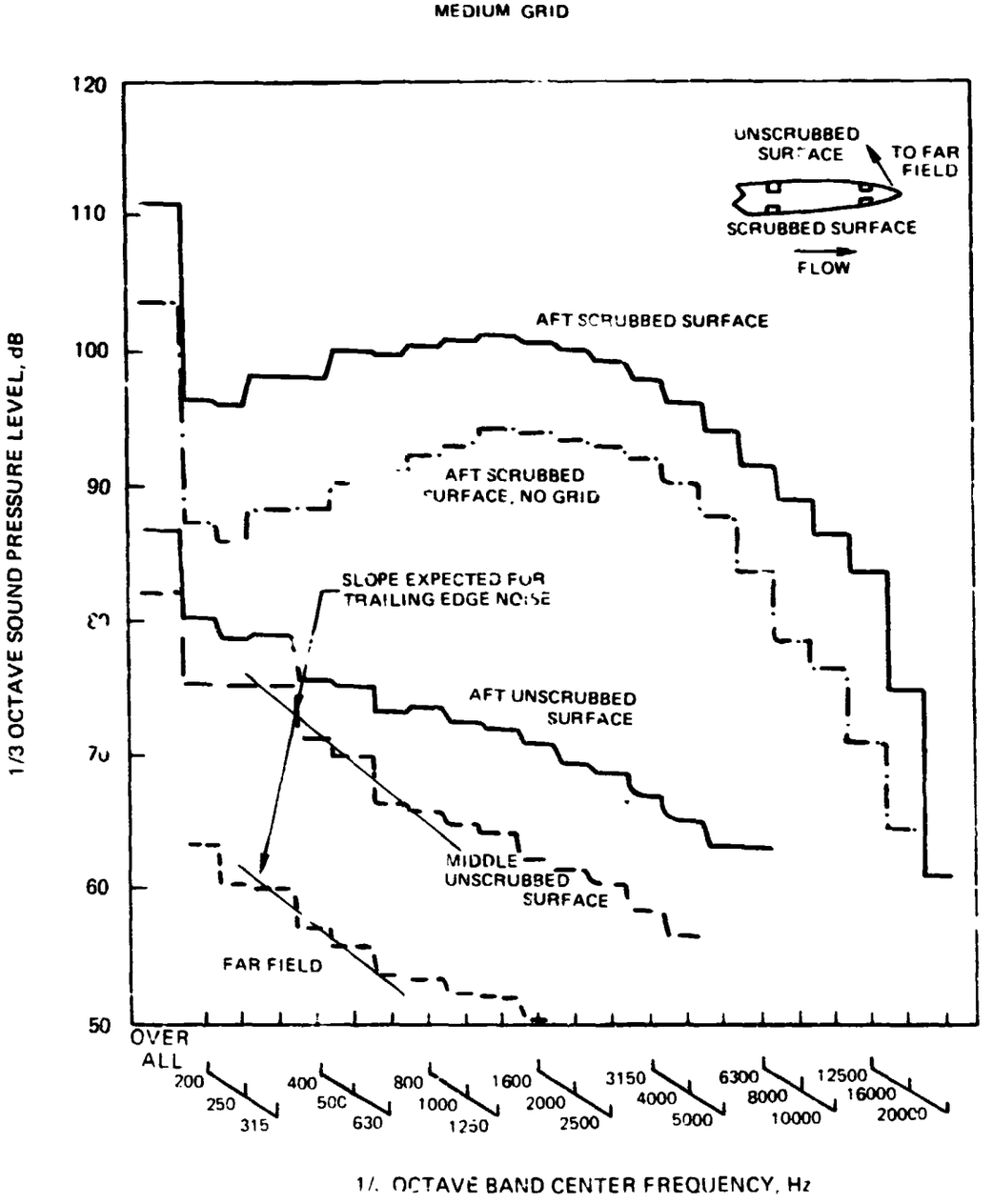

FIGURE 14. – TYPICAL SPECTRA FOR TRAILING EDGE NOISE, MEDIUM GRID.

(a) 31.5 M/SEC VELOCITY

MEDIUM GRID

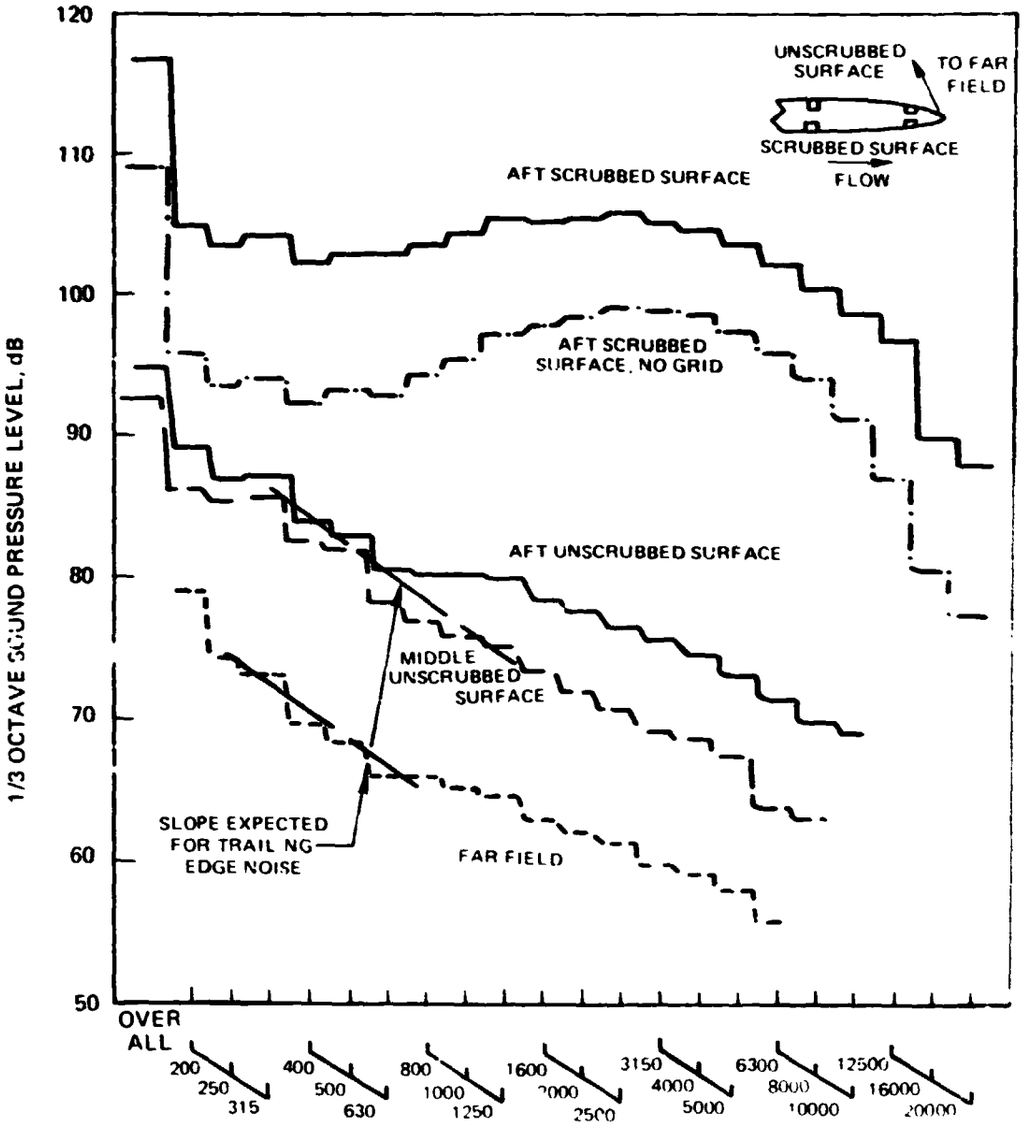

FIGURE 14. – CONTINUED. (b) 50 m/sec VELOCITY

MEDIUM GRID

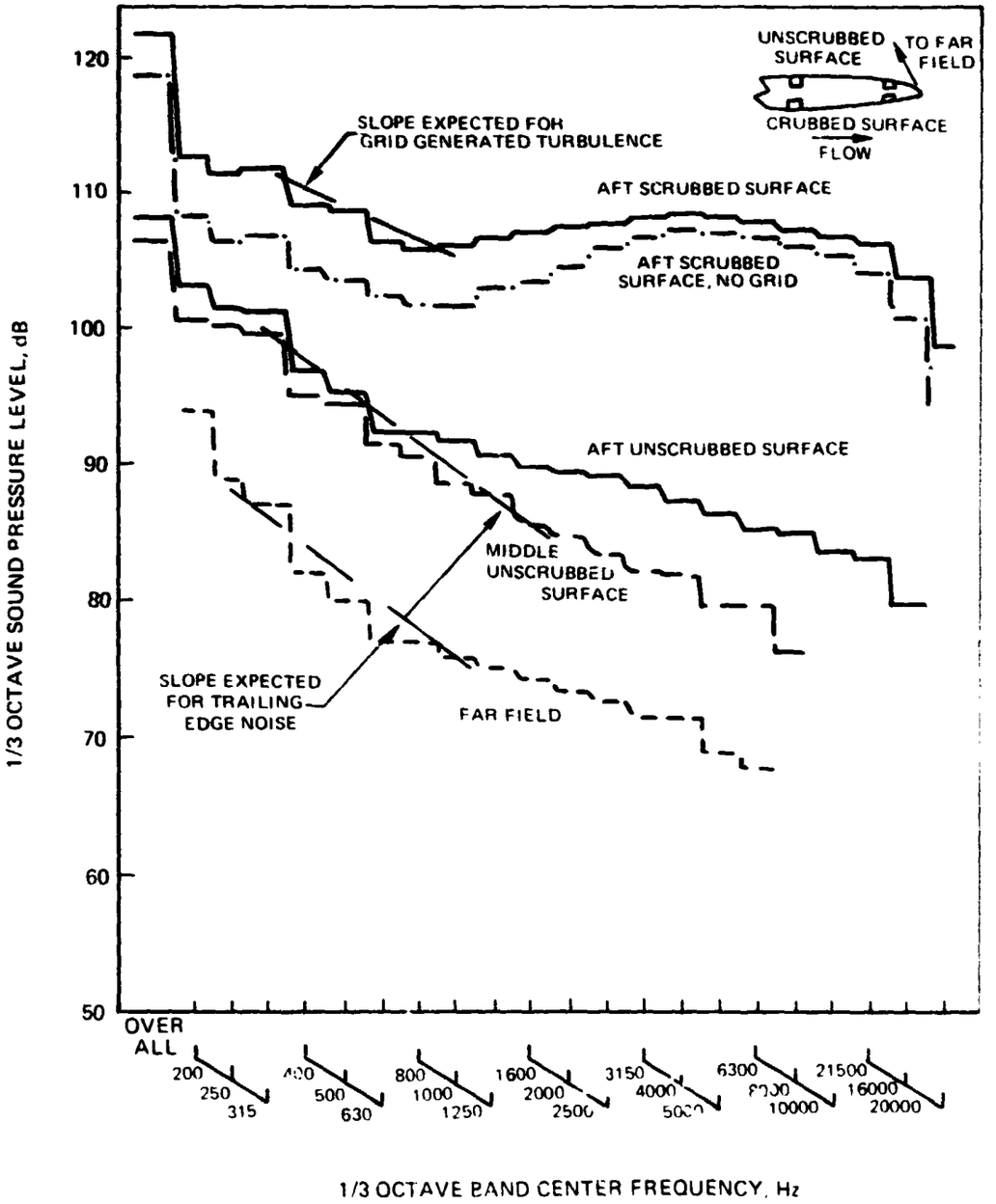

FIGURE 14. – CONTINUED (c) 80 m/sec VELOCITY M/SEC

MEDIUM GRID

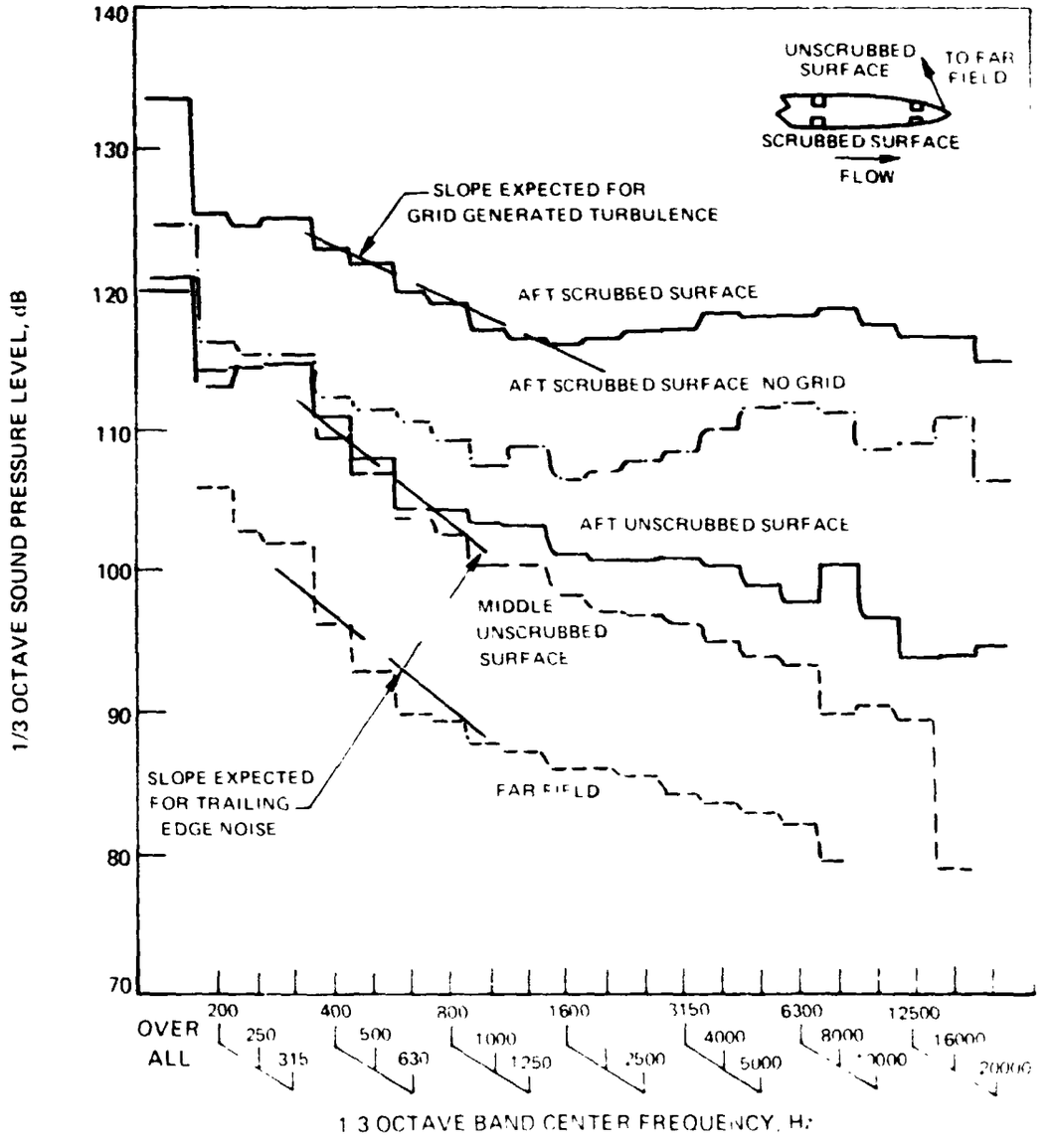

FIGURE 14. – CONTINUED (d) 125 M/SEC VELCOITY

MEDIUM GRID

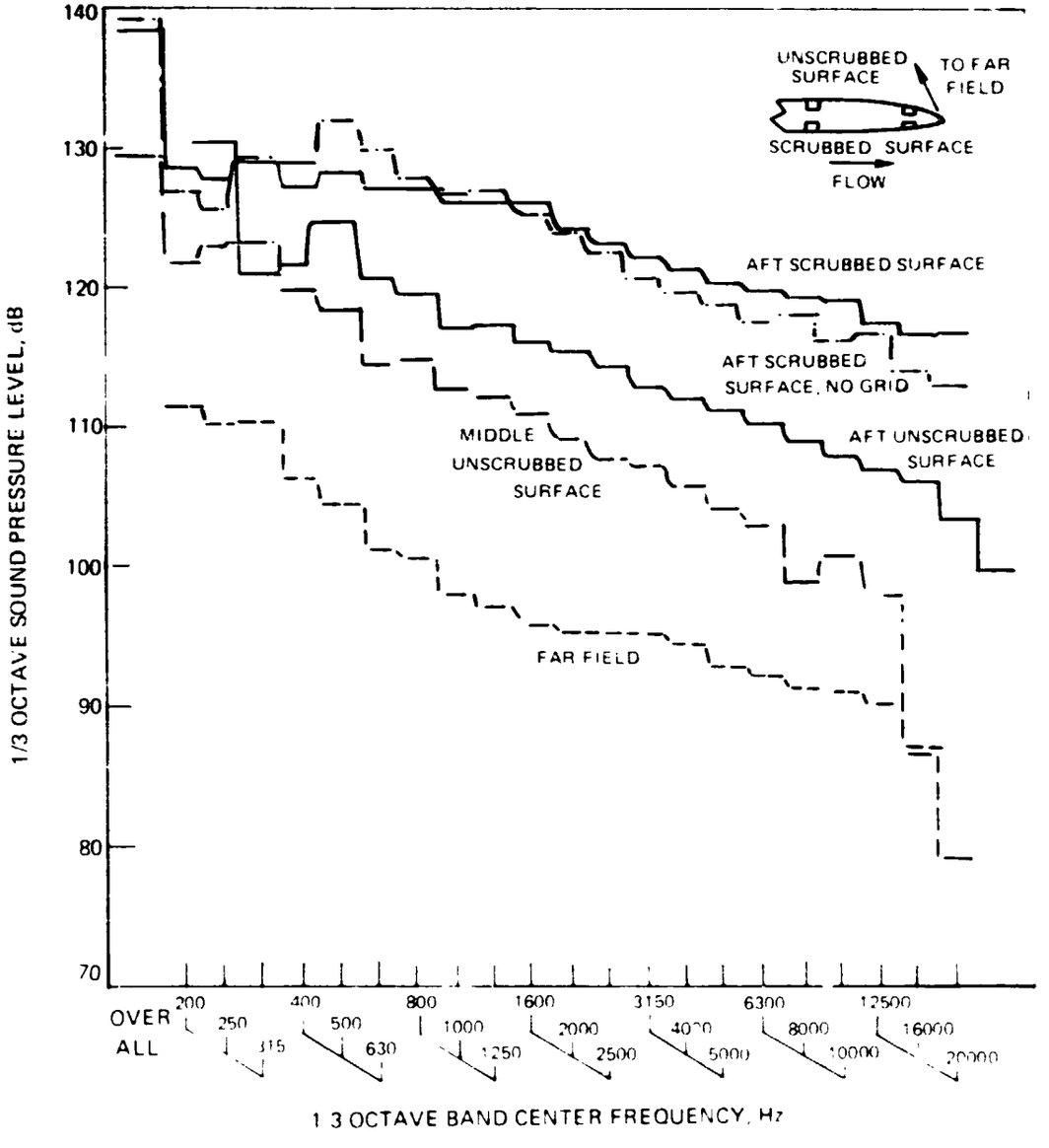

FIGURE 14. – CONCLUDED (e) 177 M/SEC VELOCITY

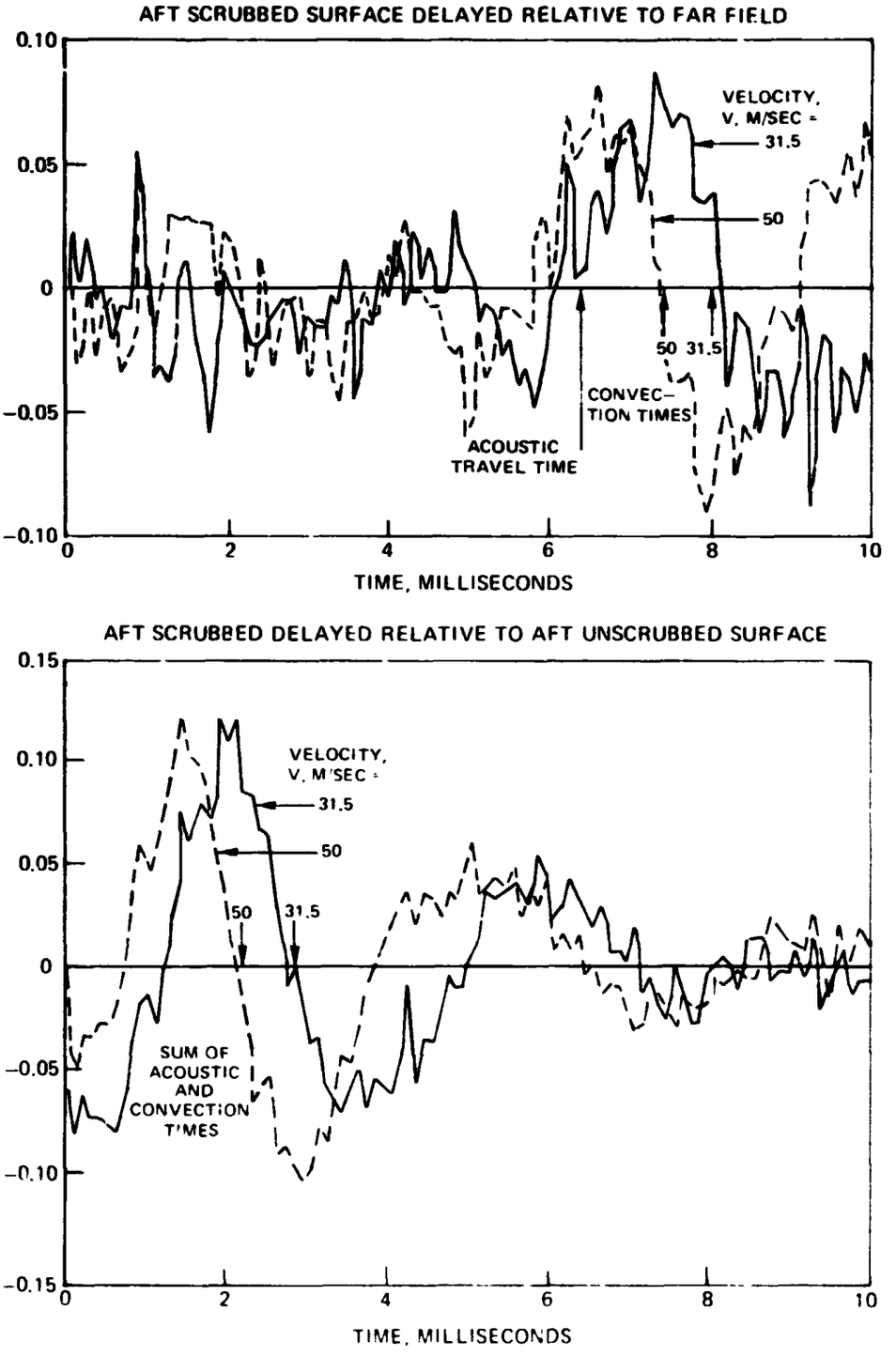

FIGURE 15. -- CROSS–CORRELATIONS OF PRESSURE SPECTRUM ON AFT SCRUBBED SURFACE WITH FAR FIELD AND AFT UNSCRUBBED SURFACE

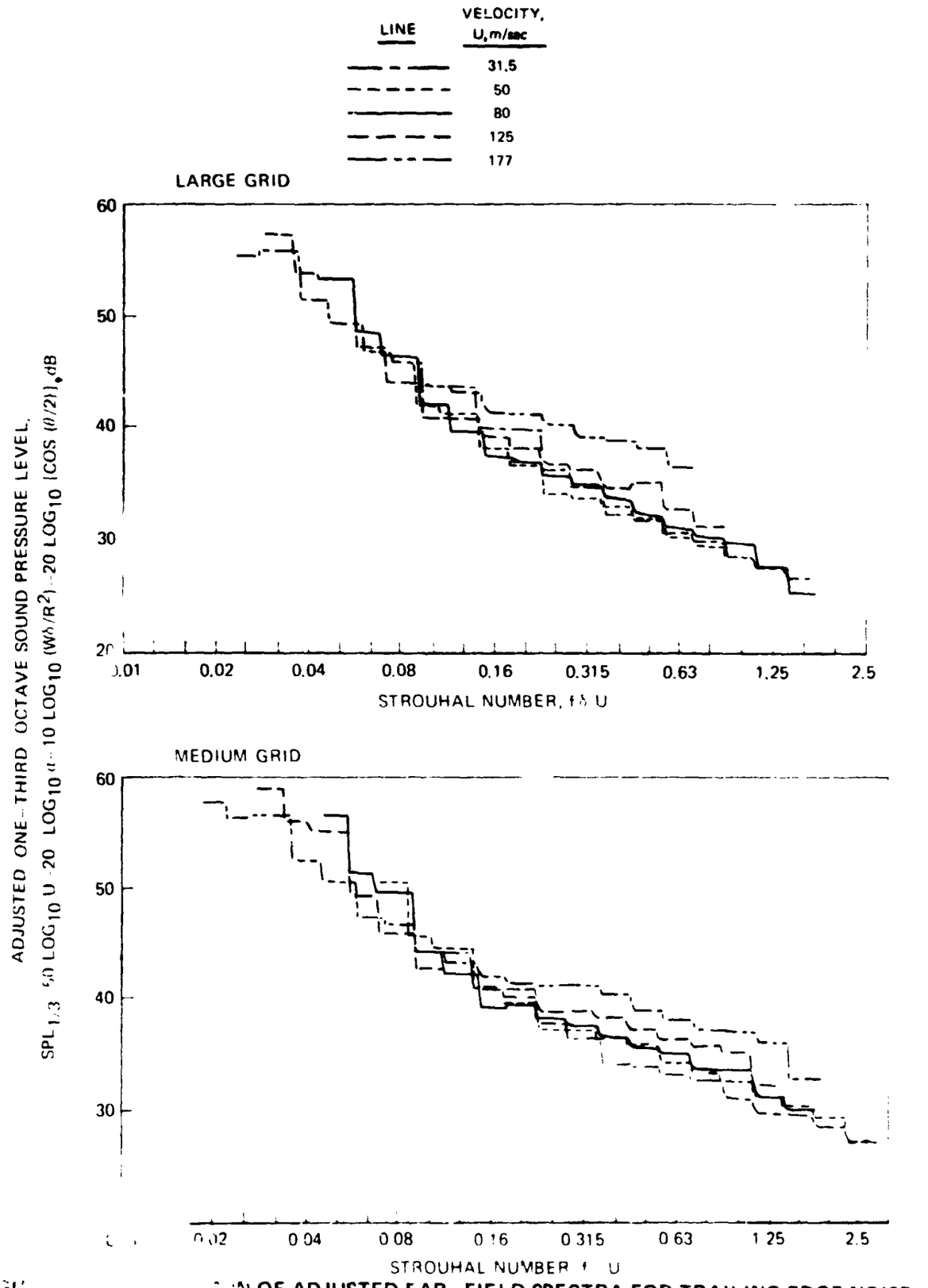

N OF ADJUSTED FAR-FIELD SPECTRA FOR TRAILING EDGE NOISE
0° FROM DOWNSTREAM, PARAMETERS OF FFOWCS WILLIAMS AND HALL.

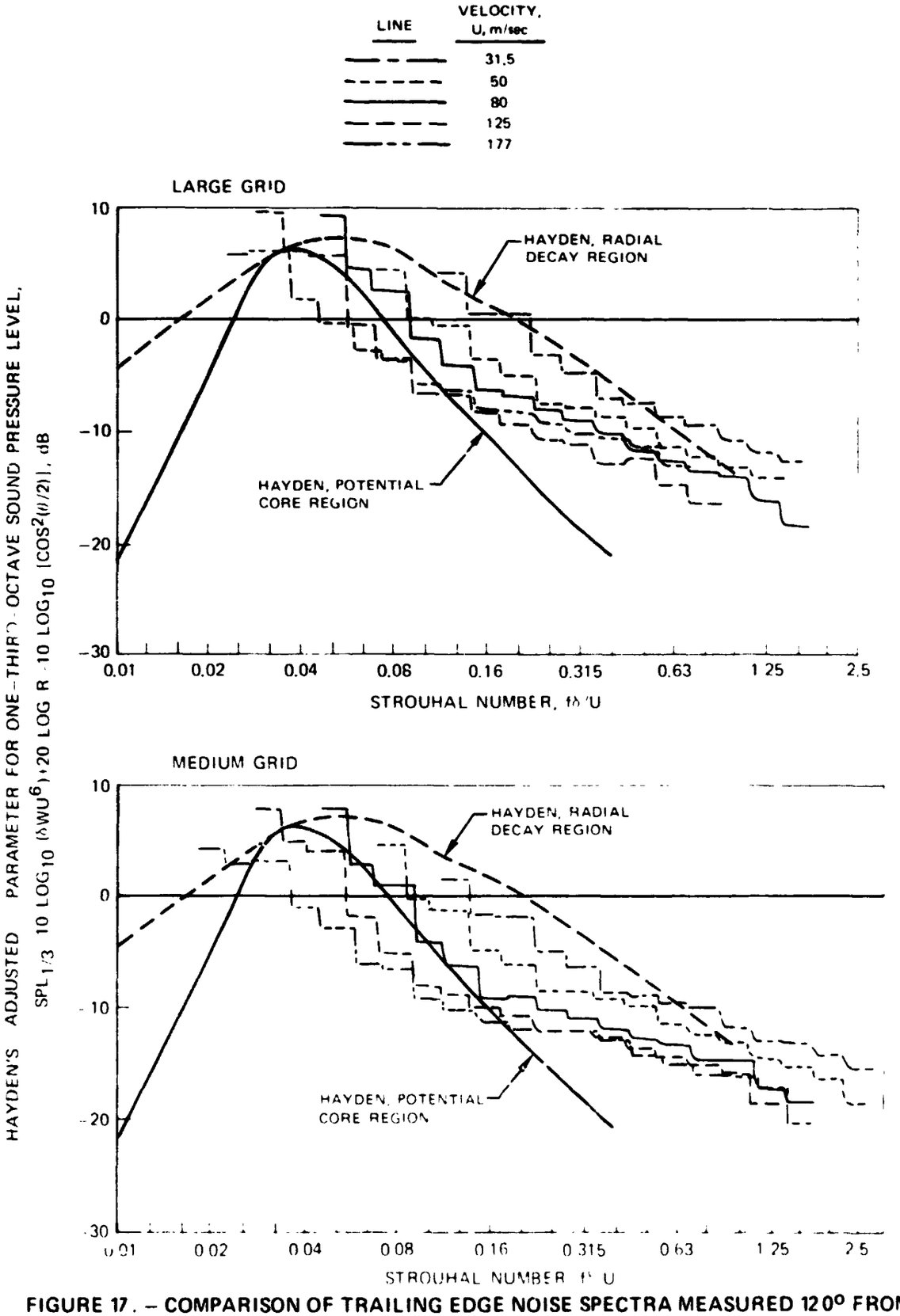

FIGURE 17. – COMPARISON OF TRAILING EDGE NOISE SPECTRA MEASURED 120° FROM DOWNSTREAM WITH HAYDEN'S PREDICTION

CORRELATION OF TRAILING EDGE NOISE SPECTRA FOR UNIFORM VELOCITY AND TURBULENCE

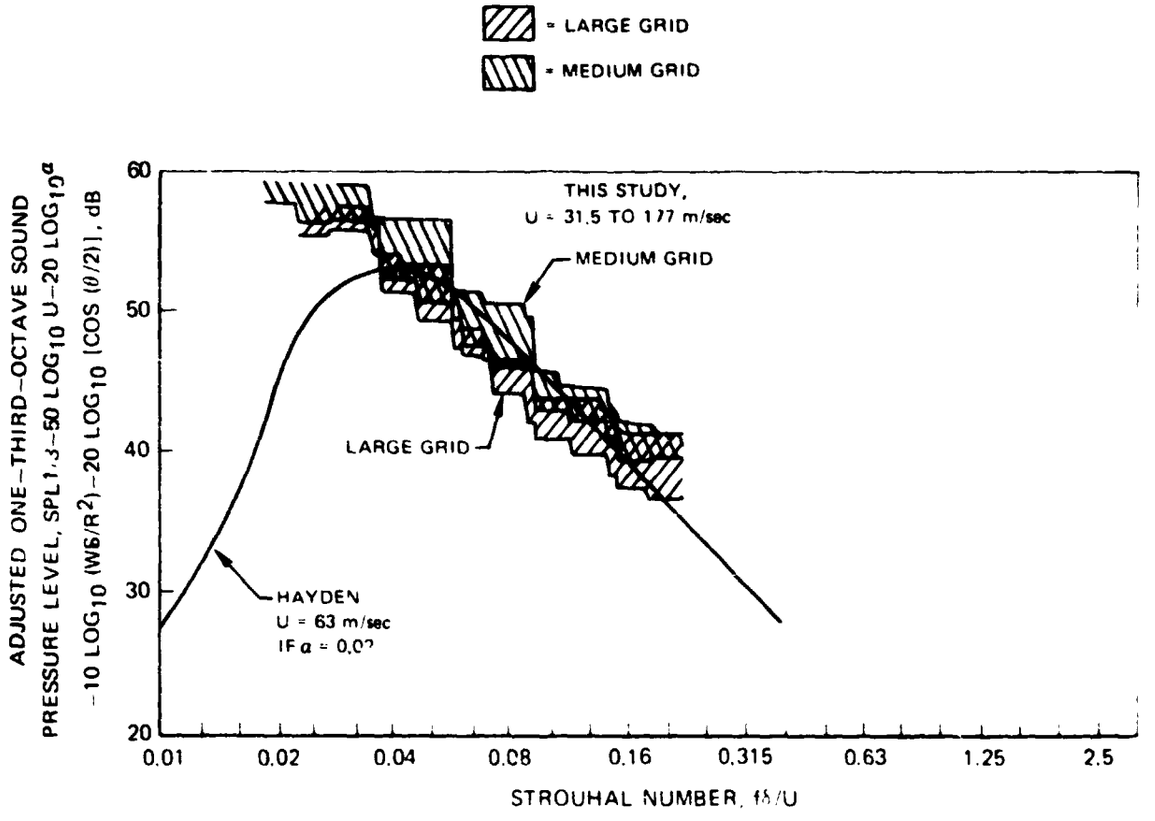

FIGURE 18. – COMPARISON OF TRAILING EDGE NOISE SPECTRA ADJUSTED BY THE PARAMETERS OF FFOWCS WILLIAMS AND HALL

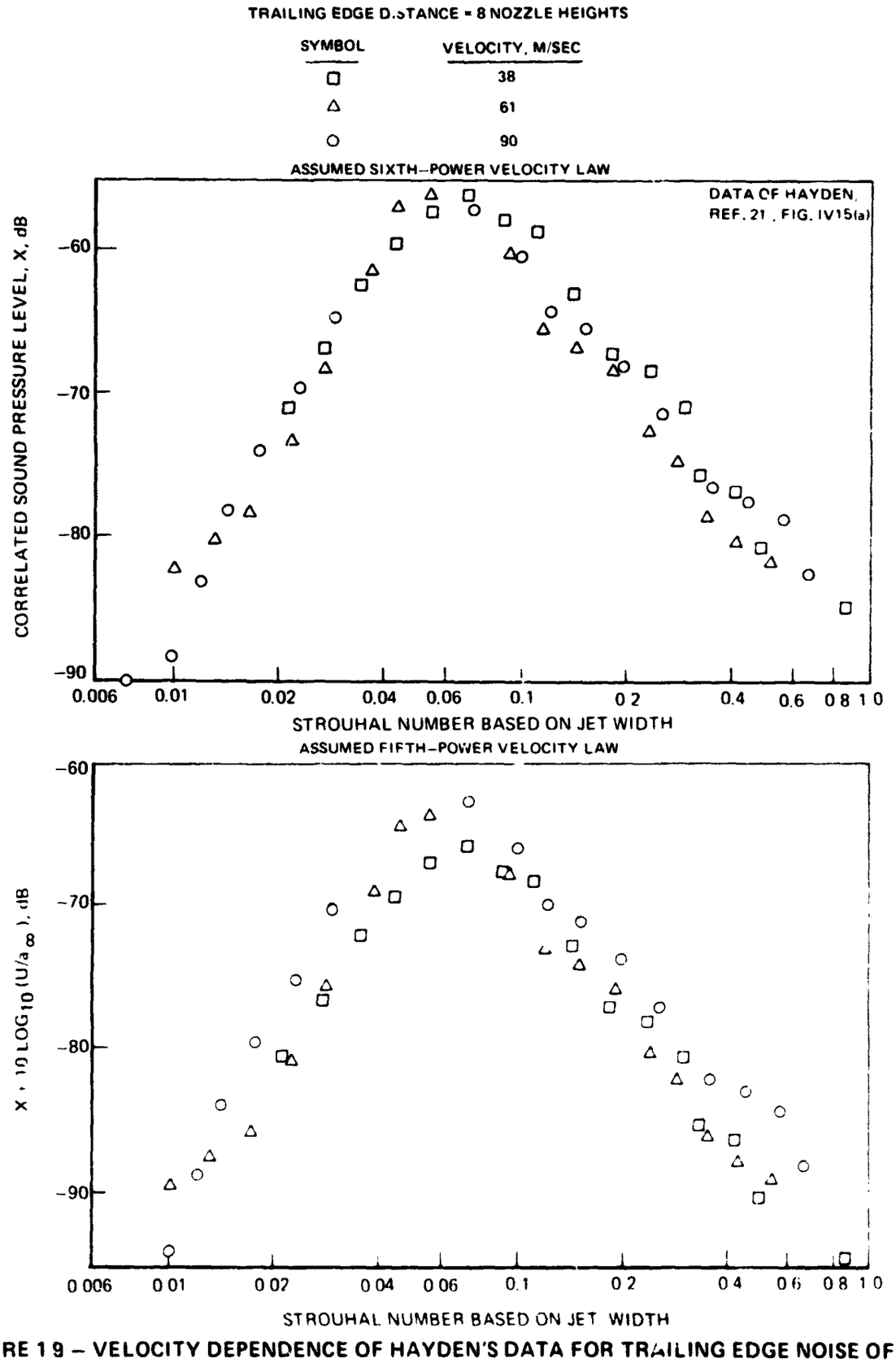

FIGURE 19 – VELOCITY DEPENDENCE OF HAYDEN'S DATA FOR TRAILING EDGE NOISE OF A WALL JET IN THE POTENTIAL CORE REGION. TRAILING EDGE DISTANCE = 8 NOZZLE HEIGHTS

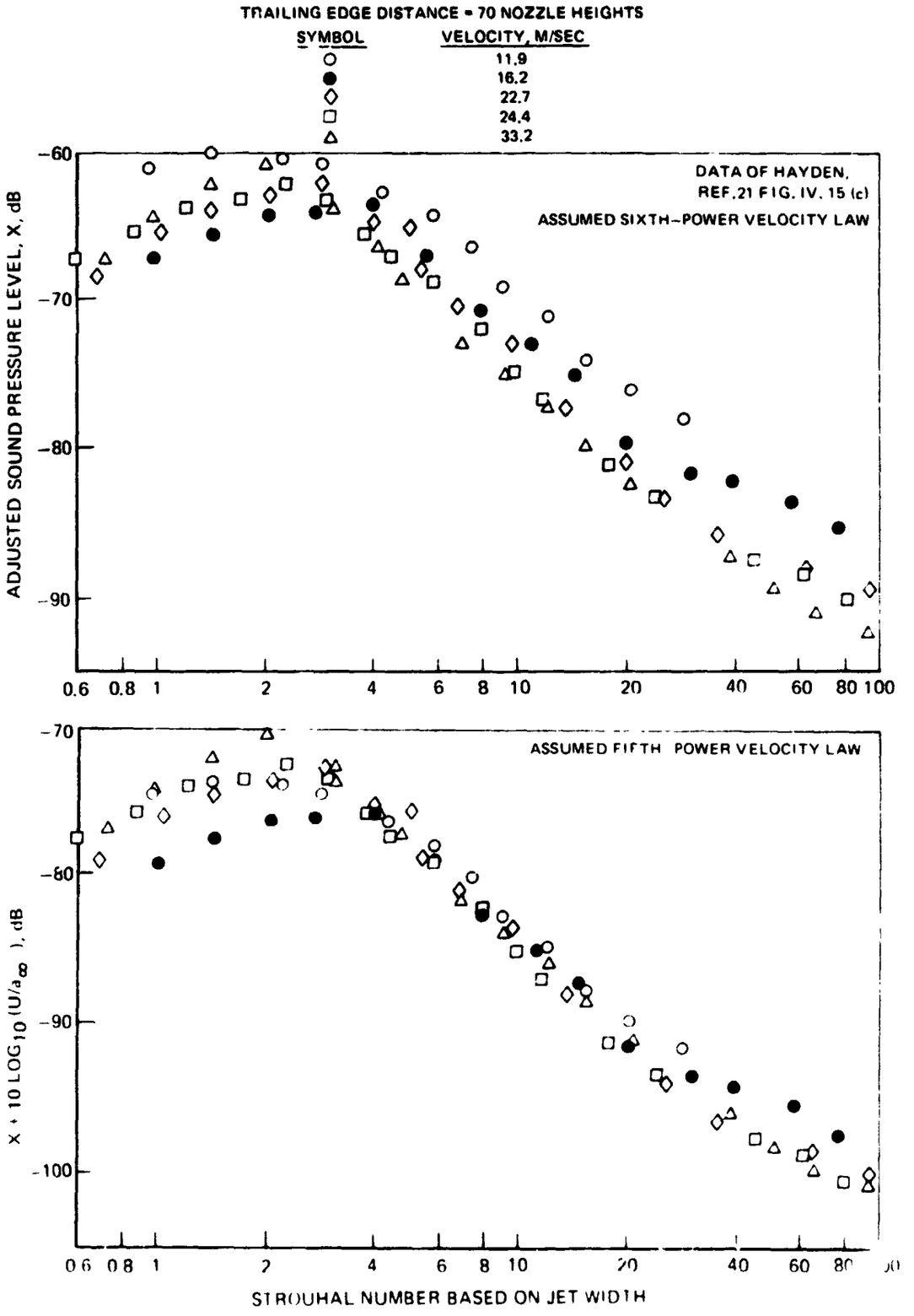

FIGURE 20. – VELOCITY DEPENDENCE OF HAYDEN'S DATA FOR TRAILING EDGE NOISE OF A WALL JET IN THE RADIAL DECAY REGION. TRAILING EDGE DISTANCE = 70 NOZZLE HEIGHTS

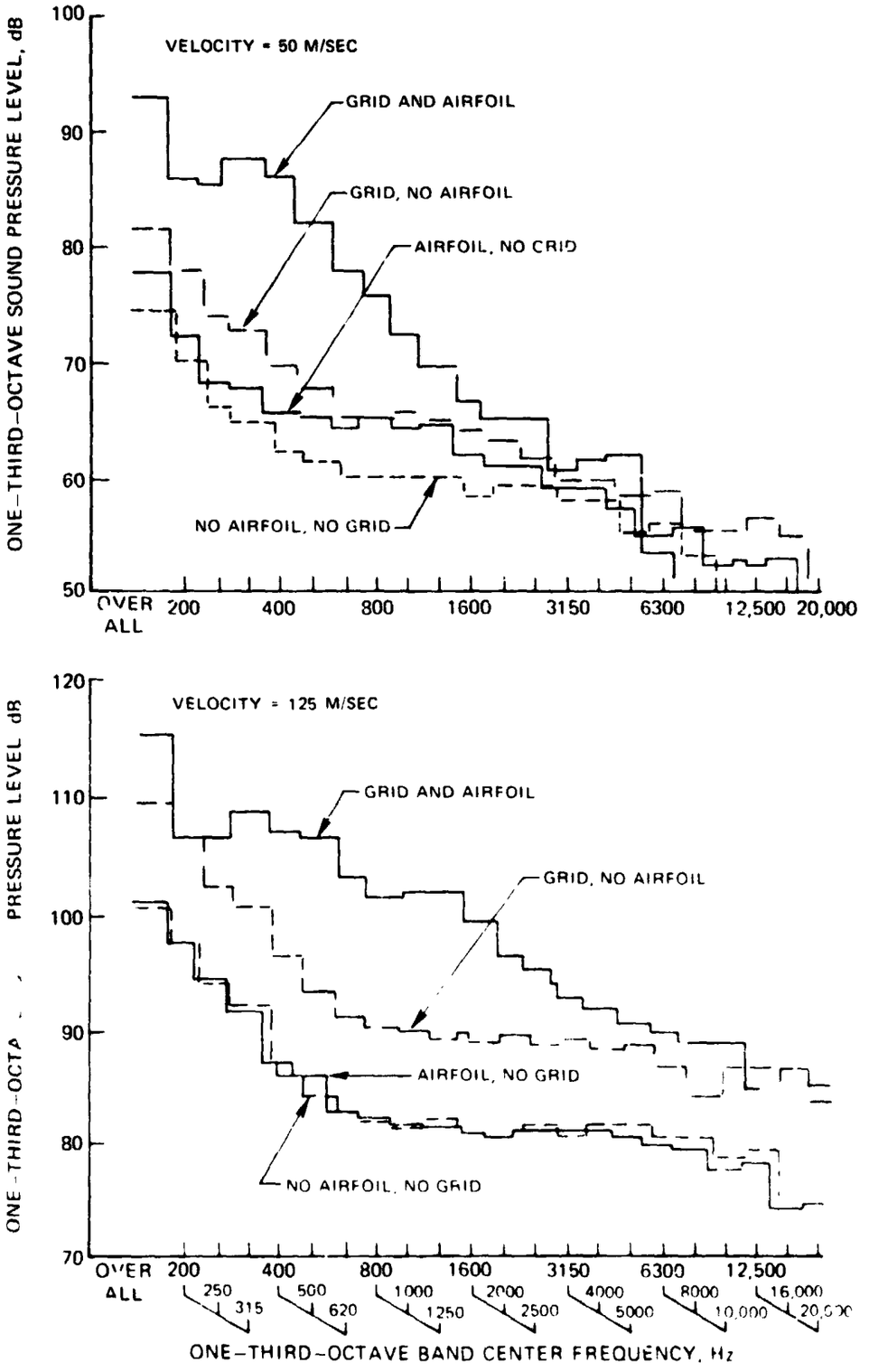

FIGURE 21. – TYPICAL FAR–FIELD SPECTRA FOR AIRFOIL WITH AND WITHOUT INCIDENT TURBULENCE FROM LARGE GRID.

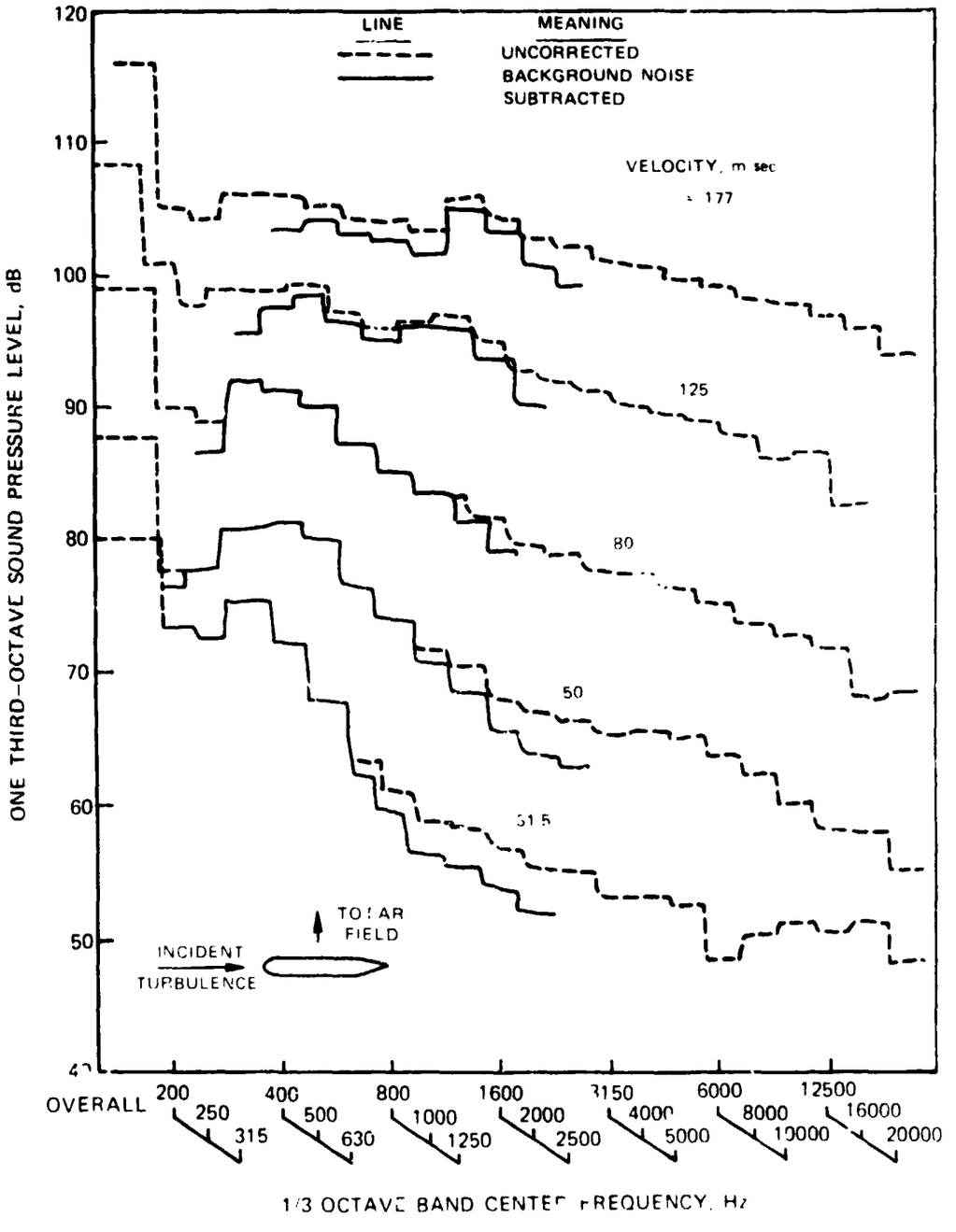

FIGURE 22. – FAR–FIELD SPECTRA FOR AIRFOIL WITH INCIDENT TURBULENCE FROM MEDIUM GRID, UNCORRECTED AND CORRECTED FOR TUNNEL BACKGROUND NOISE, 90° FROM DOWNSTREAM.

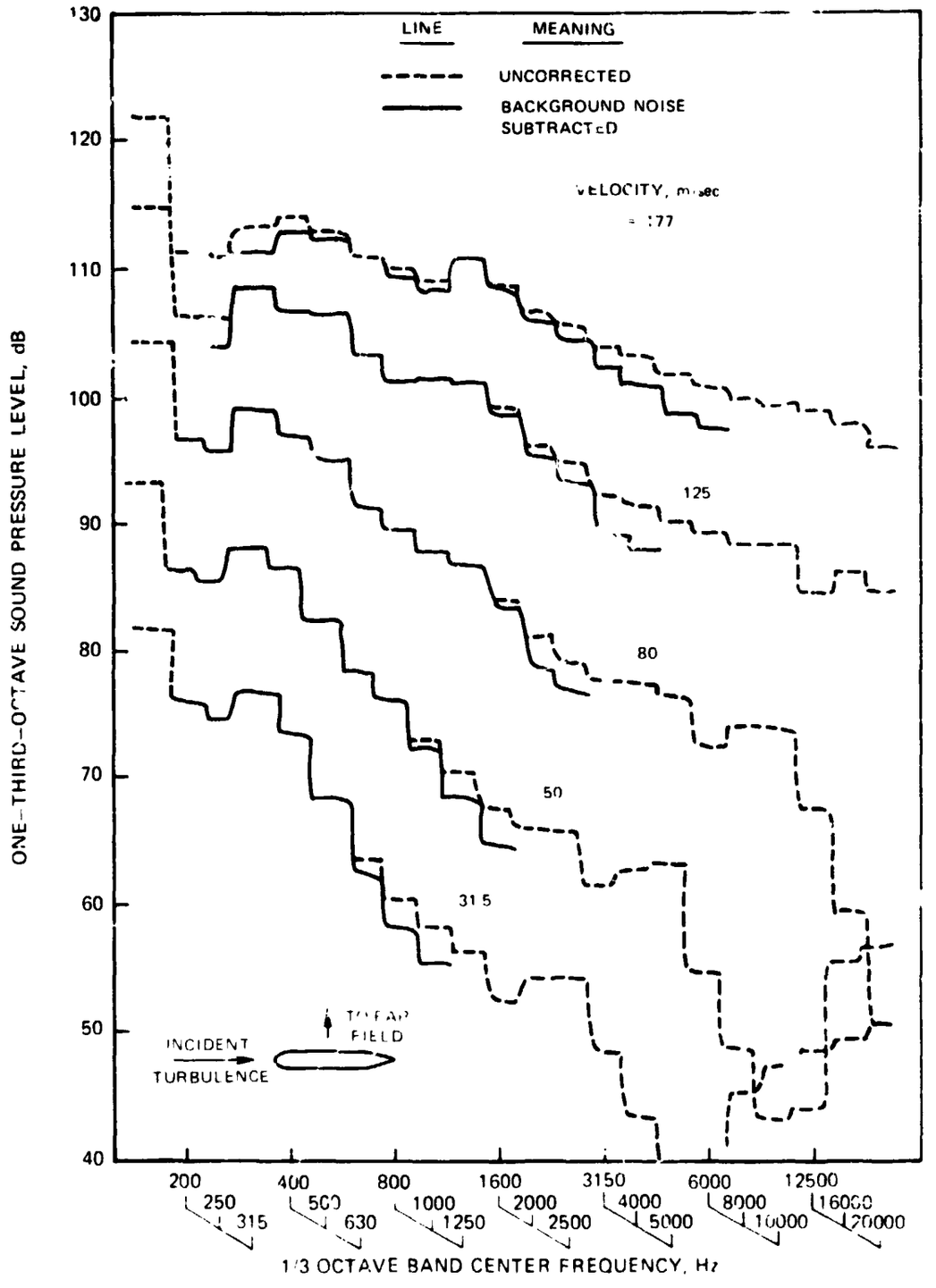

FIGURE 23. -- FAR FIELD SPECTRA FOR AIRFOIL WITH INCIDENT TURBULENCE FROM THE LARGE GRID, UNCORRECTED AND CORRECTED FOR TUNNEL BACKGROUND NOISE, 90° FROM DOWNSTREAM

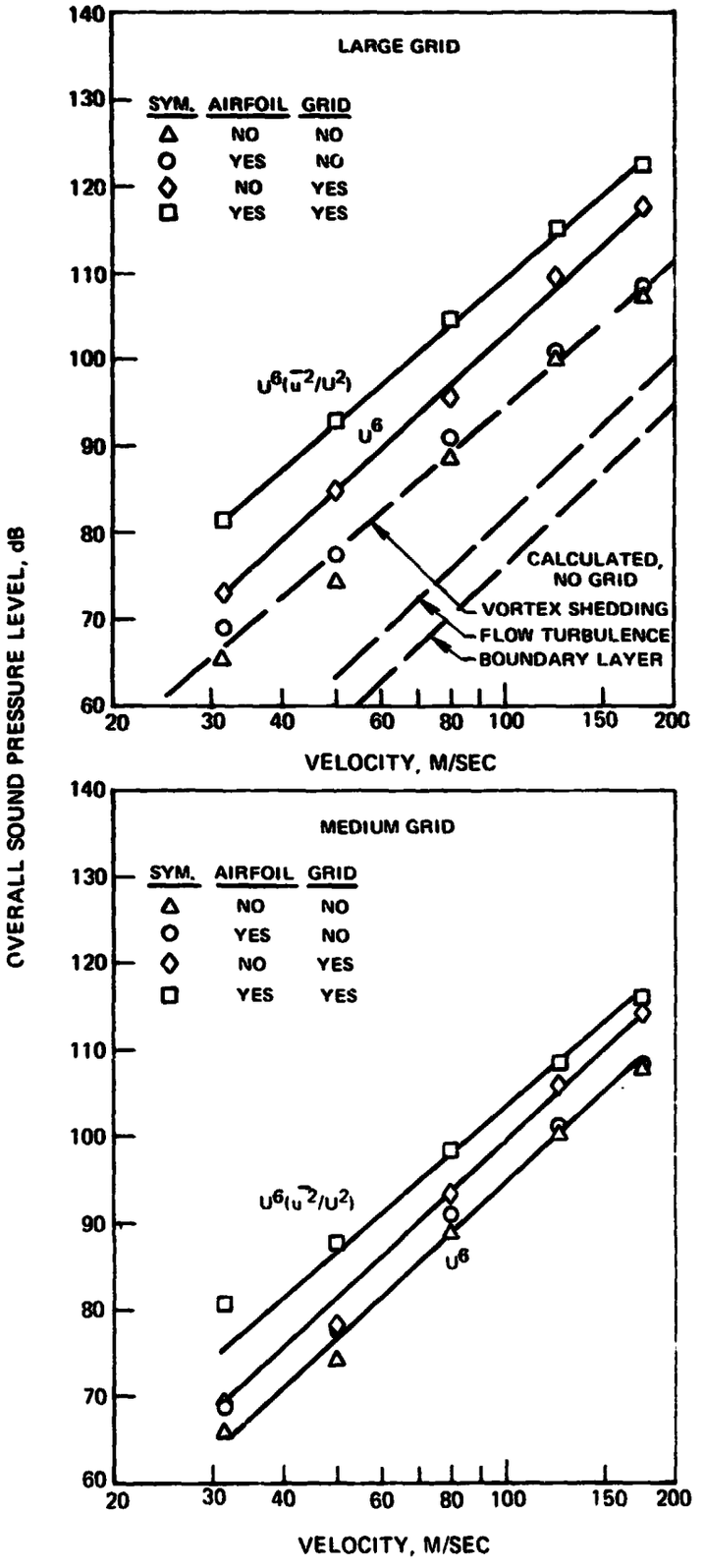

FIGURE 24. – VARIATIONS OF OVERALL SOUND PRESSURE LEVEL WITH VELOCITY FOR VARIOUS COMBINATIONS OF AIRFOIL AND GRID, 90° FROM DOWNSTREAM.

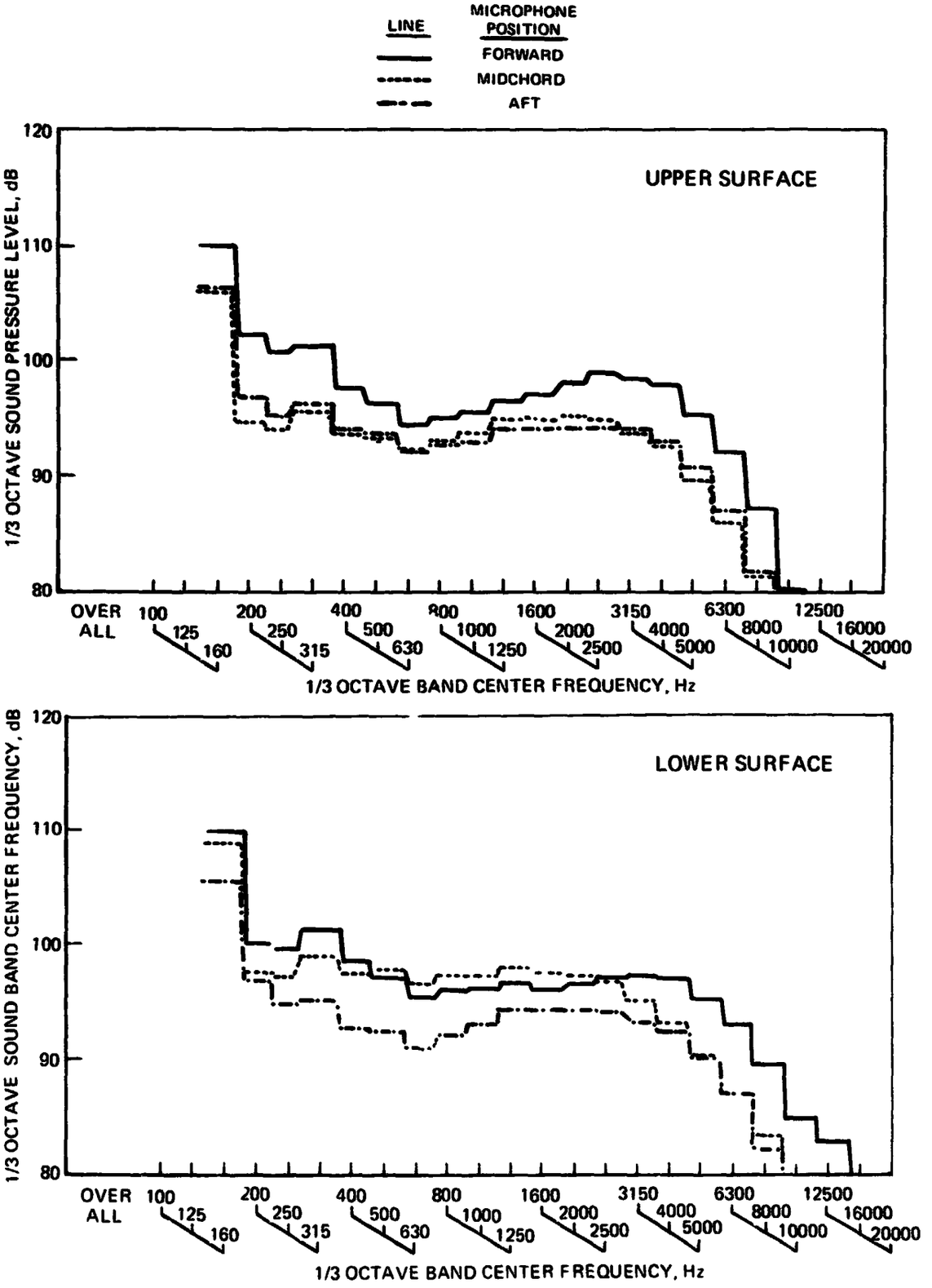

FIGURE 25. – SURFACE PRESSURE SPECTRA ON AIRFOIL WITH INCIDENT TURBULENCE FROM MEDIUM GRID. (a) VELOCITY = 31.5 m/sec.

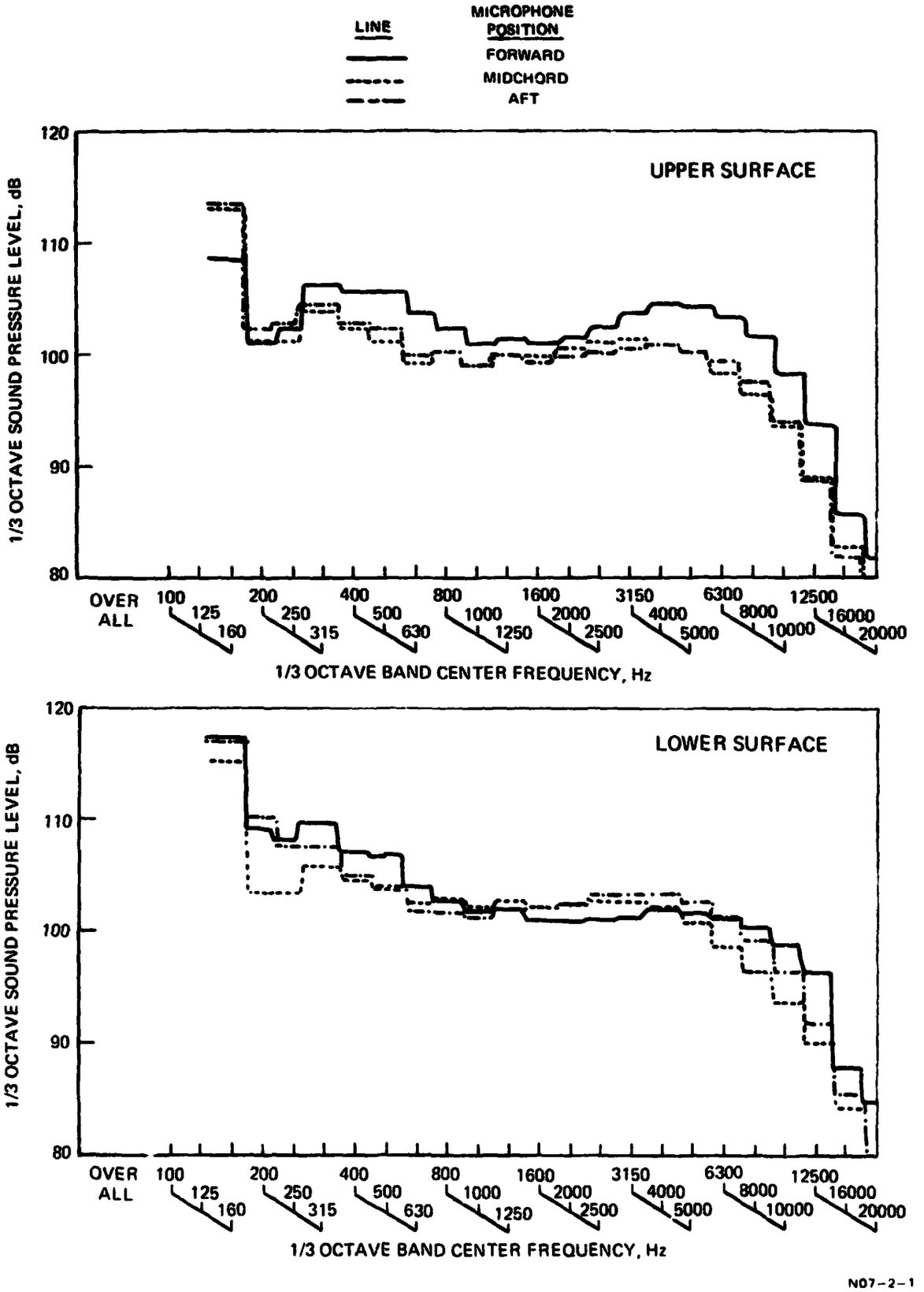

FIGURE 25. – CONTINUED, (b) VELOCITY = 50 m/sec.

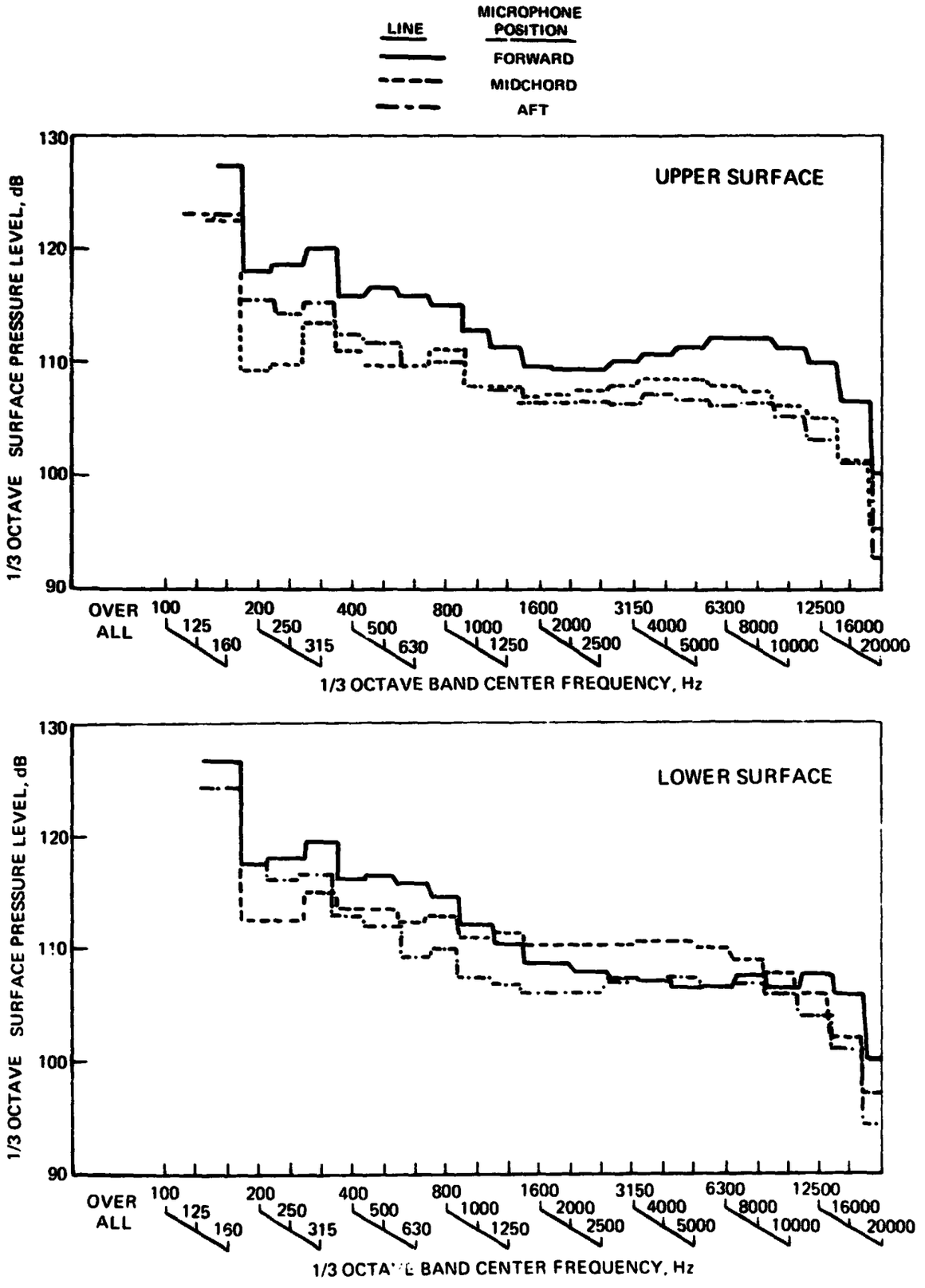

FIGURE 25. – CONTINUED (c) VELOCITY = 80 M/SEC

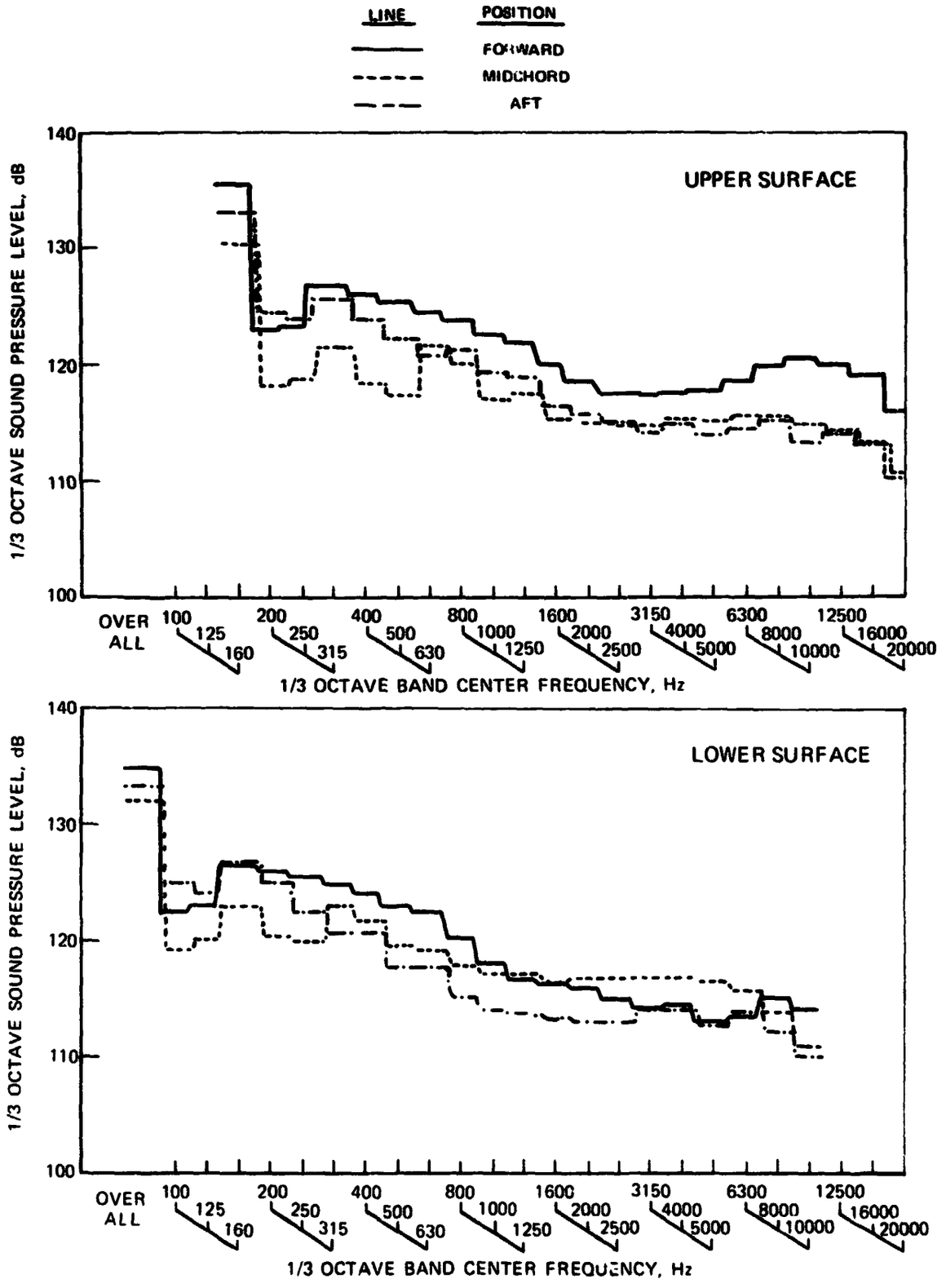

FIGURE 25. – CONTINUED, (d) VELOCITY = 125 m/sec

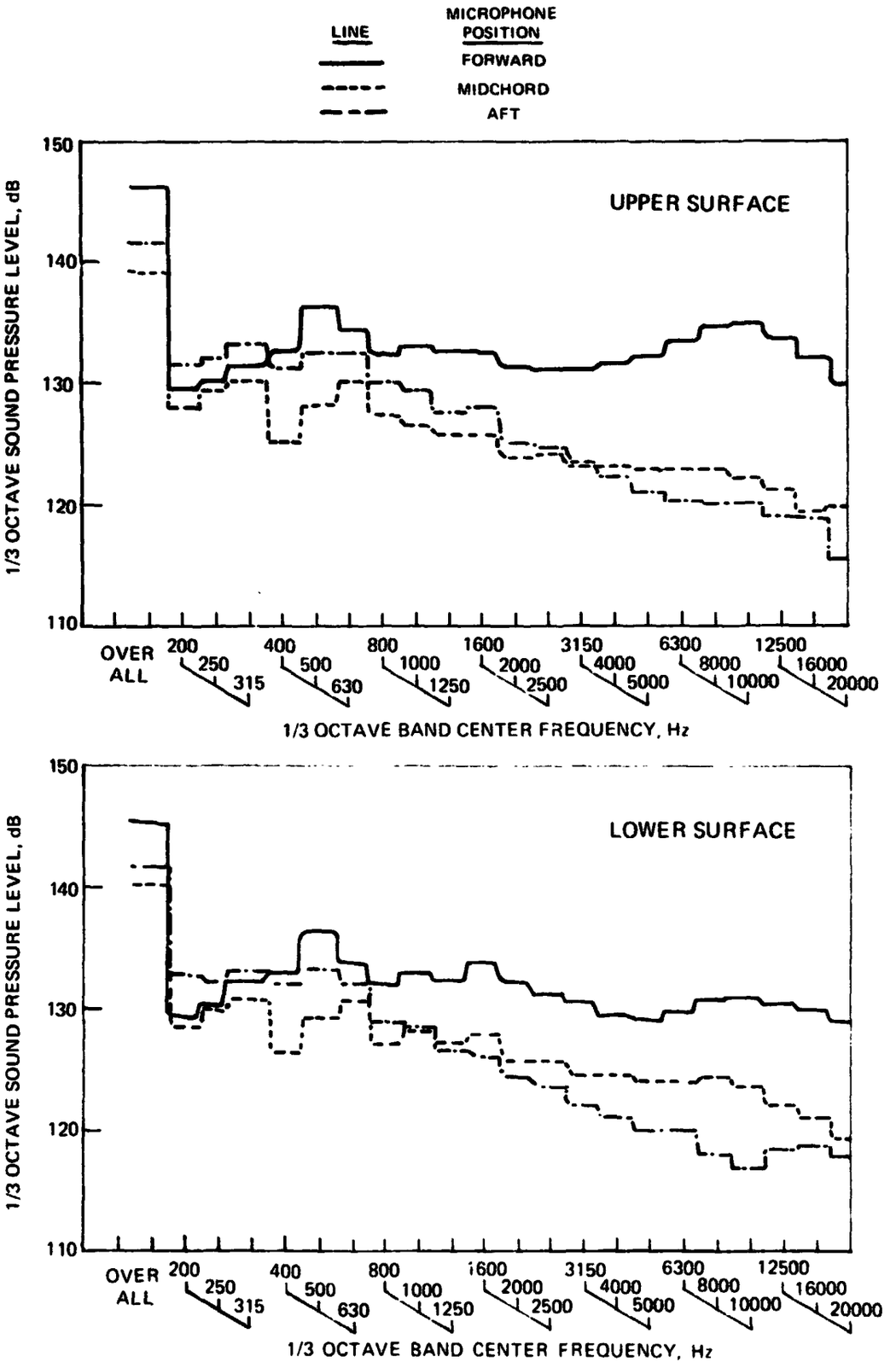

FIGURE 25. – CONCLUDED, (e) VELOCITY = 177 m/sec.

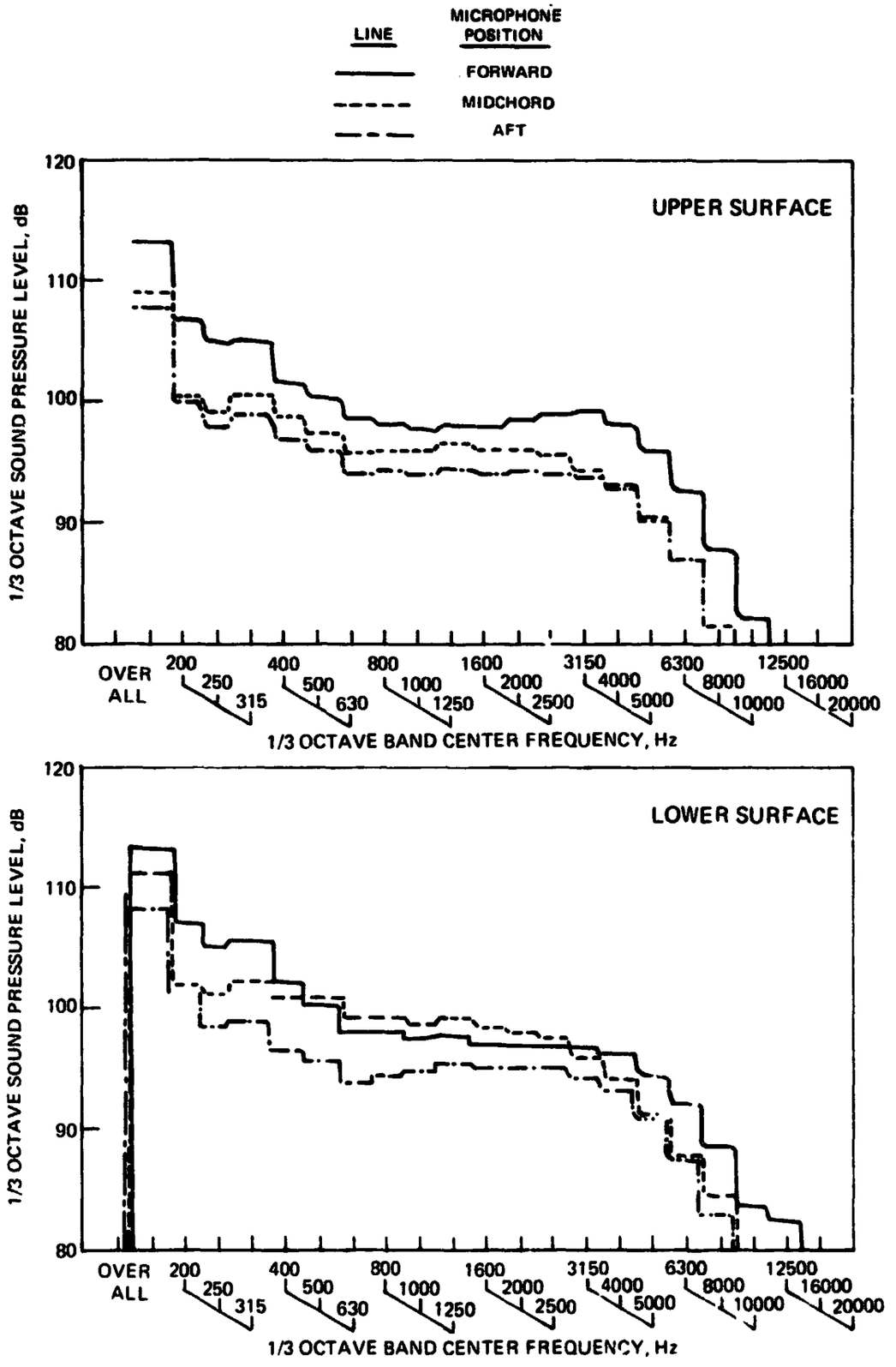

FIGURE 26. – SURFACE PRESSURE SPECTRA ON AIRFOIL WITH INCIDENT TURBULENCE FROM LARGE GRID, (a) VELOCITY = 31.5 m/sec.

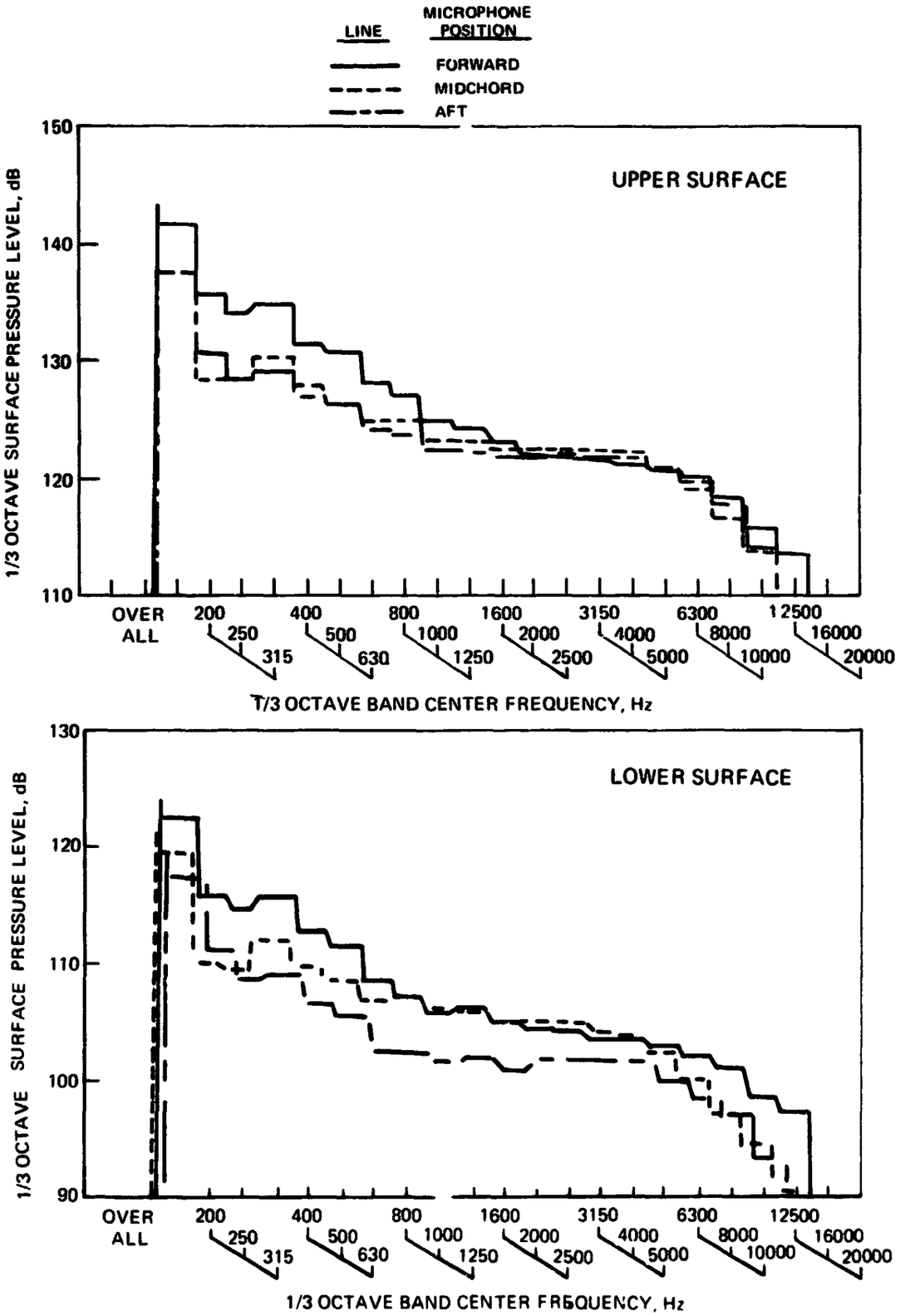

FIGURE 26. – CONTINUED (b) VELOCITY = 50 M/SEC m/sec

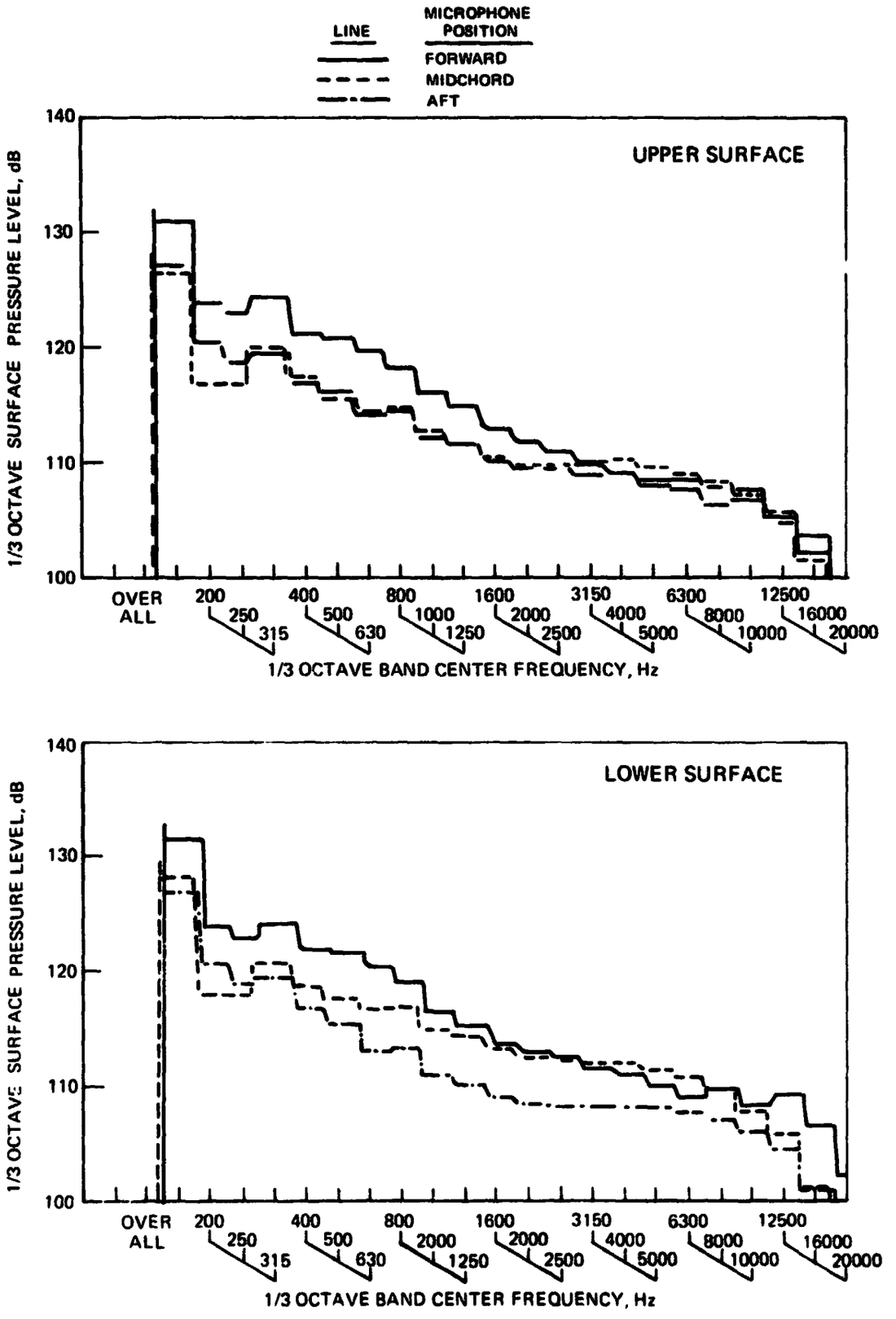

FIGURE 26. – CONTINUED (c) VELOCITY = 80 m/sec M/SEC

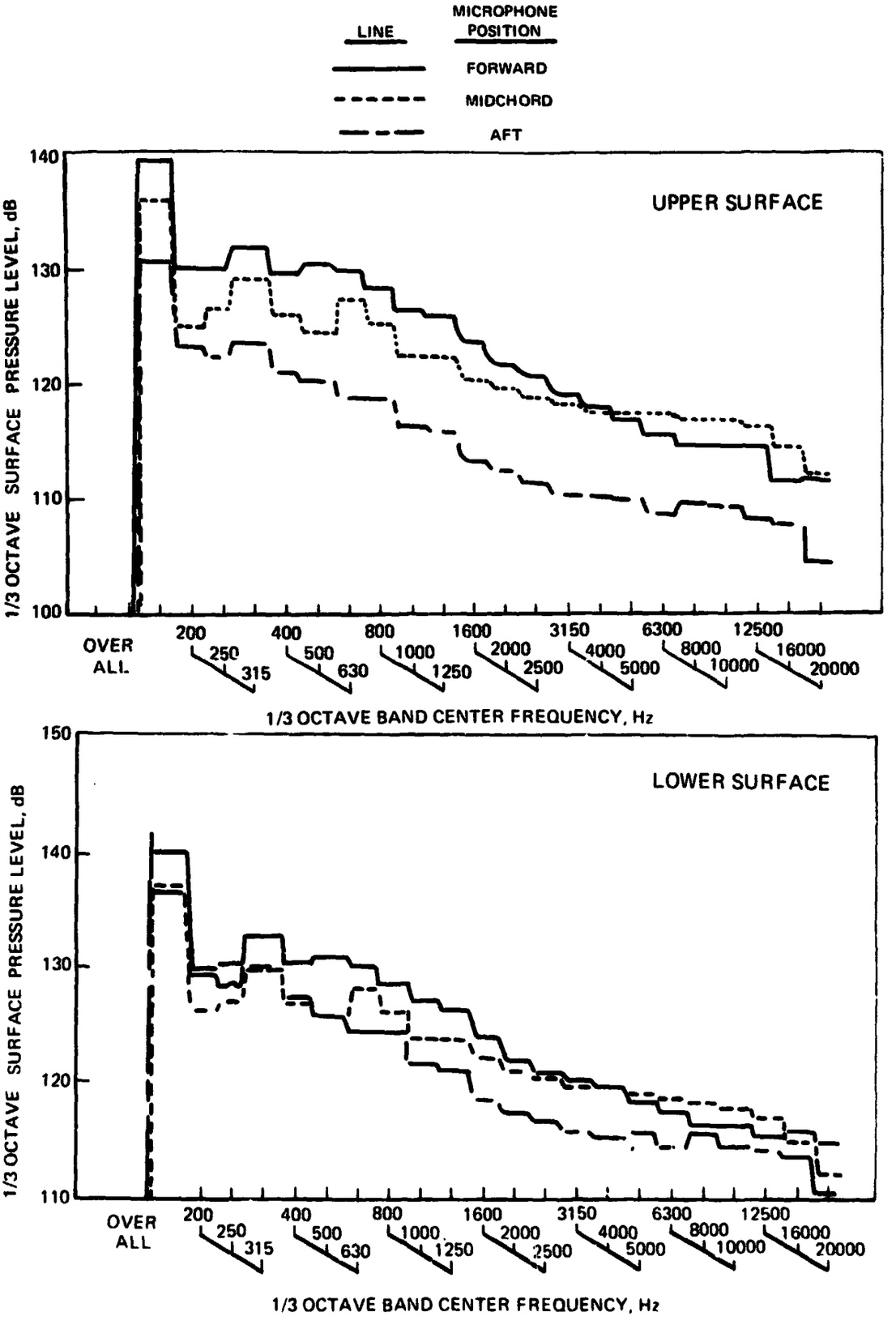

FIGURE 26. – CONTINUED. (d) VELOCITY = 125 M/SEC m/sec

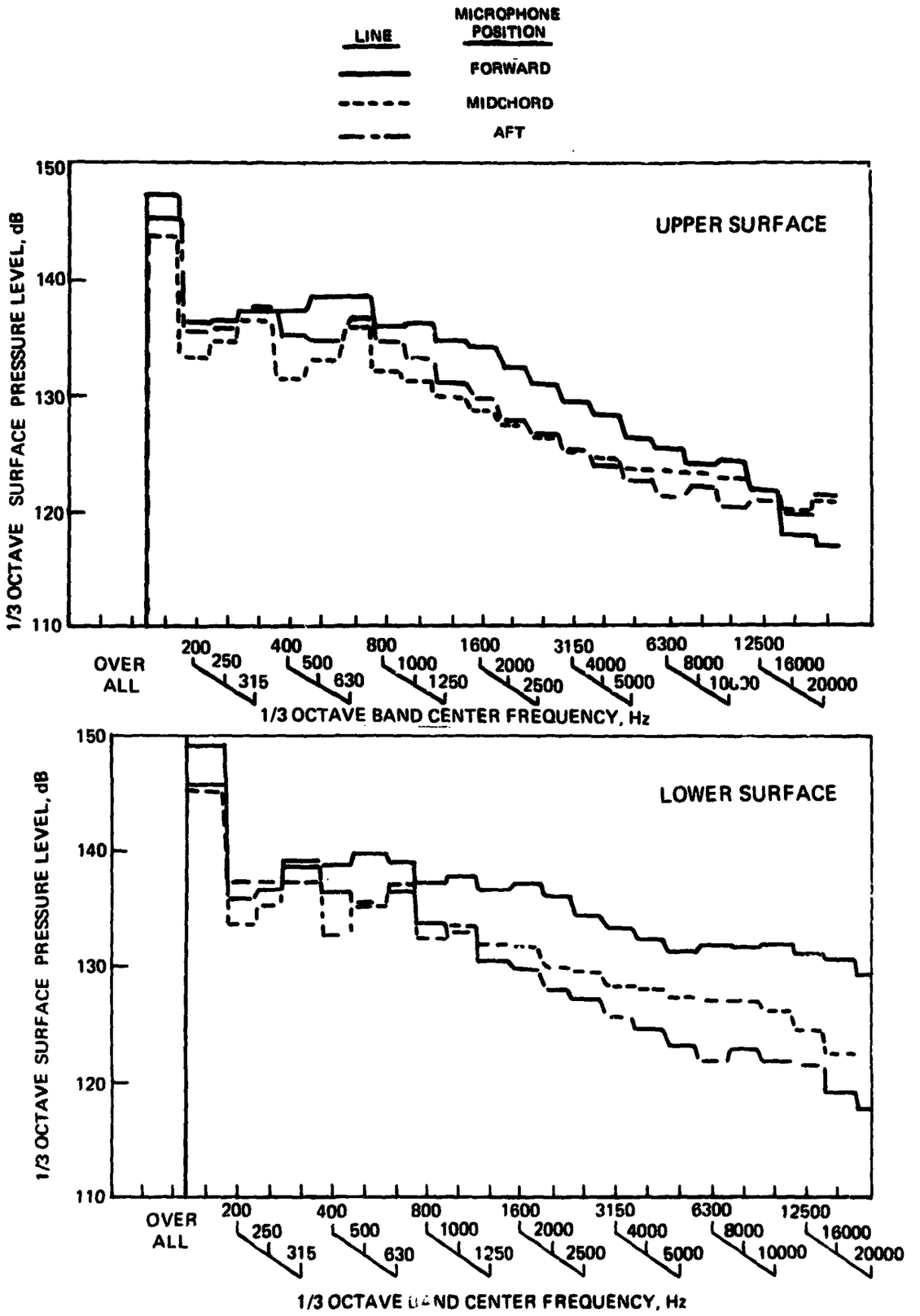

FIGURE 26. – CONCLUDED (e) VELOCITY = 177 m/sec M/SEC

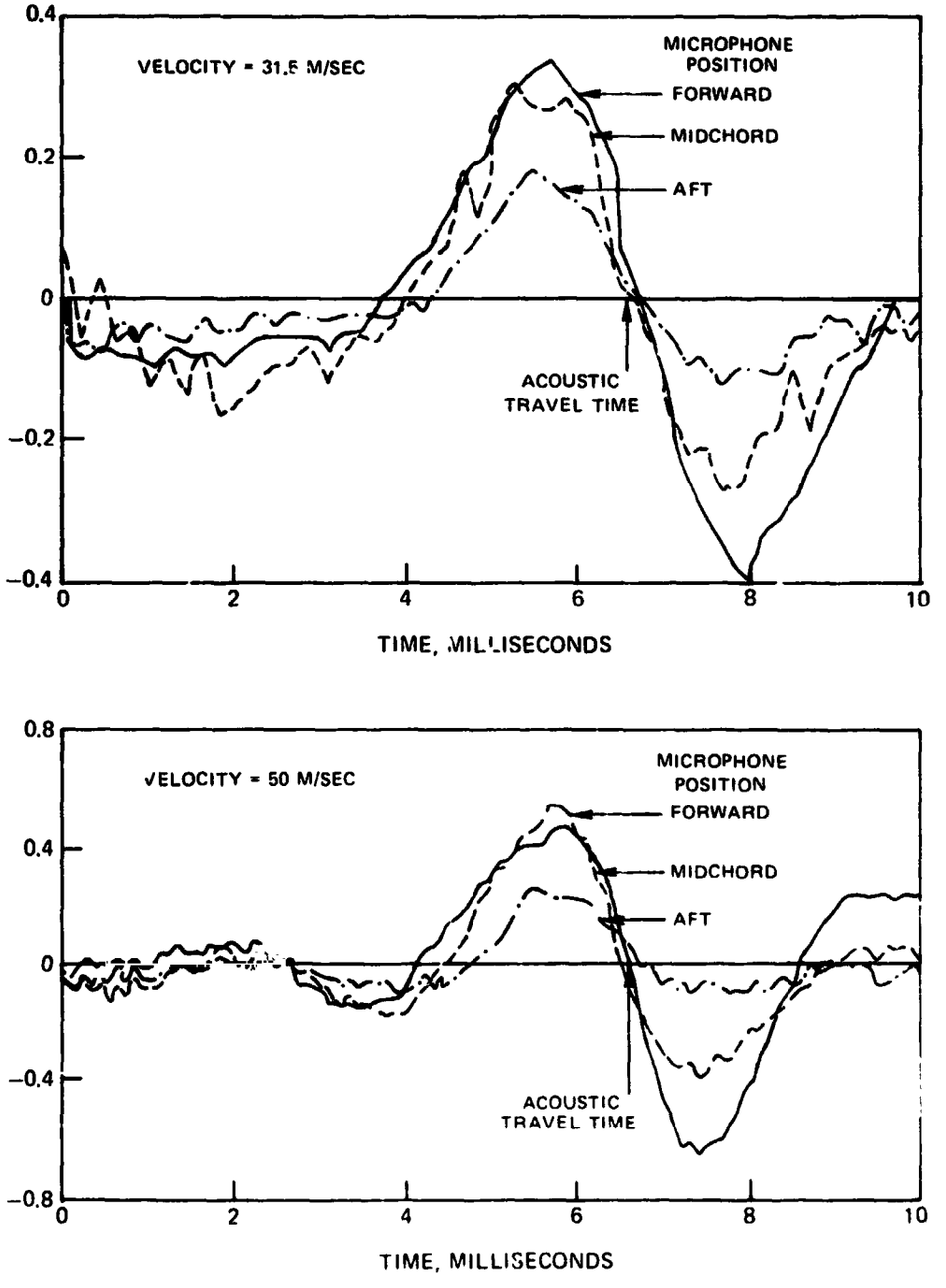

FIGURE 27. – CROSS–CORRELATIONS OF AIRFOIL SURFACE PRESSURES WITH FAR–FIELD ACOUSTIC PRESSURE FOR INCIDENT TURBULENCE

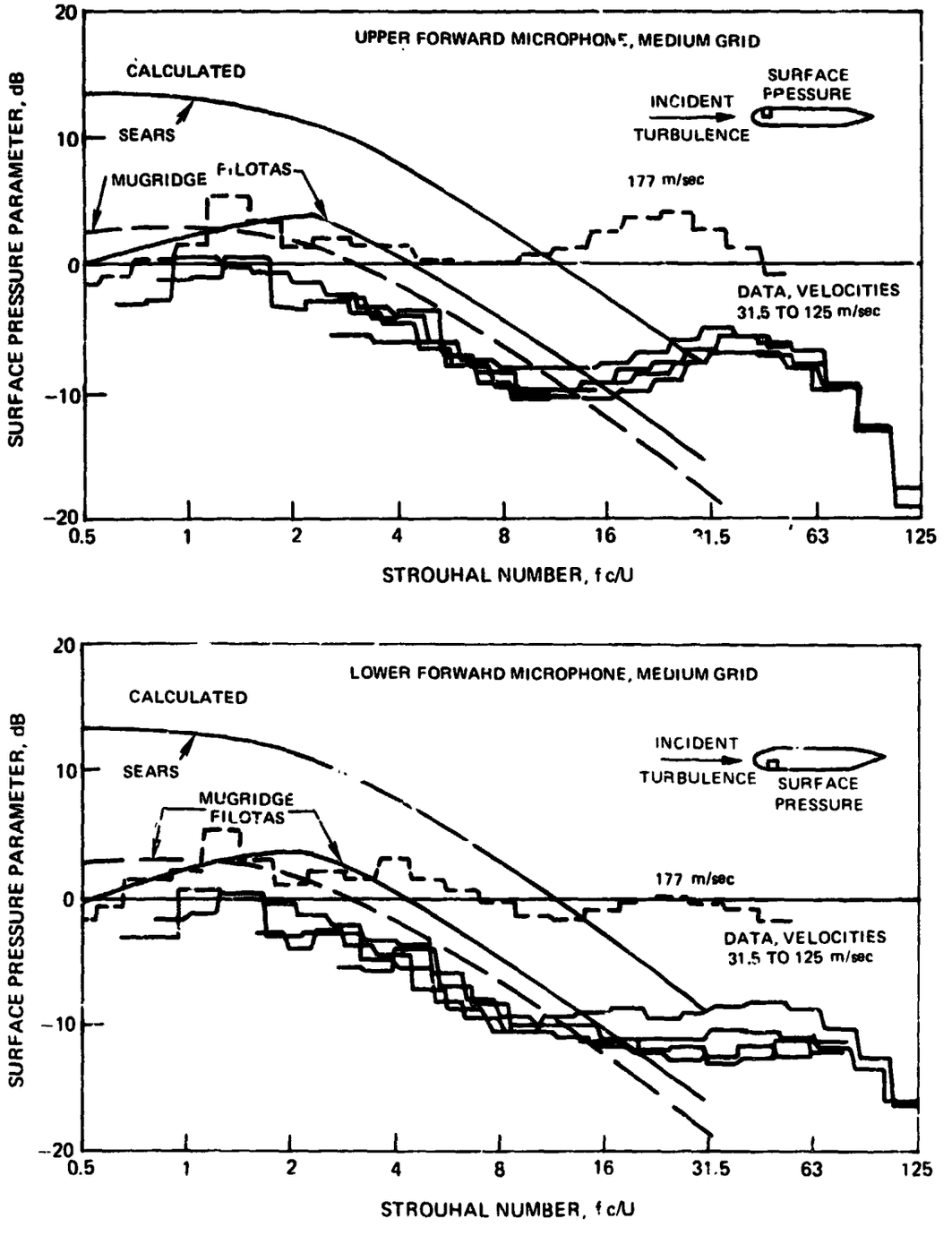

FIGURE 28. – COMPARISON OF MEASURED AND CALCULATED AIRFOIL SURFACE PRESSURE PARAMETER FOR INCIDENT TURBULENCE (a) FORWARD SURFACE MICROPHONES. MEDIUM GRID.

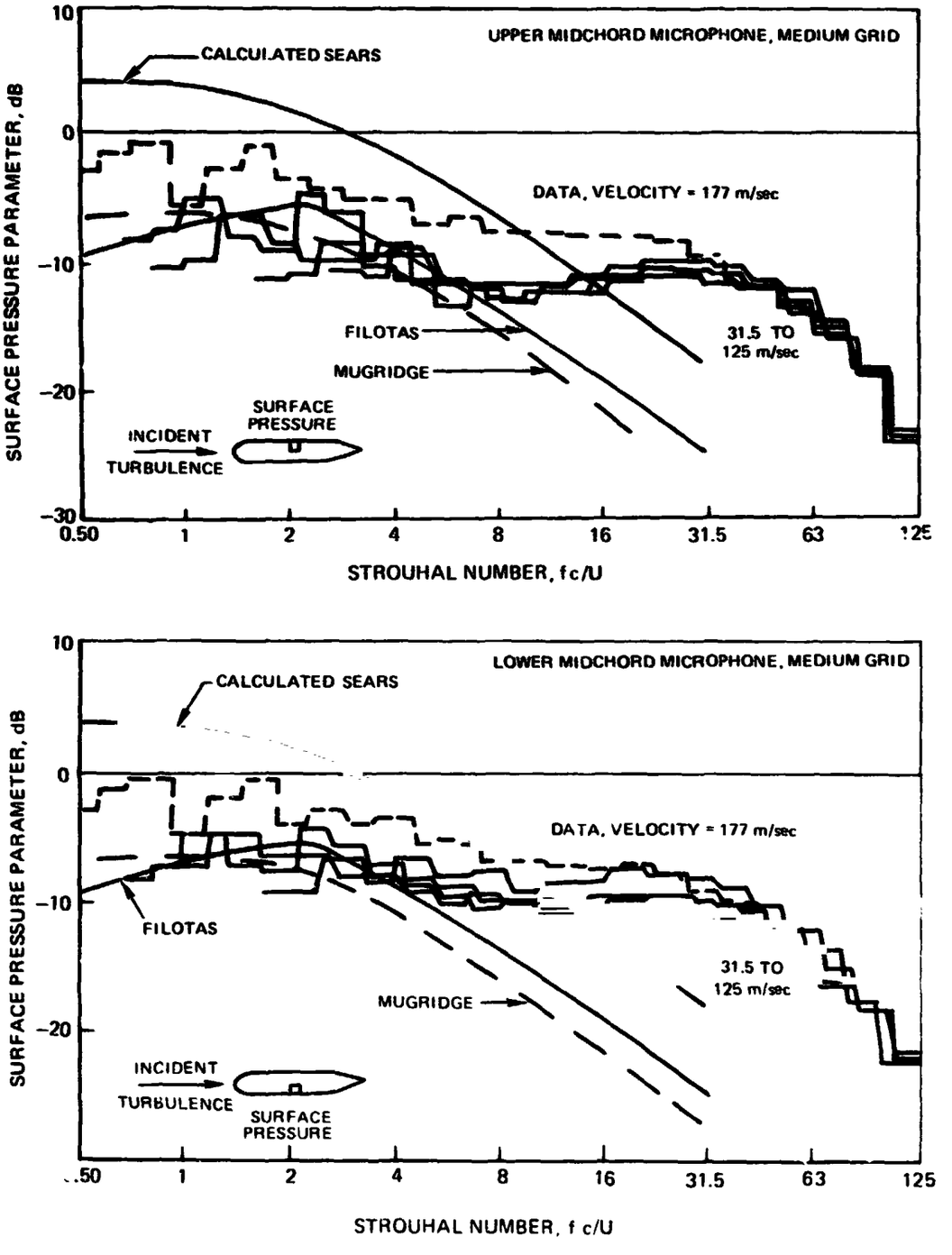

FIGURE 28. – CONTINUED. (b) MIDCHORD SURFACE MICROPHONES, MEDIUM GRID.

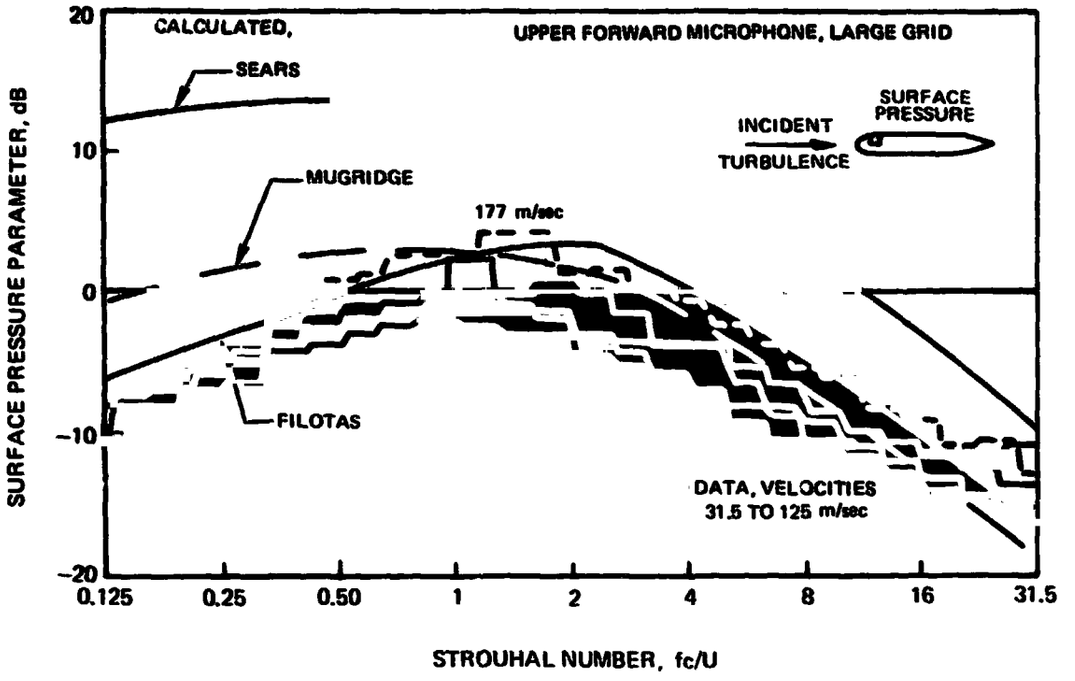

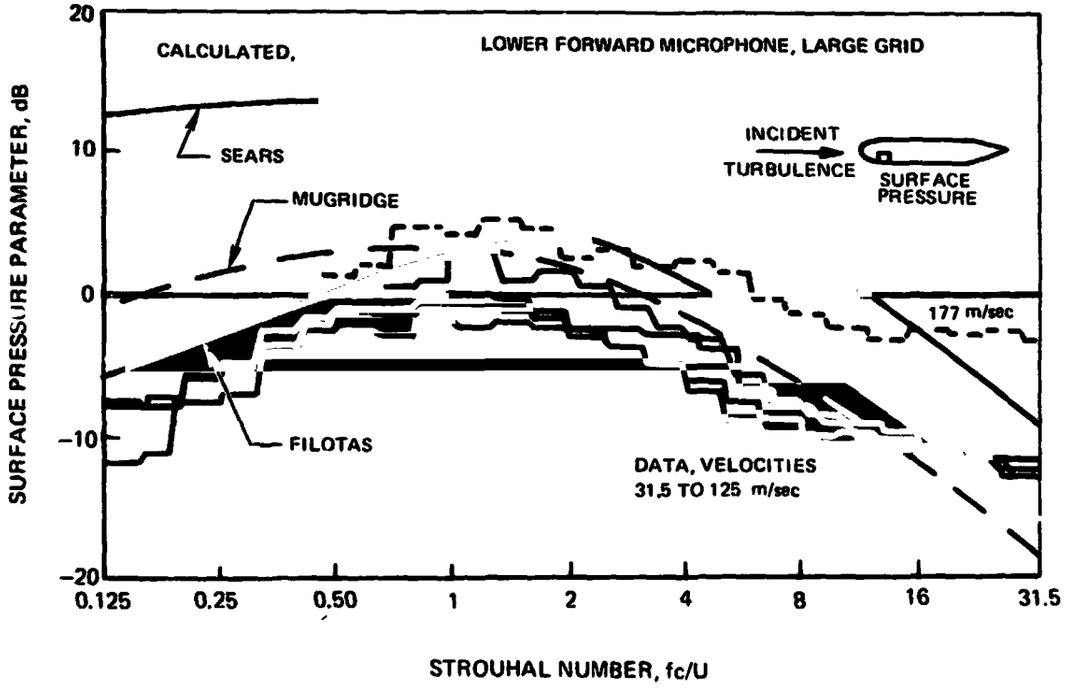

FIGURE 28. – CONTINUED (c) FORWARD MICROPHONES, LARGE GRID

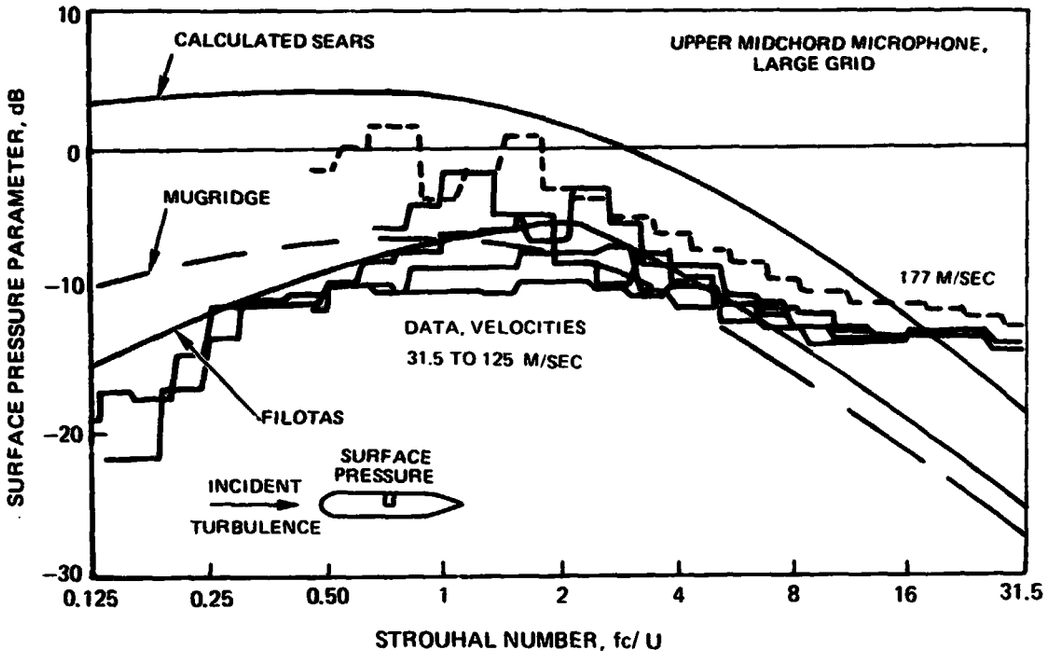

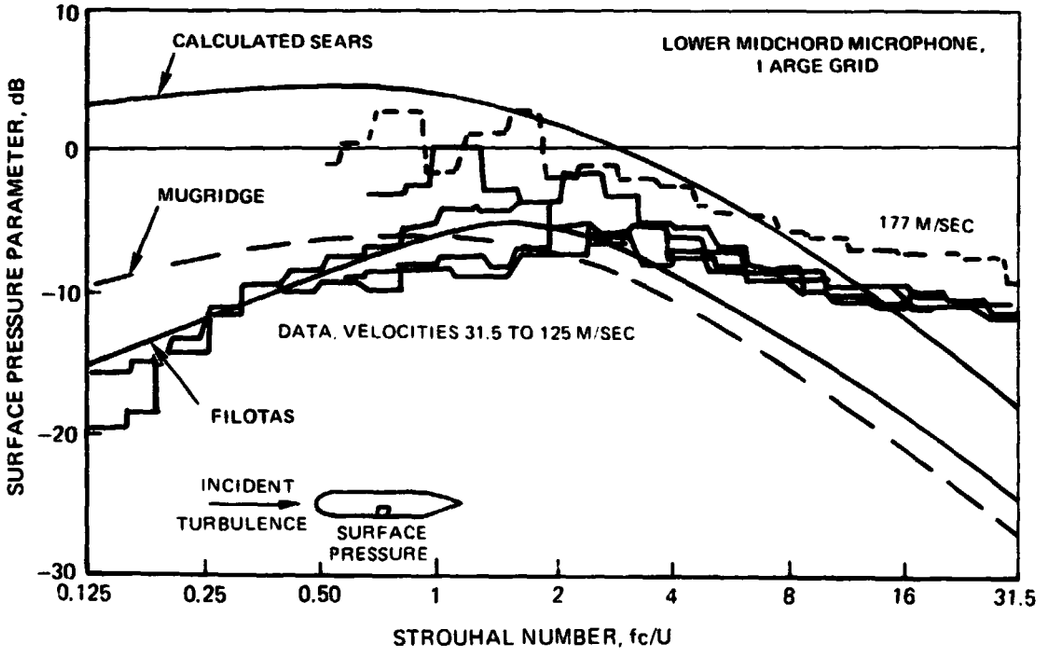

FIGURE 28. – CONCLUDED. (d) MIDCHORD MICROPHONES, LARGE GRID

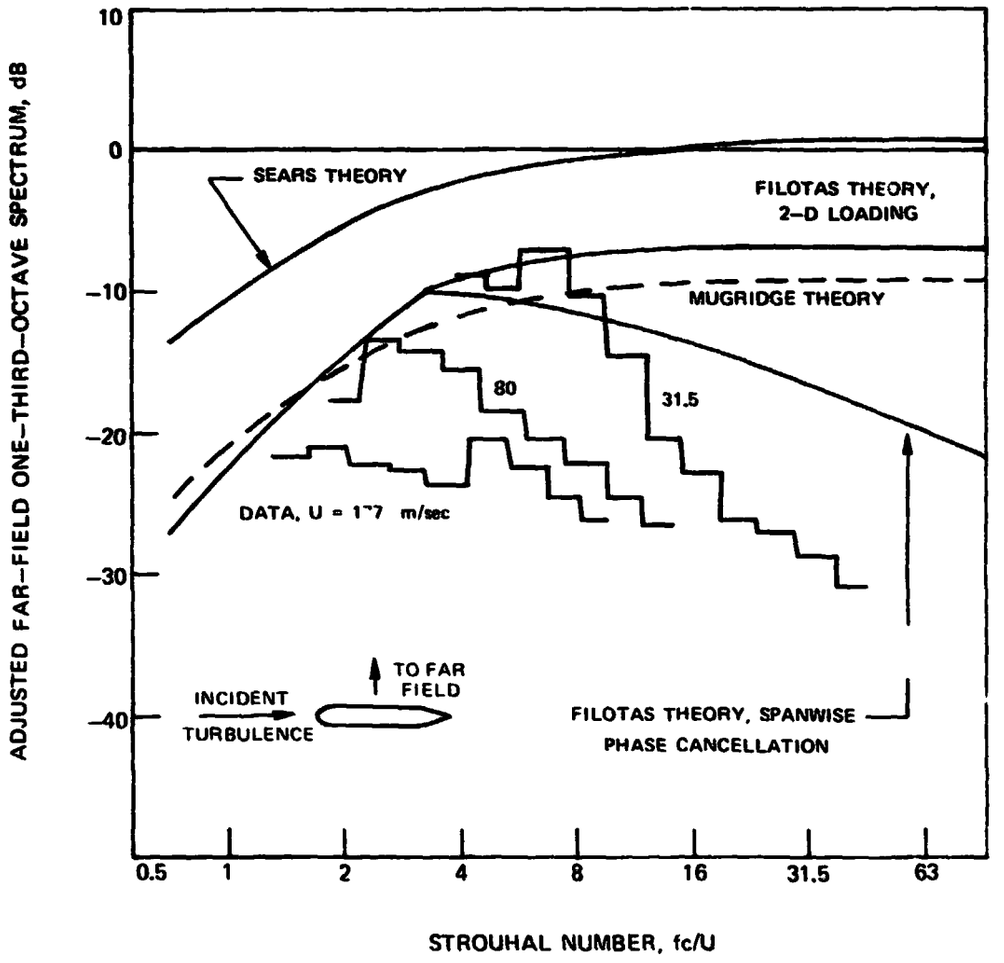

FIGURE 29. – COMPARISON OF ADJUSTED FAR–FIELD SPECTRA CAUSED BY INCIDENT TURBULENCE AT THREE VELOCITIES WITH PREDICTIONS THAT NEGLECT COMPRESSIBILITY EFFECTS

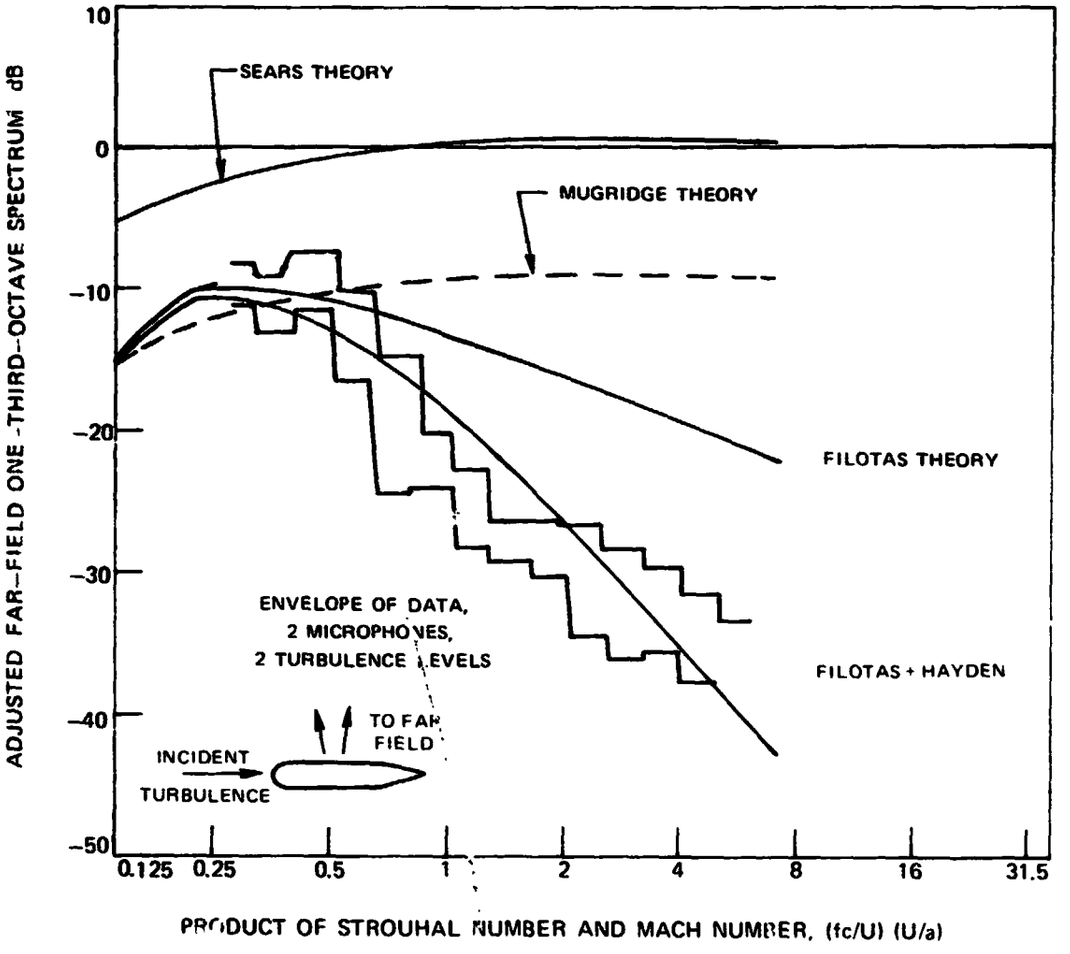

FIGURE 30. – COMPARISON OF MEASURED AND PREDICTED ADJUSTED FAR–FIELD SPECTRA CAUSED BY INCIDENT TURBULENCE (a) 31.5 M/SEC VELOCITY

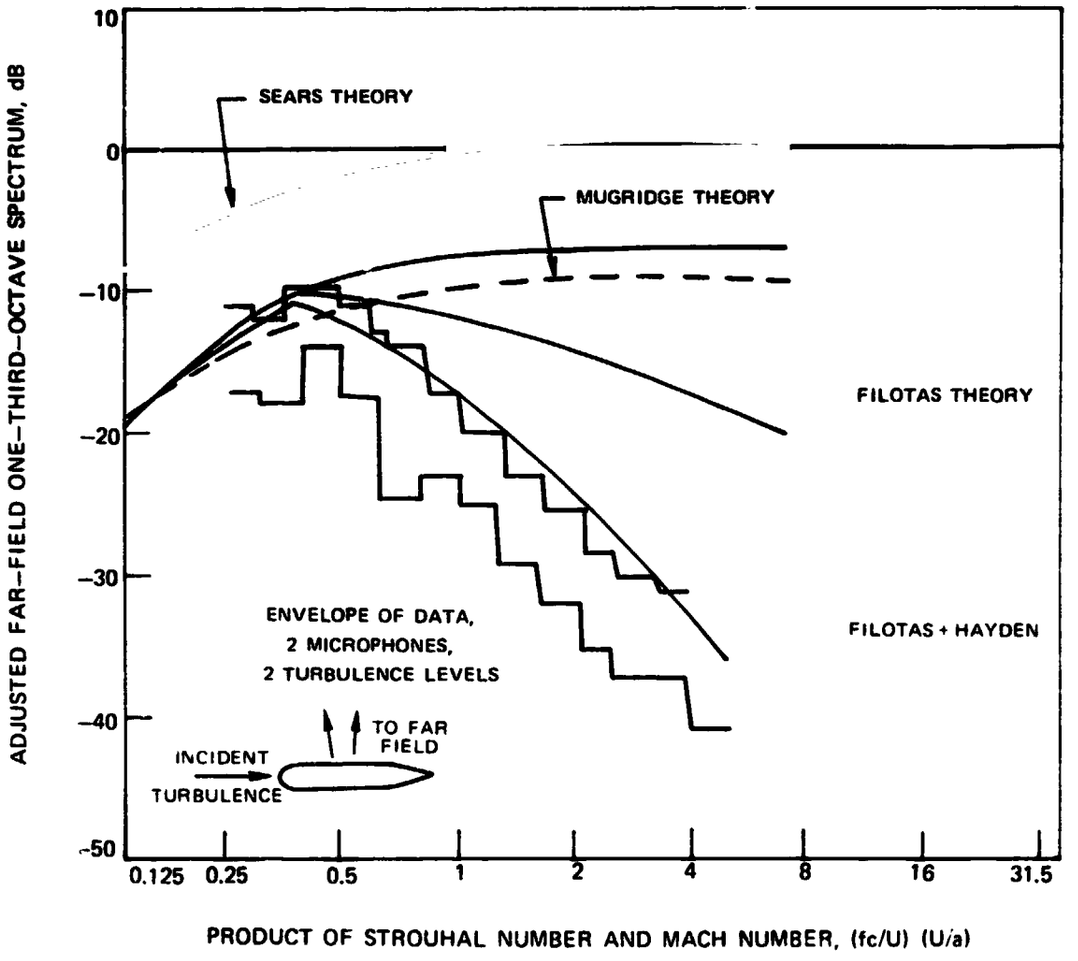

FIGURE 30. – CONTINUED (b) 50 m/sec VELOCITY

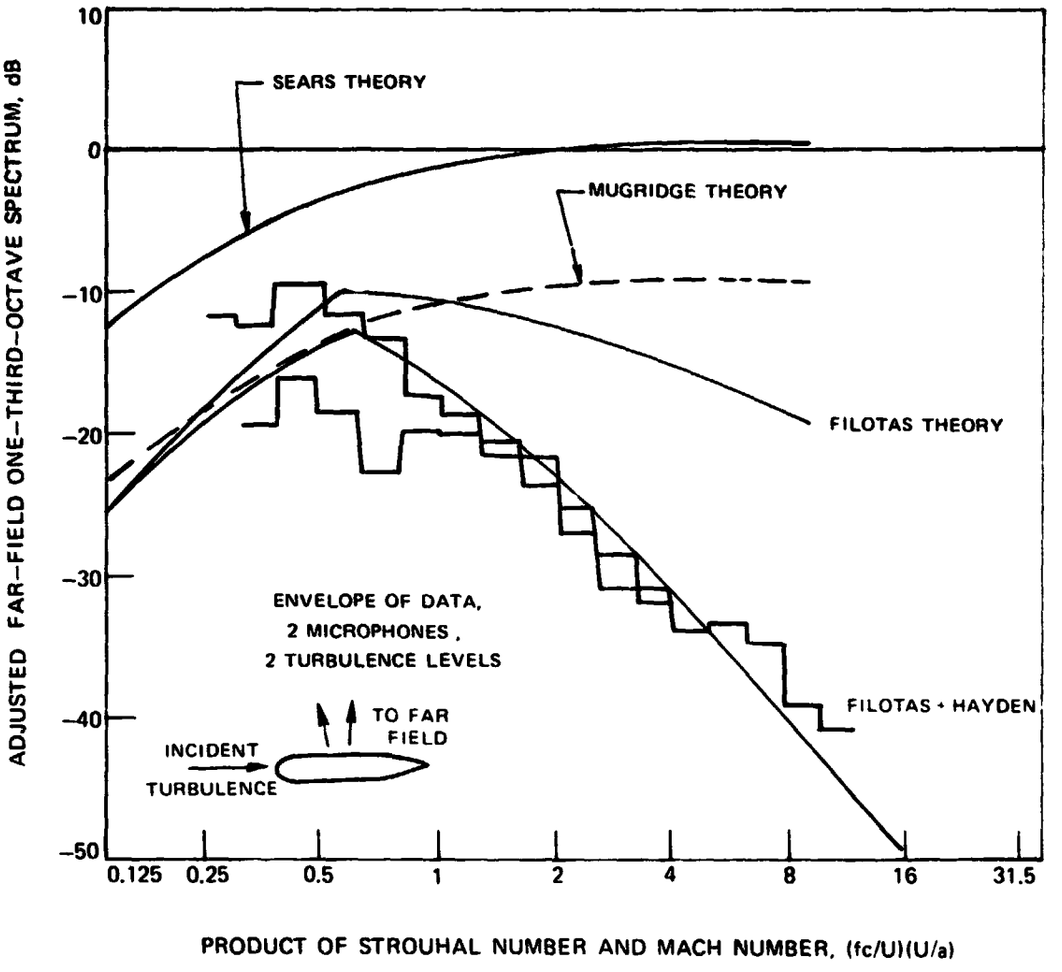

FIGURE 30. – CONTINUED (c) 80 M/SEC VELOCITY

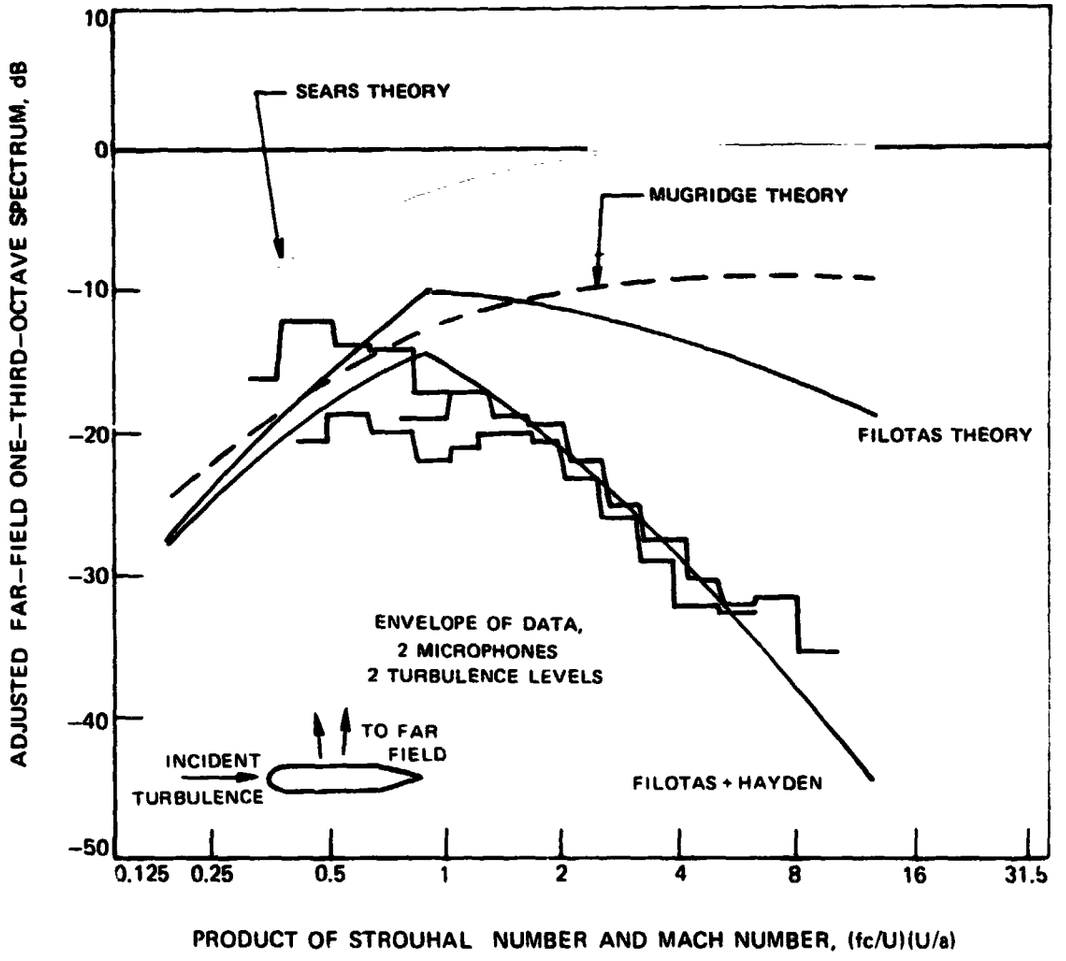

FIGURE 30. – CONTINUED (d) 125 M/SEC VELOCITY

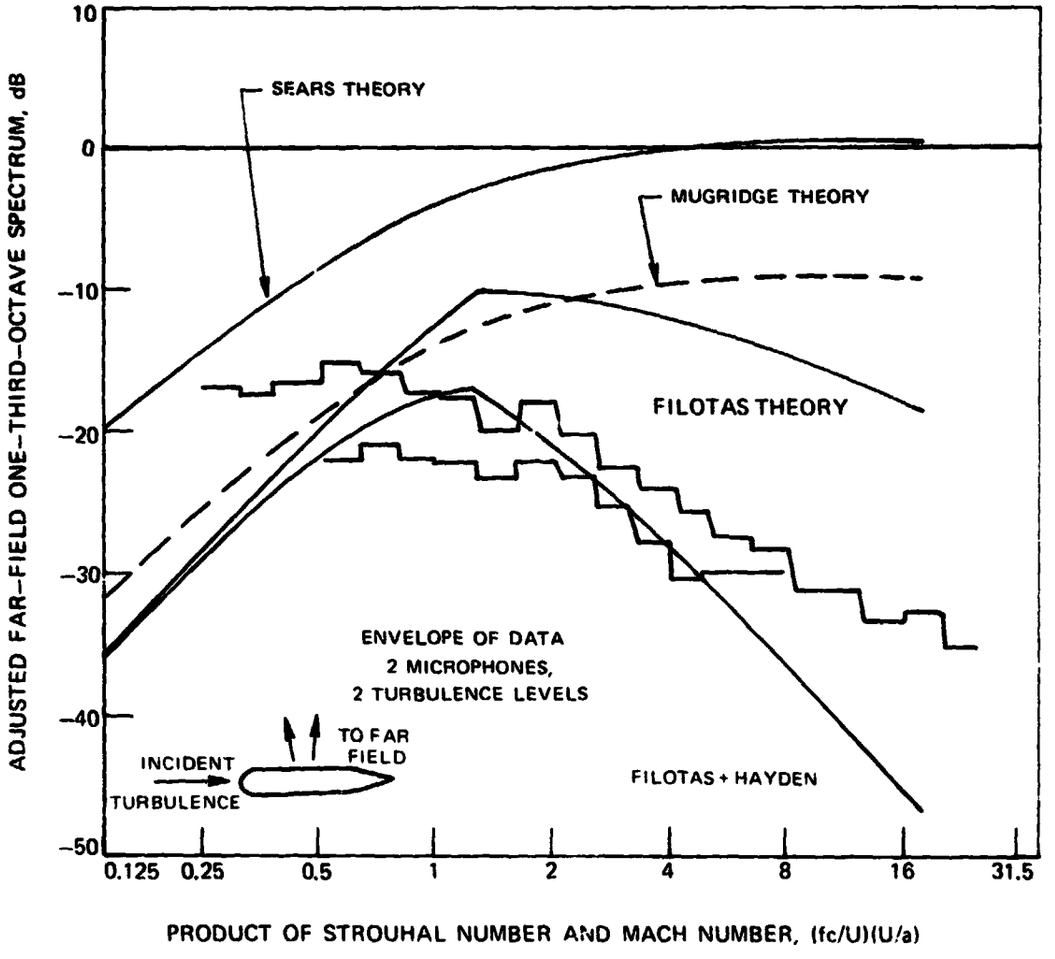

FIGURE 30. – CONCLUDED (e) 177 M/SEC VELOCITY

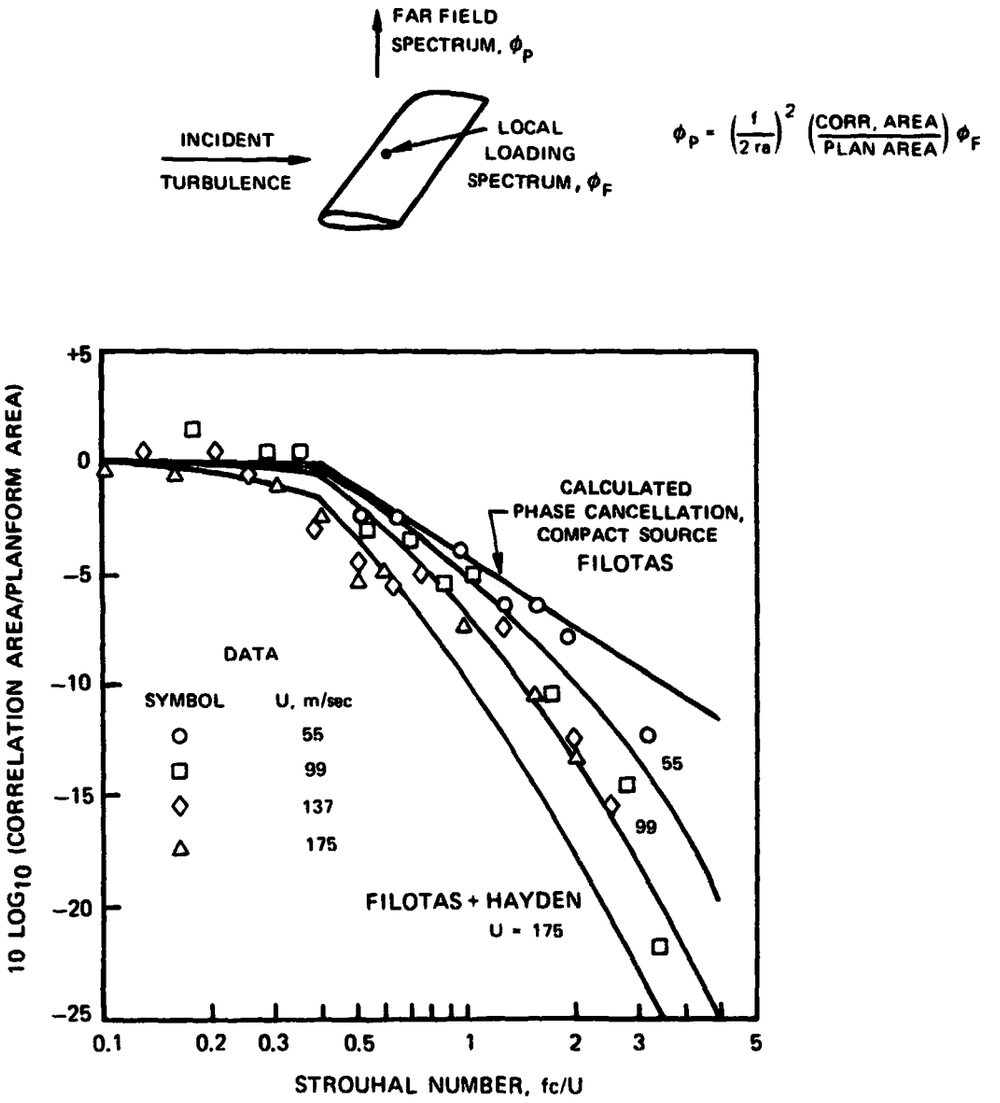

FIGURE 31. – COMPARISON OF EFFECTIVE CORRELATION AREA INFERRED BY DEAN FOR INCIDENCE FLUCTUATION NOISE WITH PREDICTIONS BY RECOMMENDED METHOD

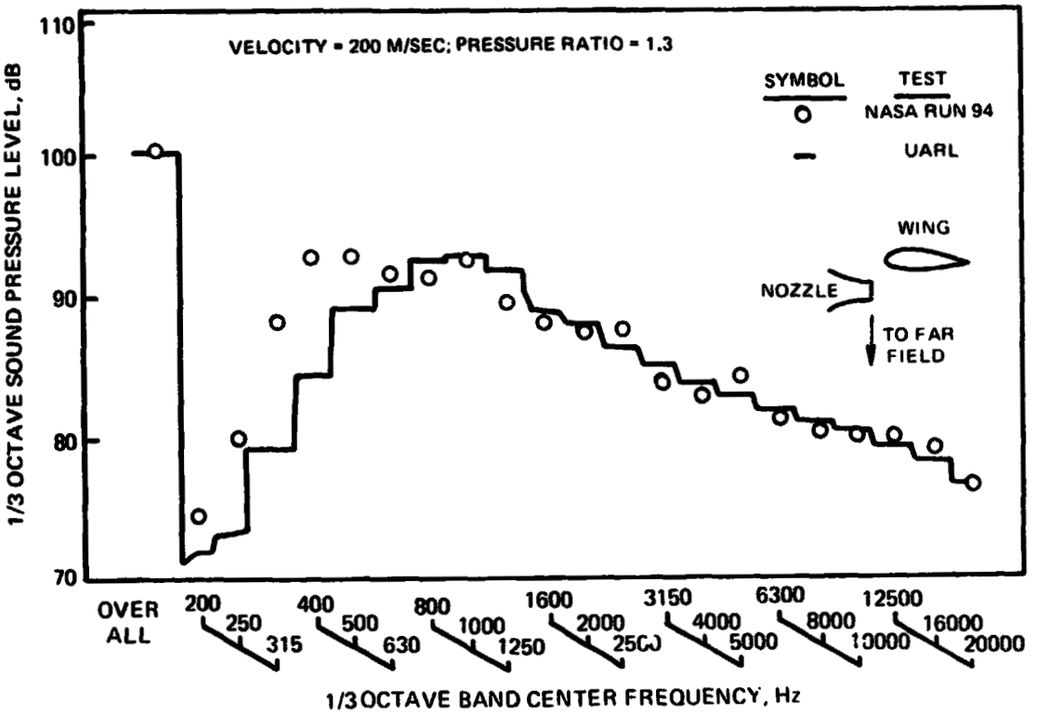

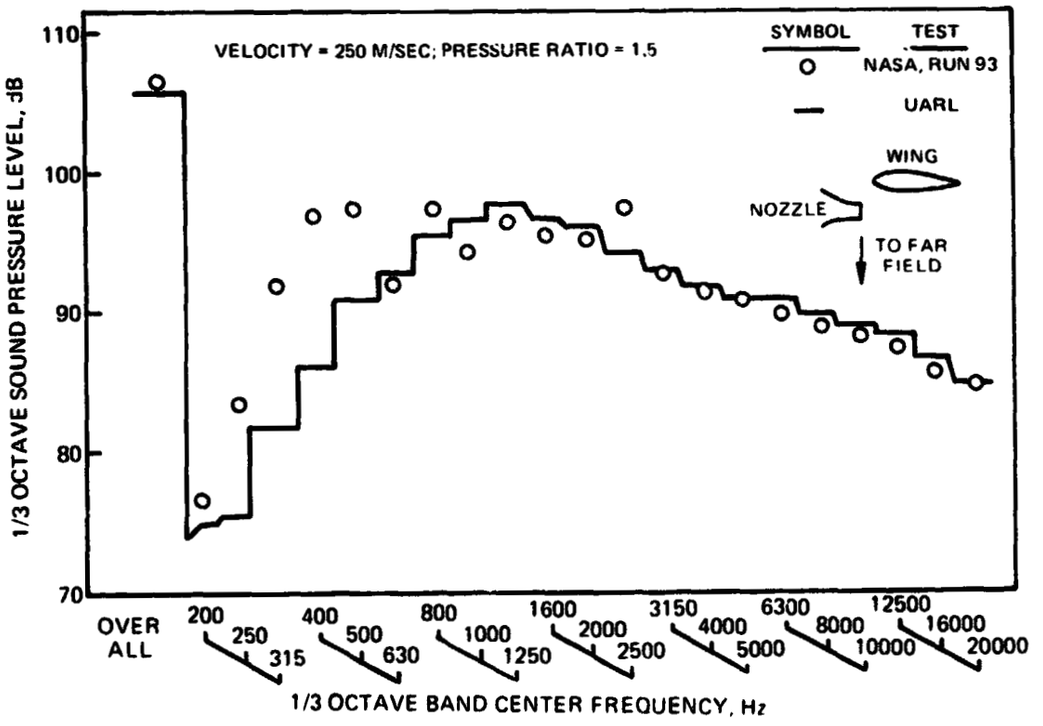

FIGURE 32.– COMPARISON OF NASA AND UARL UNDER–THE–WING EXTERNALLY BLOWN FLAP NOISE SPECTRA FOR ZERO DEFLECTION

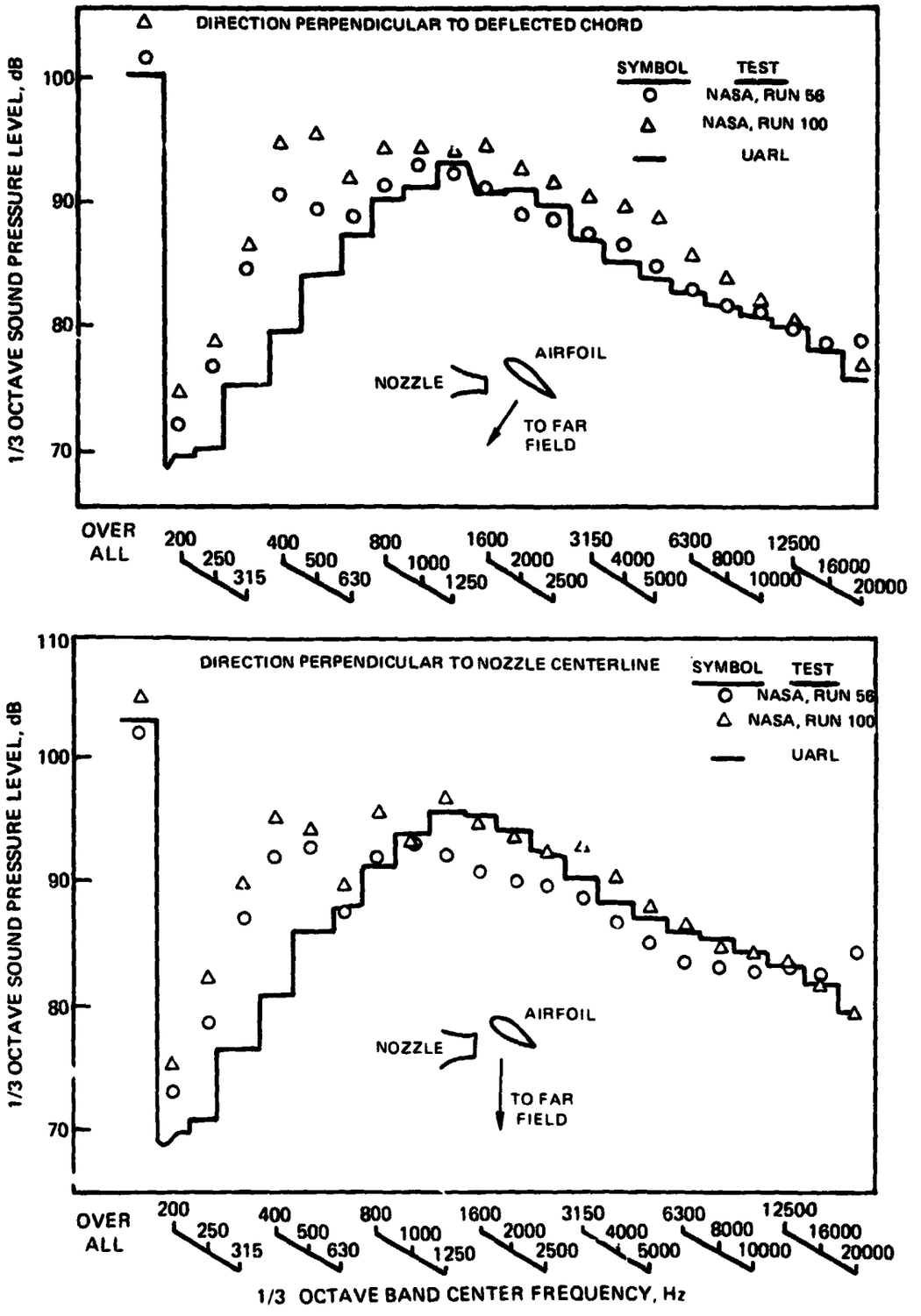

FIGURE 33. – COMPARISON OF NASA AND UARL UNDER–THE–WING EXTERNALLY BLOWN FLAP NOISE SPECTRA FOR MODERATE DEFLECTION

CIRCLE SYMBOLS ARE SUM OF UNSCRUBBED SIDE, NOZZLE DIRECT RADIATED SOUND, AND NOZZLE REFLECTED SOUND

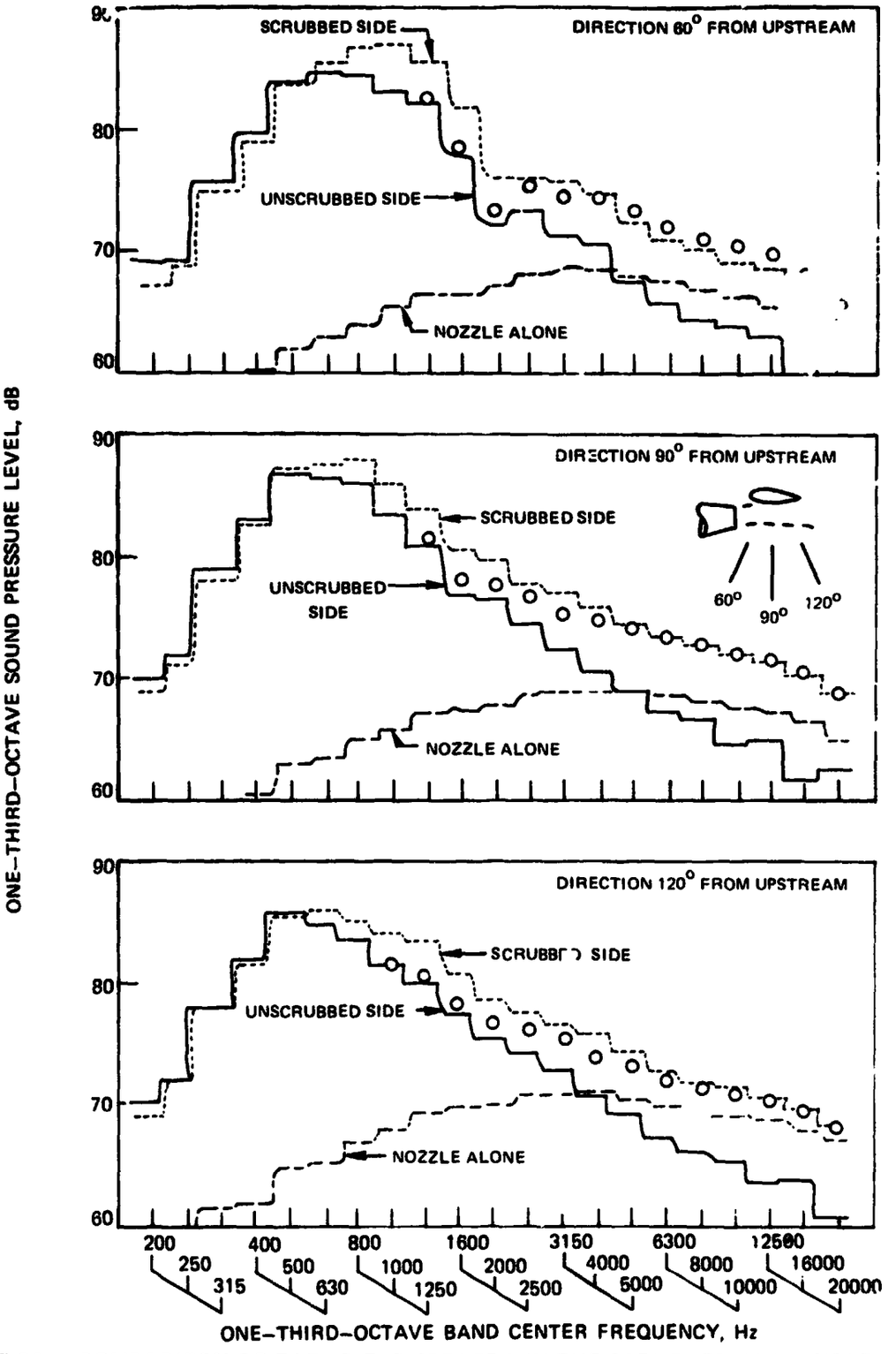

FIGURE 34. – COMPARISON OF FAR-FIELD SPECTRA IN THE SCRUBBED AND UNSCRUBBED DIRECTIONS FROM AN UNDEFLECTED EXTERNALLY BLOWN WING. (a) 160 M/SEC VELOCITY

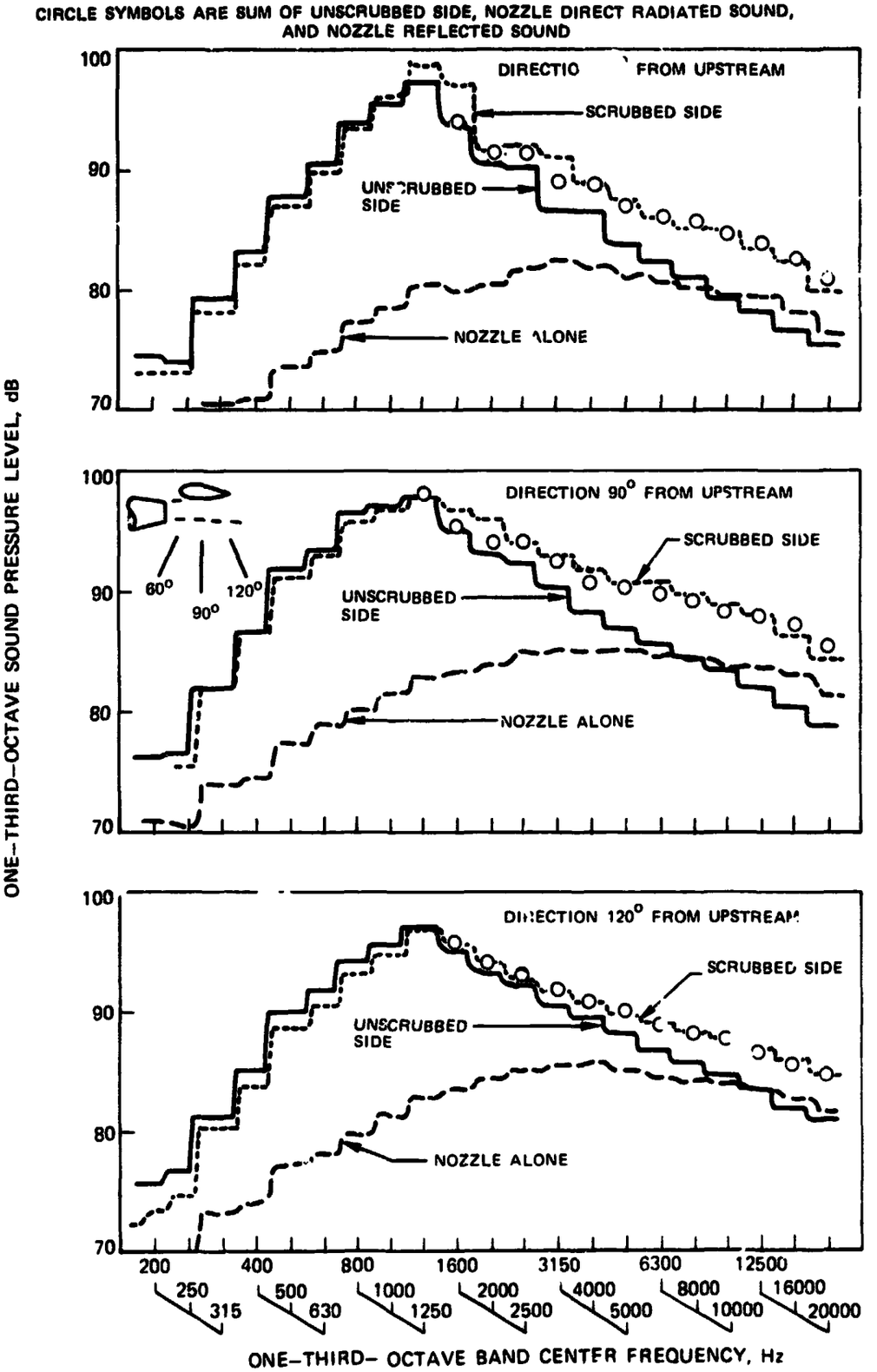

FIGURE 34. – CONCLUDED. (b) 250 M/SEC VELOCITY

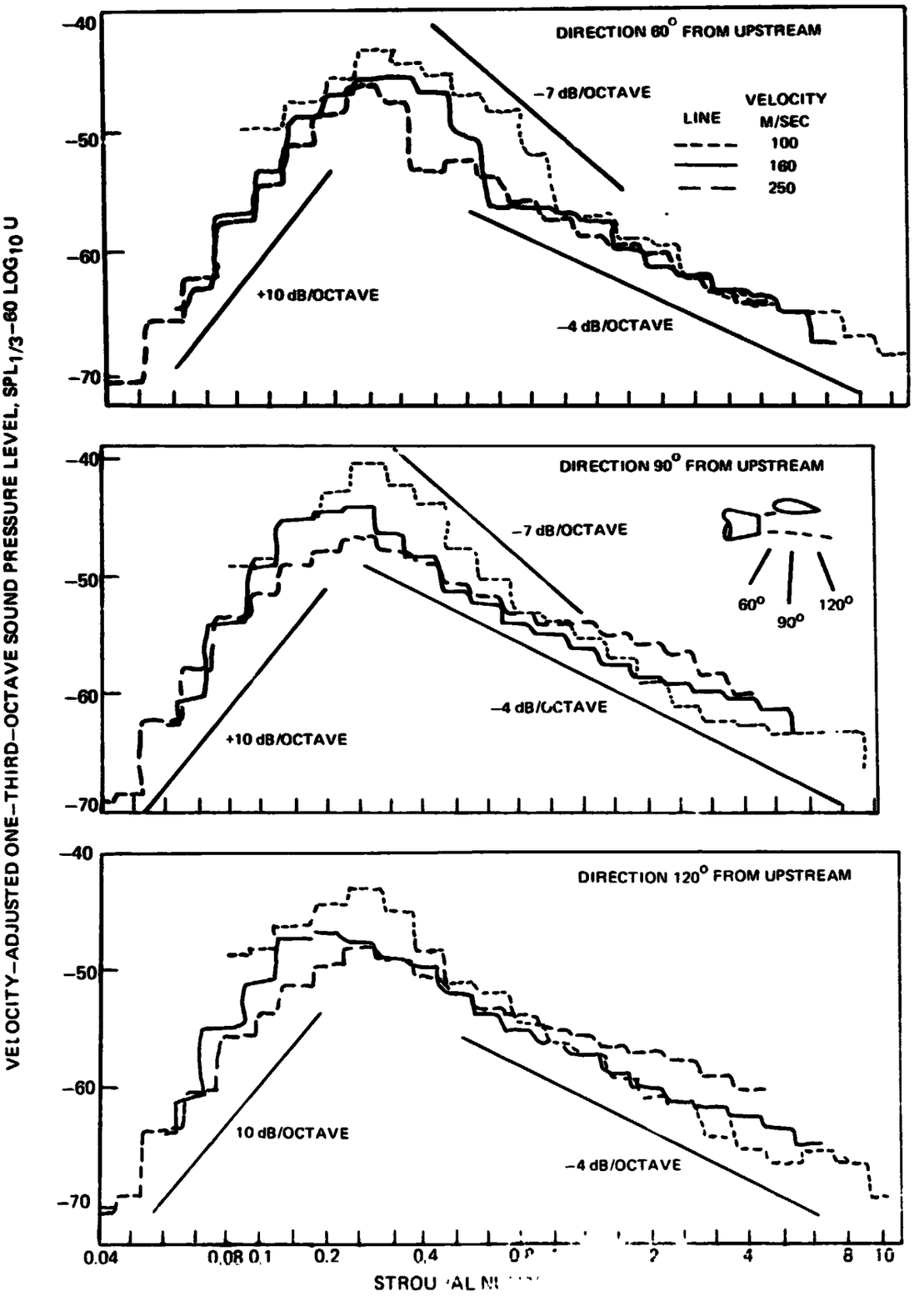

FIGURE 35. – VARIATION OF FAR FIELD SPECTRA FOR SIXTH POWER VELOCITY DEPENDENCE, WITH VELOCITY OF SCRUBBING –THE–WING INSTALLATION, 0° DEFLECTION

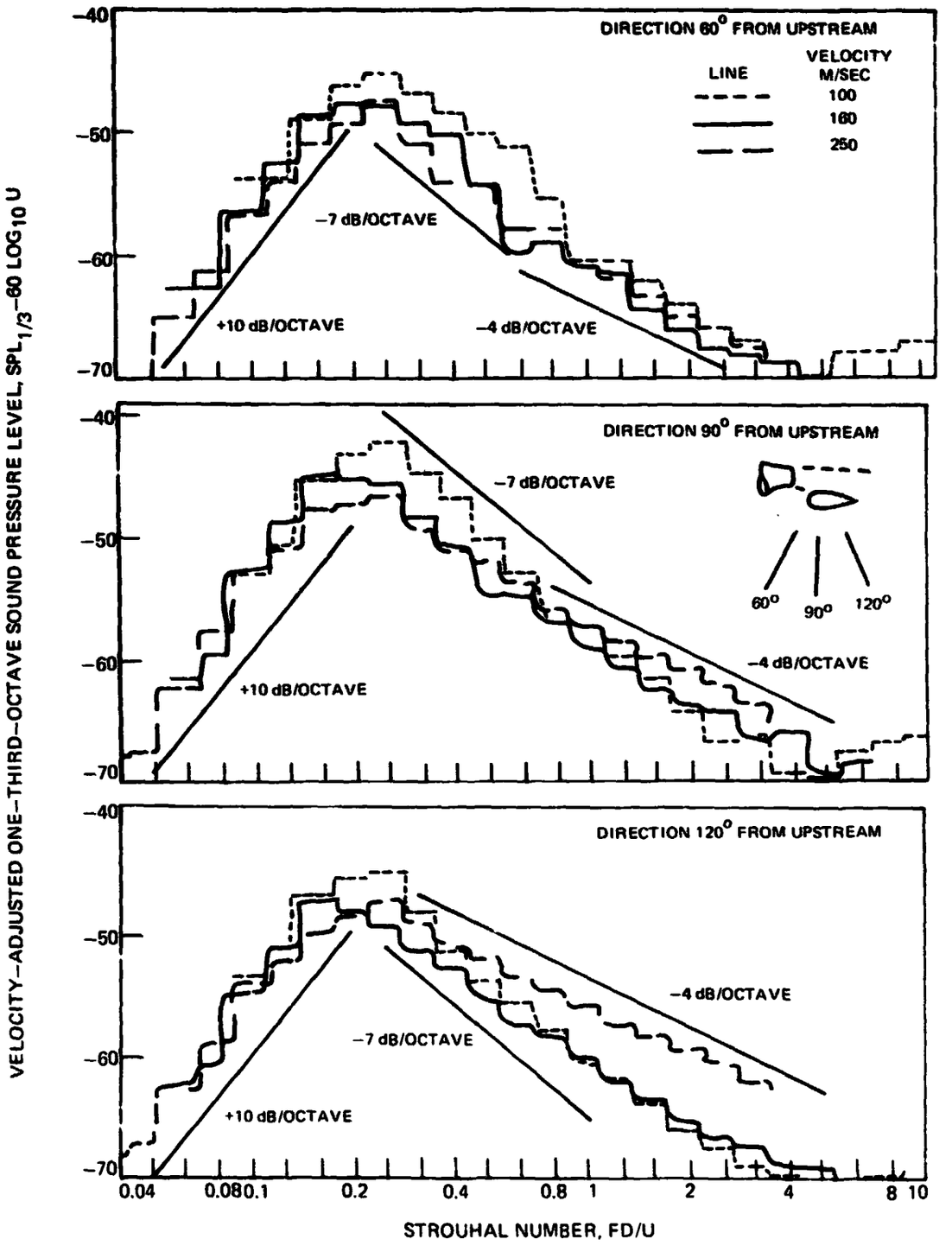

FIGURE 35. – CONTINUED. (b) OVER–THE–WING INSTALLATION, 0° DEFLECTION

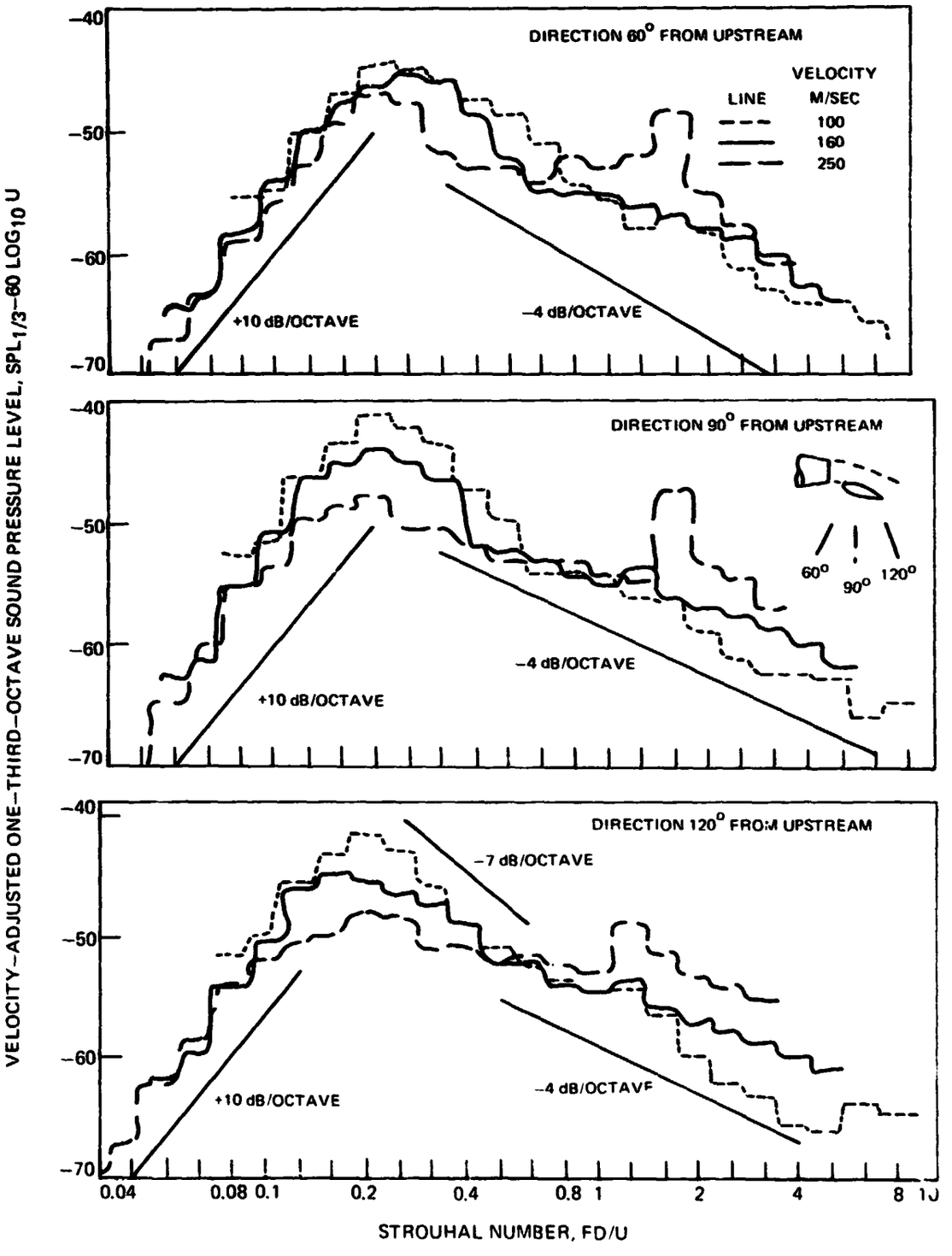

FIGURE 35. – CONTINUED. (c) OVER–THE–WING INSTALLATION, 10° DEFLECTION

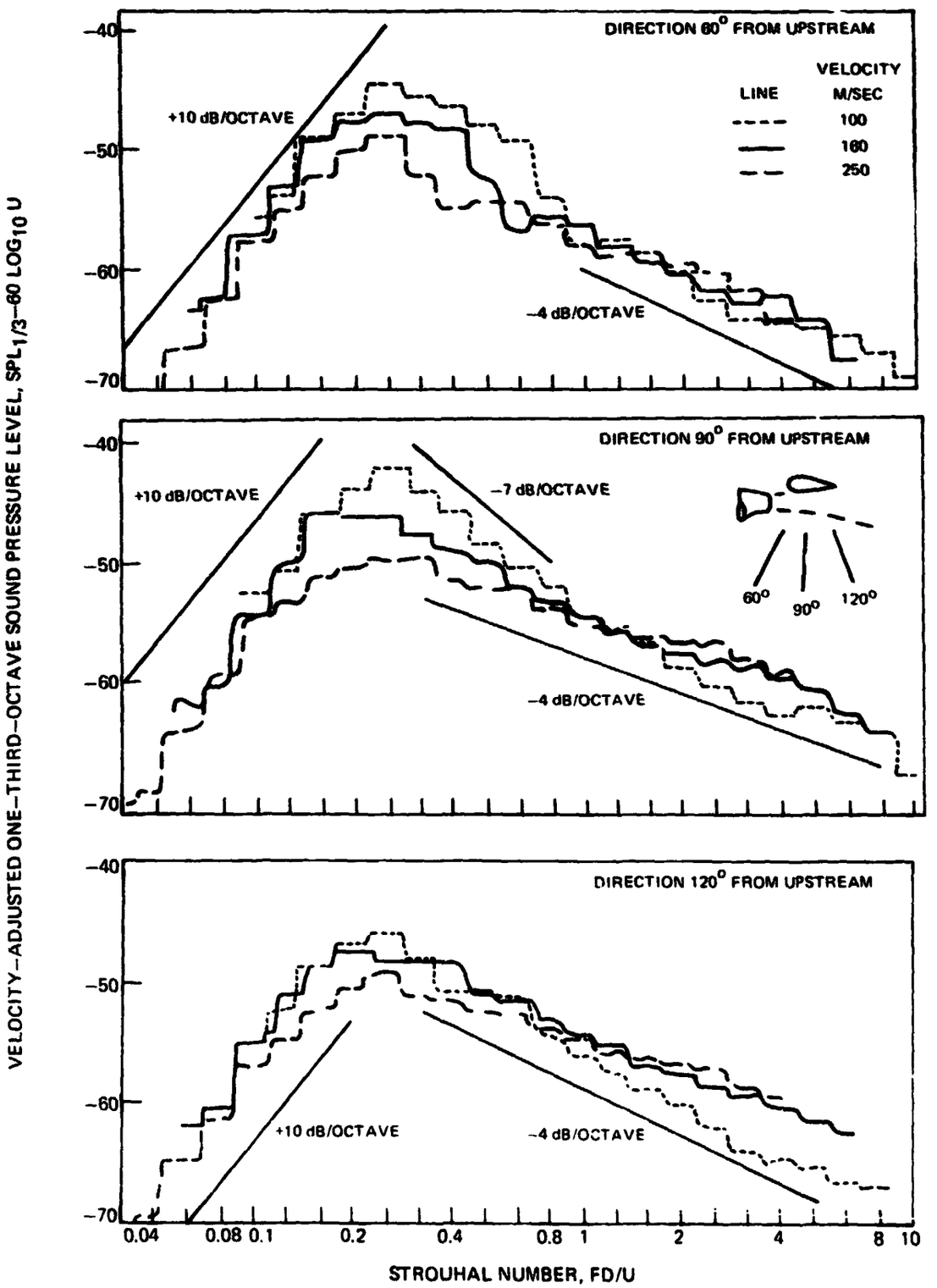

FIGURE 35. – CONTINUED. (d) UNDER–THE–WING INSTALLATION, 9° DEFLECTION

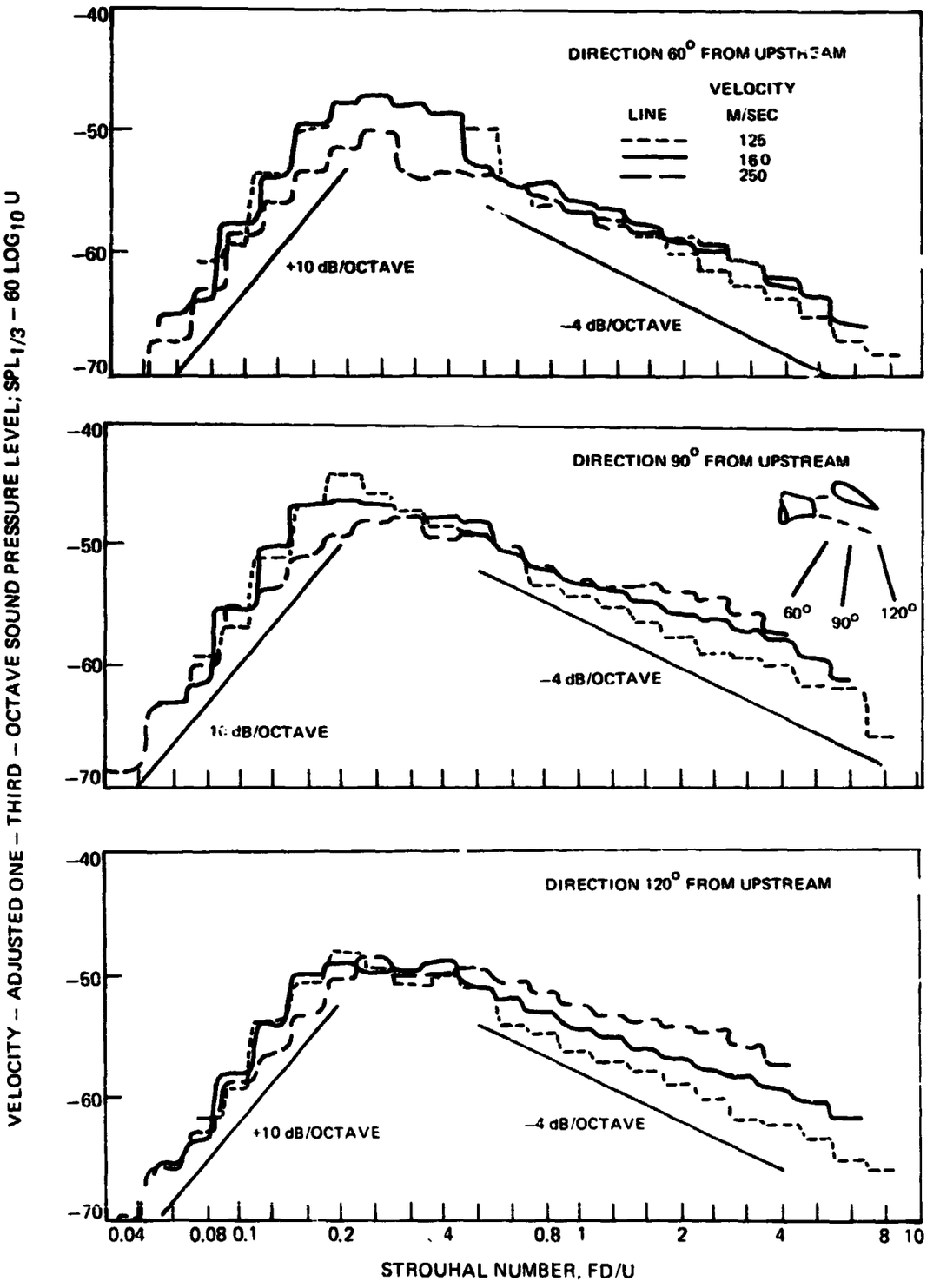

FIGURE 35. – CONTINUED (e) UNDER–THE–WING INSTALLATION, 18° DEFLECTION

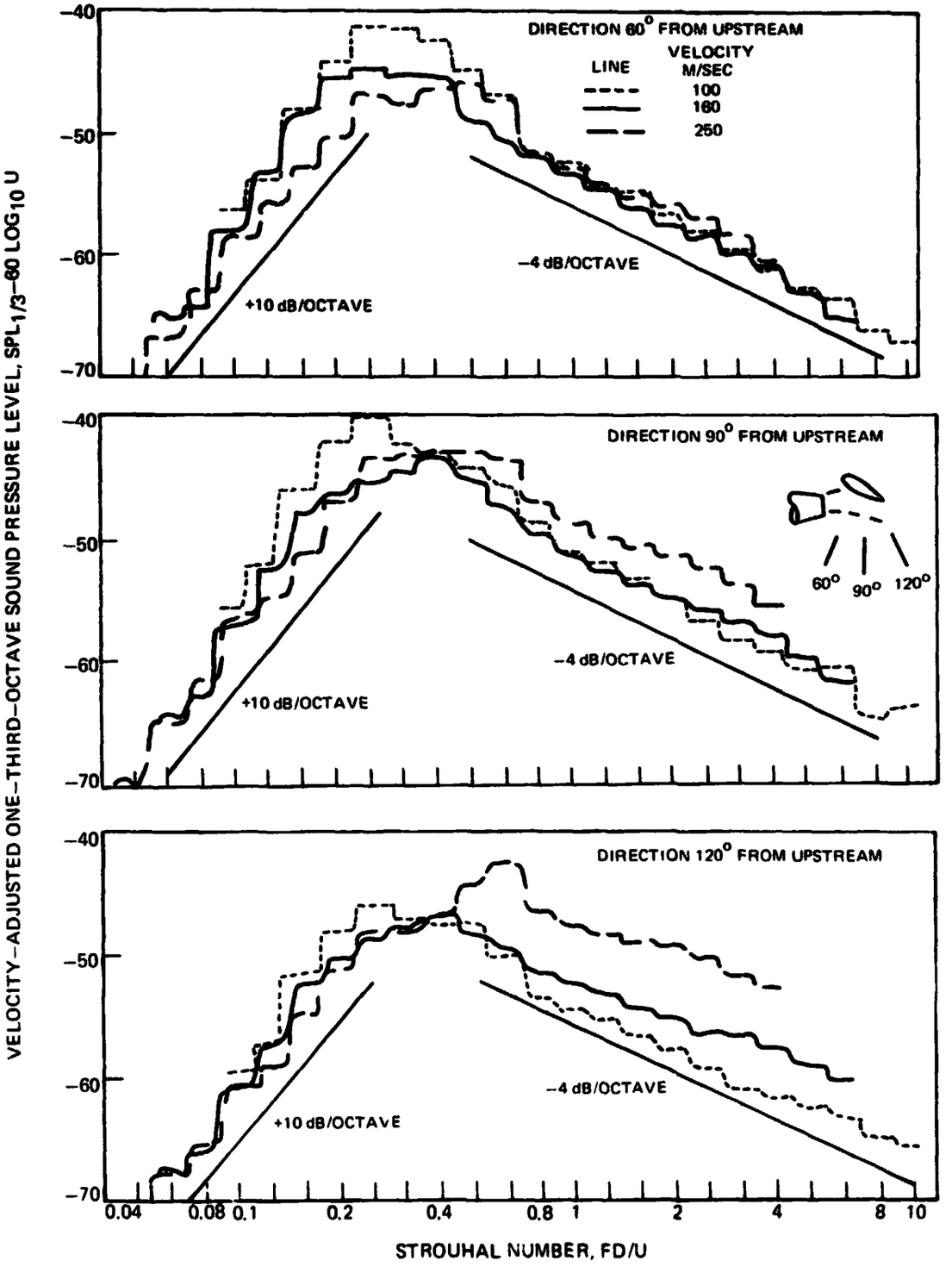

FIGURE 35. – CONCLUDED. (f) UNDER–THE–WING INSTALLATION, 30° DEFLECTION

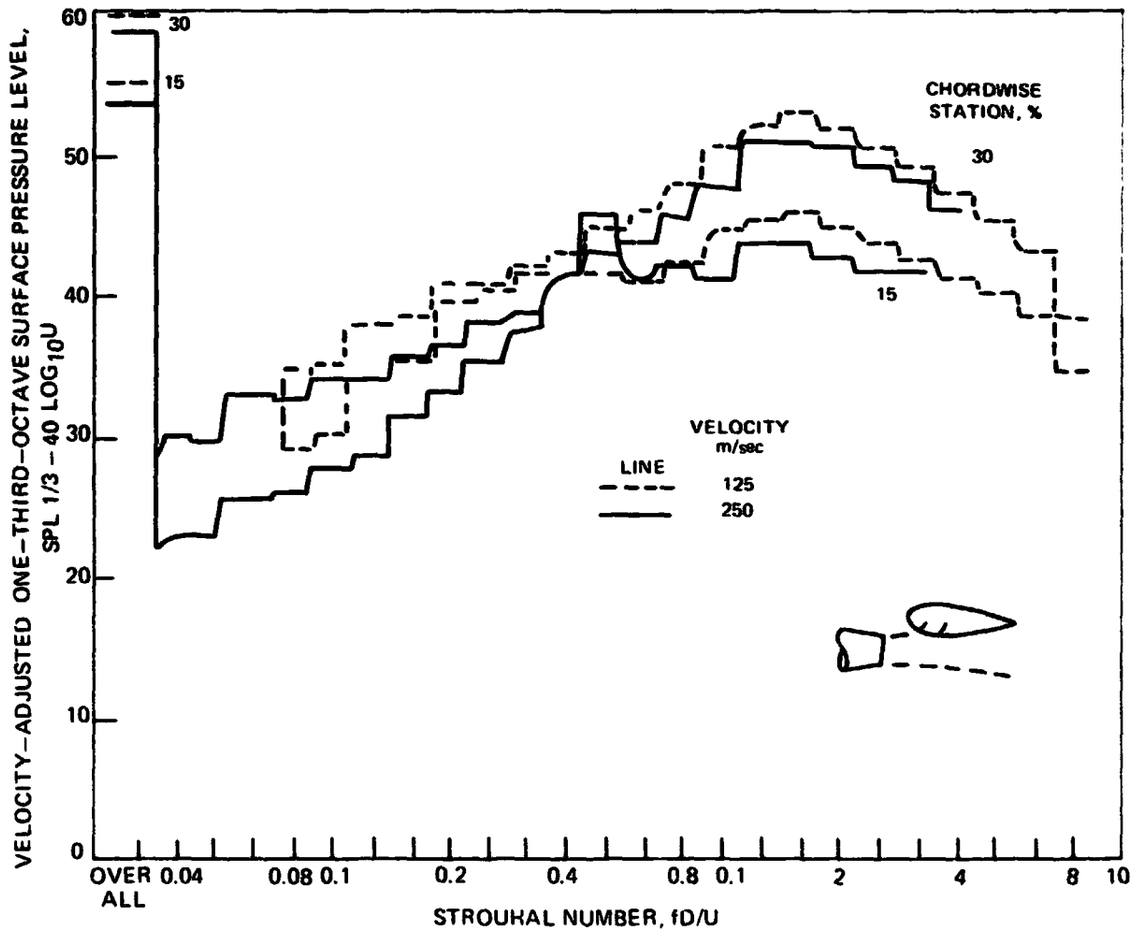

FIGURE 36. VARIATION OF SURFACE PRESSURE SPECTRA IN THE PLANE OF SYMMETRY, ADJUSTED FOR FOURTH POWER VELOCITY DEPENDENCE, WITH DOUBLING THE SCRUBBING JET VELOCITY. (a) FORWARD POSITIONS, 0^0 DEFLECTION

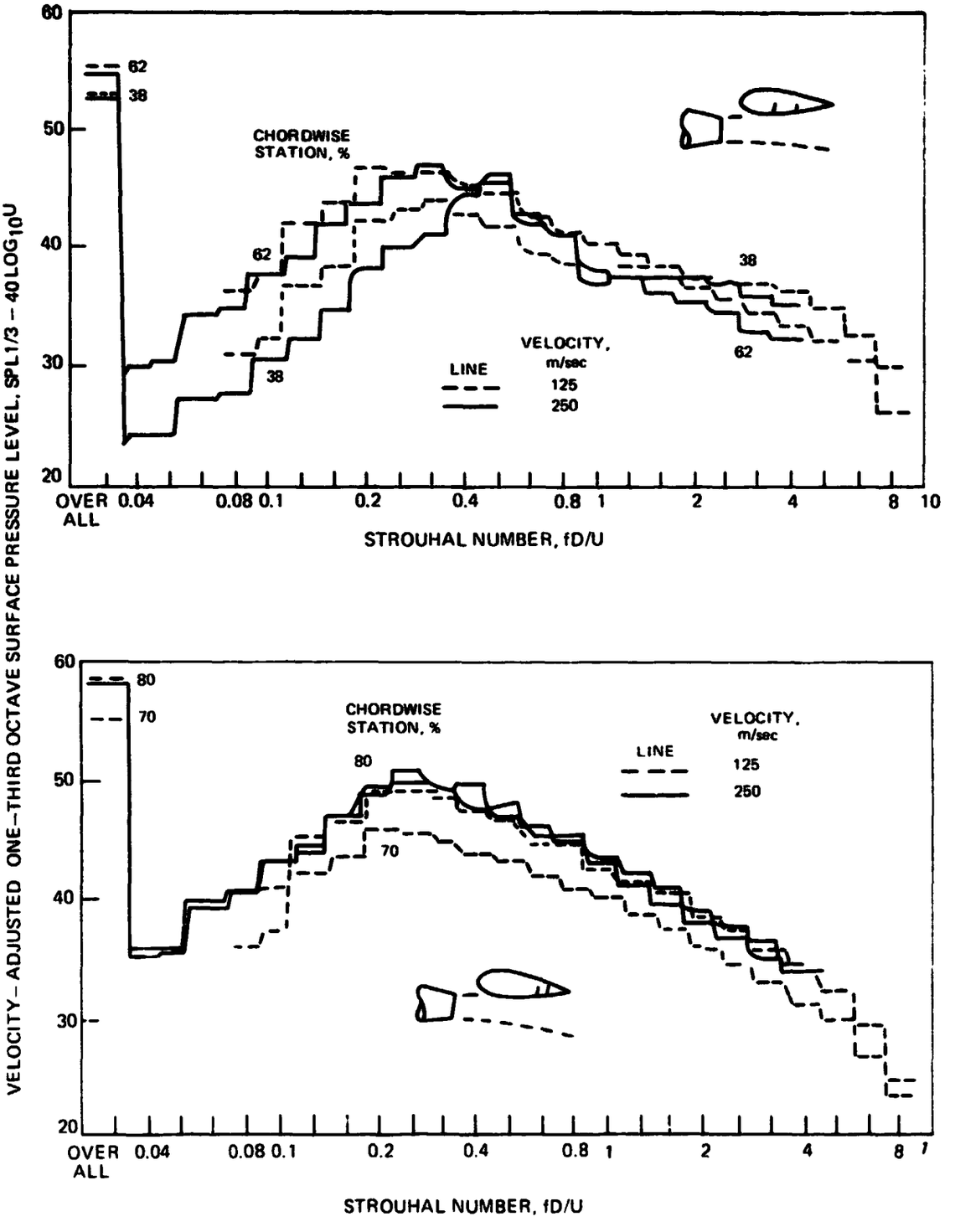

FIGURE 36. – CONTINUED. (b) MIDDLE AND AFT POSITIONS, 0° DEFLECTION.

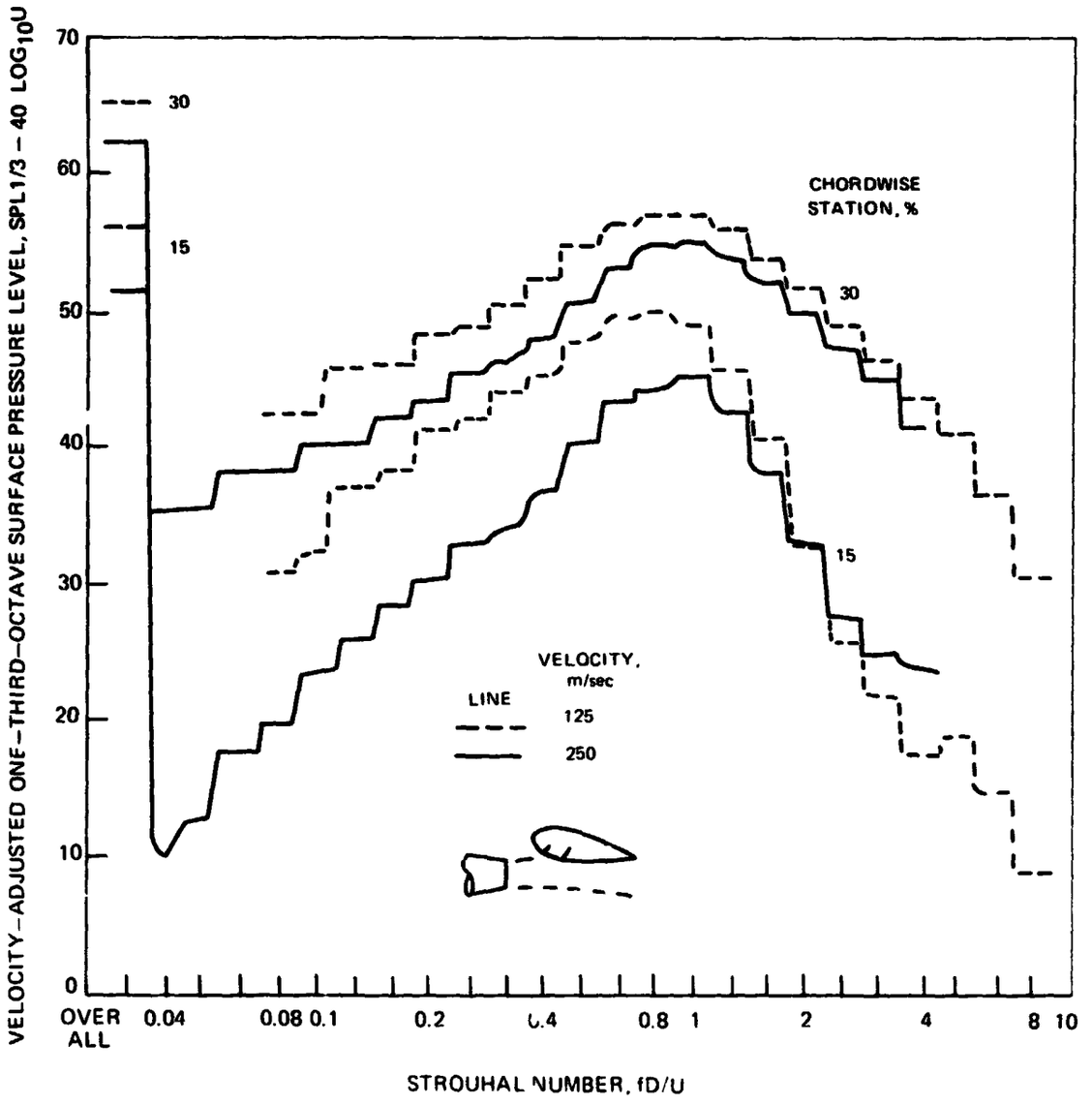

FIGURE 36. – CONTINUED. (c) FORWARD POSITIONS, 9° DEFLECTION.

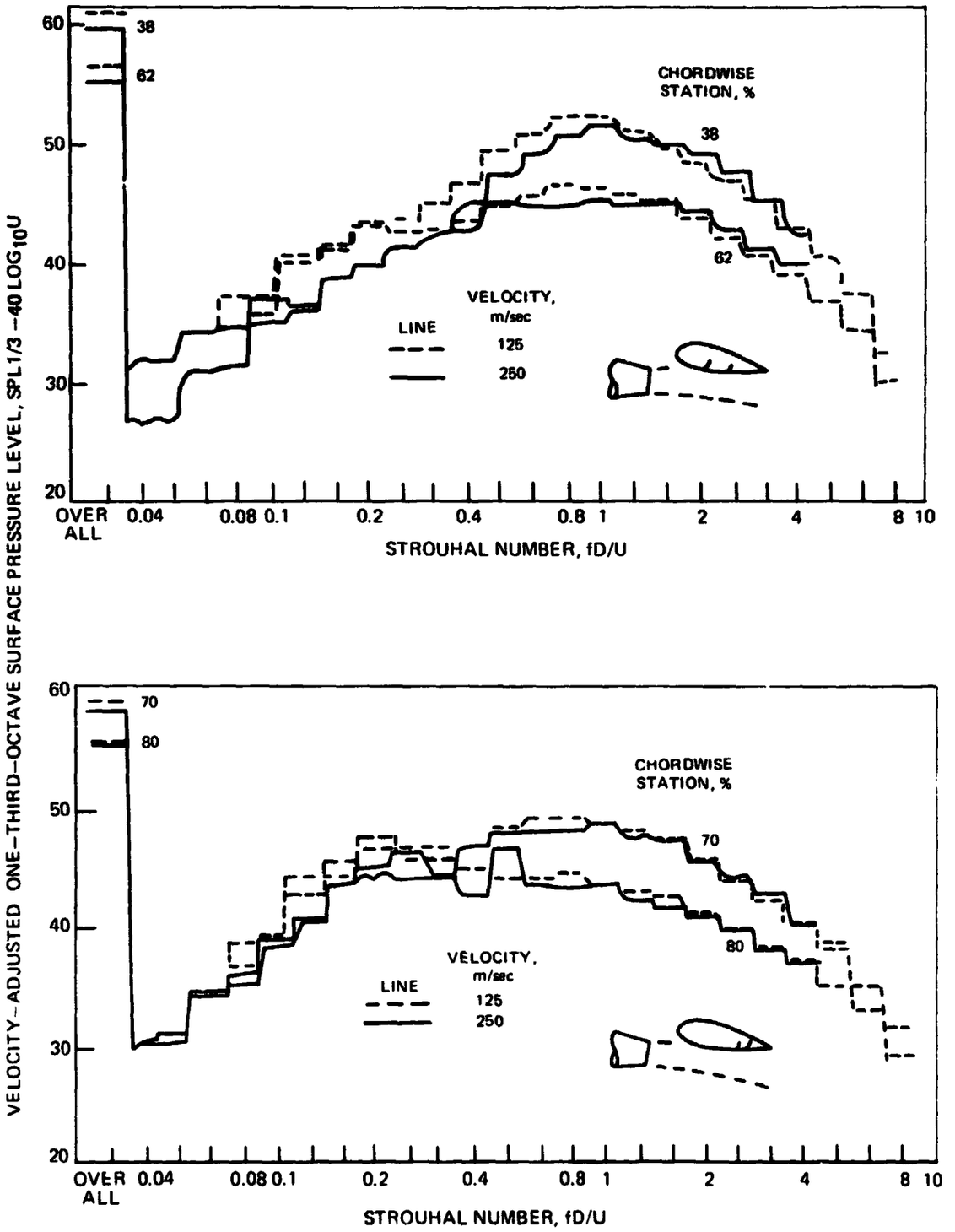

FIGURE 36. – CONTINUED, (d) MIDDLE AND AFT POSITION, 9° DEFLECTION.

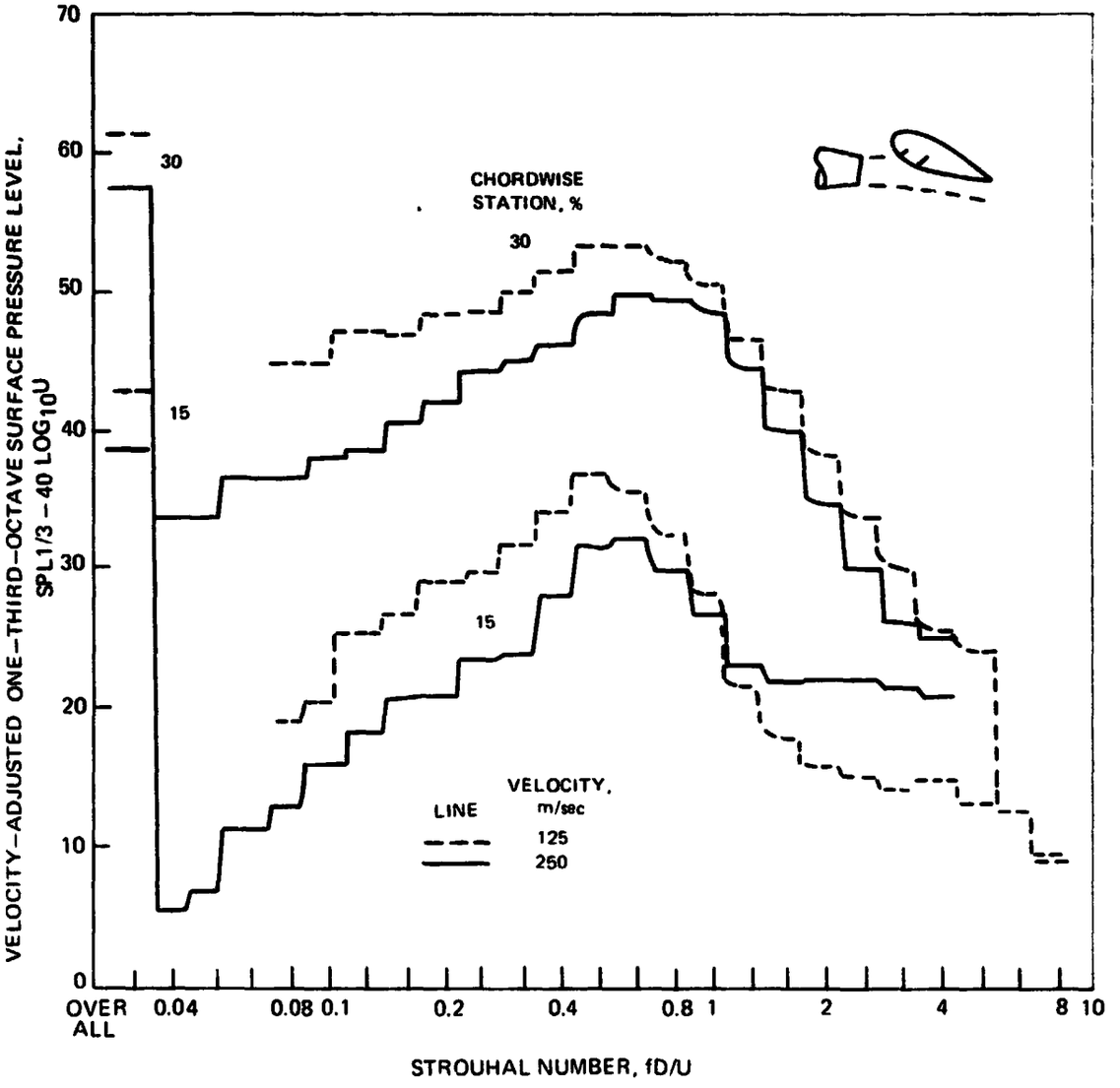

FIGURE 36. – CONTINUED. (e) FORWARD POSITIONS, 18° DEFLECTION.

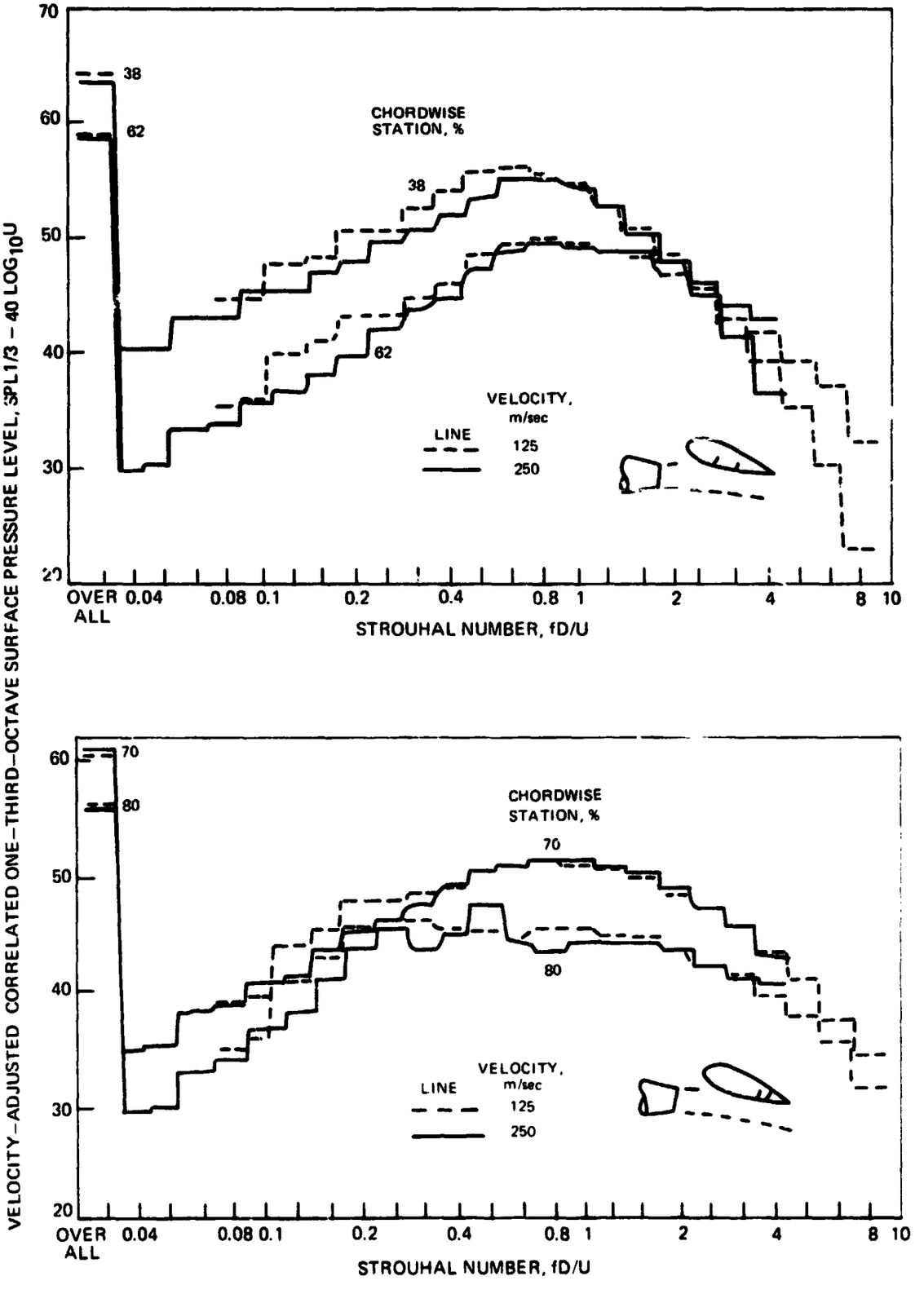

FIGURE 36. – CONTINUED. (f) MIDDLE AND AFT POSITIONS, 18° DEFLECTION.

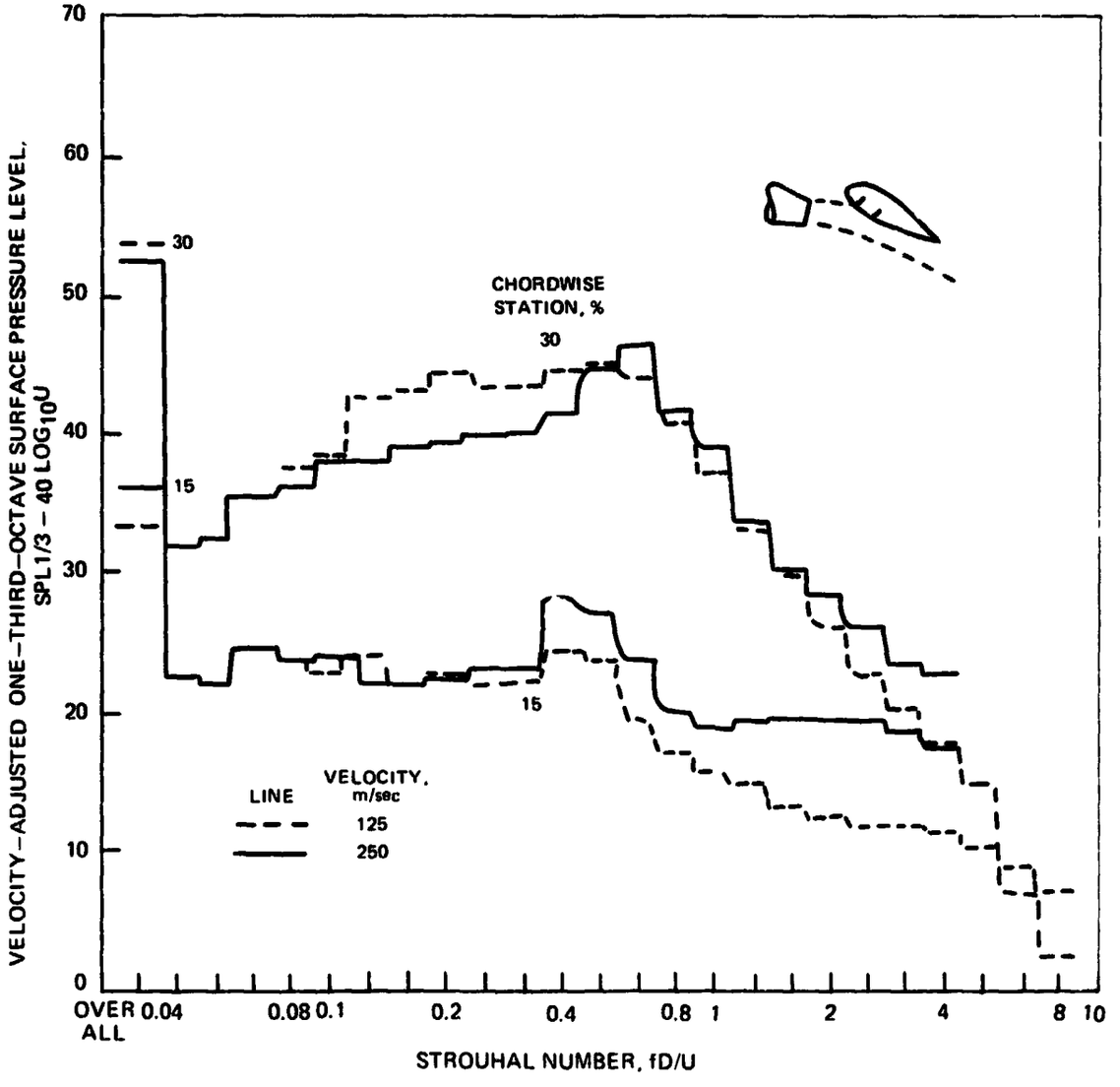

FIGURE 36. – CONTINUED. (g) – FORWARD POSITION, 30° DEFLECTION.

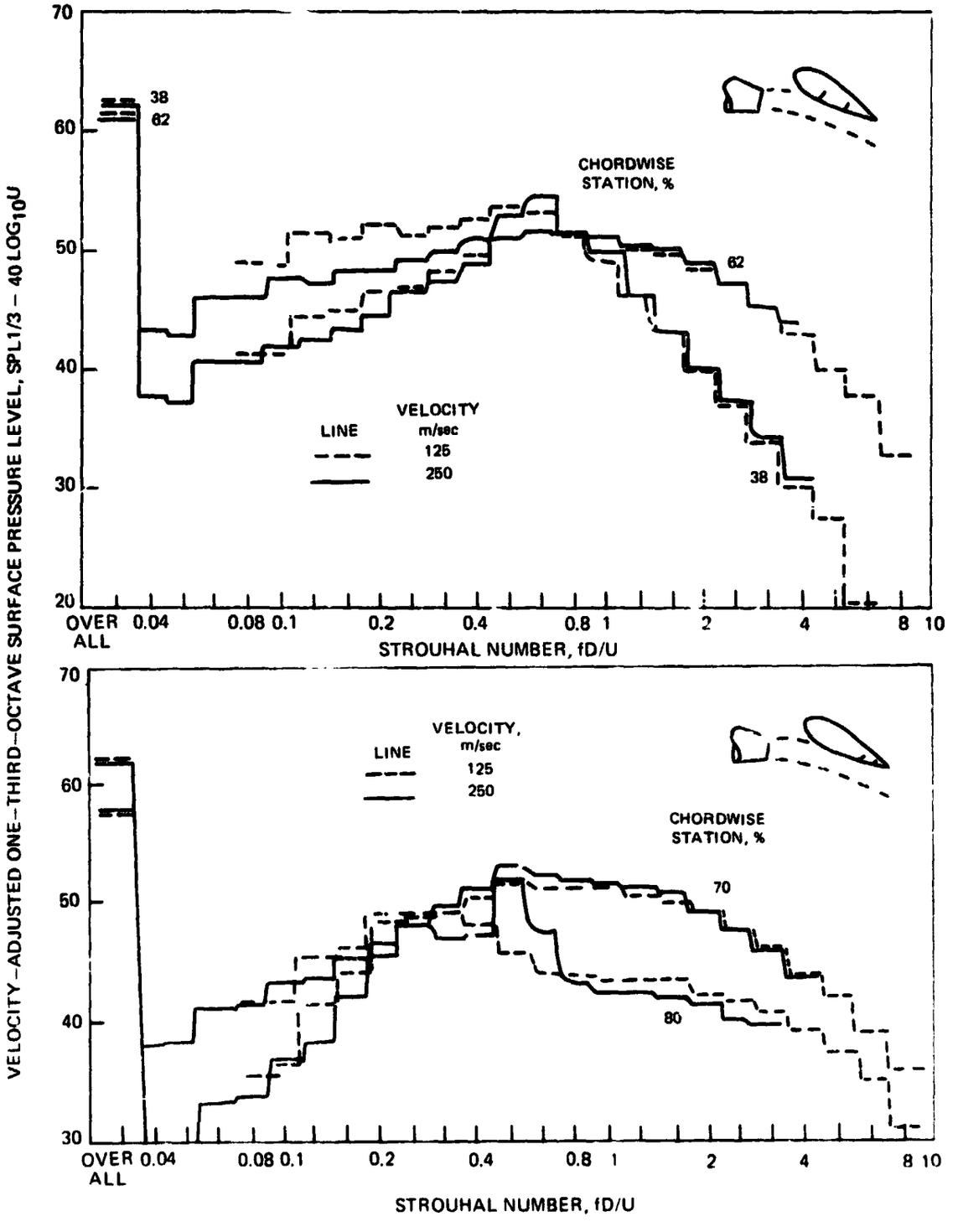

FIGURE 36. – CONTINUED. (h) MIDDLE AND AFT POSITIONS, 30° DEFLECTION.

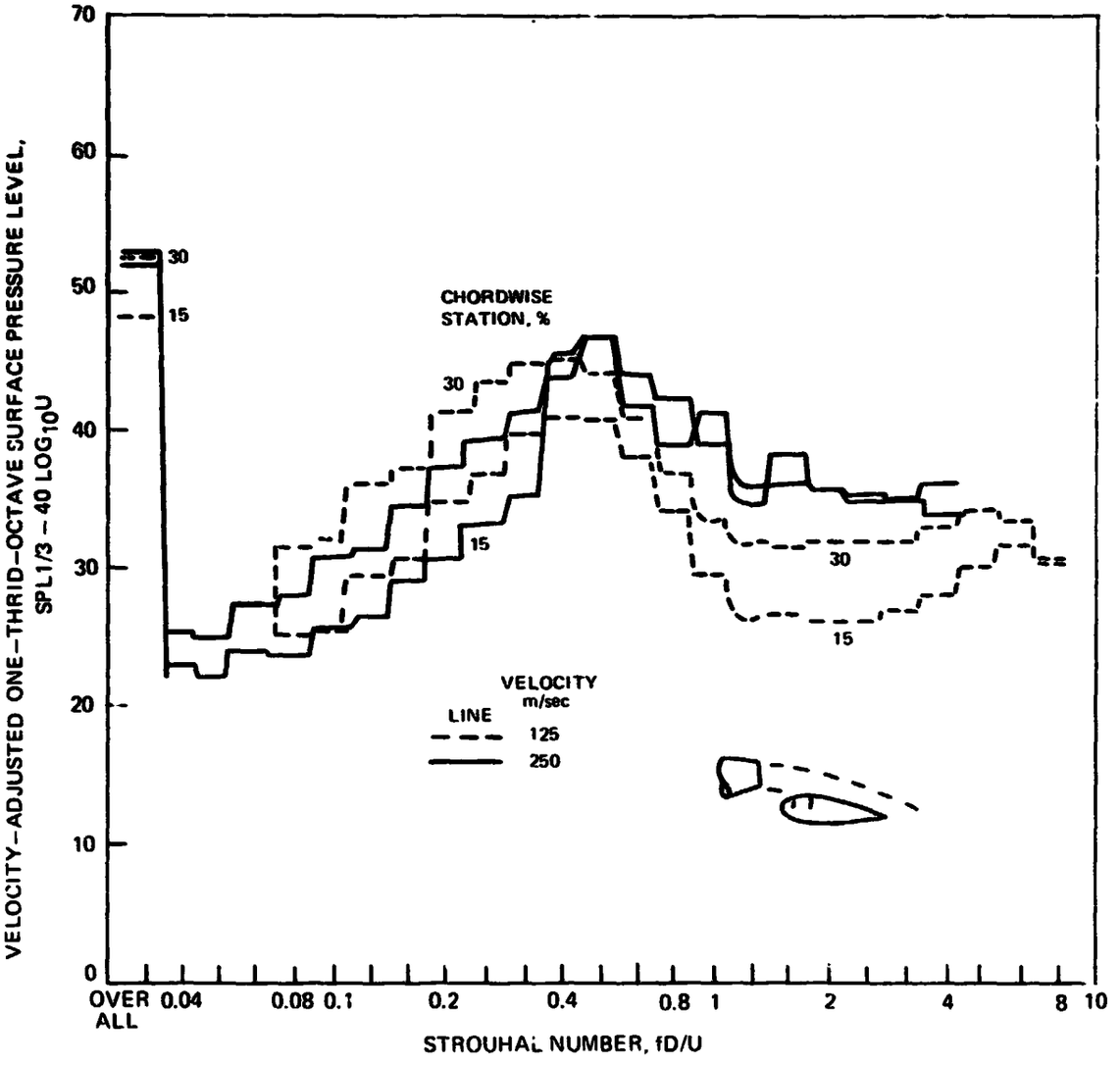

FIGURE 36. – CONTINUED. (i) FORWARD POSITIONS, -10° DEFLECTION.

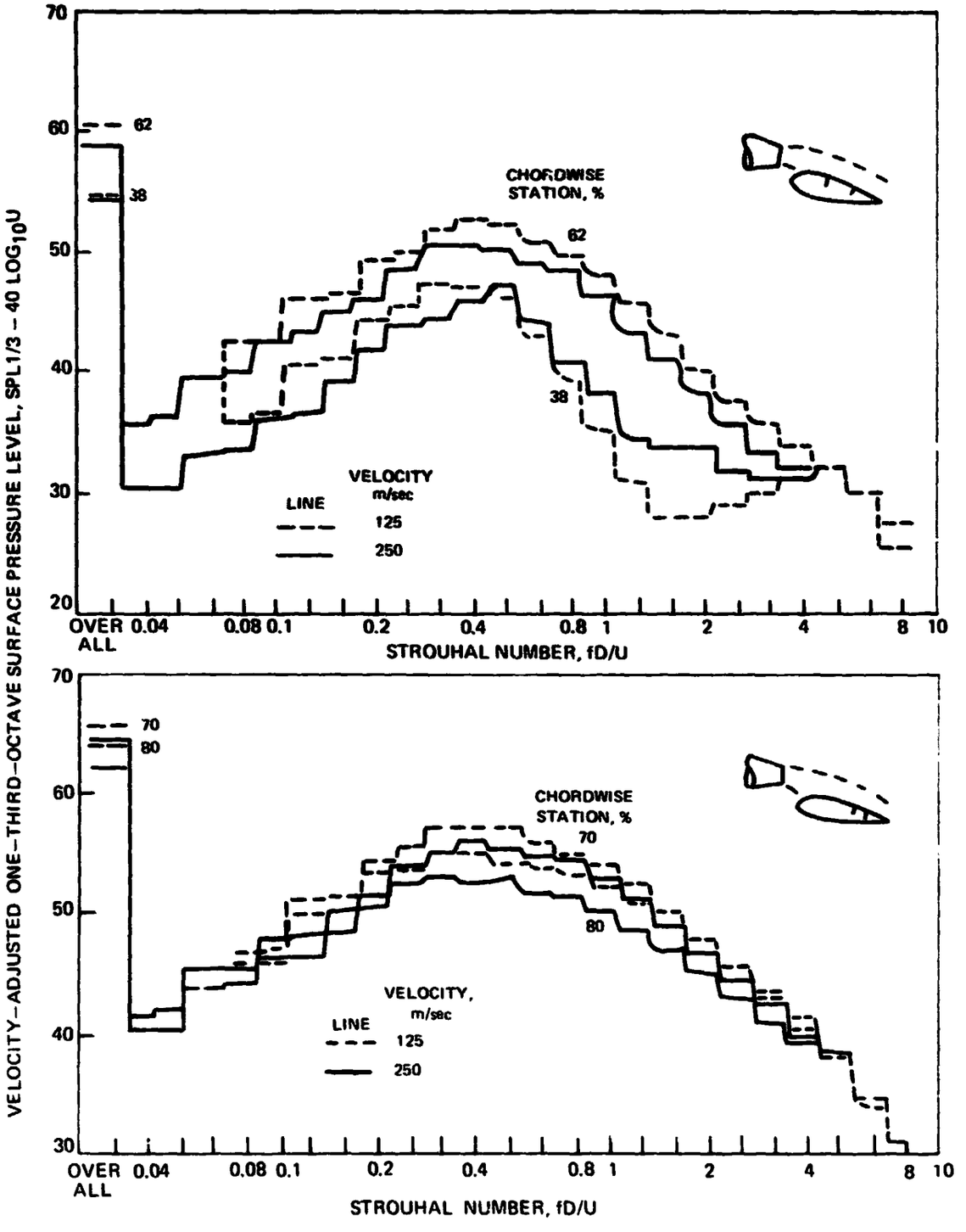

FIGURE 36. – CONCLUDFD (j) MIDDLE AND AFT POSITIONS, –10° DEFLECTION.

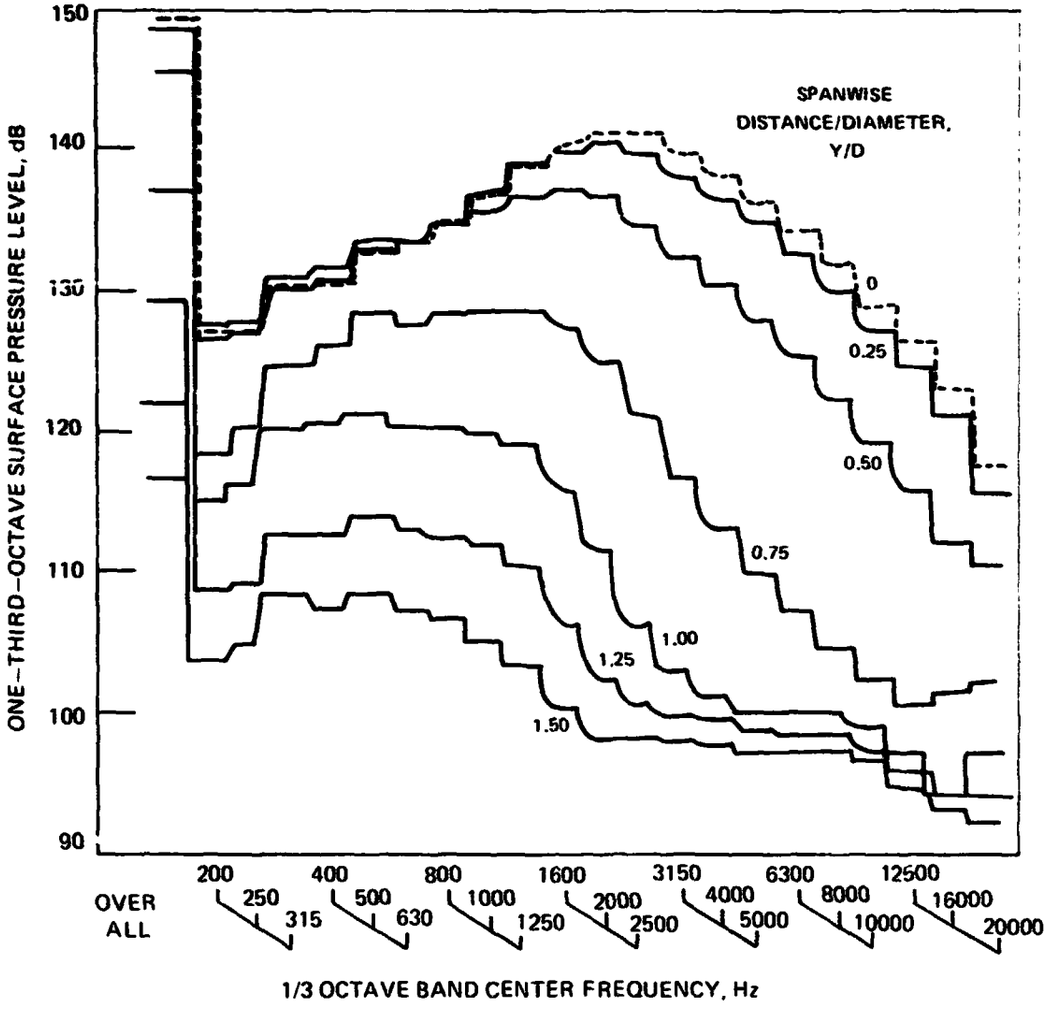

FIGURE 37. – SPANWISE VARIATION OF SURFACE PRESSURE SPECTRA ON SCRUBBED SURFACE OF DEFLECTED AIRFOIL. (a) 9 DEG DEFLECTION, 30% CHORD, 125 m/sec VELOCITY

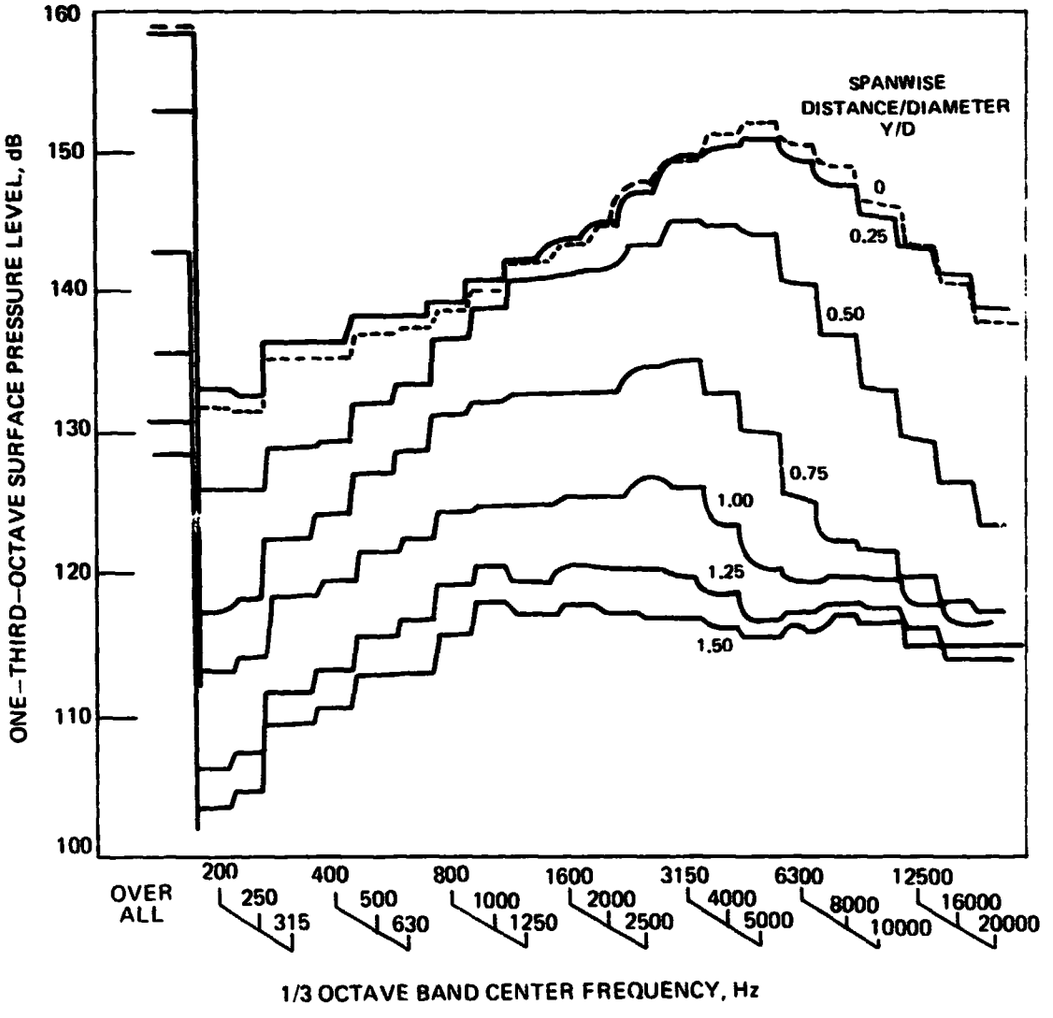

FIGURE 37. – CONTINUED. (b) 9 DEG DEFLECTION, 30% CHORD, 250 m/sec VELOCITY

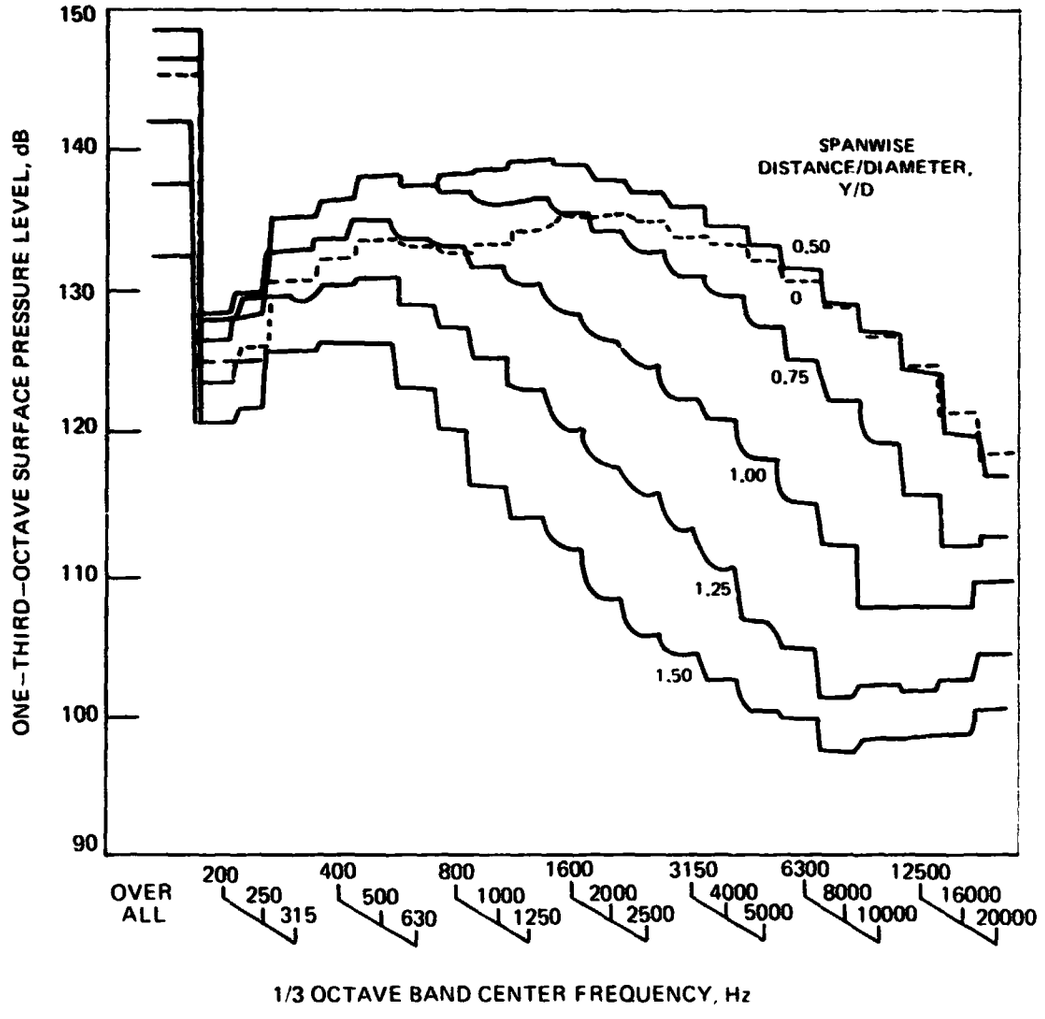

FIGURE 37. – CONTINUED. (c) 9 DEG DEFLECTION, 70% CHORD, 125 m/sec VELOCITY

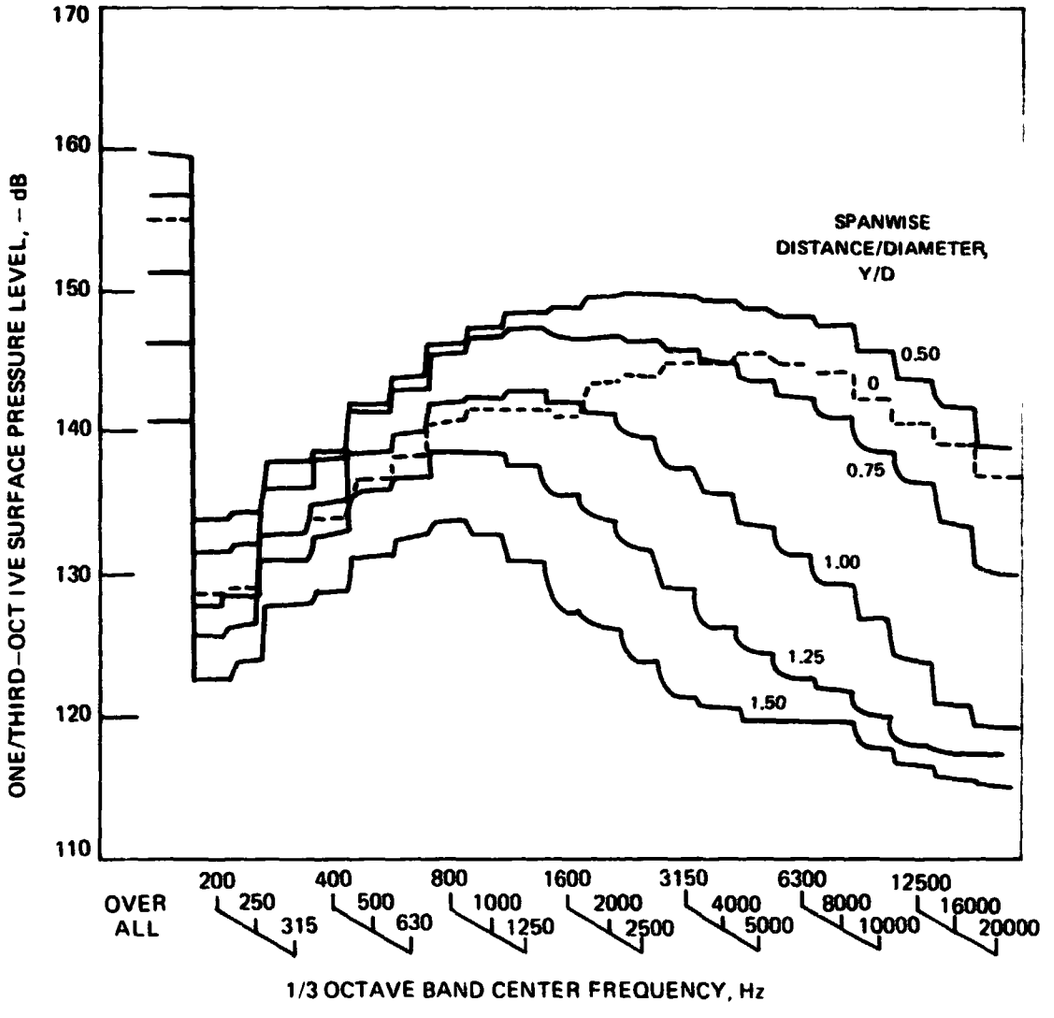

FIGURE 37. – CONTINUED. (d) 9 DEG DEFLECTION, 70% CHORD, 250 m/sec VELOCITY

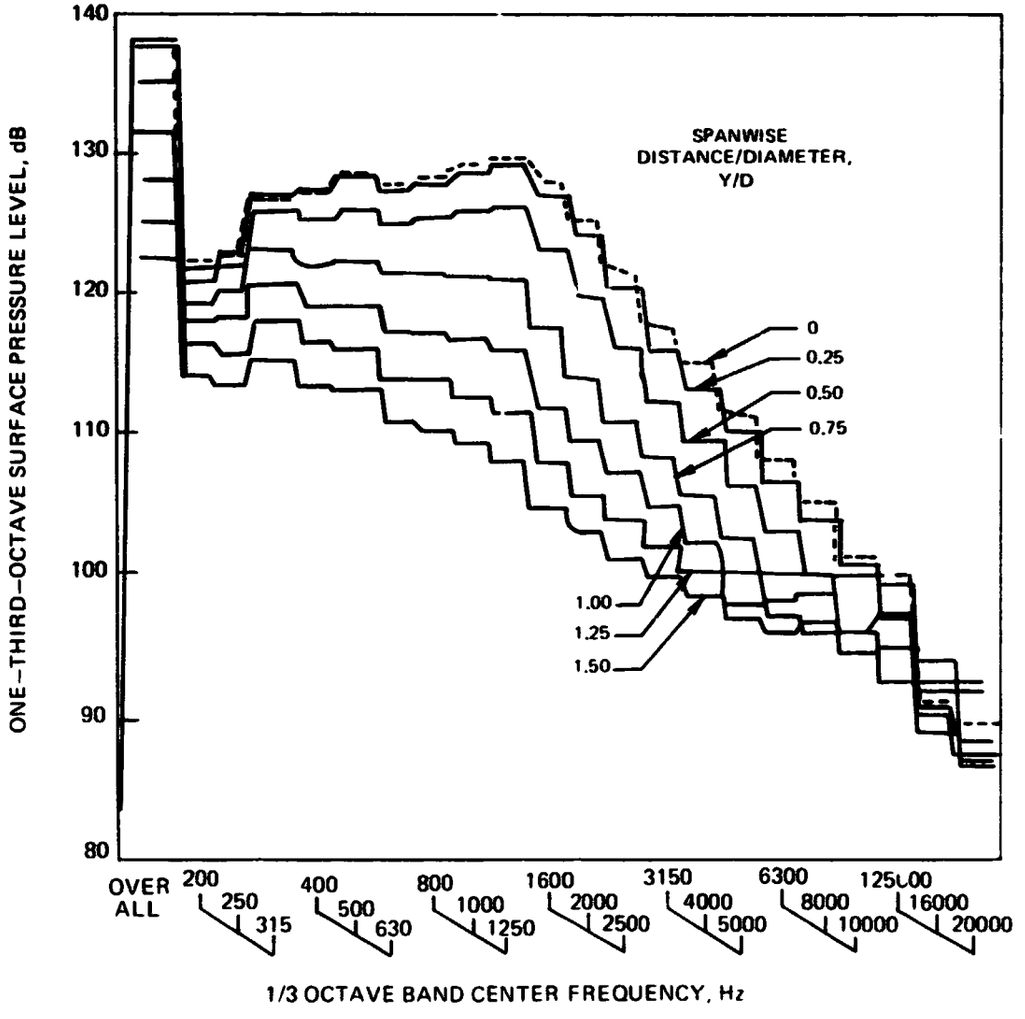

FIGURE 37. – CONTINUED. (e) 30 DEG DEFLECTION, 30% CHORD, 125 m/sec VELOCITY

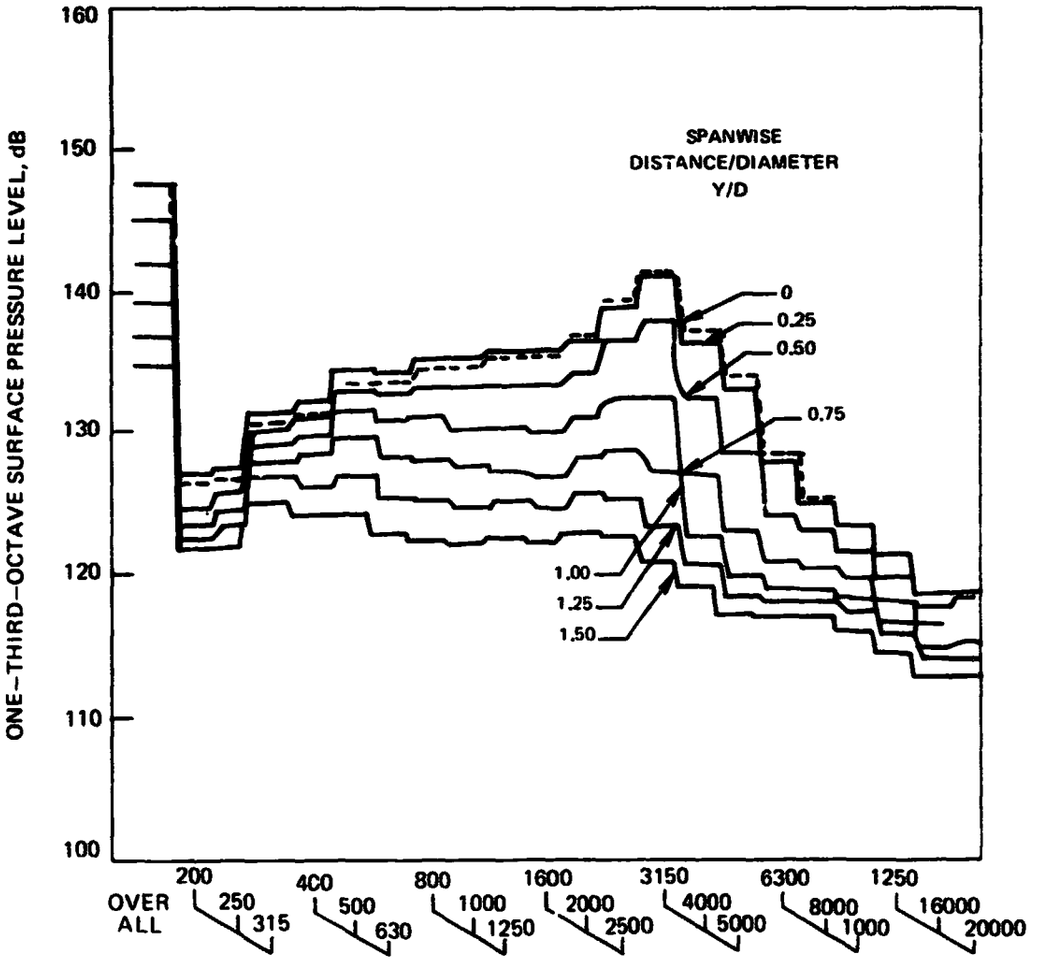

FIGURE 37. – CONTINUED. (f) 30 DEG DEFLECTION, 30% CHORD, 250 m/sec VELOCITY

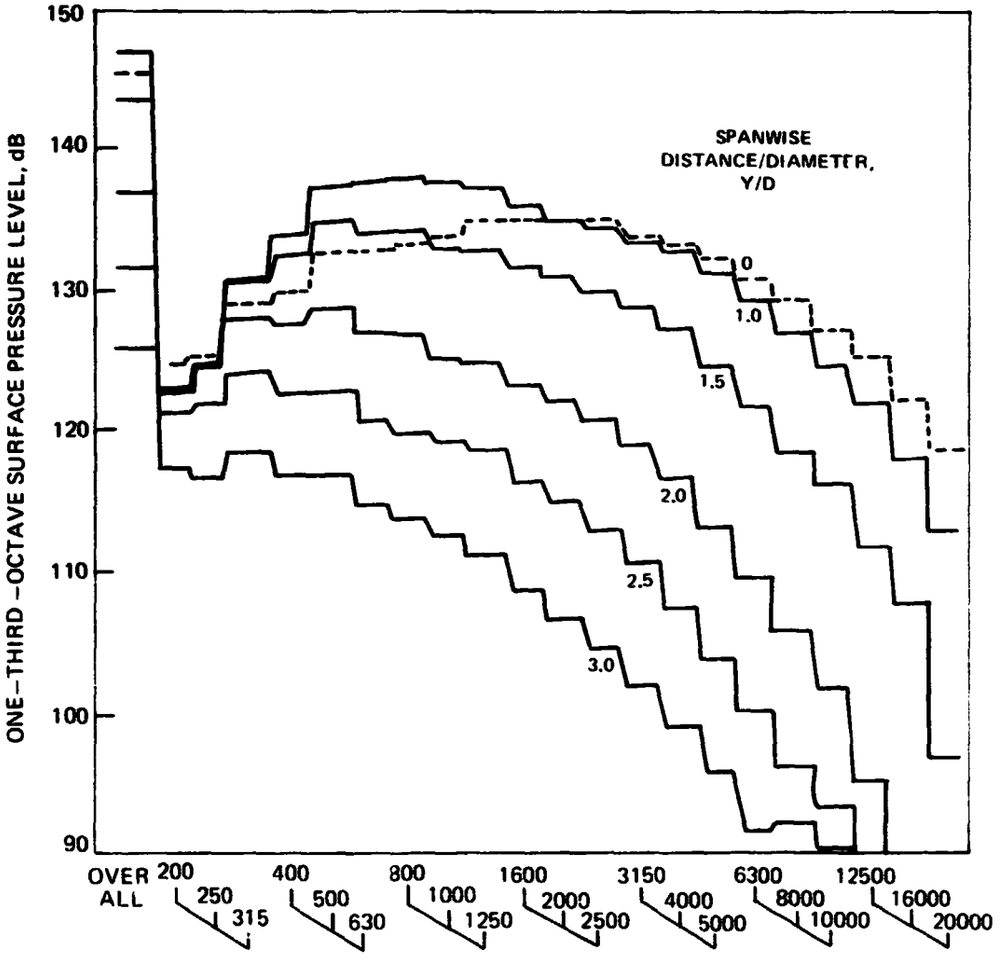

FIGURE 37. – CONTINUED (g) 30 DEG DEFLECTION, 70% CHORD, 125 m/sec VELOCITY

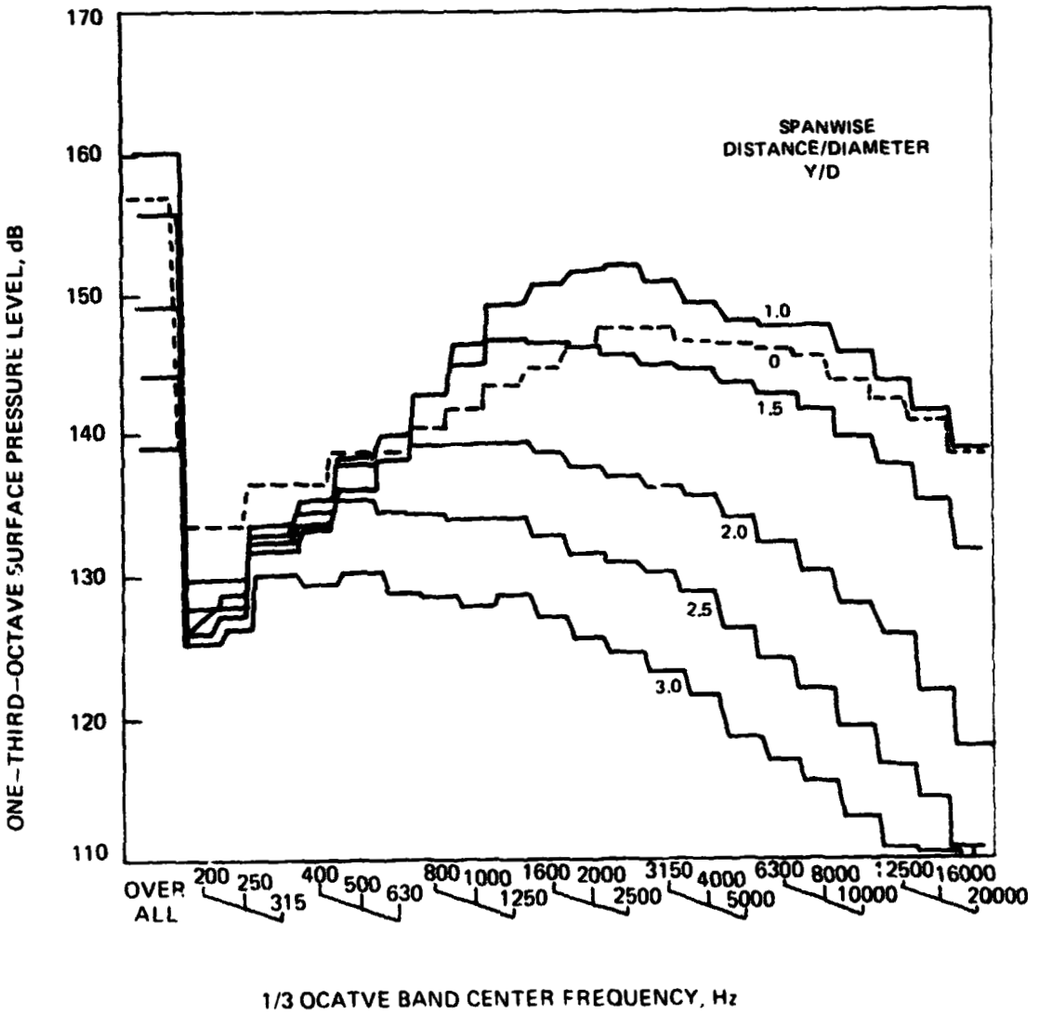

FIGURE 37. – CONCLUDED (h) 30 DEG DEFLECTION, 70% CHORD, 250 m/sec VELOCITY

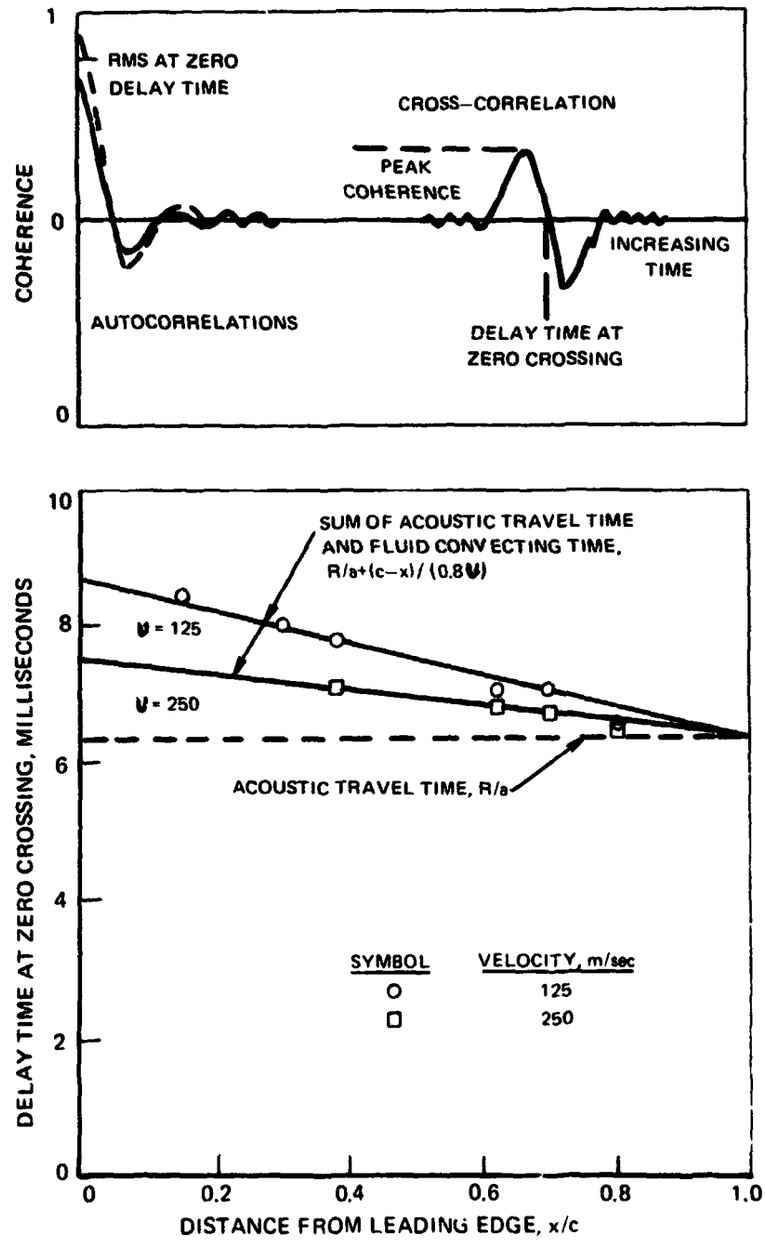

(b) DELAY TIMES AT TWO FLOW VELOCITIES

FIGURE 38. – CROSS–CORRELATIONS BETWEEN FAR FIELD AND AIRFOIL SURFACE IN PLANE OF SYMMETRY FOR 9° DEFLECTION

(c) COHERENCE OF OVERALL SIGNAL

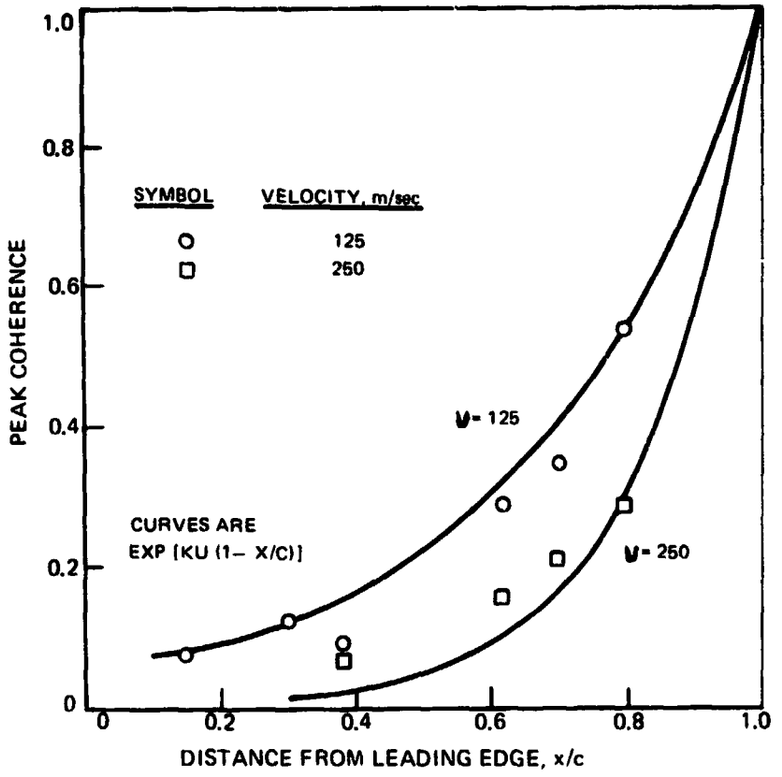

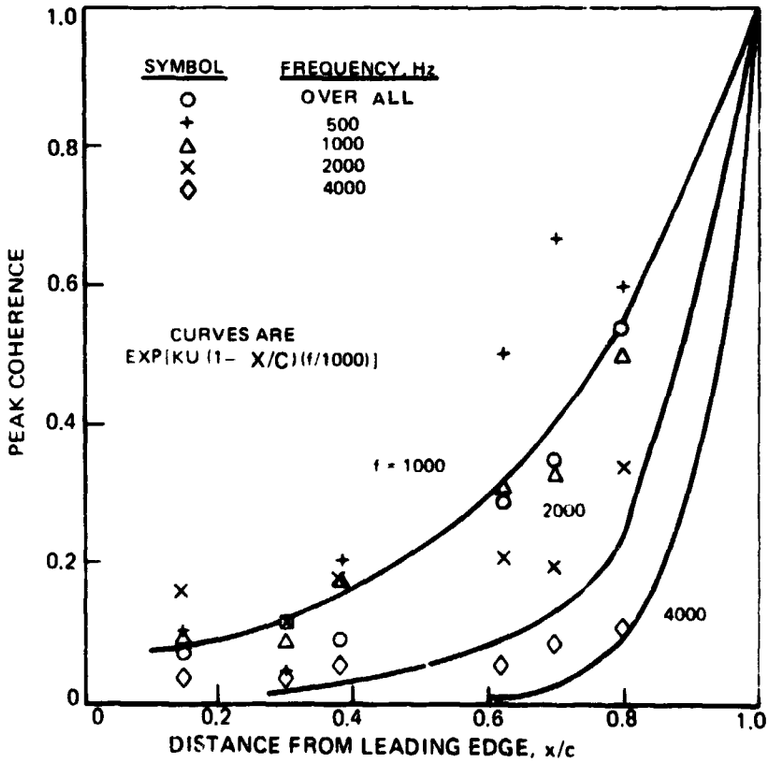

(d) COHERENCE AT OCTAVE BANDWIDTHS

FIGURE 38. – CONCLUDED

(a) DELAY TIMES

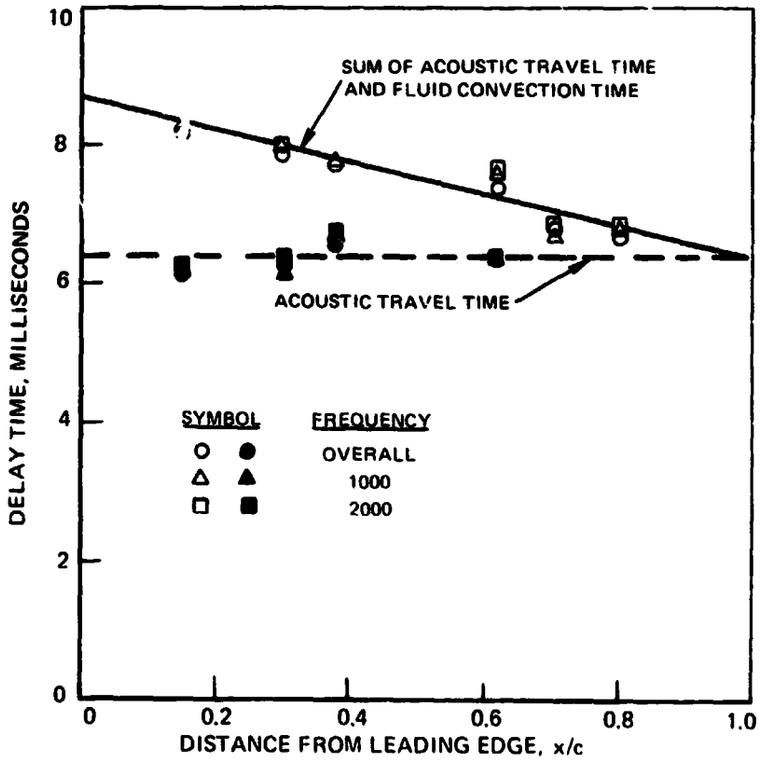

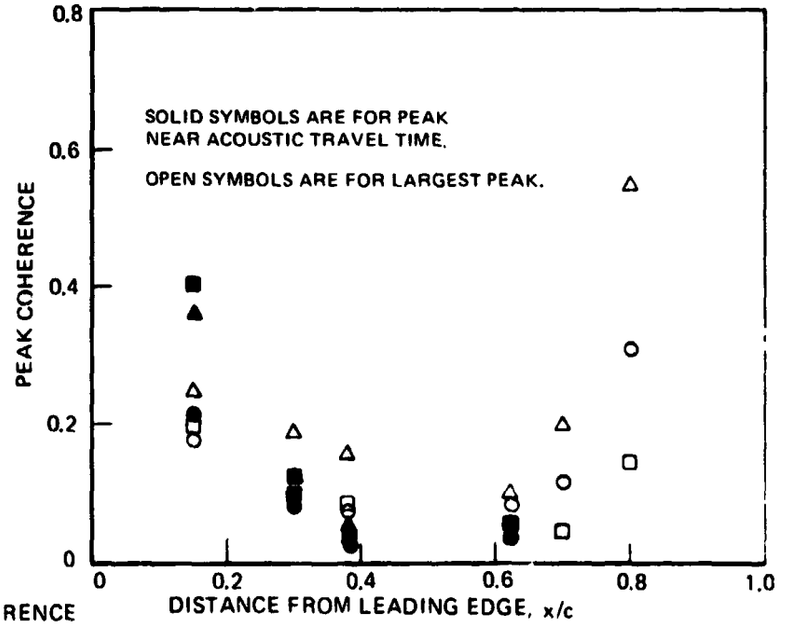

(b) COHERENCE

FIGURE 39. – CROSS–CORRELATIONS BETWEEN FAR FIELD AND AIRFOIL SURFACE IN PLANE OF SYMMETRY FOR 30° DEFLECTION ANGLE AND 125 M/SEC VELOCITY

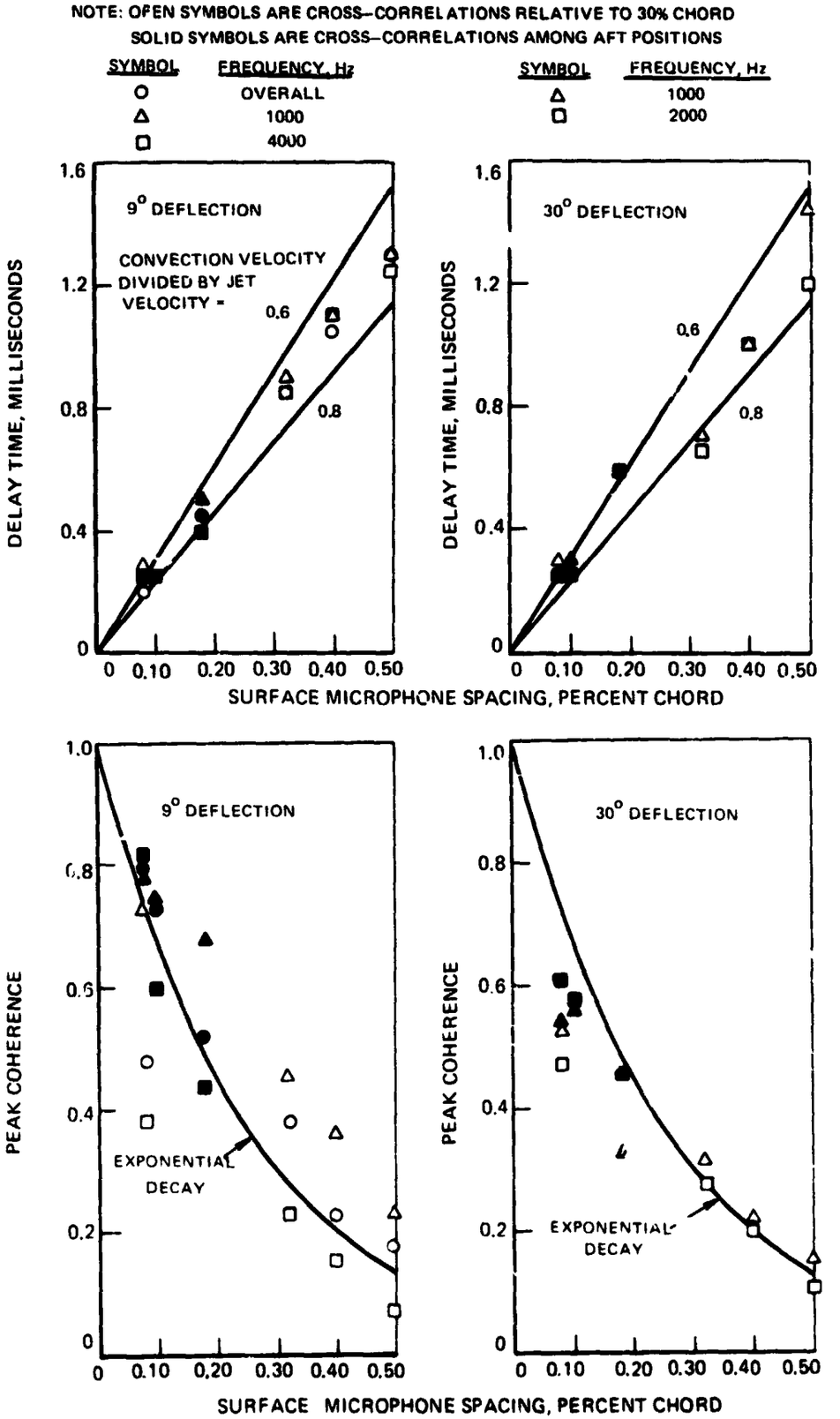

FIGURE 40. – CROSS–CORRELATIONS ALONG THE AIRFOIL SURFACE IN PLANE OF SYMMETRY FOR 125 M/SEC VELOCITY

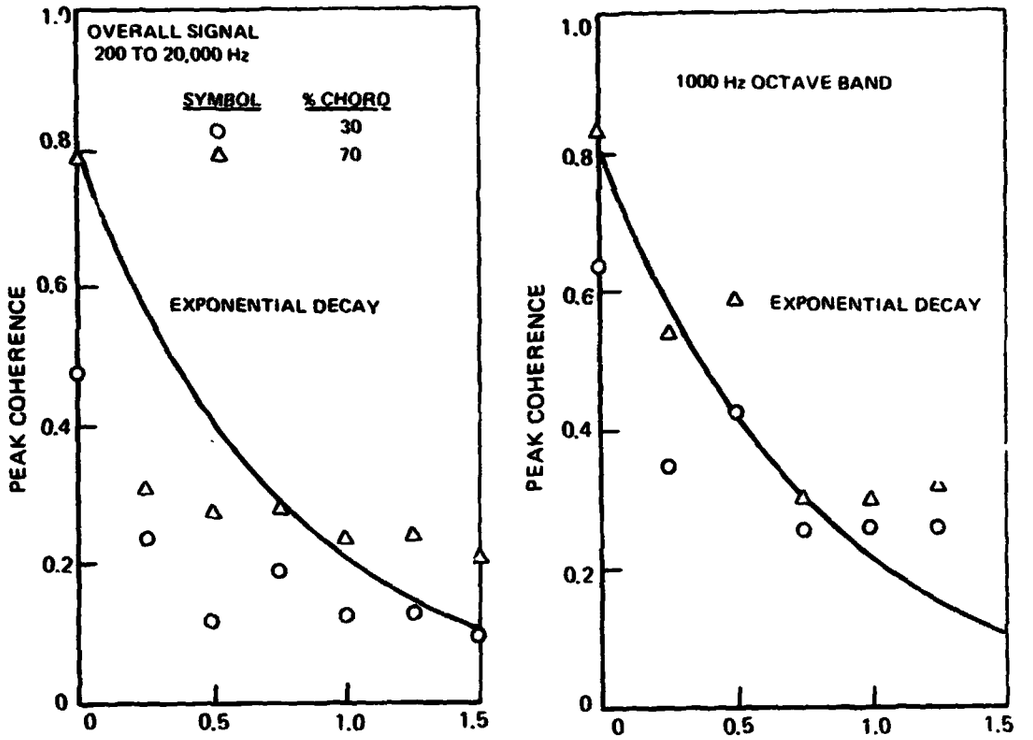

SPANWISE DISTANCE DIVIDED BY DIAMETER, Y/D
(a) COHERENCE EVALUATED AT FLOW CONVECTION TIME

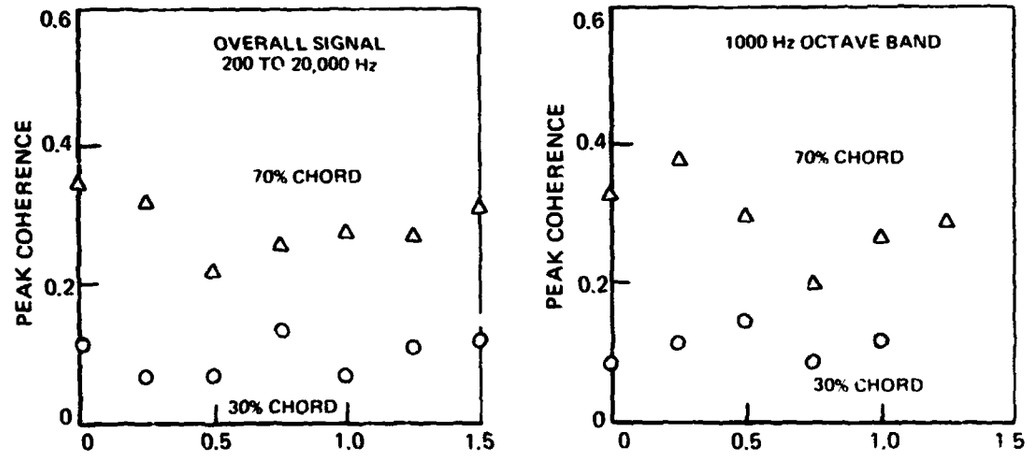

SPANWISE DISTANCE DIVIDED BY DIAMETER, Y/D
(b) COHERENCE OF SECOND PEAK IN CROSS-CORRELATIONS

FIGURE 41. – CROSS-CORRELATIONS BETWEEN SURFACE MICROPHONES AT 38% AND 62% CHORD IN THE PLANE OF SYMMETRY AND SURFACE MICROPHONES TRAVERSED SPANWISE AT 30% AND 70% CHORD, 9° DEFLECTION ANGLE AND 125 M/SEC VELOCITY